Keck Adaptive Optics Note 511

NEXT GENERATION ADAPTIVE OPTICS: SYSTEM DESIGN MANUAL

Version 2.1
March 30, 2008

Author List

Name	Function
Peter Wizinowich	NGAO Executive Committee (EC) Chair
Richard Dekany	EC Member (COO)
Don Gavel	EC Member (UCO)
Claire Max	EC Member & NGAO Science Team Chair (UCO)
Sean Adkins	WMKO Instrument Program Manager (WMKO)
From Caltech Optical Observatories (COO): Viswa Velur Anna Moore Matthew Britton Antonin Bouchez	 Optical system engineer Optical system engineer AO scientist AO scientist
From University California Observatories (UCO): Elizabeth McGrath Renate Kupke Brian Bauman Marco Reinig Chris Lockwood	 Astronomer Optical system engineer Optical system engineer AO Software engineer Mechanical engineer
From W. M. Keck Observatory (WMKO): Chris Neyman David Le Mignant Ralf Flicker Erik Johansson Jason Chin Jim Bell Drew Medeiros	 AO system scientist AO instrument scientist AO scientist AO Software Engineer Laser & electronics engineer Mechanical engineer Mechanical engineer

Approval Control

Control	Name	Function
Revised by:		
Approved by:		
Authorized by:		

Document Change Record

Issue	Date	Change Description
Version 1.0	**October 31, 2007**	
Version 2.0	**March 28, 2008**	

Table of Contents

Table of Contents

Table of Contents

Table of Contents

Figures and Tables

Figures and Tables

Figures and Tables

1 INTRODUCTION

This document describes the system design for the Next Generation Adaptive Optics (NGAO) system to be built for the W. M. Keck Observatory (WMKO). This document is one of the key system design phase deliverables as discussed in the System Design Report (KAON 575). It is intended to provide an overview of the system design, while referencing the appropriate documents which contain the details.

We begin with an overview of the system design that includes major sections on the AO system, laser facility, controls hardware and software, science operations and science instruments. The science instruments section is not at a system design level since these instruments were not part of the NGAO system design effort however, it was important to consider them from the context of the overall design and requirements.

The performance budgets are addressed in section 4. Eight system performance metrics were identified in the Science Requirements Document. For three of these metrics, background and transmission, wavefront error and ensquared energy, and high-contrast performance, we have produced associated quantitative performance budgets to identify key performance drivers. For photometric precision, astrometric accuracy, polarimetry and observing efficiency we have identified key drivers and documented these in technical reports that have informed the NGAO design..

Section 5 provides an overview of the requirements flow down and a discussion of compliance. Detailed requirements have largely not been included in the design discussions in this document because of the length of this information. The detailed requirements can be found in most of the referenced design KAONs as well as in the Functional Requirements Document (KAON 573).

The remaining two sections of this document provide a brief overview of alternate architectures that were evaluated during the system design phase and brief summaries of the trade studies that were performed.

2 REFERENCES

A list of all Keck Adaptive Optics Notes for NGAO can be found in an Appendix to the System Design Report (KAON 575). These documents are available at http://www.oir.caltech.edu/twiki_oir/bin/view/Keck/NGAO/NewKAONs.

3 DESIGN OVERVIEW

3.1 AO System Overview

All of the NGAO science cases require essentially diffraction limited performance (Strehl > 0.6) in the near-IR. A number of Solar System and Galactic science cases have requirements for at least modest Strehl in the visible wavelengths. All of the science cases also require high sensitivity with most of the targets of interest being too faint to use as references for wavefront sensing in the AO system. This high Strehl, faint object performance is required with reasonable (≥ 30%) sky coverage.

The requirements for sky coverage and high sensitivity are both met by using a laser of 589 nm wavelength to illuminate the mesospheric sodium layer, producing an artificial laser guide star (LGS) for AO wavefront sensing. Achieving the desired level of Strehl performance leads directly to a requirement for an AO system that can overcome the effect of focus anisoplanatism (the "cone effect"), a requirement that is met through use of multiple laser beacons producing a constellation of LGS as shown in Figure 1. A high order wavefront sensor is required for each LGS, and the wavefront information from these sensors is combined to produce a three dimensional description of the atmospheric turbulence over the telescope aperture using tomographic reconstruction techniques. We have concluded that a variable diameter constellation of LGS with one in the center and five equally spaced around a circle provides the optimal sampling of the atmosphere above the telescope with respect to tomography error. The radius of the circle is set at a minimum of 10" for the narrow field case, and optimized between this radius and 150" depending on the location of the deployable Integral Field Spectrograph (d-IFS) heads (see section 3.7 for a description of the science instruments) within a 150" diameter field of regard and the specific availability of tip-tilt field stars on a target-by-target basis.

Tilt anisoplanatism is removed using three NGS tip-tilt sensors operating in the near-IR. Three tip-tilt (TT) sensors are sufficient for correction of the wavefront error modes associated with tilt anisoplanatism in multiple-LGS systems. One of these sensors additional senses focus and astigmatism (FA) to reduce the quadratic mode estimation errors in the LGS tomography. Three additional point and shoot (PnS) LGS beacons are used to provide image sharpening for each of the tip/tilt stars.

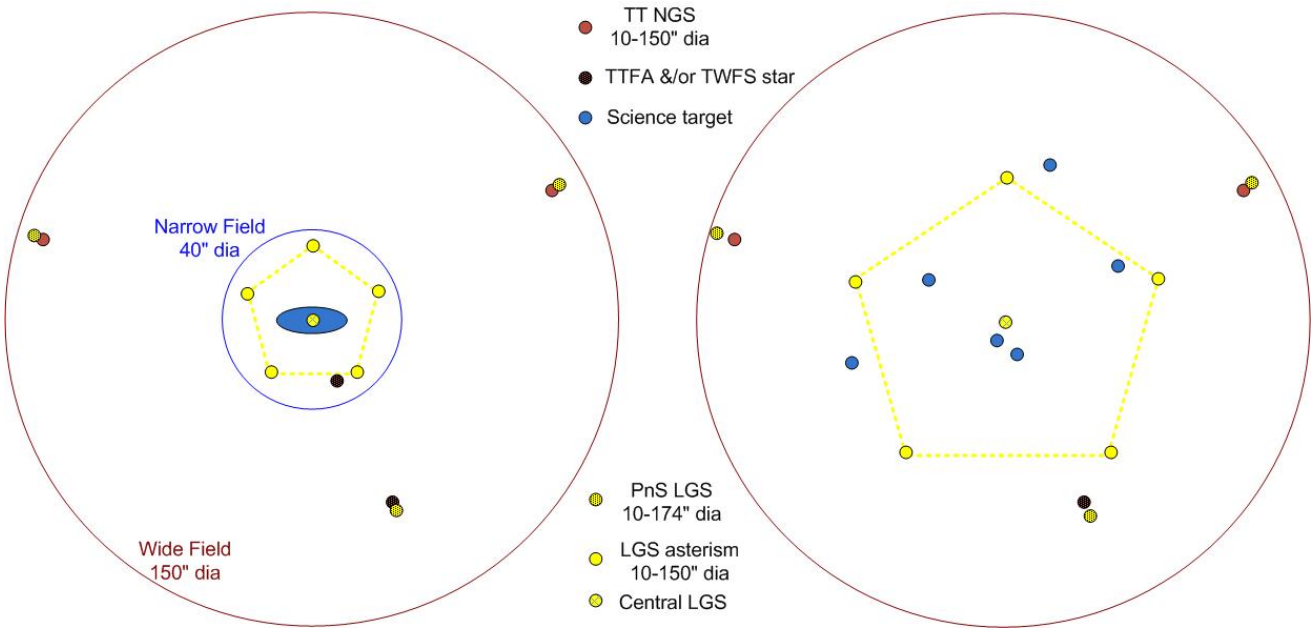

Figure 1. Narrow field (left) and wide field (right) LGS asterisms.

The Solar System and Galactic science cases all require single object observations over modest to narrow fields of view, ranging from 2" to 30". This single line of sight could be AO corrected using

a single deformable mirror (DM). However, many of the extragalactic science cases require multi-object, spatially resolved spectroscopic observations; using a number of small (1" x 3") AO corrected fields selected within a larger "field of regard". In addition, based on a combination of limiting magnitude and off axis distance for natural tip-tilt stars, an object selection mechanism is required for these stars, and such a mechanism could operate in a very similar way to the object selection mechanism (OSM) for the multi-object d-IFS. A block diagram of the AO system architecture that we have selected to deliver both high Strehl and access to multiple objects over a wide field is shown in Figure 2. We refer to this design as the "cascaded relay" because it uses two AO relays in series.

Starting at the lower left hand side of the figure, an environmental enclosure is provided to house lasers generating a total of ~150 watts in a CW format (or a pulse format with comparable sodium layer return flux). The output from these lasers is transferred (via fibers or a free space beam transfer system) to a multiple beam pattern generator and controller located at the top end of the telescope. The output of this beam pattern generator is projected onto the mesospheric sodium layer by a laser launch telescope located behind the telescope secondary mirror as shown just to the left of center in Figure 2.

Light collected by the Keck telescope is directed to the AO system shown in the lower right in Figure 2. The AO system and instruments are located on the telescope's left Nasmyth platform at the f/15 focus. The AO system is enclosed in an enclosure cooled to about -15C below ambient (~260 K) to reduce the thermal emissivity of the optical surfaces. A window is provided to isolate the enclosure from the dome environment.

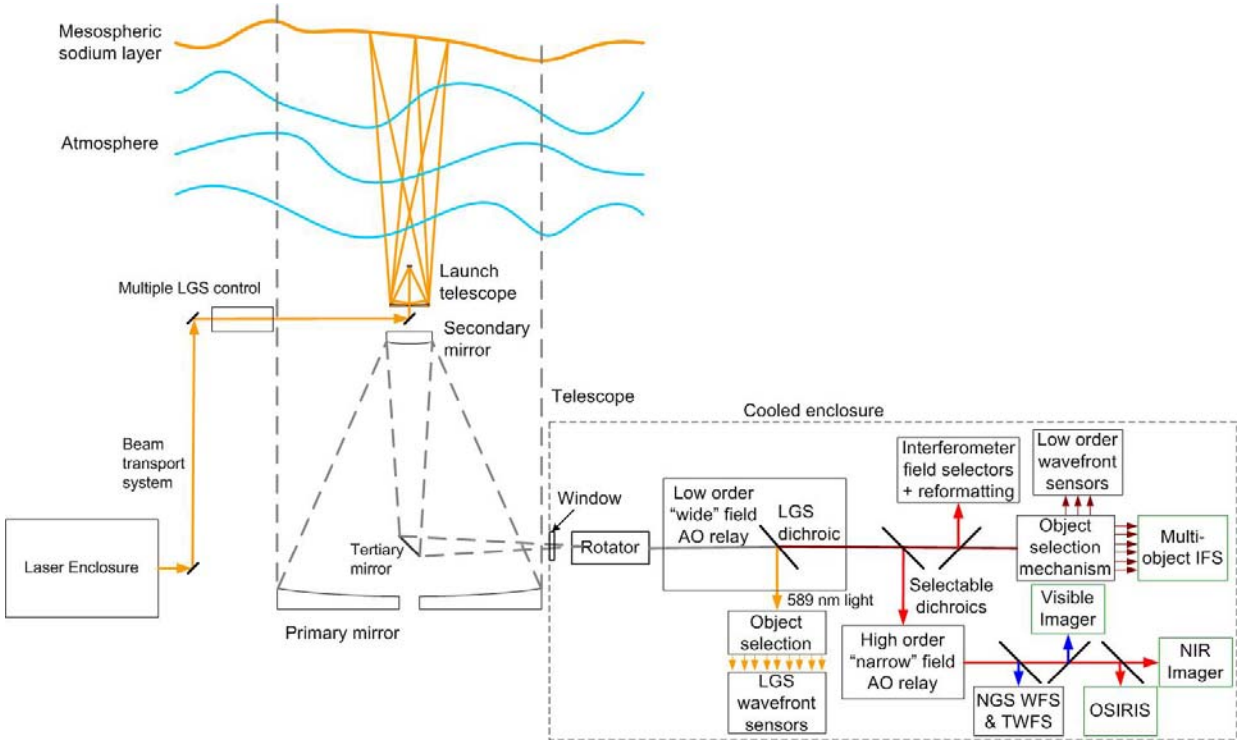

Figure 2. NGAO Block Diagram

Within the cooled enclosure, the light from the telescope passes through an image de-rotator. A "moderate" field low order AO relay incorporating a single DM provides low order AO correction (where low order refers to the order of AO correction provided by the existing Keck AO systems). This DM operates in a closed loop in conjunction with the LGS wavefront sensors. Just after the DM, a dichroic beamsplitter is used to send the 589 nm light from the constellation of LGS to the LGS wavefront sensor assembly, which includes an object selection mechanism. In the absence of a selectable dichroic the light from the low order relay is then transmitted directly to the object selection mechanism for the d-IFS and the low order wavefront sensors (i.e., the NIR TT and TTFA sensors and a NIR truth wavefront sensor (TWFS)). A fold mirror or dichroic can be inserted to feed light to the Keck interferometer.

To use the "narrow" field science instruments a selectable dichroic is inserted to send the light through a "narrow" field high order AO relay. High order refers to three times the DM actuator spacing of the low order DM. This relay provides AO corrected light to a visible light NGS wavefront sensor and TWFS assembly, and three science instruments.

For NGS AO observations only the NGS WFS is required. For LGS AO observations, the LGS wavefront sensors, three tip-tilt sensors and one of the TWFS are required.

The following is a brief summary of the key architectural features of NGAO and why they were selected (i.e., flowed down from the science requirements):

- Laser tomography to measure wavefronts and overcome the cone effect.
- A variable radius LGS asterism to maximize the performance for each science field and changing atmospheric turbulence profiles.
- LGS projection from behind the telescope secondary mirror to minimize perspective elongation.
- Location of the AO system on one of the Keck telescope Nasmyth platforms to have sufficient space for the AO system and science instruments in a gravity constant environment.
- A cooled AO system to meet the infrared background requirements. Alternate approaches such as an adaptive secondary mirror were considered.
- A K-mirror rotator at the input to the AO system to keep either the field or pupil fixed. The AO system would need to be cooled even without a rotator and this approach allows the most stability for the AO system and instruments.
- A wide-field (150" diameter) relay to feed light to the LGS wavefront sensors, tip-tilt sensors, and d-IFS science instrument.
- A conventional (5 mm pitch) DM was chosen to transmit a wide field in the wide-field relay.
- A low-order (20 actuators across the pupil) DM was chosen for the wide-field relay to limit the size of the relay, to permit closed loop AO correction on the LGS wavefront sensors and to keep the LGS wavefront sensors in their linear range, reducing the requirement on downstream open loop correction.
- Open loop MOAO-corrected near-IR tip-tilt sensors to maximize sky coverage. The MOAO approach (versus MCAO) maximizes the delivered Strehl over narrow fields. The open loop correction applies the result of the tomographic reconstruction to that point in the field. In

principle this is better than closed loop on a single LGS since focus anisoplanatism is also reduced. Near-IR sensing is used since the AO correction will sharpen the NGS image and thereby provide better tip-tilt information. We have determined that two tip-tilt (TT) sensors and one tip-tilt-focus-astigmatism (TTFA) sensor provides the optimum correction.

- Open loop MOAO-corrected d-IFS heads.
- Open loop MOAO-correction to the narrow field science instruments.
- MEMS DMs for the MOAO-correction. These are very compact devices and have been lab demonstrated to accurately go where they are commanded. Small, modest cost 32x32 element MEMS DMs provide the required correction for the tip-tilt sensors and d-IFS heads. A 64x64 element MEMS, similar to that under development for GPI, is needed to provide the required AO correction to the narrow field science instruments.
- A high order, narrow-field (30" diameter) AO relay to feed light to the narrow field science instruments (with a larger, 60" diameter, field to the NGS wavefront sensor). The science instruments fed by this relay only require a narrow-field and the narrow field facilitates the use of a single MEMs DM for all narrow-field instruments. These science instruments include near-IR and visible imagers and OSIRIS.

3.2 Telescope and Facilities

The NGAO systems must utilize and interface to the existing Observatory infrastructure. This infrastructure includes the telescope and related control systems as well as mechanical and electrical services. In some cases this existing infrastructure may need to be modified.

The NGAO design and plan currently assumes implementation on the Keck II telescope, although it would be relatively straightforward to modify the design for implementation on Keck I. The design and plan also assume that the existing Keck II AO and laser systems will be removed from the summit facility to make room for the NGAO system. In addition to providing physical space for the system this will also free up power and cooling capacity, as well as cable wrap space.

3.2.1 Telescope Model

A Solidworks model of the Keck II telescope has been generated in order to clearly define the available space and interfaces for the NGAO system. A perspective view of this model is shown in Figure 3, with a possible AO enclosure on the left Nasmyth platform. This tool can be used to provide the details of areas like the Nasmyth platform or secondary mirror socket, as shown in Figure 4, which the NGAO system will need for interface purposes. The details of this model are suitable for preliminary design. Critical dimensions will need to be field verified before detailed design.

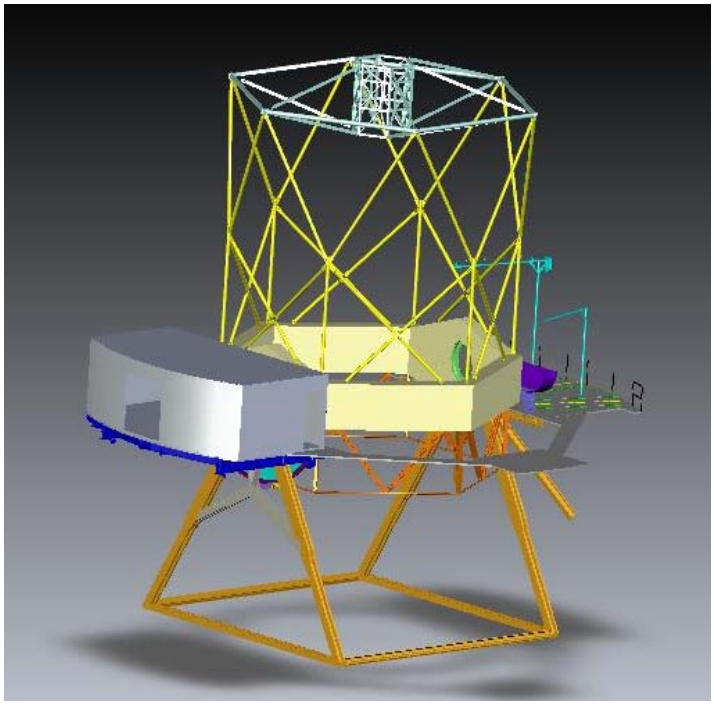

Figure 3. Telescope Solidworks model.

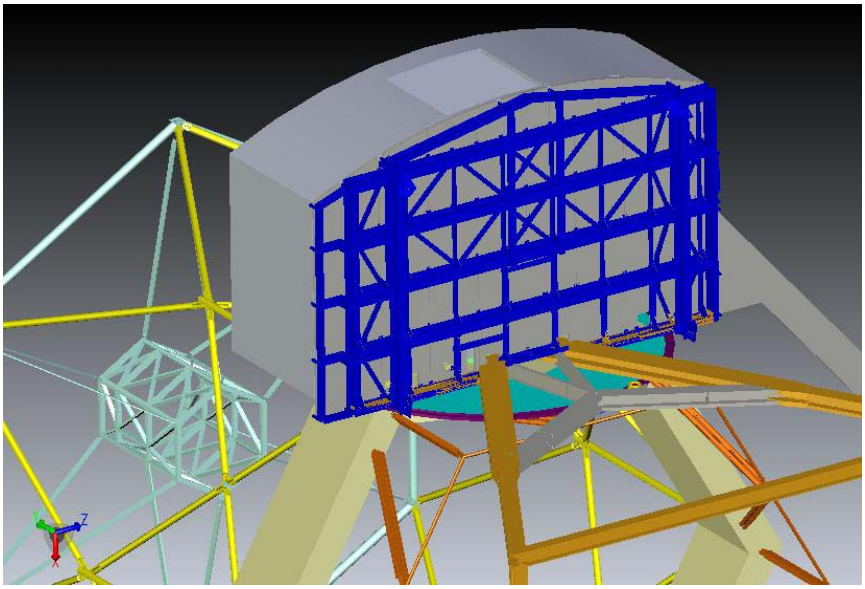

Figure 4. View from below of the telescope Nasmyth platform.

3.2.2 Facilities

The total required facility power and cooling is TBD, but several elements of these requirements have had some initial determination.

3.2.3 Interfaces

The AO system must interface to the existing telescope Drive and Control System (DCS); for example, to offload pointing and focus corrections or to request a telescope move.

3.3 AO System Description

3.3.1 AO Opto-Mechanical Design

The opto-mechanical design for the cascaded relay (see KAON 549) is summarized in this section. The AO bench, as modeled in Solidworks, is shown in Figure 5 and Figure 6. These Figures include the d-IFS, visible imager and IR imager science instruments as well as a fold to OSIRIS (the interferometer feed cannot be seen in these views). They also include the wavefront sensors and acquisition cameras. For comparison, the current Keck AO benches extend 2.4 m from the bulkhead shown in Figure 3. The final dimensions of the bench are TBD and may need to be extended to support the LGS WFS and visible imager.

The optical design, as modeled in Zemax, is shown in Figure 7. In order to follow this design it is easiest to step through the pieces beginning with the rotator and first relay. We discuss all the systems fed by the first relay before proceeding on to the second relay and the systems fed by it. The object selection mechanisms and wavefront sensors opto-mechanics are discussed in section 3.3.2.

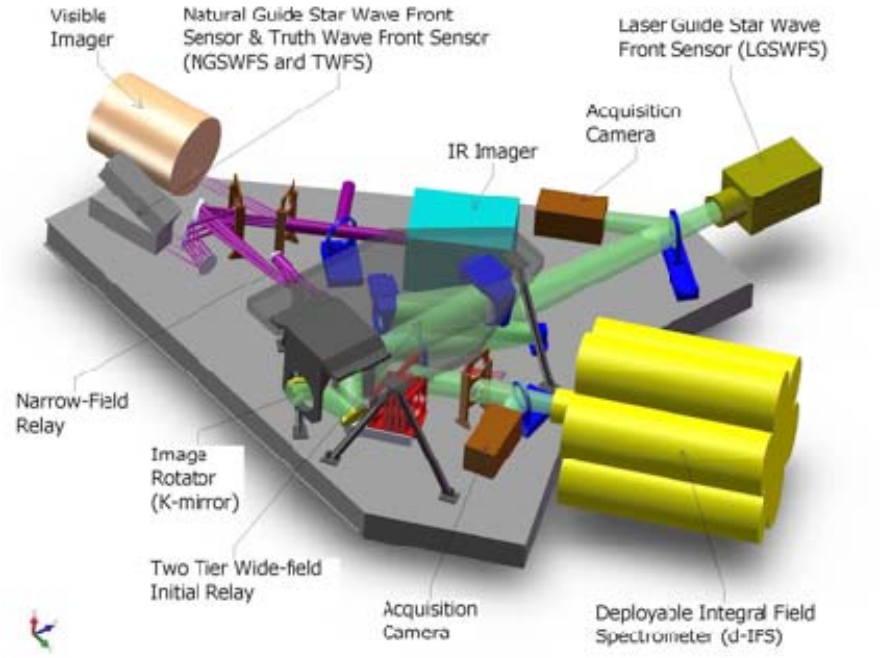

Figure 5. AO system optical layout perspective view (SolidWorks).
The optical path through the low order "wide" field relay and the high order "narrow" field relay are shown in green and purple, respectively. Light from the telescope enters through the image rotator.

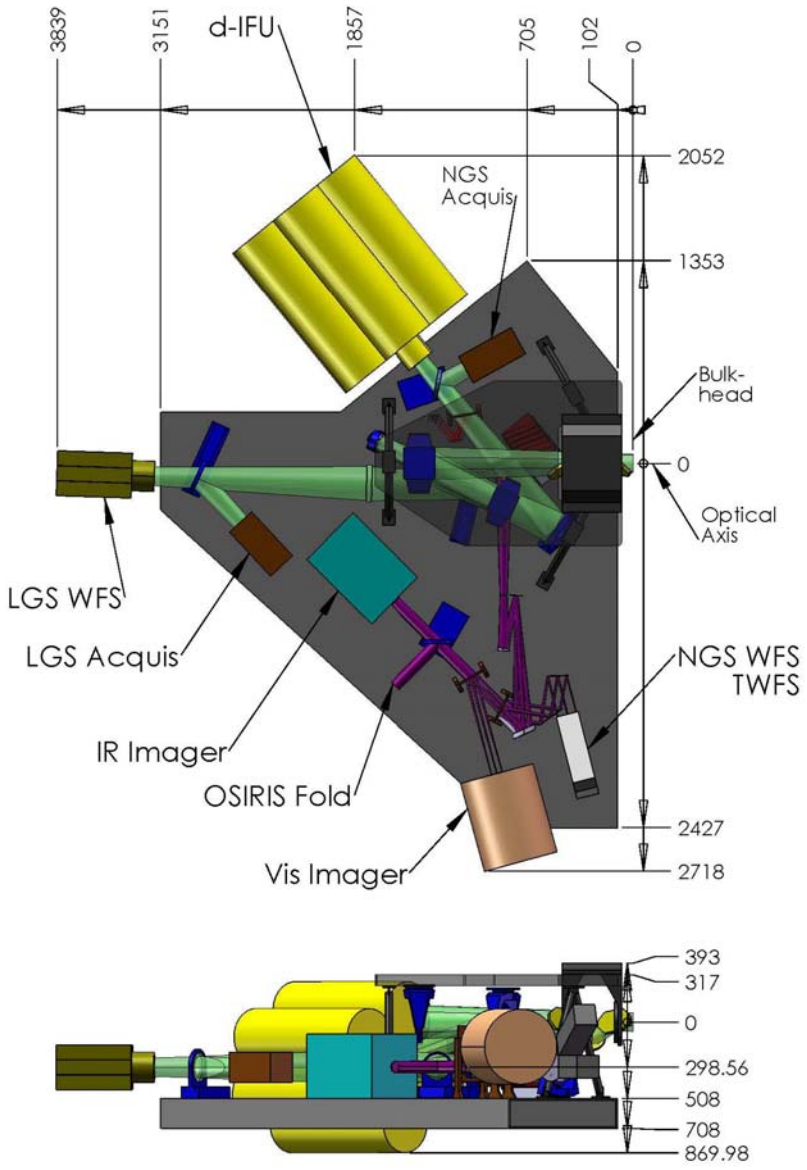

Figure 6. Elevation and plan views of the AO bench, including general dimensions (mm). *Light from the telescope enters from the right along the optical axis.*

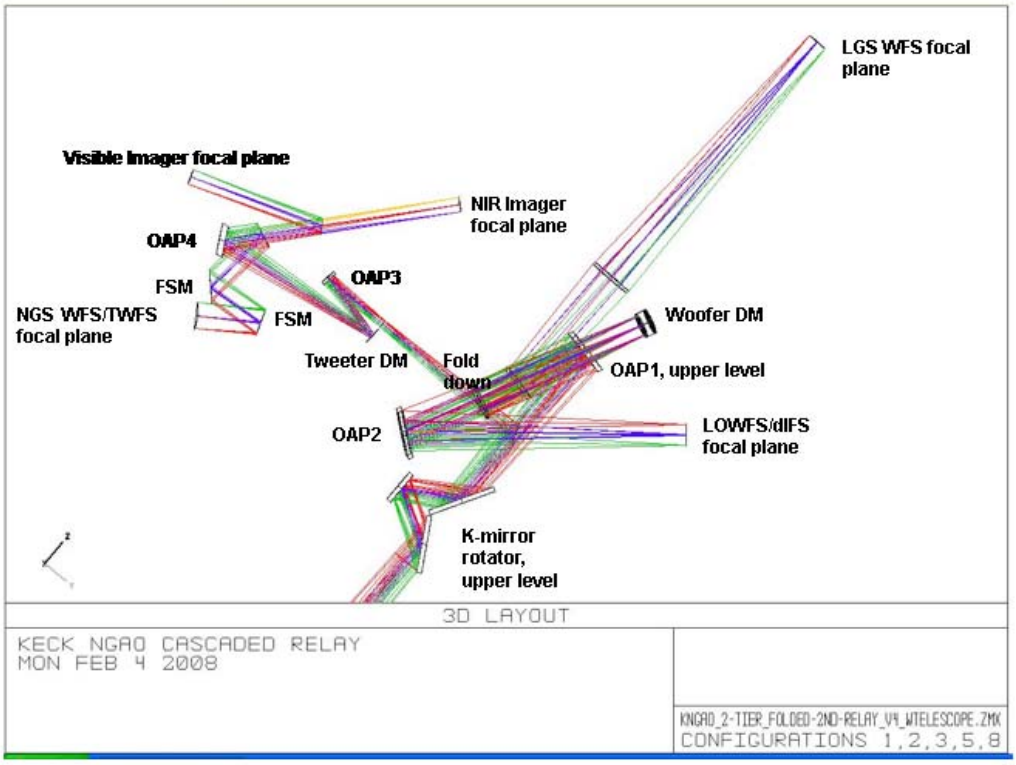

Figure 7. AO system optical layout (Zemax).
Light from the telescope enters from the bottom through the rotator.

3.3.1.1 Rotator and Wide Field Relay

The rotator and first relay are shown in shown in Figure 8. The rotator and first relay are intended to pass a wide field for the LGS and NGS and for the d-IFS science field. The relay includes a DM to provide low order wavefront correction.

The rotator is a K-mirror that can be used to either keep the field or pupil fixed. The Keck telescope's f/15 Nasmyth focal plane is located ~270 mm past the telescope's elevation bearing. The first and second rotator mirrors are located 150 mm before and after the focus, respectively. It is still to be determined to what degree having a focal plane close to these two mirrors will add thermal background effects or performance issues and how it would impact the high-contract science goals (for reference the first mirror of the existing Keck AO rotator is located 110 mm after the telescope focus). The 3-mirror rotator is sized to accommodate a 150" diameter NGS field of view (FOV) and a 175" diameter LGS FOV (for the case of an LGS at 80 km). The first and third mirrors are at 60º angles of incidence while the second mirror lies parallel to the rotation axis of the K-mirror with an incidence angle of 30º.

The first relay is a one-to-one relay consisting of an off-axis parabola (OAP) to collimate the light and reimage the primary mirror onto the DM, a flat fold mirror, the DM and a second identical OAP to converge the light with the same focal ratio as the telescope and a telecentric pupil.

The third order optical aberrations can be minimized by two approaches using a collimated beam between two identical OAPs. Of these the off-centered pupil approach was chosen since it maintains a non-tilted focal plane (Korsch, Reflective Optics, p. 171, 1991).

The focal length of the OAP was selected to map the primary mirror to a 5 mm (d_{DM}) pitch DM with 20x20 actuators. The OAP off-axis angle of 25º was chosen as the minimum angle to provide adequate space for the subsequent optics.

The rotator, OAP1 and a flat, fold mirror are all mounted to an upper tier that sits above the AO bench. The fold mirror on the upper tier and the DM on the AO bench form a periscope that changes the beam height. On both tiers the beam is parallel to the surface of the AO bench, with the beam on the upper tier ~ 300 mm above the beam on the AO bench. The two-tier approach was chosen for packaging reasons. The angle of incidence on both the fold mirror and the DM is 9.125º. This fold mirror offers the possibility of a future multi-conjugate AO option since it is conjugate to an altitude of ~9 km.

The DM is placed at a conjugate to the primary mirror and is mounted on a fast tip-tilt mount. The second OAP is located its focal length from the DM in order to project the pupil to infinity and hence a telecentric output beam.

The output of the first relay goes directly to the object selection mechanism (OSM) that feeds the d-IFS and low order wavefront sensors (LOWFS). Dichroics and fold mirrors can be inserted into this beam to feed the NGS acquisition camera, the interferometer and the second “narrow” field relay.

Some key design numbers:

- Telescope parameters (from KOTN 163 or KAON 107).
  - Telescope focal length, f_{Tel} = 149.583 m.
  - Telescope entrance pupil diameter D_{Tel} = 10.949 m
  - Telescope exit pupil diameter, D_{EP} = 1460 mm.
  - Distance from telescope exit pupil to focus, t_{EP} = 19948 mm.
  - Telescope f/#$_{Tel}$ = f_{Tel}/D_{Tel} = 13.66.
  - Telescope plate scale, PS = 0.727 mm/".
- Chosen design parameters.
  - NGS field of view diameter, Φ_{NGS} = 150".
  - Telescope primary mirror subaperture size, d_{PM} = 562.5 mm (the same as for the existing Keck AO system).
  - Rotator mirror angles of incidence are 60º for mirrors 1 and 3, and 30º for mirror 2.
  - OAP1 and OAP2 off-axis angle = 25º (corresponding to a decenter of 605 mm from the parent parabola) to provide adequate space for subsequent optics.
  - Fold mirror distance from OAP1, t_{fold} = 650 mm.

- Fold mirror and DM angles of incidence are $\alpha_{DM} = \alpha_{Fold}$ =9.125º.
- DM conjugate to the telescope primary mirror.
- DM subaperture size, d_{DM} = 5 mm.
- Output pupil from 1st relay at infinity.

- 1st order calculated parameters.
  - LGS field of view diameter, Φ_{LGS} = 175" (for the case of an LGS at 80 km).
  - OAP focal length, $f_{OAP} = (d_{DM}/d_{PM})\, f_{Tel}$ = 1329.6 mm
  - Required OAP diameter to accept the pupil and field, $d_{OAP} = (f_{OAP}/t_{EP})d_{EP} + (f_{OAP}+t_{EP})\Phi_{NGS}*PS/t_{EP}$ = 214 mm.
  - Fold mirror conjugate height, $h_{fold} = -1/\{[f_{Tel}+f_{OAP}+(1/t_{fold}-1/f_{OAP})^{-1}]^{-1} - 1/f_{Tel}\}$ = 8.75 km.
  - Distance of DM from OAP1 in order to be conjugate to the primary, $t_{DM} = [1/f_{OAP} - 1/(t_{EP}+f_{OAP})]^{-1}$ = 1418 mm.
  - Pupil distortion on the DM due to the angle of incidence, % distortion = $[1-\cos(\alpha_{DM})]*100\%$ = 1.3%.
  - Distance of OAP2 from the DM in order to project the pupil to infinity, $t_{OAP2} = f_{OAP}$ = 1329.6 mm.

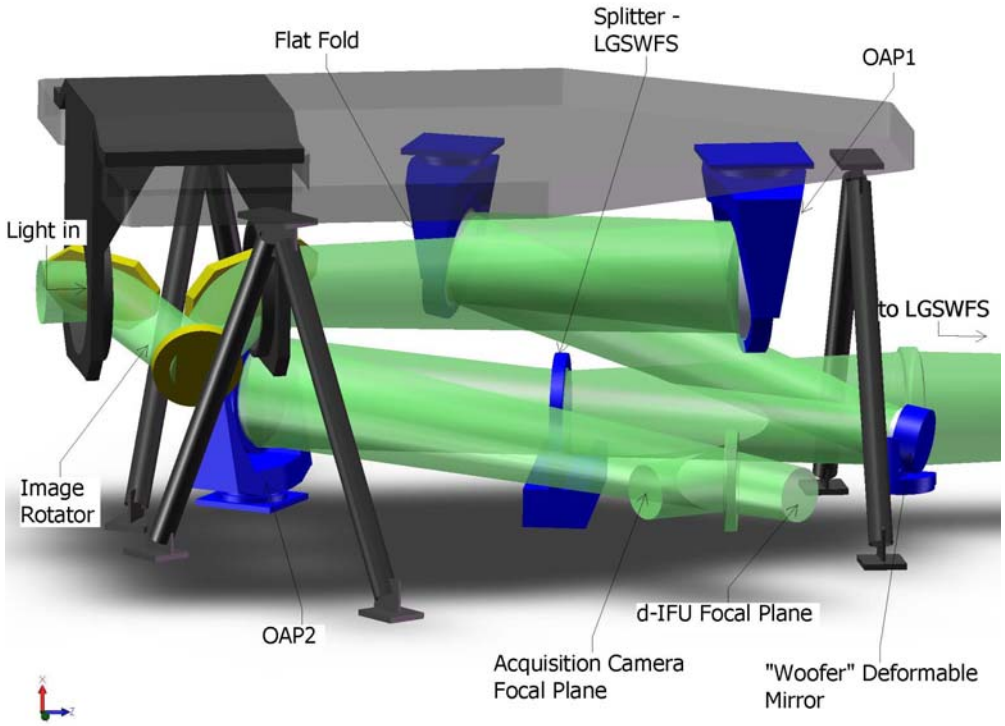

Figure 8. The image rotator and low order "wide" field relay.
Light from the telescope enters from the left and travels through the rotator to OAP1, the flat fold, the "woofer" DM. A dichroic splitter reflects the 589 nm light to the LGS WFS and transmits the remainder of the light to OAP2. A retractable mirror to feed the NGS acquisition camera is shown just before the focus.

3.3.1.2 LGS Wavefront Sensor Assembly and LGS Acquisition Camera Pickoff

A sodium reflective dichroic (i.e., retractable LGS WFS pickoff) is inserted in the collimated beam between the DM and OAP2 to send the sodium wavelength light to the LGS wavefront sensor as shown in Figure 6. A bi-convex lens is used to play the role of OAP2 and converge the light to the LGS WFS assembly. The lens' focal length and distance from the DM are the same as those for OAP2 in order to minimize aberrations and project the pupil to infinity. A retractable mirror (i.e., retractable acquisition camera pickoff) can be inserted to send light to an LGS acquisition camera (we are currently not planning to have a separate LGS acquisition camera). Both the acquisition camera and LGS WFS must translate in focus to be conjugate to the sodium layer.

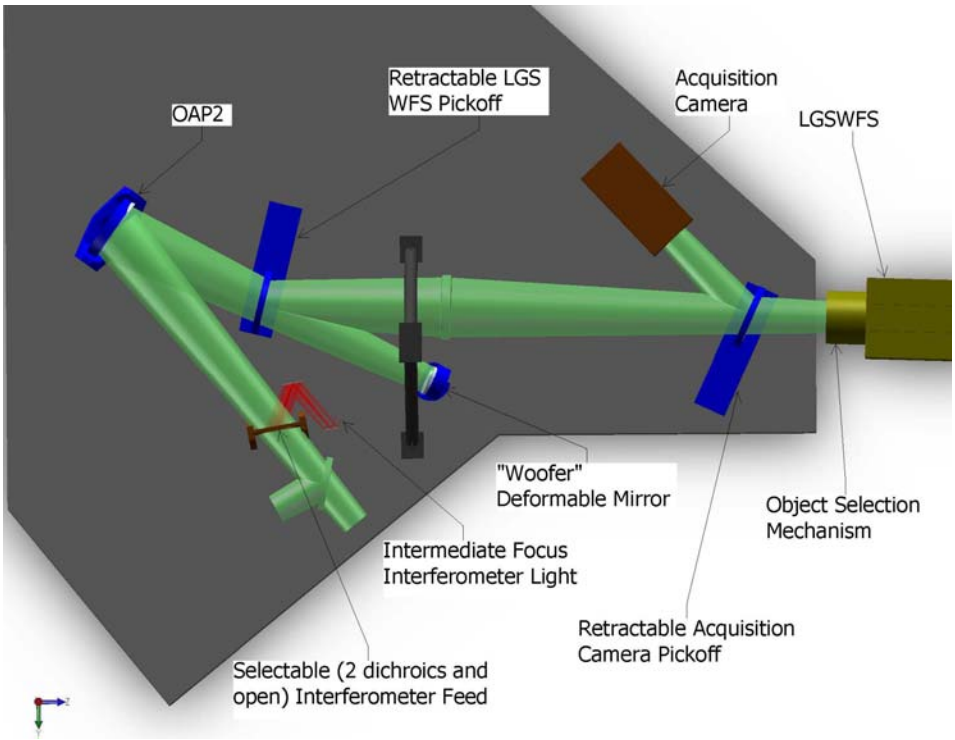

Figure 9. Laser Guide Star Wavefront Sensor and Interferometer Pickoffs.

The LGS WFS assembly consists of an Object Selection Mechanism (OSM) and nine LGS WFS. Each arm of the OSM picks up the light from a single LGS and transports this light to a single LGS WFS.

3.3.1.3 Interferometer Pickoff

Figure 6 also shows a dichroic pickoff to the Keck interferometer. This is located after the narrow field pick-off in order to most closely match the existing Keck AO system where the future interferometer pick-off is located after an IR transmissive dichroic.

The dichroic sends a 60" diameter field to a pair of field selector mirrors. The first of these mirrors is located near the focus and has a hole in it to transmit a small on-axis field. The first field selector steers the desired off-axis point to the center of the second field selector mirror, which in turn steers the off-axis field along the desired axis (parallel to the on-axis field). Similar field steering mirrors are used in the existing Keck AO system and this approach has been selected for the ASTRA upgrade to the Interferometer (ASTRA-0017).

Two options are being considered for transporting the interferometer beam to the basement. The first is to use a dual star module where OAPs are used to collimate the light and fold mirrors are used to steer the beam to the existing coude train. The second and preferred option is to insert both the on-axis and off-axis objects into single mode fibers for transport to the basement.

3.3.1.4 Acquisition Camera and Pickoff

A removable 45º incidence angle mirror folds the entire 150" diameter wide field relay output to the acquisition camera. We have determined (KAON 567 and section 3.6.2.4) that a visible camera is adequate (versus a NIR camera) and that this camera can therefore be used for both NGS and LGS acquisition. The camera will need to be on a focus translation stage to go between the NGS and LGS foci as is done with the acquisition camera for the current Keck AO system. A simple focal reducer can be used to obtain the required plate scale on the new Keck standard MAGIQ acquisition camera.

3.3.1.5 Low Order Wavefront Sensor Assembly

The light reflected by OAP2 goes directly to the NIR imager (in the absence of any fold mirrors or dichroics between OAP2 and the d-IFS). The Low Order Wavefront Sensor (LOWFS) Assembly is located directly in front of the d-IFS and consists of an Object Selection Mechanism (OSM) and four LOWFS. Two arms of the OSM feed tip-tilt (TT) sensors. A third arm feeds a tip-tilt-focus-astigmatism (TTFA) sensor and truth wavefront sensor (TWFS). A beamsplitter splits the light between the TTFA and TWFS.

3.3.1.6 Narrow Field Relay

A choice of several dichroics can be inserted in the beam between OAP2 and the d-IFS in order to send light into the narrow field relay as shown in Figure 10. This relay is intended to provide a high order of correction for the narrow field science instruments. It also provides a magnification of ~3 in order to provide separation between the instruments and an optimal plate scale for the science instruments.

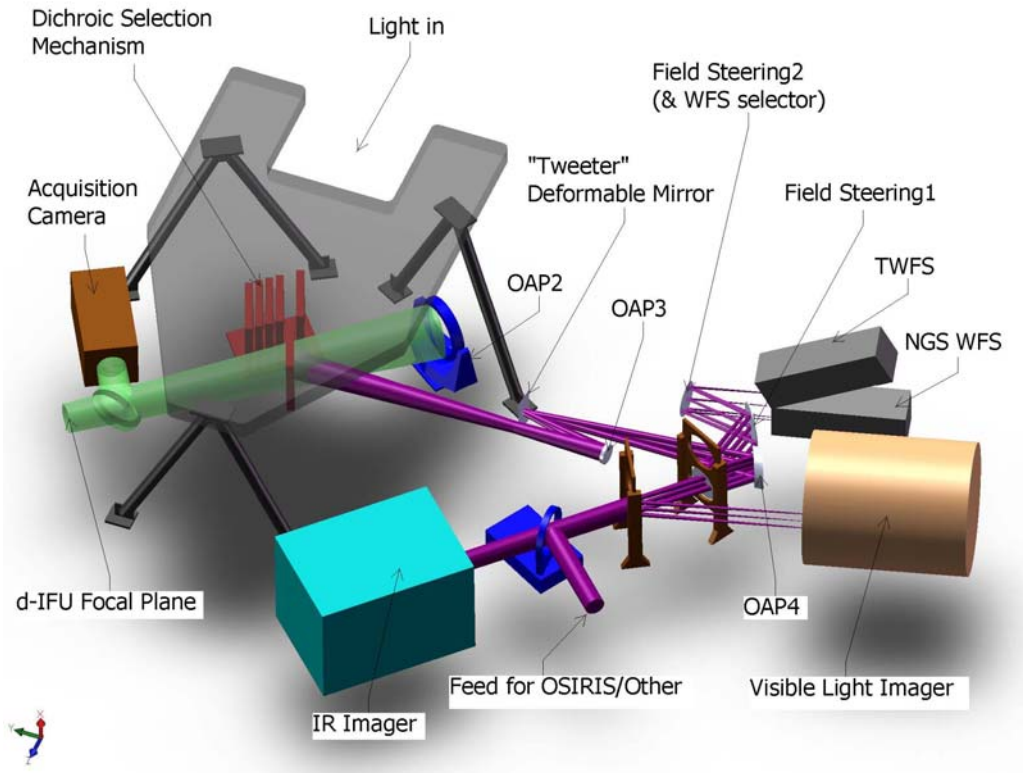

Figure 10. Narrow Field Relay.

The light reflected by the dichroic passes through focus to OAP3 which collimates the light and reimages the telescope primary mirror onto a 64x64 MEMS DM. The DM is mounted on a fast tip-tilt platform. OAP4 is chosen to provide a factor of three magnification and is located its focal length from the MEMS in order to project the pupil to infinity.

- Chosen design parameters.
  - NGS field of view diameter, $\Phi_{NGS,narrow}$ = 60" for NGS WFS and 30" for science instruments.
  - OAP3 off-axis angle = 13º.
  - Telescope primary mirror subaperture size, d_{PM2} = 176.0 mm.
  - MEMS angle of incidence, α_{MEMS} = 10º.
  - MEMS conjugate to the telescope primary mirror.
  - MEMS subaperture size, d_{MEMS} = 0.40 mm.
  - 3x magnification (f/15 input becomes f/45 out).
  - OAP4 off-axis angle = 43º.
  - Output pupil from 2nd relay at infinity.
- 1st order calculated parameters.
  - OAP focal length, $f_{OAP3} = (d_{MEMS}/d_{PM2})\ f_{Tel}$ = 340.0 mm
  - Required OAP3 diameter to accept the pupil and field, $d_{OAP3} = f_{OAP3}/f/\#_{Tel} + \Phi_{NGS,narrow}$*PS = 69 mm.
  - Distance of MEMS from OAP3 in order to be conjugate to the primary, $t_{DM} = f_{OAP3}$.

- Pupil distortion on the DM due to the angle of incidence, % distortion = [1–$\cos(\alpha_{MEMS})$]*100% = 1.5%.
- Focal length of OAP4 for a 3x magnification, $f_{OAP4} = 3f_{OAP3}$ = 1020 mm.
- Distance of OAP4 from the DM in order to project the pupil to infinity, $t_{OAP4} = f_{OAP4}$.
- Required OAP4 diameter to accept the pupil and field, $d_{OAP4} = f_{OAP3}/f/\#_{Tel} + \Phi_{NGS,narrow}$*3PS = 134 mm.

3.3.1.7 Natural Guide Star and Truth Wavefront Sensors Pickoff

The dichroic pickoff immediately following OAP4 feeds both the NGS WFS and TWFS. The dichroic is at an angle of incidence of 17º. The nominal 30" diameter field required for the science instruments was deemed to be scientifically inadequate for the NGS WFS and TWFS. The current design has a slightly offset field that extends 57" perpendicular to the bench and 54" parallel to the bench due to vignetting by the tweeter and OAP4.

A pair of field selector mirrors, similar to those discussed in section 3.3.1.3 will be used. In this case the first mirror will not have a hole in it and the second mirror is mounted on a two position rotation stage in order to provide light to one of either the NGS WFS or TWFS.

An alternate location for the NGS WFS and TWFS, in the visible imager path, will likely be implemented during the preliminary design. This location has the advantage of a shared ADC with the visible imager and only one dichroic in the beam to the IR imager when simultaneous NIR and visible observations are being performed in NGS mode.

3.3.1.8 Narrow Field Science Instrument Pickoffs

Three science instruments are fed by the narrow field relay as shown in Figure 10. The light reflected by OAP4 goes directly to the NIR imager (in the absence of any fold mirrors or dichroics between OAP4 and the NIR imager). A dichroic fold can be inserted in this path to feed the visible imager or a fold mirror can be inserted to feed the light toward OSIRIS.

In order to reuse the existing OSIRIS with NGAO, optics must be inserted in the path to convert the beam back to the initial telescope focal ratio with the pupil at the same position as provided by the telescope. This design is TBD, however similar reimaging optics were designed to use NIRSPEC with the existing AO system (KAON 201). This design consisted of two spherical mirrors and two flat mirrors and provided a magnification of 10.6 (versus only 3 in demagnification required in this case).

The interfaces to the instruments are defined in KAON 555.

3.3.1.9 Summary of Required Dichroics and Mirrors

The above sections only described the location of the required pickoffs. Table 1 provides a summary of the required dichroics and mirrors and their properties. The numbers in the NGS and LGS

columns refer to the system configurations that will be discussed in a later section. The LGS acquisition camera and fold are not required due to our decision to use a single visible wavelength acquisition camera for both NGS and LGS acquisition.

Table 1. Summary of Required Dichroics and Mirrors.

Dichroic or Fold	#	Options	NGS	LGS	Transmit	Reflect	R (extra)	Notes
	1	Out	All		All	None		Notch filter ideal. ≥
LGS dichroic	2	In		All	0.4-L	589 nm		600nm an option
LGS Acquis	1	Out	n/a	1-6	All	None		
Fold	2	Mirror	n/a	11	None	589 nm		
	1	IR transmit / vis reflect	2,3	5	JH	≤ 1 µm	K	
	2	Mirror	4-8		None	All		
	3	Out		1-3	All	None		
	4	JH transmit / K reflect		4ab, 6ab	JH	K	≤ 1 µm	Address with #1 (if can do R (extra))
	5	J transmit / H reflect		4cd, 6cd	J	HK	≤ 1 µm	
	6	H transmit / IJ reflect		4ef, 6ef, 7ef	H	< H	K	
Post Relay 1 Dichroic = Narrow Field Pickoff		JH transmit / IK reflect		7ab				Address with #1 (if can do R (extra))
		J transmit / IH reflect		7cd				Address with #5 (if can do R (extra))
	1	Mirror	2,3		None	All		
	2	Out	10	1,4-6	All	None		
Interfer-ometer Fold	3	J transmit / HKL reflect		2,3	J	HKL		
	1	Out	2,3	1-6	All	None		May need to replace mirror w/ a beamsplitter or to provide a 3rd position
Acquisition Fold	2	Mirror	10	10	None	All		
	1	IR transmit / vis reflect	All	5	Y-K	0.4-0.95µm		
NGS WFS Dichroic	2	I transmit / < I reflect			≥ 0.7 µm	0.4-0.7µm		
	3	Out		4,6	All	None		
	1	IR transmit / vis reflect			≥ 1 µm	0.7-1.0µm		
Visible	2	Out			All	None		
Imager Dichroic	3	Mirror			None	0.7-1.0µm		If #1 good then may not be needed.
	1	Out	4,7	4	All	None		
OSIRIS Fold	2	Mirror	6	6	None	z-K		

3.3.1.10 Atmospheric Dispersion Correctors

The baseline for Keck NGAO has the following Atmospheric Dispersion Corrector (ADC) needs:

1. NIR ADC in the narrow field path to the NIR imager and OSIRIS.

2. Visible ADC in the narrow field path to the visible imager.
3. Visible ADC in the narrow field path to the NGS WFS/TWFS.
4. NIR ADC (J+H) for each LOWFS.
5. NIR ADC for each d-IFS (it is TBD whether this is really required).

ADCs 2 and 3 could potentially be combined if the NGS WFS/TWFS are moved into visible imager path as discussed in section 3.3.1.7.

The atmospheric dispersion corrector (ADC) design has only been taken far enough to demonstrate that suitable ADCs can be designed. During the system design both single glass and two glass linear ADCs were evaluated. In addition there is a two glass counter rotating Amici prism design documented in KAON 134 that was developed for the existing AO system.

3.3.1.11 Optics Bench Structure

The optics bench structure is shown in Figure 11. The upper and lower tiers are both expected to be typical honeycomb core optical tables. The optimal thickness of both tiers will be determined in subsequent design phases. The separation of the two tiers is accomplished with three bipod struts. If necessary, there is clearance to make these tripod struts, allowing kinematic mount detail for the upper tier.

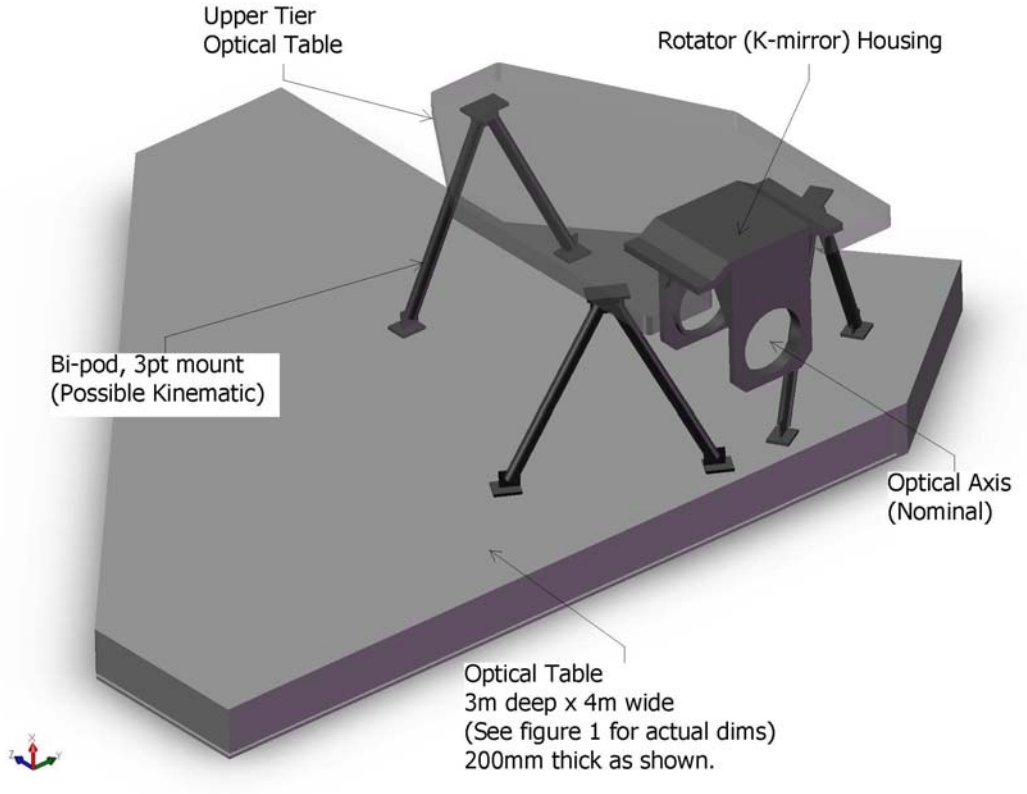

Figure 11. Optics Bench Structure.

Attachment of the optics bench to the Nasmyth platform is TBD, but will likely be similar to the mounting of the existing Keck AO benches. The clearance between the bottom of the bench and the Nasmyth platform is ~ 500 mm less than for the existing AO benches, which will make access under the bench more challenging (than for the existing benches).

3.3.2 Wavefront Sensor Opto-Mechanical Design

Two wavefront sensor assemblies are fed by the wide field optical relay: the LGS wavefront sensor assembly and the low order wavefront sensor (LOWFS) assembly. The NGS and Truth wavefront sensor assembly is fed by the narrow field relay. Each of these assemblies includes an object selection mechanism that selects the appropriate NGS or LGS and feeds the light to the appropriate wavefront sensor(s). Two versions of the same multi-target mechanism have been chosen for the LGS and LOWFS object selection mechanisms, while a different single-object selection approach has been taken for the NGS/Truth wavefront sensor assembly as described in section 3.3.1.7. The LGS wavefront sensor assembly includes nine LGS wavefront sensors. The LOWFS assembly includes four NIR sensors: two tip-tilt sensors, a tip-tilt-focus-astigmatism sensor and a truth wavefront sensor. The NGS/Truth wavefront sensor assembly includes an NGS wavefront sensor and a visible truth wavefront sensor. The conceptual design reports for the multi-target object selection mechanism and all of the wavefront sensors can be found in KAONs 562 and 551, respectively.

The design parameters for the wavefront sensors and detectors are summarized in Table 2 and Table 3.

Table 2. Baseline design parameters for the NGAO wavefront sensors.

WFS type	Location	Sensing wavelength (μm)	Input PS (μm/")	# of sub-apertures	Detector PS ("/pixel)	Filters	Field of regard (")	Object Selection
LGS WFS	in WF relay	0.589	727	16x16 32x32 64x64	1.45	none	174	θφ pickoff
TT	after WF relay	1.16 – 1.33		1x1	0.03	J+H	150	θφ pickoff
TTFA		1.16 – 1.33		2x2	0.03	J+H		shared θφ pickoff
TWFS		1.0-2.4		5x5	0.2	none		
NGS WFS	after NF relay	(0.40- or) 0.60-0.90	2254	32x32 64x64	1.5	none	50	shared field steering mirrors
TWFS		0.4-0.9		5x5	0.65	Na rejection		

Table 3. Required WFS detector characteristics.

Detector	Characteristics	# of units	Comments
CCD	256x256 pixels. RON ≤ 3e- at 2 kHz frame rate & DN ≤ 500 e-/sec @ operating temp.	10	9 LGS WFS + 1 NGS WFS
CCD	240x240 pixels. RON ≤ 3e- at 0.01-200 Hz & DN ≤ 0.001 e-/pix/sec DN	1	NF TWFS
IR detector	240x240 pixels. RON ≤ 7e- at 0.01-200 Hz & DN ≤ 0.001 e-/pix/sec.	1	WF TWFS
IR detector	Small regions. RON ≤ 7e- with 8 Fowler samples & 500 Hz data rate for the entire chip; DN ≤ 0.001 e-/sec @ 73K.	3	2 TT and 1 TTFA sensors

3.3.2.1 Low Order Wavefront Sensor Object Selection Mechanism

A design for an interim Low Order Wavefront Sensor (LOWFS) OSM has been developed in KAON 562. This interim OSM may be implemented prior to the fielding of the d-IFS. A similar OSM may be selected for the d-IFS and the two designs could potentially be integrated into a single OSM.

The LOWFS assembly is located at the focus of the first relay and contains two Tip-Tilt (TT) WFS, one TTFA WFS and one TWFS WFS. The option of a PSF monitor within this assembly is discussed in section 3.3.2.4. The NGAO LOWFS assembly is a critical part of the NGAO system as it provides the required centering accuracy and stability for acquisition and observing modes such as off-chip dithering and non-sidereal tracking.

The LOWFS assembly shown in Figure 12 attaches directly to the AO bench. The assembly can be viewed as two separate entities: the OSM consisting of a stable structural plate that supports the four roaming probe arms and the four beam-fed units located behind the structural plate that are fixed during an observation.

The LOWFS OSM probe arm is a compact 2-motor device shown in Figure 13. The 2 degrees of freedom probe arm consists of 2 individual arms: a crank arm and a lever arm, driven by 2 corresponding rotation motors: the crank and lever motors. The crank motor is secured to the main structural plate. It rotates the crank arm, and all hardware attached to it that includes the lever arm and lever arm motor, precisely about the rotation axis of the crank motor (θ rotation). The lever arm motor provides the necessary second degree of freedom by rotating the lever arm and all associated optics (φ rotation).

The lengths of the crank and lever arms were chosen to provide full coverage of the LOWFS OSM field of view. Any position in the LOWFS OSM field of view can be acquired by calculating appropriate values for θ and φ, noting that due to a mirror reflection there are always two possible solutions. Four basic configurations of the LOWFS OSM probe arms are shown in Figure 14, including (a) the non-LGS observing mode; (b) a probe arm at full range; (c) “home position” where all probe arms are outside the field and (d) a random configuration for LGS mode. The probe arm

tips can be designed to approach very closely; this design allows the positioning of two probe arms on two NGS with only 5" separation.

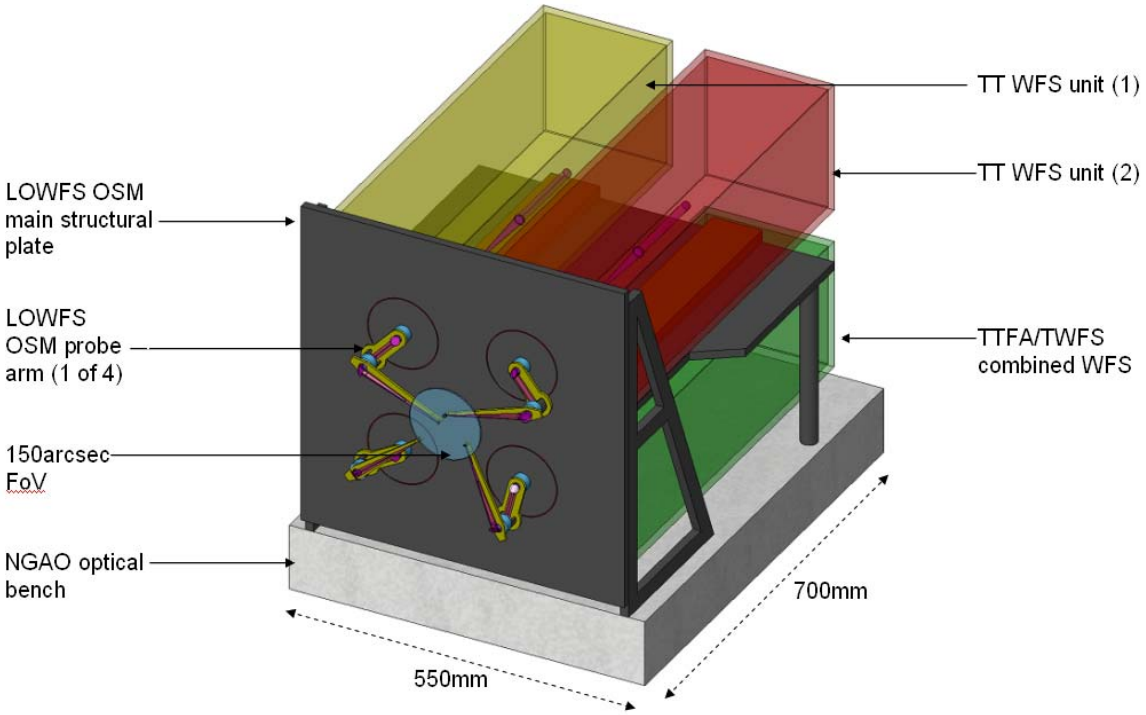

Figure 12. The LOWFS assembly.

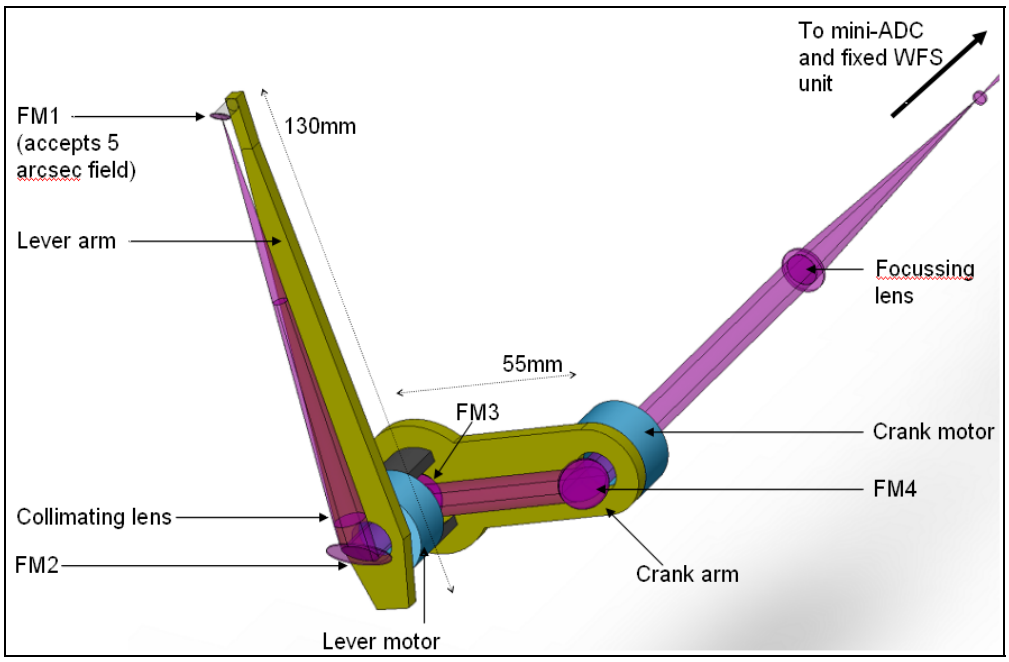

Figure 13. LOWFS OSM probe arm.

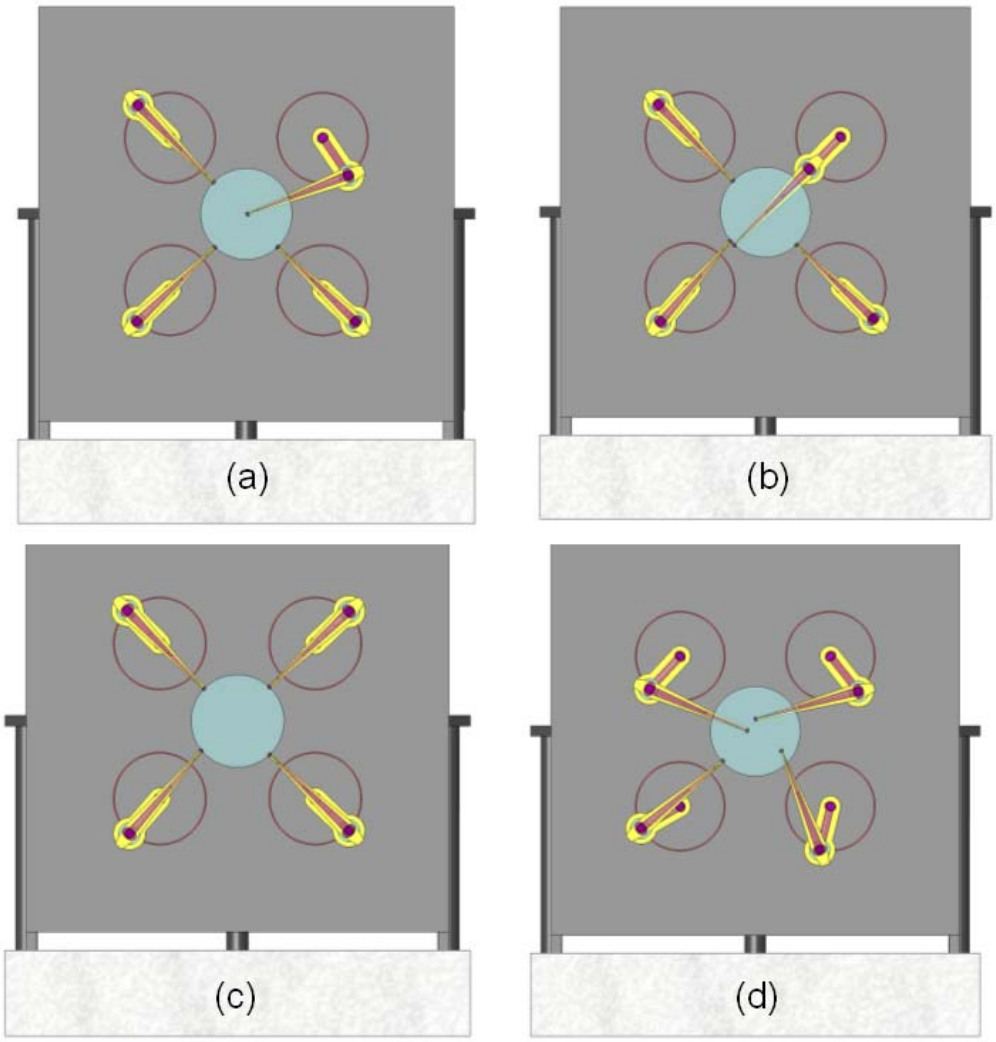

Figure 14. Four configurations of the LOWFS OSM arms.
(a) one TT on-axis with the remaining 3 probes unused; (b) one probe arm fully extended; (c) all probe arms at the home position at the edge of the 150" diameter field; and (d) a random field with all 4 probes in operation.

The telecentric feed from the AO system makes the LOWFS optical design relatively simple. The immediate benefit of this to a focal surface probe arm design is that the probe arms can patrol a *flat* field and not require any tilt of the optics to compensate for changing angle.

The LOWFS OSM focal surface is curved with a radius of -1320 mm. As the probe arm moves from the center to edge of the field, this results in a defocus of approximately 1 mm. The broadening of the beam at the probe arm is negligible however the focus position of the re-imaged star at the WFS unit will change by a corresponding amount. Note that this focus change is a smaller issue than the ~7 mm of focus change when a dichroic is inserted or removed from in front of the LOWFS assembly.

A solution to the focus issue is to position all four LOWFS units on linear slides. The units are moved to the correct focus position at the start of an acquisition procedure and do not need to be tracking devices. An alternative solution is to keep the LOWFS units completely fixed and to place the probe arm focusing lenses on linear stages. This may be preferable and will be evaluated during preliminary design.

Optically the probe arm could be a simple relay, as shown in Figure 15, with a collimator, to produce a pupil, and a focusing lens. The design to incorporate a MEMS DM, and possibly a pupil stop, at the reimaged pupil is TBD.

A 5" diameter field of view was chosen as a reasonable size of field to be large enough to always hit the target, but small enough to allow close positioning of the probe arms. The field can be stopped at the WFS if required. The focal length of the focusing lens will be determined as part of the WFS design.

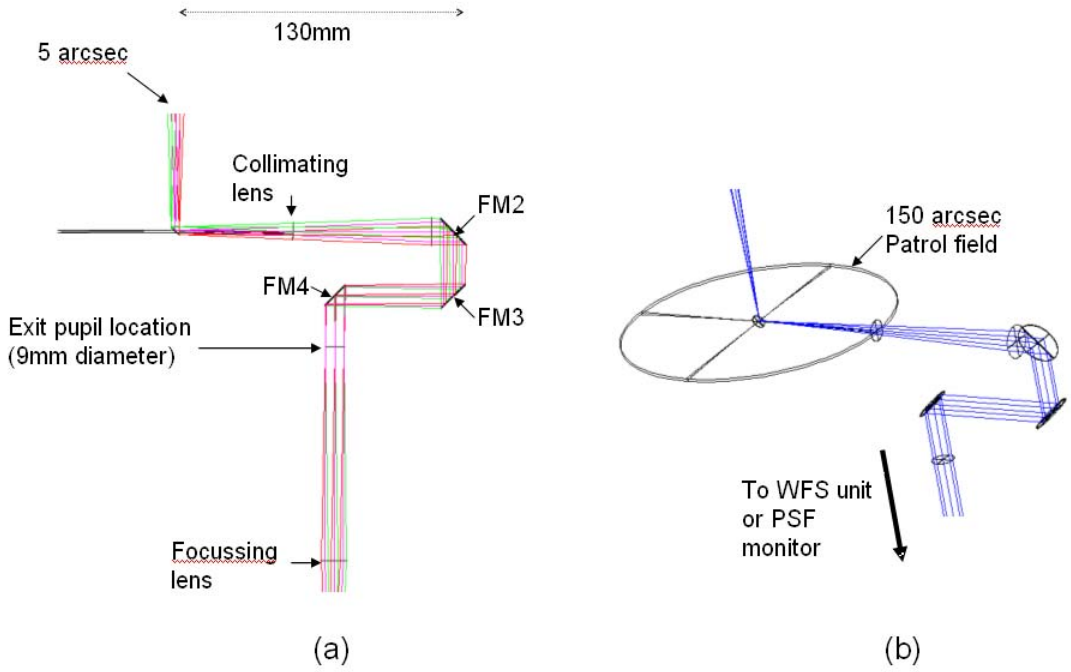

Figure 15. (a) Zemax model of LOWFS probe arm. (b) Probe arm patrol field.

The advantages of a θ/φ probe arm design for this application are:

1. The optical pathlength is naturally and accurately preserved as a function of field position.
2. As only four pick-offs are required one can allow larger mechanisms than otherwise allowed, resulting in readily available off-the-shelf rotary mechanisms using conventional worm gears rather than custom piezo or hybrid devices.
3. The theta/phi arm naturally allows for a fixed feed to the non-tracking WFS unit.
4. The arms can be balanced about the center of mass for each arm if this is needed for fine positioning.

There are two disadvantages of a theta/phi mechanism:

1. The pupil rotates as a function of field position, by ±180°. This creates a varying rotation of the woofer DM with respect to the DM and lenslet arrays inside the TTFA and TWFS unit. The TT and PSF monitor units contain no lenslet arrays and the effect can be calibrated in software. A solution to this is to include an extra non-tracking rotation mechanism in the WFS unit that rotates the entire unit about the z axis as a function of field position. However, the low order nature of the TTFA and TWFS units is most likely sufficient that this mechanism is not required in the LOWFS assembly, and we therefore propose the effect to be calibrated in software.
2. In general, linear motors are more accurate than rotary.

3.3.2.2 Tip-Tilt (Focus and Astigmatism) Sensors

The three Low Order Wavefront Sensors (LOWFS) operate at near-IR wavelengths to improve the availability of suitable stars of sufficient brightness. Optimal performance is obtained using combined J and H band light, but a selectable beam splitting dichroic will allow sending one or more near-IR bands in combination to the tip-tilt sensors with the remainder of the near-IR and the visible light passing to the narrow field instruments. At least one sensor will be of at least order 2 x 2 subapertures to provide sensing of focus and astigmatism as shown schematically in Figure 16. Each tip-tilt star will be AO corrected using a MEMS DM with a pointable LGS beacon positioned near each tip-tilt star to maximize this correction.

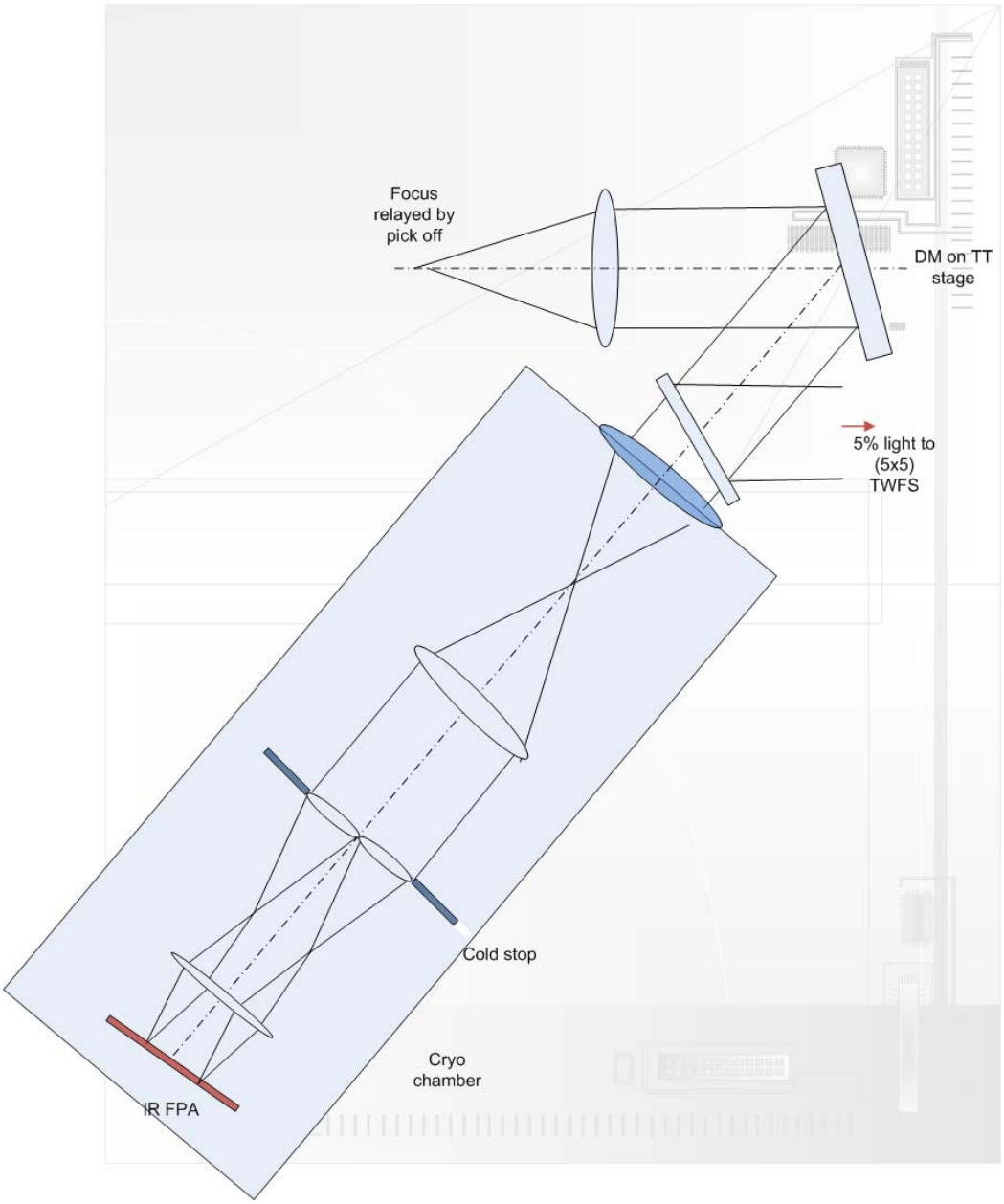

Figure 16. Tip, tilt, focus and astigmatism (TTFA) sensor schematic.

3.3.2.3 Truth Wavefront Sensors

The Truth Wavefront Sensors (TWFS) are used to calibrate biases that arise when using LGS in an AO system; we refer to this as the Low Bandwidth Wavefront Sensor in the existing Keck AO system. The biases are principally caused by the elongated nature of the LGS when viewed by sub-apertures of the LGS wavefront sensor and the changing sodium layer density profile. The truth wavefront sensor measures these biases by sensing the wavefront from a NGS. These biases are

slowly varying and are of a low spatial order. So, a NGS WFS using long exposures and only measuring the lowest spatial wavefront error is sufficient.

The truth sensor has been estimated to be a 5x5 sensor (Figure 17) with detailed error budgets for the same still in the works. The baseline design will have two truth sensors as these sensors are to be placed as close as possible to the science instrument. The wide field TWFS sensor will be a NIR sensor while the narrow field TWFS is conceptualized to be a visible sensor. The wide field TWFS will be used for d-IFS science while the narrow field TWFS will be used for all narrow field LGS science.

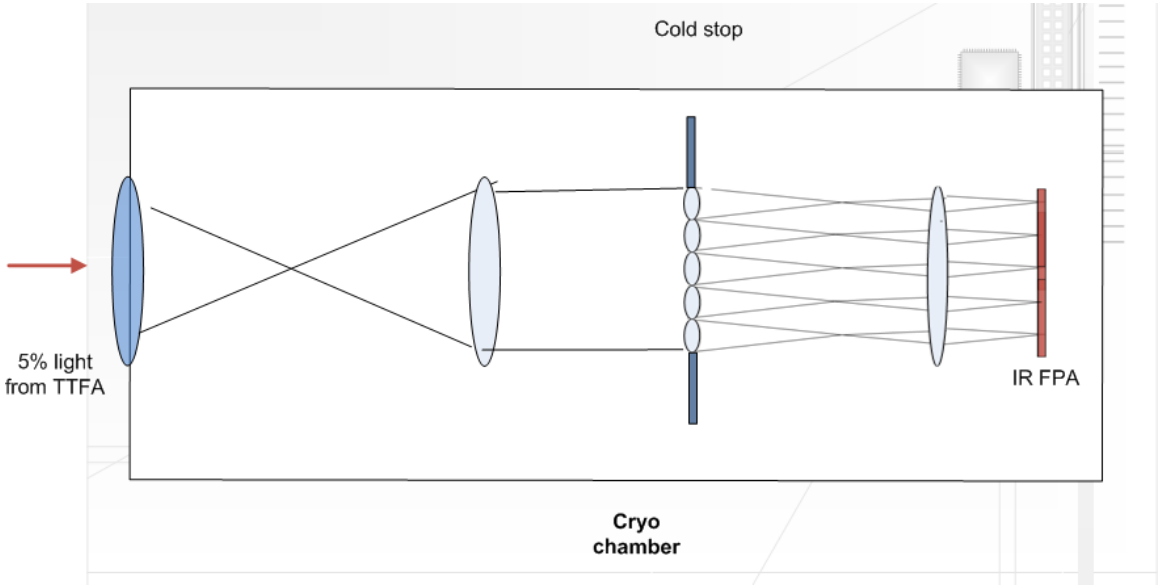

Figure 17. Wide field truth wavefront sensor (TWFS) schematic.

The wide field TWFS will share ~5% of the light to the TTFA sensor. The plate scale for this TWFS is the same as the TT sensors (0.2"/pixel). The Strehls are ~20% in H-band and 10% in J-band; well within the range to be able to sense TT on the core of the PSF.

The visible TWFS plate scale was chosen based on a median seeing limited spot size of 0.65". Current estimates suggest that the visible TWFS can go down to 21.5 mag with a 10 second integration time and achieve 35 nm of total TWFS error.

3.3.2.4 PSF Monitoring Camera

The design discussed above has allowed for a PSF monitoring camera. Since this camera would only be potentially useful for PSF monitoring for the d-IFS we are currently not planning to design or implement such a camera. If scientifically useful it should be implemented as one of the d-IFS channels.

3.3.2.5 LGS Wavefront Sensor Object Selection Mechanism

There are a total of nine LGS wavefront sensors in the baseline NGAO design. The asterism is novel in the sense that there is a fixed central guide star with a 5 star asterism around it on the vertices of a regular pentagon and there are 3 additional point and shoot lasers that can be pointed anywhere in the field of regard to MOAO sharpen the 3 TT(FA) stars. The asterism diameter can be varied between 20" and 174".

Figure 18 is a schematic view of one of the eight LGS θ/φ pickoff probe arms. These pickoffs are intended to be very similar to the LOWFS object selection mechanisms described in section 3.3.2.1. A conceptual mechanical enclosure for the LGS WFS is shown in Figure 19.

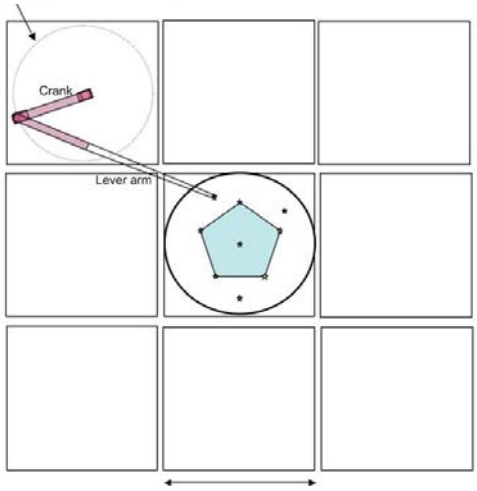

Figure 18. Plan view of the LGS object selection θ/φ pickoff scheme.

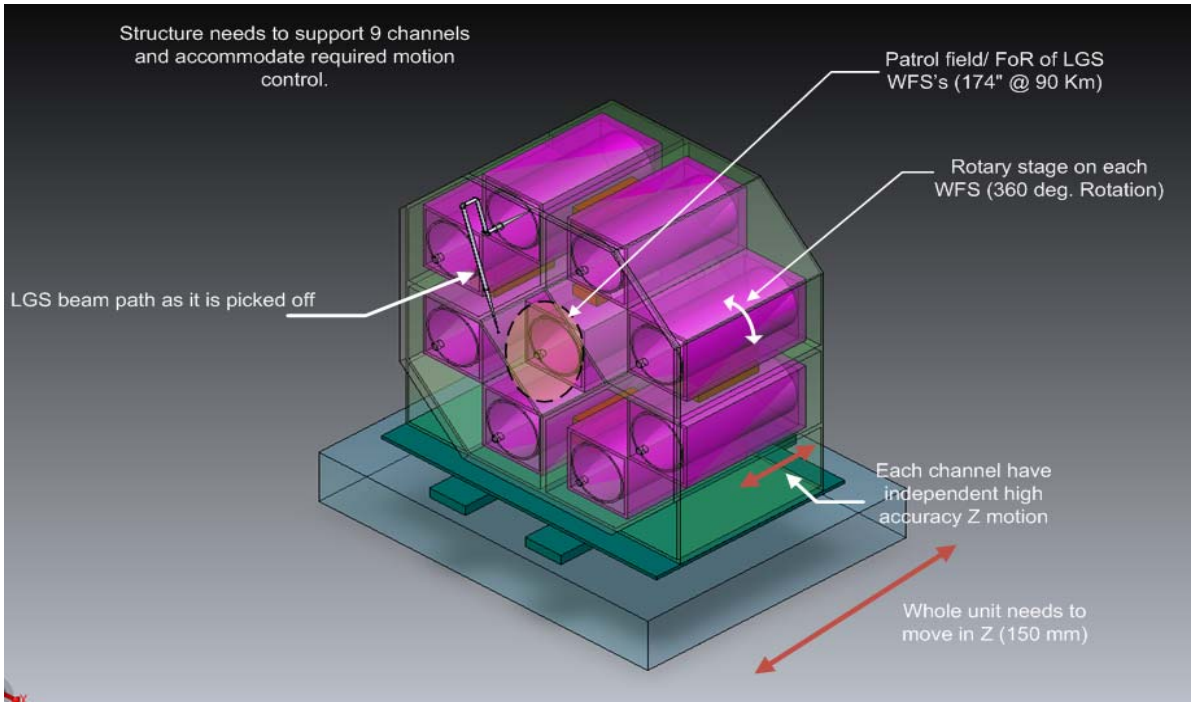

Figure 19. LGS WFS assembly enclosure.

Note that the LGS are always maintained fixed with respect to the LGS WFS OSM. When the AO rotator is used in fixed field mode this is accomplished by the laser launch facility maintaining the LGS asterism fixed on the sky via its own rotator. When the AO rotator is used in fixed pupil mode this is accomplished by not having the LGS asterism rotate on the sky.

3.3.2.6 LGS Wavefront Sensors

The LGS wavefront sensors are Shack-Hartmann (SH) sensors with up to 64 x 64 subaperture sampling of the pupil. For the LGS wavefront sensor detectors we anticipate using a very low noise CCD based on the CCID-56 to minimize the laser power required in each beacon. This detector is nominally 256x256 pixels with 3 electrons read noise at 2 kHz frame rates and < 500 electrons/sec of dark current at the operating temperature. A descope to an existing 240x240 pixel CCD and 60x60 subapertures is a potential fallback option.

A single LGS WFS channel is shown schematically in Figure 20. This is very similar to the existing Keck AO WFS design (the existing optical design is documented in KAONs 137 and 375) and a preliminary optical design has been performed. The WFS is positioned such that the LGS image is located at the field stop. The entire mechanism, including object selection mechanism, must translate in focus to remain conjugate to the sodium layer. Pupil reimaging optics reimage the telescope pupil (i.e., woofer DM) onto the lenslet array and relay optics relays the images produced by the lenslet onto the camera with the required magnification. A lenslet switching mechanism allows multiple pupil sampling scales and a translation stage allows the relay lens and camera to refocus for different lenslets.

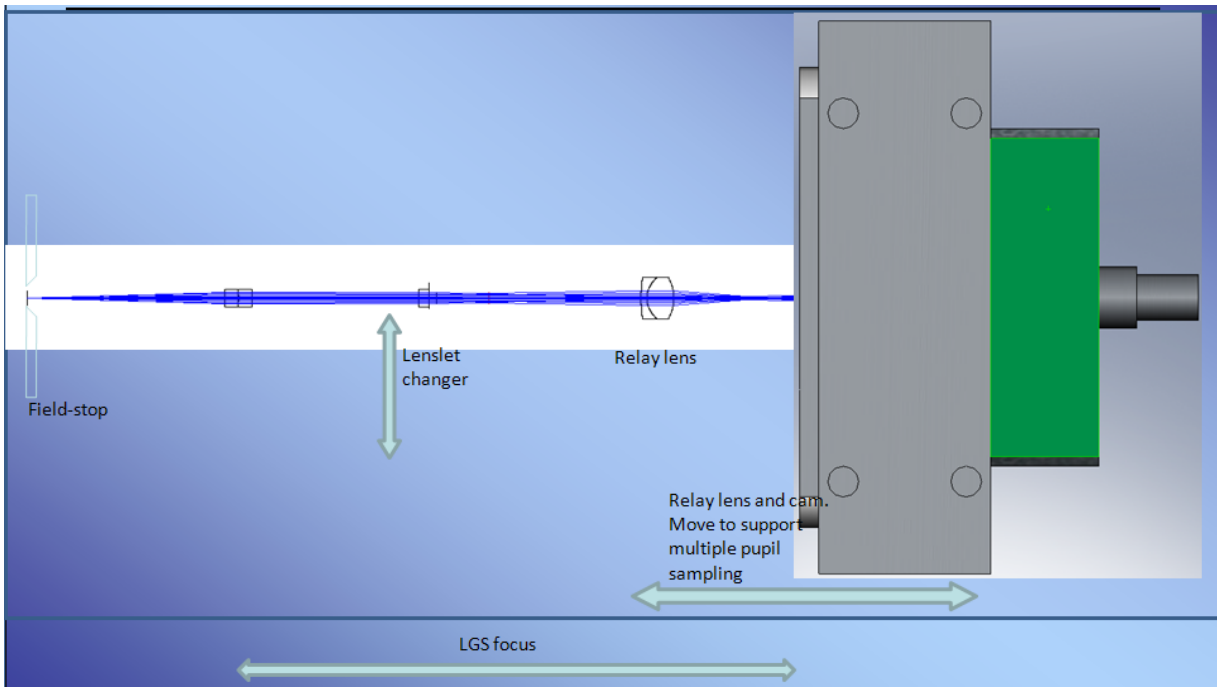

Figure 20. Schematic of a single LGS WFS channel.

3.3.2.7 NGS Wavefront Sensors

The NGS WFS and narrow field TWFS pickoff is performed with a pair of field steering mirrors as discussed in section 3.3.1.7. The NGS WFS opto-mechanical design will likely be similar to that of the LGS WFS and will use the same CCD.

3.3.3 AO Optical Performance

To determine the performance of the optical system, several sources of optical degradation were analyzed using Zemax in the wavelength passbands used by the individual science instruments and wavefront sensors. The passbands are defined in KAON 530.

The optical relay was modeled in conjunction with the Keck primary and secondary mirrors, to ascertain the combined effects of the two optical systems.

Field points used were the maximum off-axis fields defined for each instrument. The wavefront errors and RMS spot radii quoted are the worst-case for the field points analyzed.

According to Zemax, the working f/# of the wide-field relay is f/13.66 and of the narrow-field relay is f/46.89. Airy disk sizes are defined by

$$r_{airy} = 1.22\lambda F/\# \qquad (1)$$

and the depth of focus (DOF) is defined by $DOF = 4\lambda(F/\#)^2$.

In Zemax, both the woofer and tweeter DMs were defined as "Zernike Fringe" surfaces. This allowed a placement of Zernike terms on the mirror surface, to mimic the correction capabilities of an actual DM and derive an "uncorrectable" wavefront error (errors which could not be corrected with a DM). Examination of the Zernike Fringe Coefficients and spot diagrams indicated that the bulk of the wavefront error was due to astigmatism and coma, therefore the Zernike fringe surfaces were optimized only for those coefficients (optimizing in Zemax with too many variables is slow and sometimes fails to converge in a realistic fashion).

3.3.3.1 Wide Field Relay Optical Performance

3.3.3.1.1 Optical Performance to the Deployable Integral Field Spectrograph

It is assumed that the d-IFS is used in MOAO mode, and that the DM in each arm can apply low-order correction optimized for that field position. Thus field-dependent aberrations can almost completely be removed.

When the d-IFS is in use, there will be no dichroic in the converging beam ahead of the instrument. Lateral color and chromatic focal shift are therefore very close to null (with a negligible contribution from the tilted LGS WFS dichroic in collimated space). Image analysis results are shown in Table 4.

Table 4. Optical performance to the d-IFS

Instrument	λ bands	F/#	FOV (″)	Field Curvature (mm)	RMS WFE (nm)	Spot Size (μm) at J	Spot size (mas)	Airy radius (μm) at J
d-IFS	J, H, K	15	150	1430	8.6	1.25	1.7	19.5

3.3.3.1.2 Optical Performance to the Low Order Wavefront Sensors

The LOWFS optical selection mechanisms share a focal plane location with the d-IFS science instrument. Because the LOWFS must also be used with the imagers located in the narrow-field relay, it will often be the case that the dichroic splitter for the second relay, or the interferometric dichroic, are inserted between OAP2 and the LOWFS focal plane.

This dichroic location introduces several issues. When the ~ 20 mm thick dichroic is removed or installed, the focus will shift by ~7 mm along the optical axis and ~1.5 mm in the direction of the dichroic tilt. The LOWFS assembly will be mounted on a translation stage to adjust for this focus shift.

The insertion of the dichroic also leads to lateral color (see Figure 21) and a chromatic focal shift. The lateral color will be minimized by introducing a small wedge angle to the second surface of the dichroic (on the order of tenths of a degree; see KAON 107 for how this was done with the existing Keck AO system dichroics). The tilted dichroic will introduce astigmatism which can be removed by the LOWFS DM.

Table 5 gives aberrations during simultaneous observations in J and H bands, the largest bandpass the LOWFS is likely to utilize. No wedge angle has yet been included on the second surface of the dichroic.

Table 5. Optical performance to the LOWFS in simultaneous J and H-bands.

Instrum (mode)	λ (μm)	F/#	FOV "	Field curv. (mm)	RMS WFE (nm)	RMS Spot Radius (μm)	RMS Spot Radius (mas)	Airy radius (μm)	Lateral color (μm)	Chrom. Focal shift (μm)	Depth of focus (mm)
LOWFS	1.17-1.78	15	150	1320	15.6	18.6	10.7	19.5	24.4	70	0.9

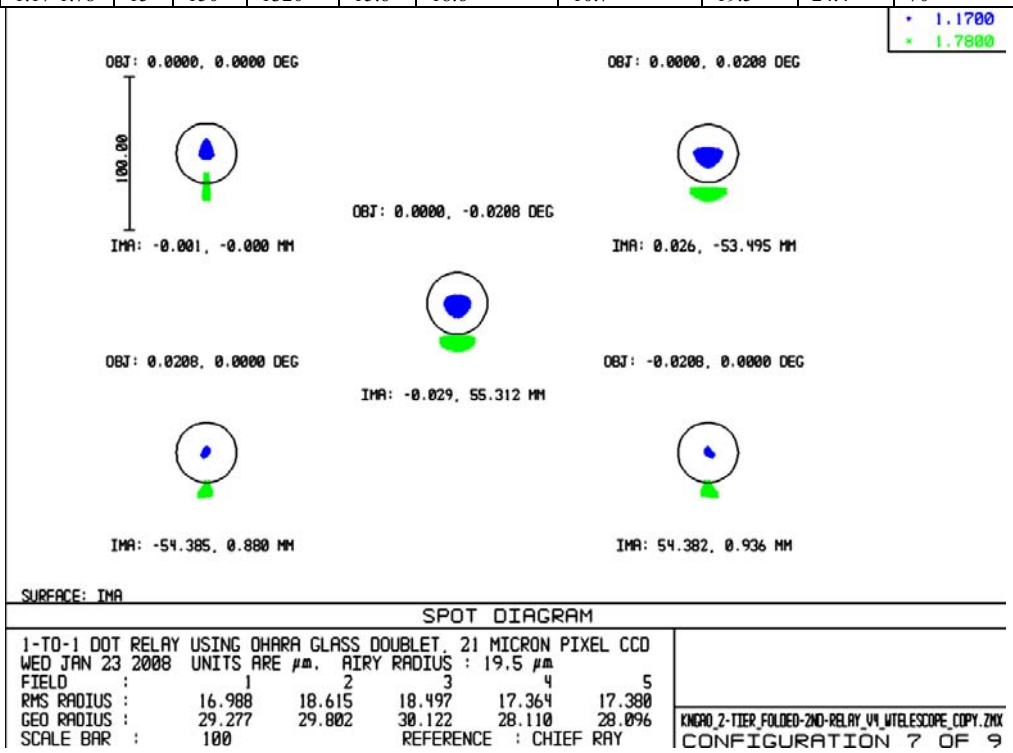

Figure 21. Spot diagrams delivered to the LOWFS focal plane showing lateral color without a wedged dichroic.

3.3.3.1.3 Optical Performance to the Interferometer Field Selectors

When the interferometer is in use, there will be a dichroic in the converging beam ahead of the instrument similar to the existing Keck AO system (although this is not necessary in LGS mode). The narrow field performance should be comparable to the existing Keck AO systems. The impact on the polarization has not yet been evaluated. Relatively shallow angles have been chosen in the wide field relay in order to minimize polarization effects.

3.3.3.1.4 Optical Performance to the Laser Guide Star Wavefront Sensors

The LGS WFS dichroic pick-off is located in the collimated space between the woofer DM and OAP2. The current simple design reimages the LGS, over their 174" diameter field, using a 1-glass biconvex lens. The lens chosen need only work at the sodium wavelength, so chromatic aberrations are not an issue. This lens was optimized for 90 km, but other zenith angles may be considered in

future optimizations (the performance varies by only 10s of mas between 90 and 180 km, so this is not seen as a huge potential improvement). Table 6 details the performance of the LGS WFS relay.

Table 6. Optical performance to the LGS WFS versus conjugate height.

Conjugate height	FOV, arcsec	Field Curvature (mm)	RMS WFE (μ)	RMS Spot Radius (mas)
90 km	174	650	2.8	415
180 km	162.5	650	3.1	440

Of concern are the almost half-arcsec spot sizes of the LGS WFS (see Figure 22). This is a significant fraction of the 1.45" pixels proposed for the LGS WFS; note that 4x4 pixels are used per subaperture. These aberrations stem from using OAP1 at a finite conjugate. An Alvarez-style corrector plate has been suggested as a solution.

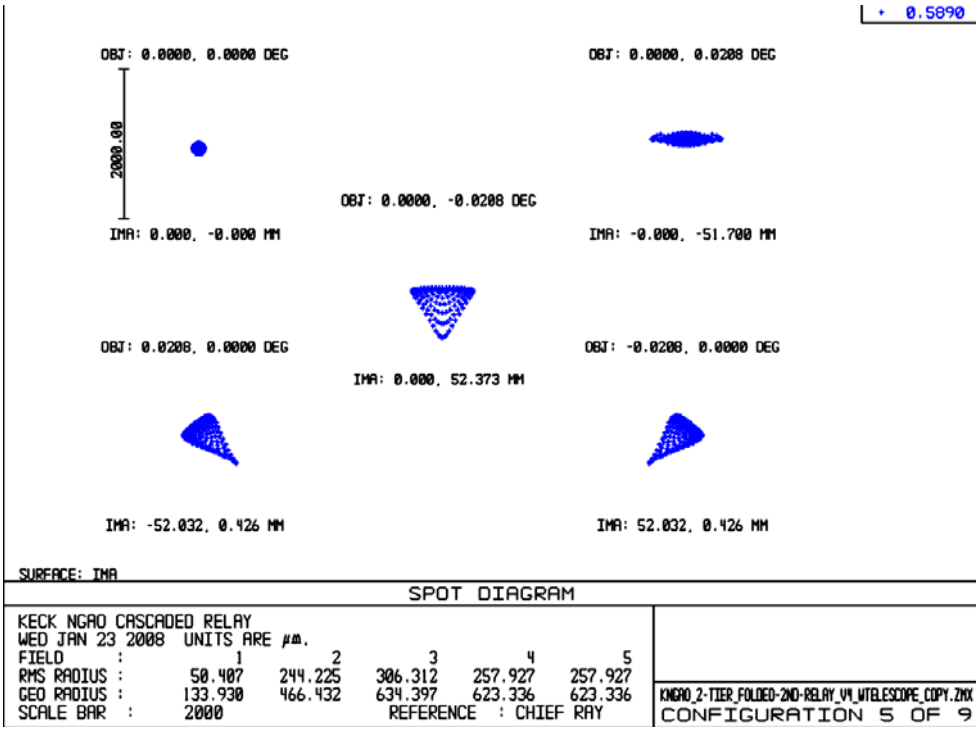

Figure 22. Spot diagrams delivered to the LGS WFS at 180 km conjugate.

3.3.3.2 Narrow Field Relay Optical Performance

It is assumed for the narrow-field instruments that the tweeter DM applies correction across the entire 30" diameter field of view. The performance values in Table 7 assume that the NGS/TWFS dichroic is in place. RMS spot radius takes lateral color into account, but like the LOWFS, this can be minimized by putting a wedge angle on the second surface of the NGS/TWFS dichroic.

Table 7. Performance to the narrow field instruments.

Instrument (mode)	λ (μm)	F/#	FOV "	Field curv. (mm)	RMS WFE (nm)	RMS spot radius (μm)	RMS spot radius (mas)	Airy radius (μm)	Lateral color (μm)	Chrom. Focal shift (μm)	Depth of focus (mm)
NIR Im, Y-band	0.97-1.07	46	30	277	15.6	17.5	7.8	55.1	4	11.8	8.4
NIR Im, J-band	1.17-1.33	46	30	277	15.6	18.3	8.2	66.4	5.5	17	10
NIR Im, H-band	1.49-1.78	46	30	277	15.6	20.9	9.4	84.6	10.78	34	13
NIR Im, K-band	2.03-2.37	46	30	277	15.8	24	10.8	115.3	17	53	18
Vis. Im,	0.7-0.97	46	30	277	15.8	22.2	10.0	39.7	12.8	42	6
NGS/TWFS	0.4-0.7	46	54	277	36	32.3	14.5	22.7	0	0	3.5

Lateral color is well inside the Airy radius for all instruments in this f/46 beam, so a wedge on the NGS/TWFS dichroic may not be necessary. Chromatic focal shift is negligible compared to the depth of focus. Note that the NGS/TWFS encounters only reflective optics, and therefore does not suffer from chromatic aberrations. Note, also, that none of the analyses include the effects of the ADC which will be required in each instrument's beam path.

The second relay OAP performance degrades with field angle. The large field of the NGS WFS/TWFS therefore exhibits much more wavefront error, as seen in Figure 23 and Figure 24, over its 54" diameter field than the science instruments over their 30" diameter field.

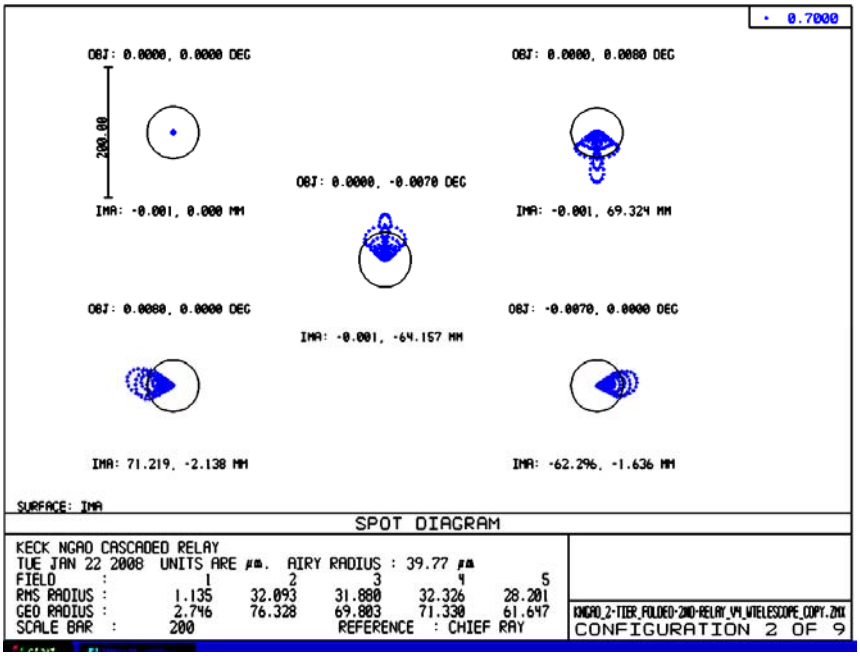

Figure 23. Spots at the on-axis and extreme field angles to the NGS WFS.

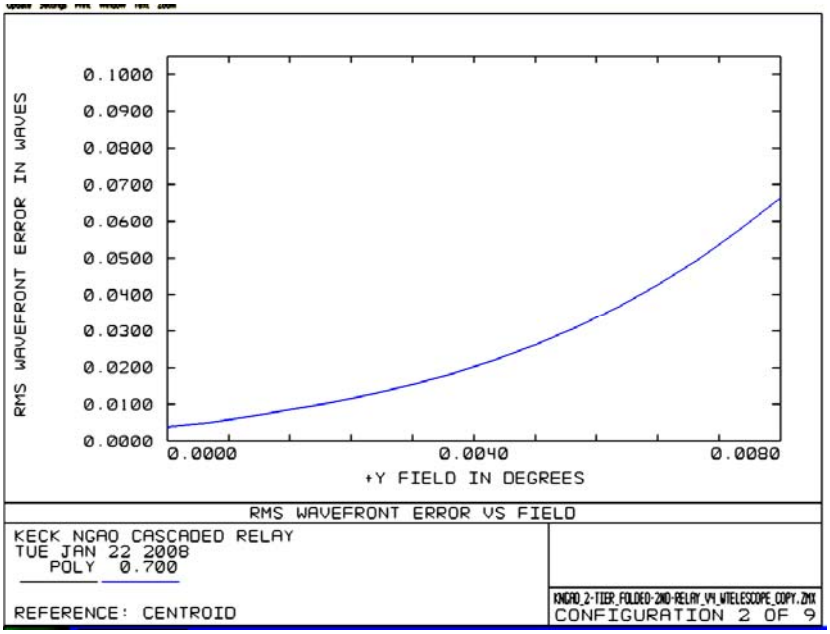

Figure 24. RMS wavefront error to the NGS WFS versus field.

3.3.3.3 Atmospheric Dispersion Correction

As mentioned in section 3.3.1.10 the ADC design has only been taken far enough to demonstrate feasibility. As shown in Figure 25 an f/15 ZnSe linear ADC can have < 10 mas or residual dispersion for λ = 0.9-2.5 μm. The rms wavefront error for this design is < 40 nm over this wavelength range. An f/45 version of this ADC has better rms wavefront performance, as shown in Figure 26, and can be shorter because of the slower beam (100 mm long in this example). A two-glass linear ADC generally has better performance, but at the cost of transmission due to the extra surfaces and glasses.

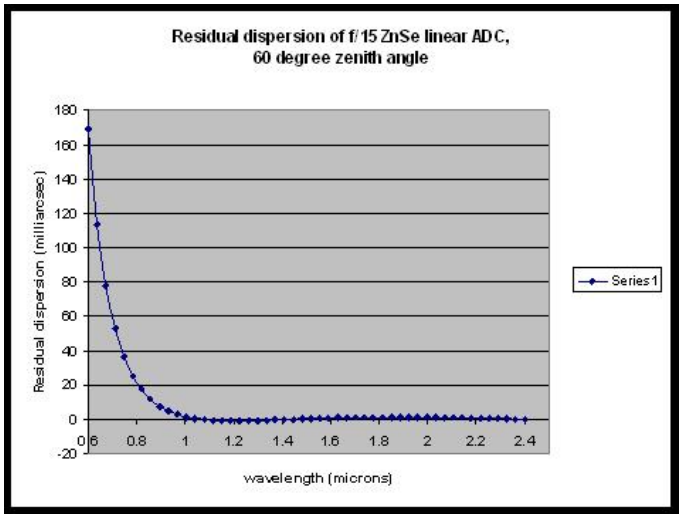

Figure 25. Residual dispersion of f/15 ZnSe linear ADC at 60º zenith angle.

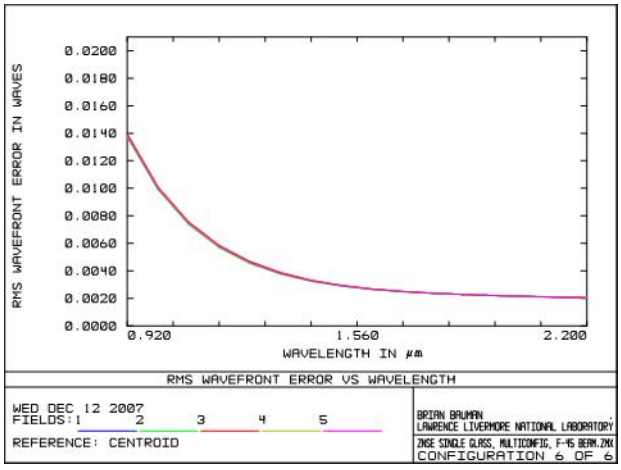

Figure 26. F/45 ZnSe linear ADC rms wavefront error.

3.3.3.4 Pupil Distortion

Pupil distortion in the NGAO cascaded relay manifests itself in several ways. The first two of these are evaluated in this section: the degree to which a grid of points on the primary mirror maps to a square grid on the DM and the field dependent pupil aberrations.

Two other factors (not evaluated here) are: pupil tilt on the DMs (this manifests itself not only as an uncertainty in the conjugate height of the correction, but also in plate scale errors that can degrade the astrometric accuracy) and DM-to-lenslet mis-registration and scale errors (these are dependent on the pupil reimaging optics chosen for the wavefront sensors).

In the analysis, the telescope primary became the "object", and field points were defined on the edges of the primary mirror. Observed field angle was set by adjusting the "stop" size placed at the Nasmyth focus to accommodate a 150" diameter field for the woofer, and a 30" diameter field for the tweeter in the narrow-field relay. Results are shown in Table 8. Figure 27 and Figure 28 and display grid distortion and the pupil PSFs for the woofer DM. Figure 29 and Figure 30 show the same things for the tweeter DM.

Table 8. Characteristics of the pupil image on the deformable mirrors.

	Diameter (mm)	Field (″)	# actuators	Curvature (mm)	Max Grid Distortion	Pupil PSF (μm)
DM1, woofer	100	150	20x20	5500	0.4%	400
DM2, tweeter	25	30	64x64	500	0.2%	38

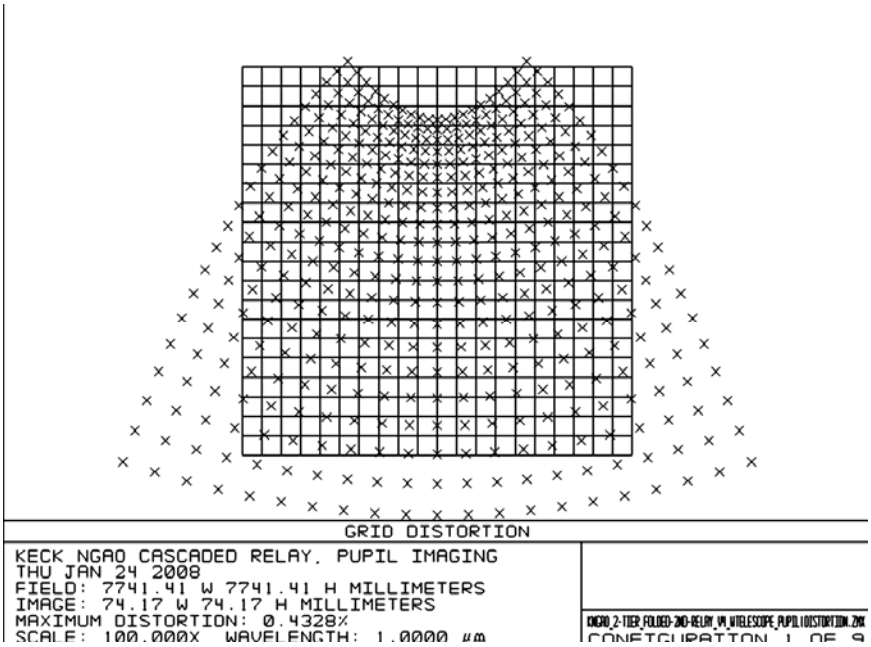

Figure 27. Grid distortion at the woofer DM location, magnified by 100.

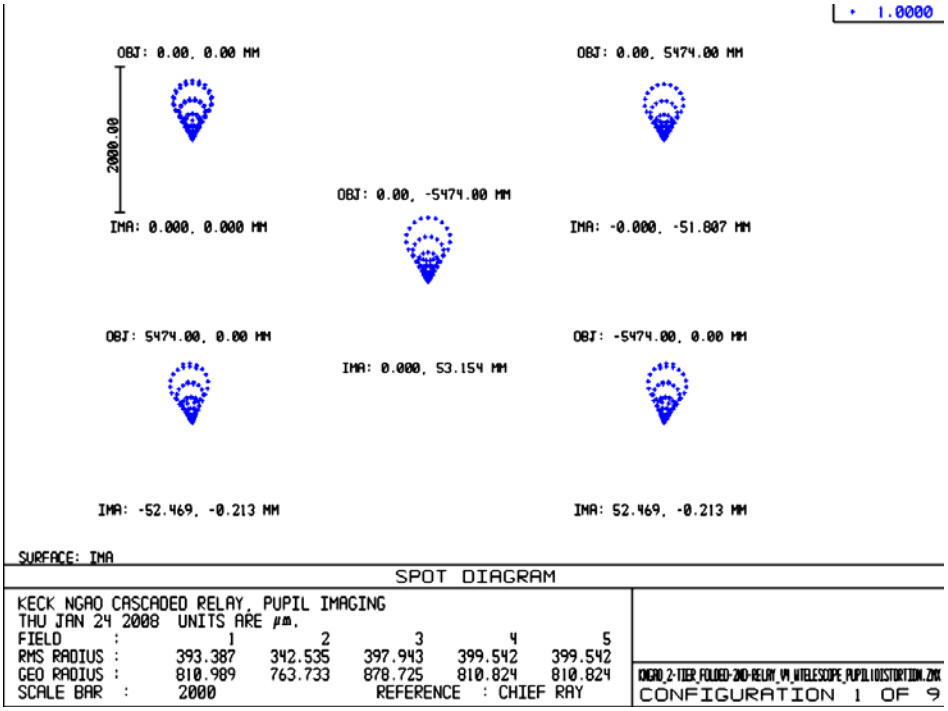

Figure 28. Spot diagrams for 5 locations on the primary mirror imaged onto the woofer DM.
Field considered is 150" diameter. Chief rays from the on-axis field angles make up the point of the comatic pattern, while chief rays for75" off-axis field angles make up the outer "radius" of comatic points.

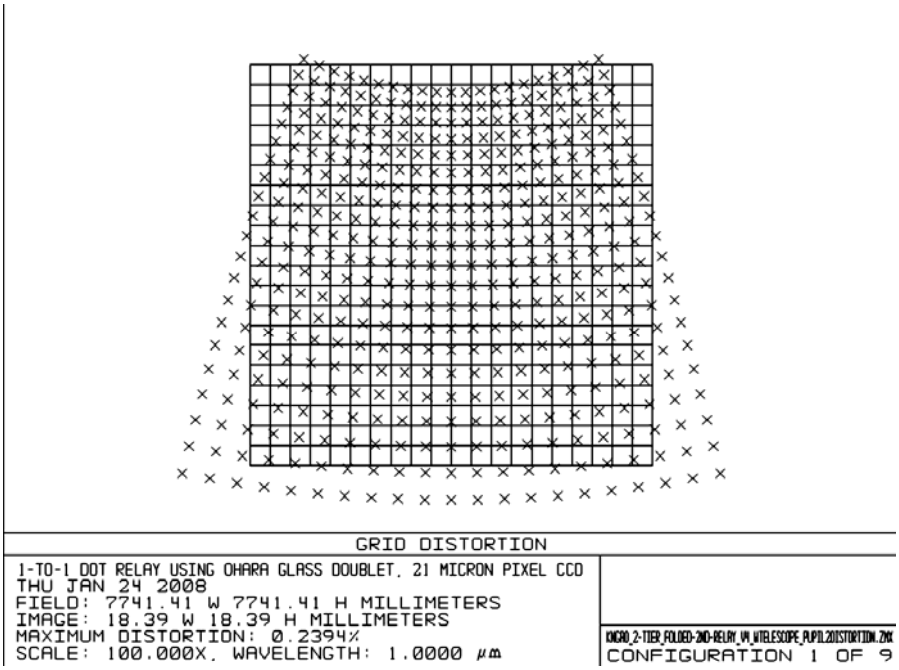

Figure 29. Pupil grid distortion at the tweeter DM position, magnified by 100.

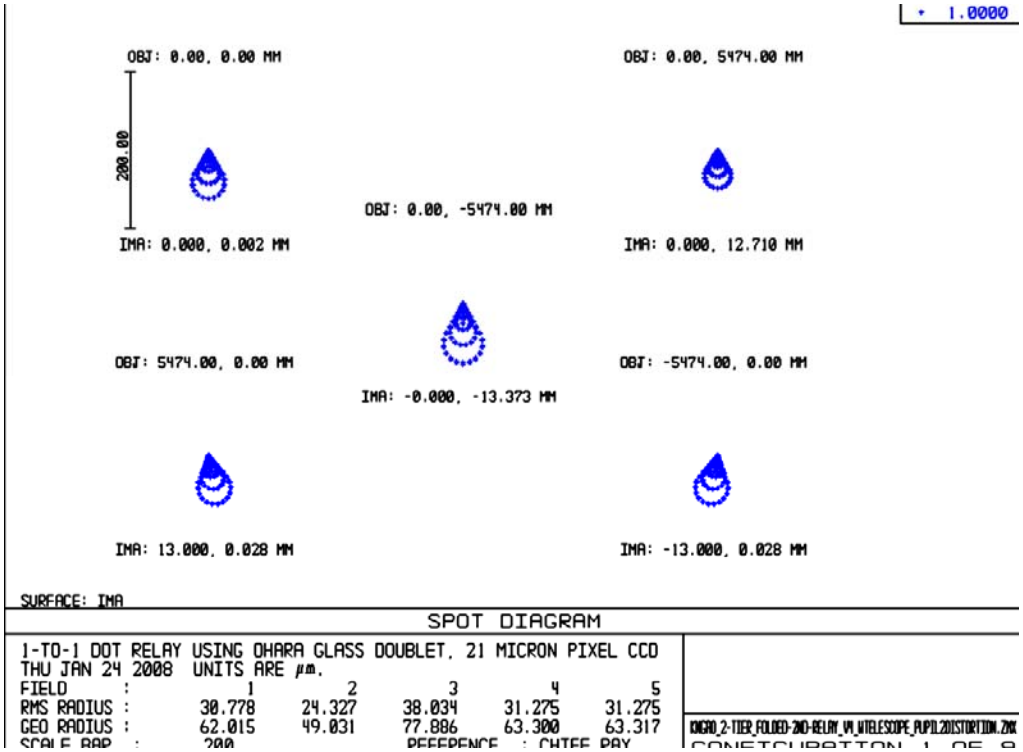

Figure 30. Spot diagrams for 5 positions on primary mirror imaged onto the tweeter DM.

3.3.4 AO Enclosure

The AO enclosure conceptual design is documented in KAON 563. The 3D model shown in Figure 3 was developed to support this design. The current design makes full use of the entire left Nasmyth platform and covers an area of 6.1 x 9.1 m. A working height of 2.59 m is provided with an overall working height of 3.35 m.

The cold room requirements include ≥ -20º C operating temperature, class 10,000 clean room and humidity ≤ 50%. Entrance to the main room will be via an ante-room (2.4x2.4x3.35m).

A proposal for feasibility and budgetary cost was solicited from a commercial supplier of cold/clean rooms, Harris Environmental Systems, Inc. The equipment supplied as part of the proposal includes all floors, walls, ceiling, redundant cooling and clean room process equipment, piping from the Keck machinery room and installation. A number of issues have been identified that will need to be addressed during the preliminary design, including extending the enclosure into the elevation bearing and identifying azimuth wrap space for the refrigeration system.

An alternate approach, which may need to be selected for cost reasons, is to only cool the AO bench itself. The visible and NIR imagers would be inside this enclosure and the fronts of the d-IFS and OSIRIS might mate to this AO bench cold area.

3.3.5 Alignment, Calibration, Diagnostics, Metrology and Monitoring

KAON 568 outlines the requirements and a design concept for alignment, calibration, diagnostics, metrology and monitoring. The following systems are envisioned to provide these types of information for NGAO:

- Standard sources for flux (flat field) and wavelength (spectral line) calibration of instruments.
- Astrometric source for instrument field distortion calibration.
- Simulated NGS and LGS sources for calibration, optical testing, and alignment.
- Atmospheric simulator.
- Wavefront measurement capability in each science instrument.
- Metrology (TBD).
- Atmospheric profiler.

3.3.5.1 Instrument Calibration Source

The standard sources for instrument calibration would likely be an integrating sphere with white light and spectral sources. These could be placed at an entrance of the AO bench as a facility that could be shared by all the instruments and provide calibration of the AO system detectors and instrument flat field correction simultaneously.

Based on the Keck OSIRIS experience, it is suggested that a flat field source can be constructed from an integrating sphere and optics that project the sphere's output port onto the telescope exit pupil. Both a white light and spectral lamps could be used with the same sphere.

3.3.5.2 Astrometric Calibration Source

The current Keck NIRC2 instrument is equipped with a precision grid of small holes at a focus inside the instrument. This point spread function (PSF) grid is used to map the optical distortion of the instrument across its field of view. A similar gird would likely be placed at the NGAO input focus for astrometric calibration of the AO and the instrument. Each astrometric instrument may also have its own internal grid source like the current NIRC2 instrument.

3.3.5.3 NGS and LGS Simulated Sources

Simulated NGS and LGS sources would be located at the input focus at the front of the AO bench. These simulated sources are used for:

- Checking optical alignment (registration) between the AO system and instruments
- Point spread function and field aberration verification and calibration
- Testing atmospheric dispersion compensators (ADC)
- Calibrating chromatic aberrations
- Measure DM-to-lenslet registration
- Measure DM influence functions
- Non-common path aberration calibration
- Closed loop AO tests

The simulator discussed in the next section would be designed to have several diffraction limited and seeing limited NGS sources. The LGS sources would attempt to mimic the elongation of laser guide stars, as closely as possible. These sources would be used in combination with the wavefront measurement capability of the AO system to calibrate each deformable mirror and each wavefront sensor. The point source is also used to verify the registration between wavefront sensors and deformable mirrors. The point source would also be used the measure instrument non-common path aberrations.

The NGS and LGS source simulators will be located on the telescope side of the AO rotator. The current design places the infinity focus inside the K-mirror between the first and second mirrors. The location of the LGS focus is even further inside the K-mirror. If single mode fibers or pinholes are used to generate a reference wavefront for the AO system, some means will be needed to relay these optical "clean beams" from their source to the AO focus. This optical design task may prove challenging with regards to the requirements for RMS wavefront error for the NGS sources. Non diffraction limited sources will have somewhat relaxed requirements. If the same optical relay is used for both NGS and LGS sources then some means will be needed to correct the focal difference between LGS and NGS sources. A schematic is shown in Figure 31. This relay is shown as two lenses similar to the existing Keck AO system simulator. However, the need to operate across both

visible and NIR wavelengths and over a wide field will likely require a reflective optical design. Since the aberrations resulting from the LGS source passing through the 1-to-1 optical relay is static, predictable, and of relatively low spatial order, small optical correctors could be built into each LGS source. A novel method used at the Gemini telescope, is inclusion of a low cost 19 channel deformable mirror inside the point source generator used to calibrate its active optics wavefront sensors.

3.3.5.4 Atmospheric Simulator

A simulator is needed to test the AO system's ability to correct atmospheric turbulence, especially tomographic reconstruction over the NGAO field. In current AO practice, turbulence simulators pass a reference beam through a distorted optical surface that mimics atmospheric turbulence or through a turbulent fluid (mixing cold and hot air). Both these aberrating media could be used in a source simulator which would be placed close to the input focus of the AO system.

The point source simulator can serve as an atmospheric simulator if rotating phase plates are inserted into the system as shown in Figure 31. In order to meet the requirement on operation to a wavelength of 2.5 μm the phase plates will need to be made of etched IR grade fused silica similar to those made by Silios in France. If transmission to 1.6 μm is acceptable then plastic materials may be used, at a considerable cost savings, similar to phase screens made by Lexitek in Massachusetts.

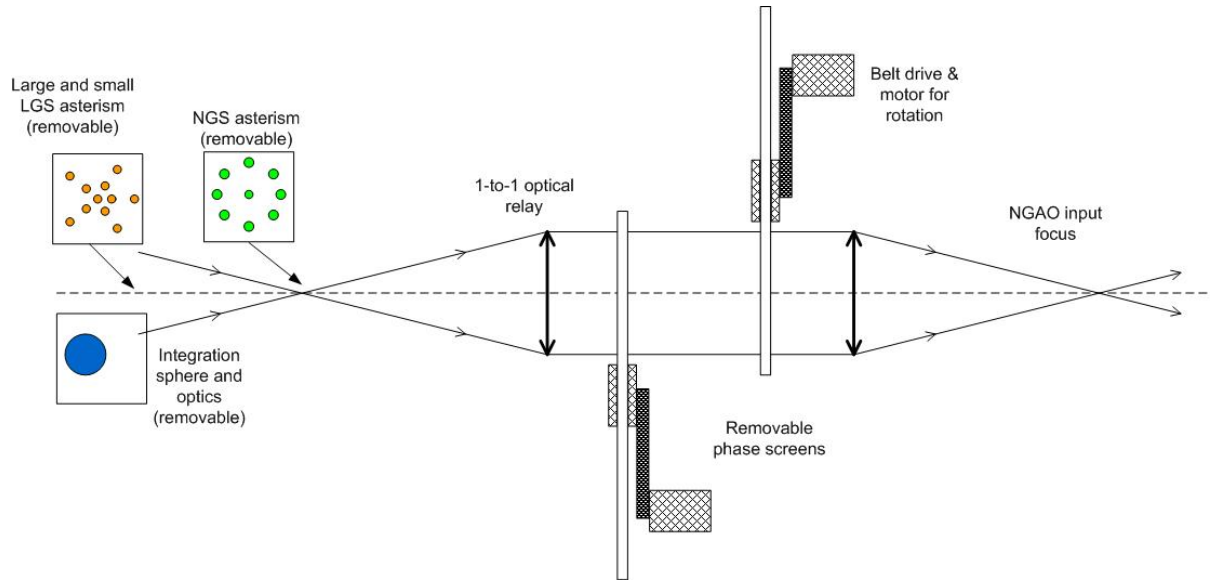

Figure 31. Schematic of a combination atmospheric simulator, LGS and NGS source simulator, and radiometric calibration source.

3.3.5.5 Science Instrument Wavefront Measurement

The instrument should be able to determine the aberration differences between the AO system and the instrument optical trains, the so-called "non-common path" aberrations. At present, AO systems meet their performance specifications by placing a shape on the deformable mirror that cancels

instrument aberrations; this shape is the "zero point' for dynamic correction of the atmospheric distortion. An alternative would be to require much tighter tolerance on the optical quality of the instrument. The measurement of these wavefront errors and correction by the AO system has proven adequate in present AO systems and appears to work at tolerances typical of extreme AO systems (see references in KAON 568). A number of techniques are available for measuring these aberrations including, phase diversity algorithms, fiber optic interferometers, point-diffraction interferometers, and 'on-instrument' wavefront sensors. Most of these techniques would make use of an optical source located at the input focus of the AO optical system.

3.3.5.6 Metrology

A metrology system could potentially be needed to monitor and correct for the alignments between the NGAO system and the science instruments, especially given the tight tip/tilt requirements and the significant non-common path between the LOWFS and the narrow field science instruments. A "metrology like" alignment system (KAON 35) was proposed originally for the Keck AO system. Some parts were installed in the NIRC2 camera but it was later decided not to be needed. A laser metrology system for the Palomar AO system was also considered but was not installed.

3.3.5.7 Atmospheric Profiler

The initial requirements and design for an atmospheric profiler are KAON 552. A profiler was deemed to be useful for NGAO for the following reasons:

- Acceptance testing and performance verification (in order to know the performance versus the current conditions).
- Diagnostic tool during observing.
- Aid to planning observations.
- Improve accuracy or speed up the convergence of the laser tomography algorithm.
- Useful as an aid in estimating the AO PSF across the instrument field of view.

The highest level requirements were determined to be:

- Measure atmospheric profile at low resolution in six or more altitude bins between 1 km and 20 km altitude.
- Measure the profile once every 2 minutes.
- Measurement accuracy of 10% or better for r_0.
- Operate automatically when conditions are suitable for operating the Keck telescopes.
- Small physical size.

A brief overview of the available technologies for optical measurement of atmospheric turbulence is given in KAON 552. A MASS/DIMM system was recommended as the best system to meet the NGAO requirements. The NGAO team has significant experience utilizing and interpreting the data from the TMT MASS/DIMM that is located on Mauna Kea (KAONs 415, 420 and 496). Continued

use of this TMT system and/or of a joint Mauna Kea facility are being pursued. The proposed location for the Mauna Kea facility is shown in Figure 32.

Figure 32. TMT seeing monitor superimposed on proposed Mauna Kea seeing monitor site.

3.4 Laser Facility Description

3.4.1 Laser Facility Optical Design

3.4.1.1 Laser Facility Optical Requirements

The NGAO error budget modeling (see section) assumes that sodium laser returns typical of what has been demonstrated at Starfire Optical Range (SOR) can also be achieved for NGAO. During the development of the NGAO system design, the various factors affecting the rms measurement noise and the rms temporal error on the wavefront sensor were analyzed and a combined specification for the laser guide star (LGS) wavefront sensor and LGS facility were developed. The NGAO error budget WFS measurement noise accounts for the standard photon and read noise sources. In addition, it also includes errors from the spot elongation of LGS beacons, lenslet diffraction, lateral diffusion in the CCD, and the level of AO correction provide by the deformable mirror in the first relay of the NGAO system. The error budget also accounts for the optical and atmospheric transmission, the beam quality of the laser, and the wavefront error of the entire laser transport optics. The NGAO laser system requirements are based on an assumed return efficiency from the sodium layer of 150 photons/cm2/s/W. The FWHM of the resulting spot at the sodium layer must correspond to 1.1 arc seconds in standard NGAO seeing conditions (r0 = 16.0 cm, q0 = 2.7 arc seconds). The laser launch telescope must be 50 cm in diameter and the laser transport optical system must have a rms wavefront error of 40 nm rms or less.

As part of the system design process, the NGAO team made a detailed trade study of the tomography error associated with various arrangements or asterisms of LGS. The results of this study by Ralf Flicker are documented in KAON-429 and the results were confirmed in another study (KAON-475)

by comparison to two other AO computer simulations. These studies concluded that the original NGAO five LGS asterism, 4 at the corners of a square plus one in the center, was not sufficient to meet the error budget requirement for tomography error in the case of wide field d-IFU science observations. A new baseline was adopted with 6 LGS, 5 in a regular pentagon and one at the center. In order to be optimized for both wide field and narrow field science cases, it was proposed that the LGS asterism should be able to be contract and expand about the central beacon. The implications of this feature on wavefront sensor performance show a preference for an asterism that is continuously variable in radius over one that can only be varied in discrete steps, this effect is most pronounced as the LGS asterism size increased over 40 arc seconds in radius. Based on studies of sky coverage, Richard Dekany proposed that three LGS be dedicated to AO correction or "sharpening" of the three LOWFS natural guide stars. These three LGS were christened "point-and-shoot" laser guide stars. Because of these studies, a 9 LGS asterism was adopted as the baseline for NGAO architecture.

Based on the current understanding of LGS tomography error the performance of the NGAO system is a relatively weak function of the LGS asterism. Some experimentation will likely occur during the initial on-sky testing of the LGS tomography system to explore performance based on several LGS configurations.

Another design decision was to have the LGS constellation projected such that the orientation of the central asterism and the "point-and-shoot" LGS remains fixed with respect to the sky during most observational scenarios. Most observations occur in a "field-fixed" mode with the AO K-mirror keeping natural stars fixed in the AO field of view (FOV). In this mode, the LGS projection system must rotate the LGS asterism as it is projected in order for the asterism to appear stationary in the AO FOV. A less used mode of the AO system is a "pupil-fixed" mode, where the AO K-mirror keeps the telescope pupil fixed in the AO FOV. The projected LGS are also kept fixed with respect to the telescope in this mode. However, as seen in the AO FOV the natural star will appear to rotate to relative to the LGS asterism. The "point-and-shoot" LGS will not remain fixed relative to the LOWFS stars, this is acceptable because the science cases that require "pupil-fixed" mode are narrow field and in most cases, the science object is bright enough to use as a tip tilt reference source. In the "pupil-fixed" mode, the projected LGS and the LGS wavefront sensors maintain the same orientation during an observation; therefore the LGS wavefront sensors can remain fixed with respect to the AO FOV in both observing modes. This design choice requires that the LGS projector can rotate the uplink laser beams as needed.

3.4.1.2 Laser Facility Optical Design

An overview diagram of the laser facility optics is provided in Figure 33. Three major blocks are shown: the laser enclosure, the beam transport optics and the top end beam transfer optics located behind the telescope's secondary mirror. The laser output is first divided into the desired number of LGS by a switchyard shown within the AO enclosure.

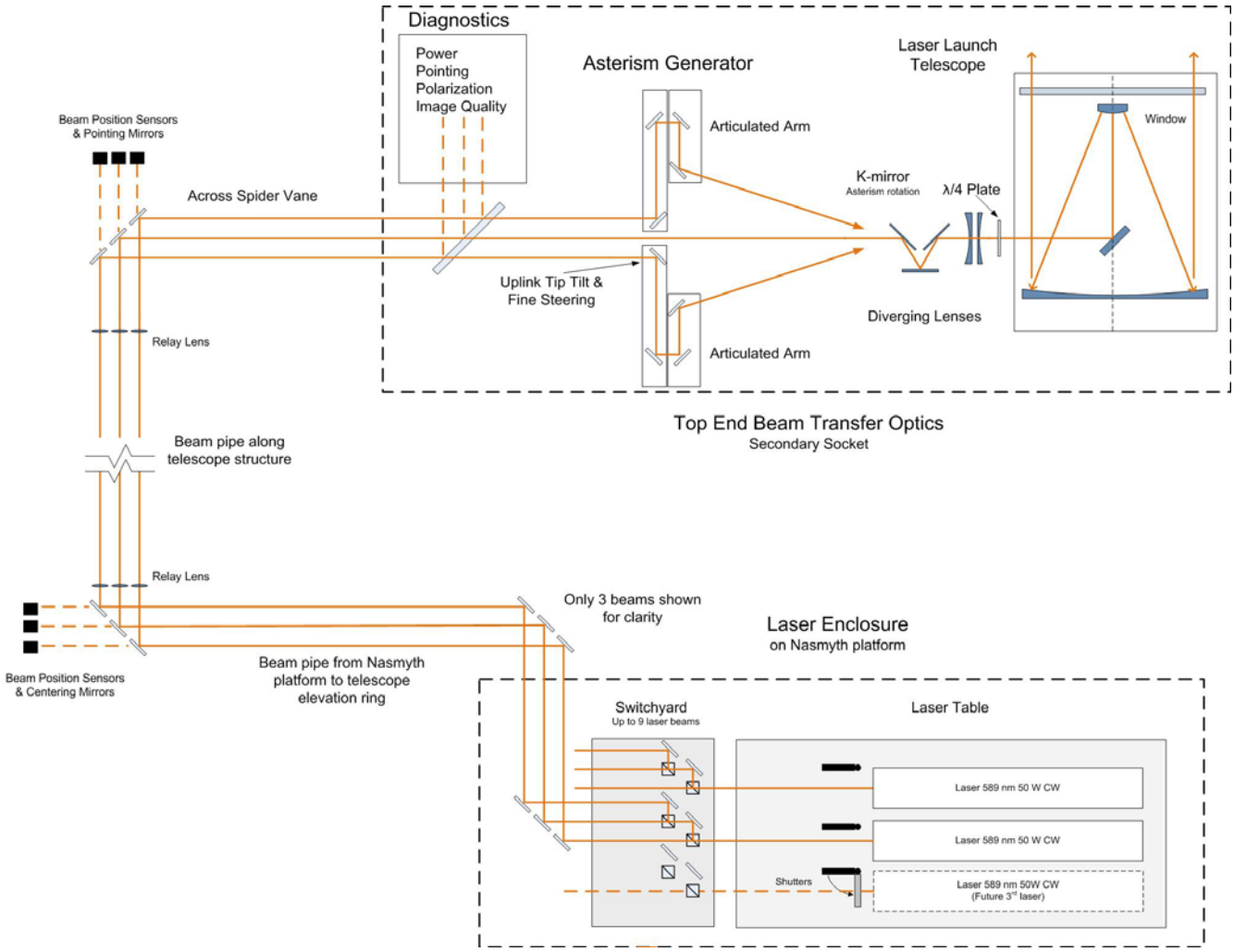

Figure 33. Laser facility optical schematic.

The required asterisms, and the corresponding number of LGS, are summarized in Table 9. The formatting of the laser beams is accomplished by motorized beamsplitters and mirrors that accept the 50 W input beams from the two laser systems and direct them to the proper outputs at the desired power. One can generate four 12.5 W beams using two sets of three 50/50 beamsplitter to produce Asterism 1. A second set of beam splitters can be used to produce Asterism 2 using a 33/66 beamsplitter followed by a 50/50 beamsplitters which will produce three 16.7 W beams. These same splitters can be used with three 50W laser systems to produce the nine LGS Asterism 3. Shutters on each beam are used to permit diagnostic measurements of any individual output beam. The switchyard will also have a low-power HeNe "surrogate" lasers that can be switched into the optical path to provide 594.1 nm laser beams, an inexpensive wavelength that is resonantly close to 589 nm, to permit testing of the beam transfer optics without requiring the high power laser systems.

Table 9. NGAO asterisms versus laser power.

	Asterism 1	Asterism 2	Asterism 3
Total laser power	100 W	100 W	150 W
Lasers	2 x 50 W	2 x 50 W	3 x 50 W
Main asterism	"Box plus one" or quincunx	Triangle	Pentagon plus one
Point and Shoot lasers	3	3	3
Total number LGS	8	6	9
Watts per guide star	12.5W	16.7	16.7
Beam splitters	4 50/50 splitters per laser	33/66 + 50/50 per laser	33/66 + 50/50 per laser

After the laser are reformatted to produce the desired asterism they will transported from the Nasmyth platform enclosure to the telescope structure and up the side of the telescope tube. For both safety and cleanliness, the entire optical train of the laser facility must be enclosed in a light and dust proof mechanical structure. The proposed location for these folds optics and the beam pipes are shown in the figures of section 3.4.3. The tube structure is outside the footprint of the primary mirror and crosses behind the secondary mirror support structure. The Keck telescope top end is significantly larger than the primary mirror, which affords space for location of fold optics at the top end of the telescope.

A feature of the proposed optical design, for the case of the laser not being on the elevation moving part of the telescope, is that the fold mirrors at the bottom and top of the telescope structure must track as the telescope moves in elevation. In addition the beam tube running parallel to the telescope Surrier truss must change length as the telescope move in elevation as well. It has been suggested that this tube can be a series of several nested tubes in a "telescoping" arrangement, similar to an architect's blueprint storage tube or a sailor's spyglass. If such an arrangement is not possible, the tracking mirror can be moved from the top of the telescope to a location on the telescope tube just above the tracking flat located on the roof of the AO enclosure, a much more compact tube could be fitted over these mirrors, this appears mechanically with the draw back of requiring more fold mirrors.

After the folds at the top end of the telescope the beams will travel over the top of one of the secondary mirror supports or "spiders". Next the beams will travel down into the secondary mirror structure and into the launch telescope. Beams will be arranged to pass along the spider in a compact fashion inside a tube so that laser light does not scatter into the telescope. Relay lenses along the path will maintain the beam diameter and exit pupil. Two of the mirror in each beam will be controllable in tip and tilt these mirrors will maintain the centering and pointing of the beams at the input to optics located behind the telescope secondary. A slow update control loop will be responsible for correcting for the flexure of the telescope structure with elevation. The update may be done exclusively with look-up tables or with feedback from position sensitive photo-diodes or imaging cameras.

The use of fibers would greatly simplify the design of the beam transport optics. Although the Keck I laser system will be using fibers to transport powers comparable to the power per guide star in Table

9, the Keck I laser will use a mode-locked laser that is not affected by Stimulated Brillouin Scattering like a narrow width CW laser source would be when passing through a single mode fiber. The European Southern Observatory has used a narrow line CW laser with a single mode optical fiber at powers as high as 10 W. This is accomplished by first passing the laser through an electro-optical modulator, making it no longer a narrow line width source. The purpose of the phase modulator is to broaden the laser line width before the laser is injected into the single-mode relay fiber. Based on numbers at the Laboratory for Adaptive Optics web page the ESO laser would produce about half the return of an equivalent power narrow bandwidth CW laser. This appears to be an unacceptable loss for the NGAO system. Future advances in the efficiencies in fiber throughput should be considered as well. Crystal Fibers from Denmark has developed a 589 nm capable fiber with an 8 db/km loss. Current fibers losses are 10 db/km.

In order to produce the required laser asterisms the nine laser beams must be steerable about the field of view of the laser launch telescope in a flexible way. In particular the "point-and-shoot" concept requires the laser beam to be pointed at arbitrary locations about the field of view. Given the small image (plate) scale of any practical laser launch telescope the laser beams must be positioned fairly close to each other if they are brought to focus before being transmitted out of the launch telescope. Although a steering mirror array, similar to a MEMs deformable mirror was proposed as an asterism generator its location close to focus makes it susceptible to laser damage. In addition bringing the laser beams to focus can produce problems with air breakdown unless the optics work at very slow focal ratios or the area around focus is evacuated. As a means of avoiding these problems the laser launch telescope is used in combination with a diverging lens so that the laser beams do not go through focus.

We propose using a series of steering arms to position the laser beams about the field of view; the steering arm would be similar to the probe arms proposed for the laser guide star wavefront sensor [5]. The asterism generator would have 8 arms using θ-φ mechanisms and would be arranged in a 3 by 3 grid with the center being empty to allow the on axis laser to pass straight through. These eight mechanisms can be made to achievable mechanical tolerances by using a magnification for the laser launch telescope of about 60. The down side of this arrangement is that the asterism generator and the laser launch telescope must be separated by about 2 meters. This will likely require folding the beam inside the secondary socket in order to make the optical system fit in the available space. The feasibility of this design will be determined during preliminary design phase.

The diagnostic system directs a small fraction (1%) of each of the laser beams through a beamsplitter into a diagnostics package that will include power meters, polarization sensor, point diagnostics and laser wavefront quality diagnostics.

The linearly polarized output of the lasers is converted to circularly polarized light prior to projection by the laser launch telescope to maximize the efficiency of exciting the sodium in the atmosphere. This is accomplished by quarter-wave plates in each beam. The wave plate rotation must be adjustable to account for variations in polarization as the laser beams are directed through the optical elements in the beam train.

The laser launch telescope is a Cassegrain reflecting telescope. When used in combination with the diverging lenses in Figure 33 it functions as a Keplerian afocal telescope with a magnification of about 60. This high total magnification allows the separation for a reasonable scale for the asterism generator optics.

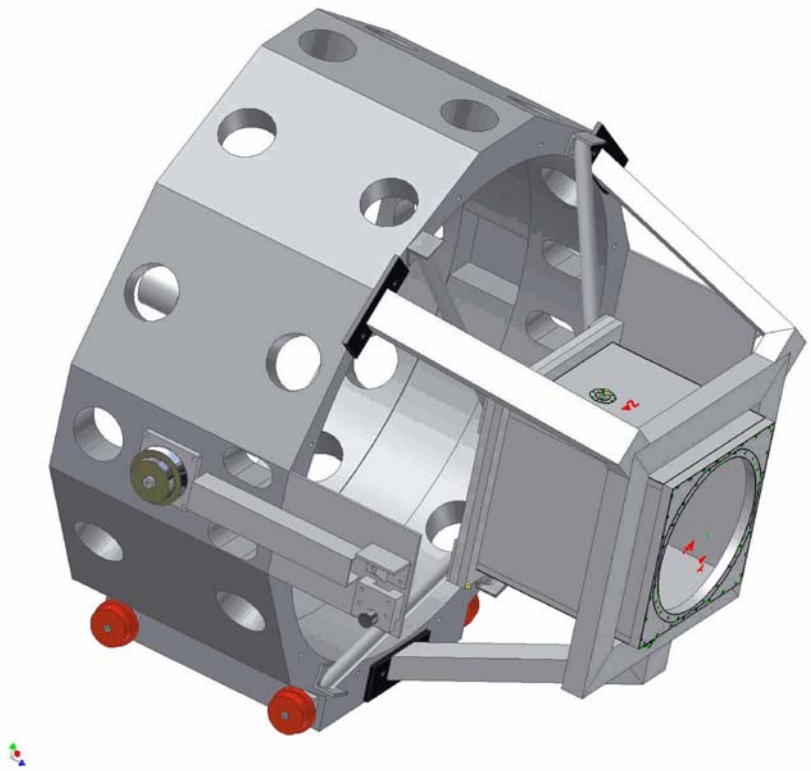

Figure 34. Secondary mirror module and Keck I laser launch telescope.

An evaluation was performed of the benefits of uplink compensation in KAON 509. For the moment we have decided to proceed without uplink compensation.

3.4.2 Lasers

Laser power estimates for NGAO have converged around the need for a total power of 150 watts for the purpose of generating multiple laser guide stars to support tomographic reconstruction of the atmospheric turbulence. In this discussion we will focus on laser systems that have demonstrated power levels of at least 50 watts since this power level appears to be commensurate with our requirements.

A laser choice has not yet been made for NGAO however two types of solid state sum-frequency lasers systems are the most likely candidates for consideration:

1. A single frequency laser system. Once example is the laser built for the Starfire Optical Range (SOR). This laser system has the highest measured return per Watt of the existing

lasers. A second generation, two frequency laser is currently under development by the Air Force Research Laboratory on the basis that this will allow even greater return efficiency.

2. A mode locked laser system. One such system, built by Lockheed Martin Coherent Technology (LMCT) is in use at Gemini-North with a power output of ~12 watts. In a combined Keck/Gemini experiment the Gemini-North laser system was demonstrated to have twice the return of the Keck dye laser. A higher power laser system based on this laser design is currently being constructed for the Gemini South Observatory and the Keck I telescope. This is the only 589 nm guide star laser built by a commercial supplier.

We also intend to monitor the progress of fiber lasers. ESO is working with Volius to develop a Raman fiber laser and LLNL also continues to develop their fiber laser. Volius is currently building a low power sodium wavelength laser for Keck. The LLNL fiber laser will be demonstrated in the VILLAGES experiment at Lick.

As discussed in KAON 582 the general plan of both single frequency and mode locked lasers are similar, but each design differs in a number of key details that are helpful to understand when considering the development issues and risk areas for each approach.

The laser system consists of two infrared laser sources, one operating at a wavelength of 1064 nm and the second at a wavelength of 1319 nm. The light from these two lasers is overlapped spatially and temporally in a non-linear optical crystal (such as lithium triborate or LBO) to produce a sum frequency mixing product at 589 nm.

The power required for the IR laser sources is determined primarily by the efficiency of the sum frequency generation (SFG) process. While non-linear materials have been experimentally demonstrated that can produce higher conversion efficiencies, the most proven material remains LBO. Single pass conversion in LBO has efficiencies of ~35%, while resonant enhancement designs can have efficiencies of ~65%. Table 10 lists the IR power levels required to obtain 50 watts at 589 nm for these two conversion schemes.

Since the SFG process requires one photon at each input wavelength to produce one photon at the sum frequency, an optimum condition for operation of the SFG is obtained by adjusting the power levels of the two inputs to yield a photon balanced condition, that is, the power of the 1064 nm source is set to 1.24 times the power of the 1319 nm source.

Table 10. IR laser powers for various SFG efficiencies to give 50W SFG output.

SFG Configuration	Estimated Conversion Efficiency	Total IR power	1064 nm power	1319 nm power
Single pass	35%	143	79	64
Resonant enhancement	65%	77	43	34

An important characteristic of a laser system for guide star applications is a stable output power and frequency. Stable power is particularly important for wavefront sensing configurations that require

subtraction of the Raleigh scattered flux to improve the quality of the wavefront sensing. In the SFG process the output frequency and power stability are determined by the stability of the inputs, and for the wavelengths of interest for the infrared sources there are two alternatives for high stability and stable frequency operation: mode locked lasers or single frequency lasers.

At the infrared wavelengths of 1064 nm and 1319 nm, it is relatively easy to build a solid state laser using optically pumped Nd:YAG as the gain medium in conjunction with an external cavity. In CW operation the output of such a laser consists of a number of frequencies each corresponding to one of the axial modes in the cavity. Each mode has random phase with respect to any other mode, and while the power output of this laser appears continuous, over time the phase relationships of the modes will vary, resulting in interference between them and a corresponding fluctuation in the laser output. By using active mode locking, a technique to modulate the gain of the laser cavity in synchronization with the round trip time, the laser output becomes a well-defined pulse with a repetition rate equal to the round trip time and with a stable amplitude. For a given laser configuration the output spectral bandwidth of the mode locked laser is determined by the width of the pulse. Maximizing power output and stability tends to favor narrower pulse widths, resulting in a correspondingly wider bandwidth.

Mode locked oscillators, such as the oscillators used in the current LMCT design, are capable of relatively high power outputs, from tens to hundreds of watts, but they typically have output spectral bandwidths of 500 to 1500 MHz.

Single frequency operation requires that only a single laser mode be allowed to propagate in the laser cavity. One commonly used design for single frequency lasers is the non-planar ring oscillator or NPRO. These are easily tuned and reliable devices, but only produce low output powers, typically less than 1 watt. The have very narrow output line widths of 10 KHz or less.

While a mode locked oscillator could be used directly to drive the SFG process, as the power levels increase the beam quality of the laser tends to decrease. The efficiency of the SFG process is directly affected by the beam quality and matching of the input beams, and as a result current implementations use mode locked oscillators in conjunction with optical power amplifiers to reach the required power levels for the SFG output.

The optical power amplifier is pumped with light from high power laser diodes. The energy supplied to the gain medium is released by stimulated emission at the wavelength of the input laser beam. Efficient operation of optical power amplifiers requires that the input beam extract most of the pump power in order to prevent spontaneous emission in the amplifier, this becomes a particular problem when operating at 1319 nm. This leads to a relatively high input power requirement for the first stage of laser amplification, typically 10 to 15 watts minimum. In properly designed amplifiers the output beam quality is determined primarily by the input beam quality, and with careful attention to detail reasonable performance can be obtained.

As a result, since a mode locked power oscillator offers relatively high output power, it is well suited to optical power amplification, and the resulting systems using several stages of optical amplification can easily reach the power levels required in Table 10 for single pass SFG operation.
In the laser systems currently being developed for the Gemini South Observatory and the Keck I telescope, mode locked oscillators followed by power amplifiers provide the IR sources, and single pass SFG is used to generate the 589 nm output. The single pass SFG configuration is relatively tolerant with respect to input beam quality, with the SFG process acting as a "spatial mode cleaner" due to the fact that the non-overlapping portions of the input beams are not converted.

As noted earlier, lasers that offer single frequency operation such as the NPRO have lower power outputs, making them ill-suited as the input to an optical power amplifier. An alternative approach is to injection lock a high power oscillator using a single frequency laser such as an NPRO. By injection locking a slave laser, such as a ring laser, the slave laser is forced to operate on a single mode at the same frequency as the injection laser. This approach is used in single frequency laser system in operation at SOR. In this laser system design two injection locked lasers are used in conjunction with a resonant enhancement SFG. A fundamental requirement of such a design is precise mode matching between the two input beams and the resonant SFG cavity. This leads to a requirement for essentially diffraction limited performance for both injection locked oscillators and results in very high output beam quality from the SFG.

As can be appreciated from Table 10 the two approaches differ significantly in terms of IR power requirements, and therefore in terms of operating efficiency. In addition the two approaches are likely to differ in output beam quality, and are clearly differentiated by their output spectral bandwidths.

The literature contains a number of discussions of the photon return efficiency of various laser systems. The largest uncertainty in the current understanding is the degree to which optical pumping occurs with a narrow bandwidth source and circular polarization.

In July 2005 a simultaneous projection test of the Gemini North and Keck II laser systems was conducted. Each Observatory made observations of both projected spots. The results are summarized in KAON-419. Based on these results the return efficiency for the Gemini North laser system was 22 photons/s/cm^2/W. This is a mode locked laser system with an output spectral bandwidth of ~1 GHz. This is approximately twice the return efficiency of the Keck II dye laser.

For the single frequency laser system we reference the results of tests at SOR in the latter half of 2005. It appears that all of the reported results are for powers measured prior to the laser beam transport and launch optics, so for comparison with the Gemini North results, and with the methodology employed in the NGAO simulations to compute launched laser power we have corrected the reported power values by assuming launch path transmission of 82%.

Using results reported for circular polarization in this time period and correcting for the presumed launch path transmission, we obtain a range of photon return efficiencies from 90 to 229 photons/s/cm^2/W. The mean of four reported values is 146 photons/s/cm^2/W, while the mean of the

range of values given in the conclusions is 162 photons/s/cm^2/W after correction for launch path transmission. As a result we have adopted an "average" photon return of 150 photons/s/cm^2/W for a single frequency laser system with circular polarization.

The laser power required is determined from the NGAO system design error budget assumptions as follows:

1. Total guidestar photon return at the top of the atmosphere: 14868 photons/s/cm^2
2. Photon return efficiency: 150 photons/s/cm^2/W
3. Uplink transmission losses for an observation at a 30º zenith angle: ~34%

This leads to a requirement of 150 watts total laser power, and for the purposes of this discussion we assume that this will be provided by three 50 watt lasers for the reasons given above. It should be noted that for cost reasons the NGAO system design also considers a possible phased deployment of lasers, starting with a 100 watt total power requirement delivered by two 50 watt lasers, and then adding a third 50 watt laser at a later time.

The key NGAO system requirements that are flowed down to the baseline optical performance requirements for the NGAO laser systems are as follows:

1. 150 watts total laser power, 50 watts per laser
2. Beam transport via either free space or single mode optical fiber
3. Tunable off the sodium lines for Rayleigh calibration
4. Emission compatible with the NGAO passbands
5. The optical requirements for the NGAO laser systems are driven by the assumption of a return efficiency of 150 photons/s/cm^2/W. As discussed in the section on return efficiency, to date this performance has only been achieved by a single frequency laser system with 10 MHz line width and a circularly polarized beam derived from a linearly polarized output with a high degree of polarization purity. The photon return assumption also implies precise tuning to the peak of the sodium D_{2a} line. While this also appears to down select to the SOR laser system design, it is conceivable that a single frequency design could evolve from the technologies used in the laser systems under development for the Gemini South Observatory and the Keck I telescopes.

A more extensive treatment of laser systems for NGAO, including baseline requirements for all of the essential parameters (optical, mechanical, etc.) may be found in KAON-582.

3.4.3 Laser Enclosure and Beam Transport Mechanical Design

The choice of laser will significantly impact the location of the laser on the telescope and the approach to laser beam transport. In the absence of a specific laser selection we have had to evaluate several location and transport options. The favored location for beam transport simplicity and for maximizing the laser power delivered to the sky would be on the elevation moving portion of the telescope, or even behind the telescope secondary mirror, if the laser could be compact enough and could accept a changing gravity vector. Alternatively the laser would be located on the azimuth

moving portion of the telescope. A third option of locating the laser off the telescope, as done for the majority of the Keck II laser, would be the option of last resort.

The favored beam transport approach because of its simplicity, especially if the laser can not be on the elevation ring of the telescope, is to use single mode hollow core photonic crystal fibers to transport the light to the launch telescope located behind the secondary mirror. However our current baseline assumes that a multiple mirror based beam transport system would need to be implemented.

The expected size of an LMCT-type laser will likely require it to be located on the part of the telescope that does not move in elevation. On the other hand the short pulse laser format may allow the use of single mode fiber transport since the pulse duration is too short to excite stimulated Brillioun scattering in the fiber. The more compact size of an SOR-type laser may allow it to be housed on the elevation moving portion of the telescope, assuming that a changing gravity vector can be made acceptable, but the continuous wave laser format is not compatible with fiber transport.

The laser enclosure conceptual design is discussed in KAON 570 and KAON 564. Three cases were considered during the system design. All three cases include beam transport concepts that do not rely on fibers. For reference, the Keck II telescope including the existing AO and laser enclosures and laser launch tube are shown in Figure 35.

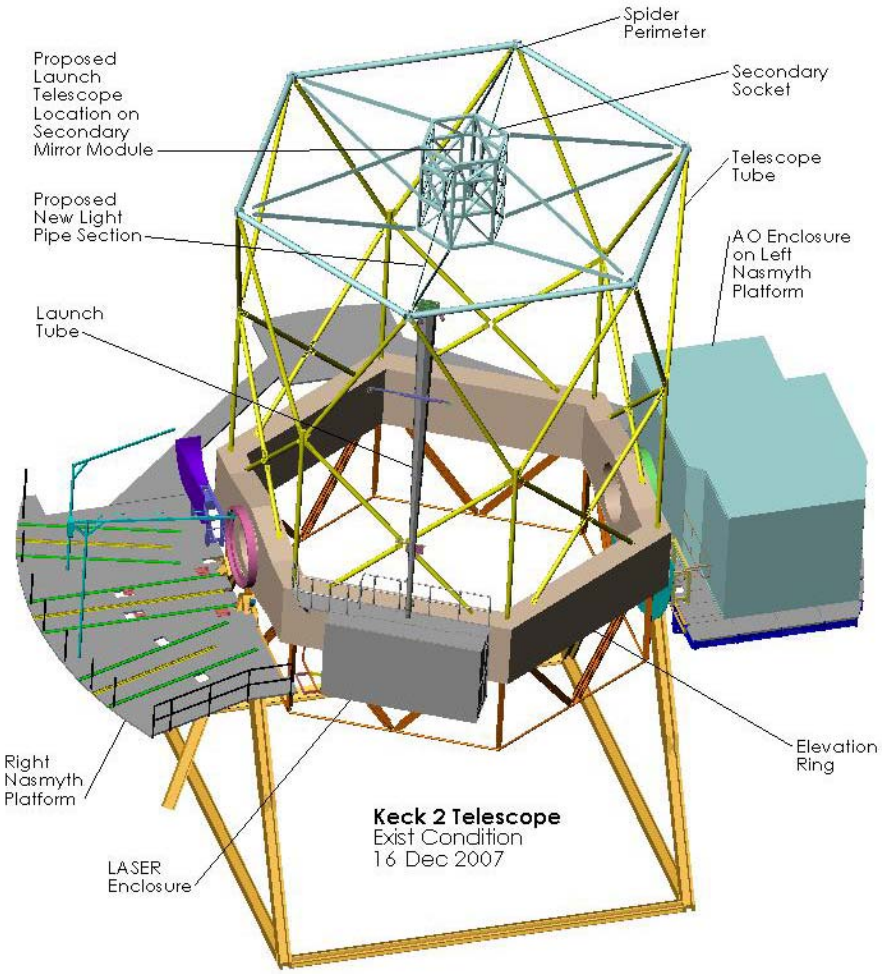

Figure 35. Existing Keck II Telescope and laser location case 1.

The first case considered is for a laser that can operate with a changing gravity vector. In this case the laser could be mounted on the elevation ring of the telescope. One option would be to house the laser in the existing laser enclosure on the right-front wall of the elevation ring (assuming it meets the size and weight restrictions). The laser electronics that do not have to be co-located with the laser could be housed in an electronics enclosure on or below the left Nasmyth platform, similarly to the existing auxiliary laser electronics and cabling would run through one of the existing elevation cable wraps. The laser transport optics and beam path could be enclosed in a tube running up the telescope tube to the perimeter of the spider (similar to the existing launch tube) and across to the launch telescope behind the secondary mirror.

If the laser cannot be tilted then it needs to be housed on the part of the telescope that moves in azimuth. Two options were considered for this scenario. The ideal option of transporting the laser beam onto the elevation portion of the telescope along the elevation axis was not considered since this axis is blocked by the AO system on the left Nasmyth platform and NIRSPEC and DEIMOS on the right Nasmyth platform.

One option would be to house the laser in the existing AO electronics or a new room at this location as shown in Figure 36. The NGAO electronics could then be housed in a new enclosure under the Nasmyth platform. The laser beam could then be directed out through the enclosure roof and folded toward a gimbaled mirror at the elevation ring edge of the enclosure roof. This mirror would track as a function of telescope elevation to maintain the beam centered on a gimbaled mirror at the top of the spider which would in turn track to maintain the beam direction toward the launch telescope behind the secondary mirror. A telescoping tube between the two gimbaled mirrors could be used to enclose the beam as the distance between the gimbaled mirrors changed versus elevation.

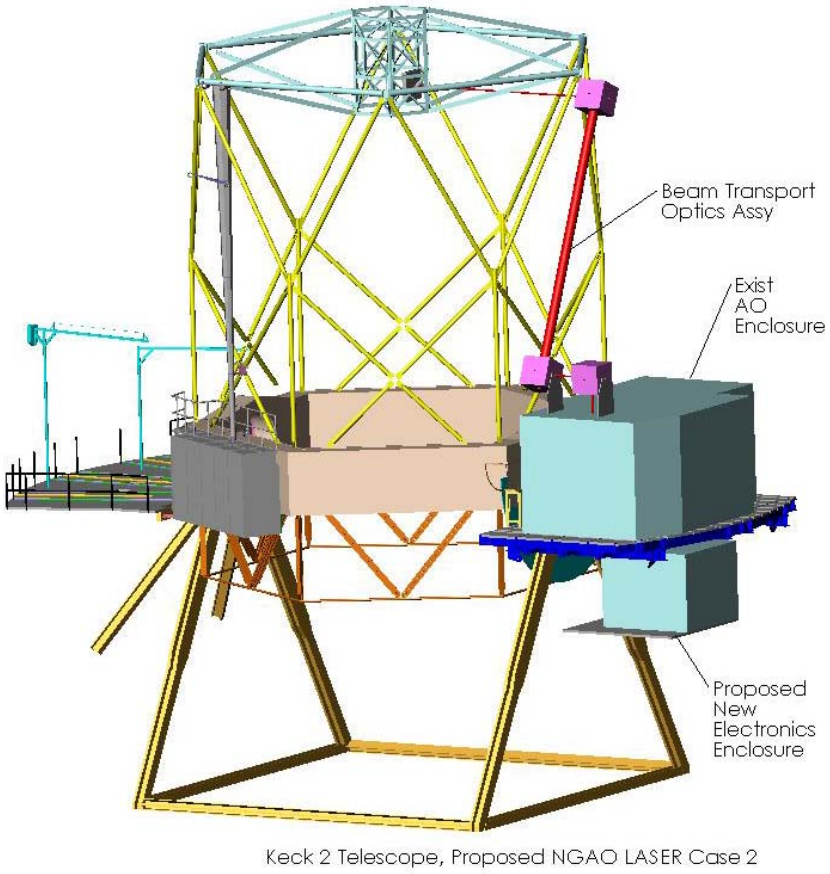

Figure 36. Laser location case 2.

The second option considered would be to build a new platform and laser enclosure between the existing left Nasmyth and Cassegrain platforms as shown in Figure 37. The beam transport system in this case could be similar to that proposed in case 2 with the addition of an extra fold mirror on the top of the new laser enclosure to fold the beam to a fold mirror on top of the AO enclosure.

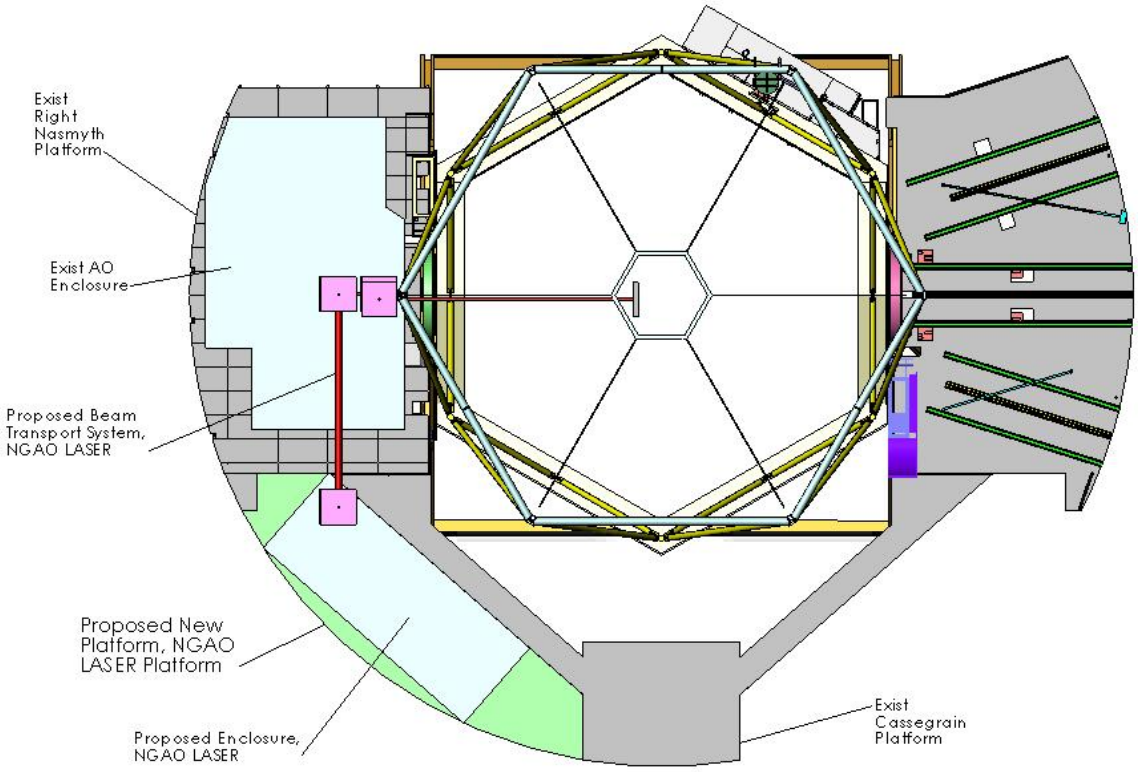

Figure 37. Laser location case 3.

If the laser were to be mounted on Keck I instead of Keck II the same options as above would exist, except that for case 1 there is no existing laser enclosure on the elevation ring. In addition, a laser enclosure has been implemented on the right Nasmyth platform of the Keck I telescope as shown in Figure 38 and Figure 39 that could potentially be reused for the NGAO lasers. The laser bench accommodates a 20W LMCT laser.

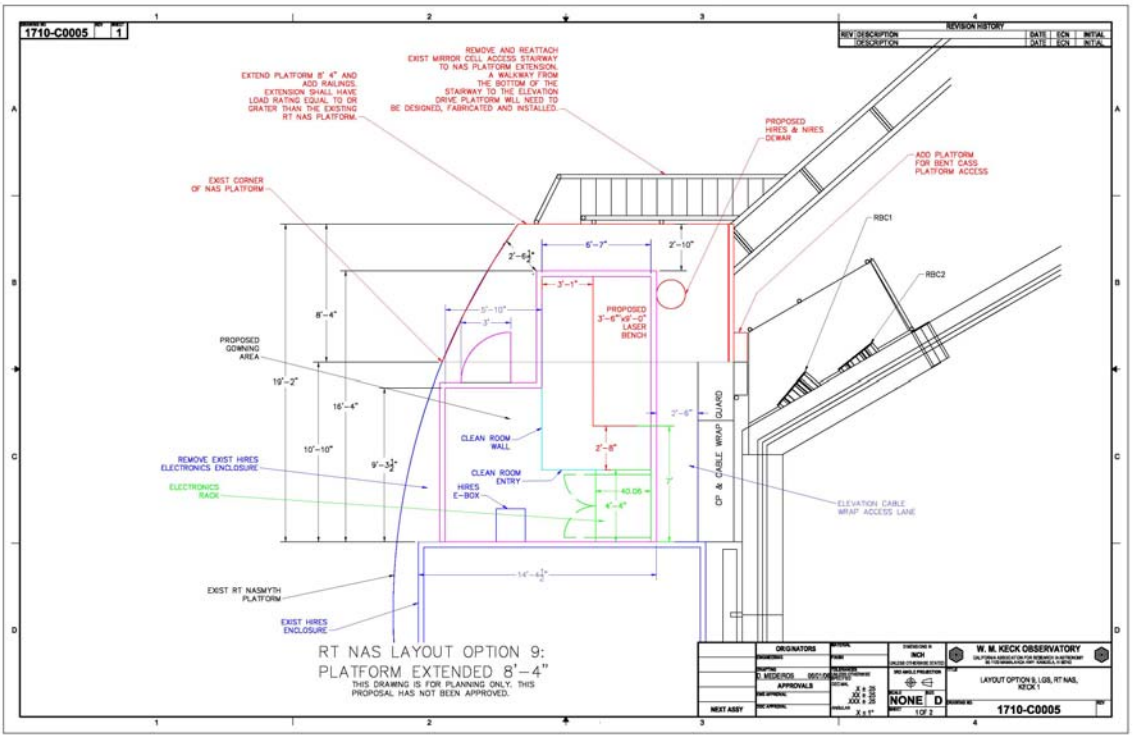

Figure 38. Laser enclosure location on the Keck I right Nasmyth platform.

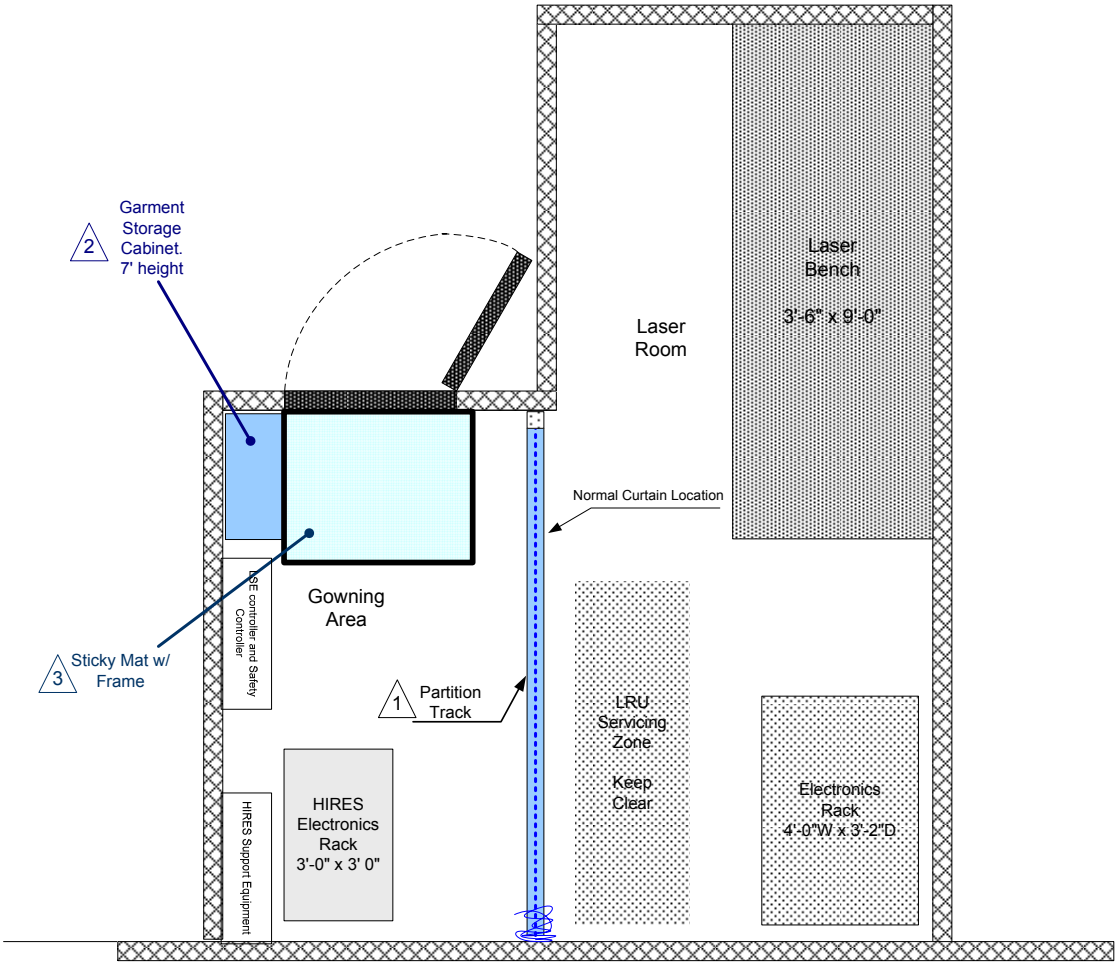

Figure 39. Keck I laser enclosure.

As partly illustrated in Figure 37, the laser enclosure will house also house heat exchangers and power supply racks for the laser, optics for the beam transport system, the safety system and the beam transport control system electronics. Estimated sizes of the components in the laser enclosure are given in KAON 570. Since the heat exchangers, electronics rack, and the beam control system will put sizeable amounts of heat into the environment, the laser enclosure will need to be thermally isolated and temperature controlled. Provisions must also be made for personnel to operate in this environment. With the heat exchangers and electronics rack, provisions will be necessary for vibration isolation of these units. The heat exchangers will have pumps and motors while the electronics system will contain fans for cooling. Vibration must be controlled since these components will be on the telescope. From a safety point of view, the interior of this room will be exposed to laser radiation. This enclosure must be light tight with proper engineering controls to not allow laser radiation to escape.

A second enclosure will reside within the telescope secondary module. The laser launch telescope will interface to this module for mechanical support and receive the laser beams and project them to the sky. The enclosure's functions are to provide a suitable environment for the beam splitters and

beam steering systems that format the beams into the appropriate LGS asterism. The enclosure also provides a mechanism to contain the laser light from these subsystems. This enclosure will need to be thermally isolated since it is in the secondary module and is likely to produce more than the allowed 100 W radiated into the dome environment. This heat can be reduced via glycol cooling. Vibration mitigation is not expected to be needed at this location since liquid cooling is expected to be the primary heat removal element.

Glycol cooling will be the primary heat removal medium for this system. Figure 40 shows the components requiring glycol. Glycol will be pumped from the mechanical room through the telescope to laser enclosure, the secondary of the telescope. The bulk of the cooling will be needed to operate the two laser heat exchangers. Estimates of the heat capacities are provided in KAON 570.

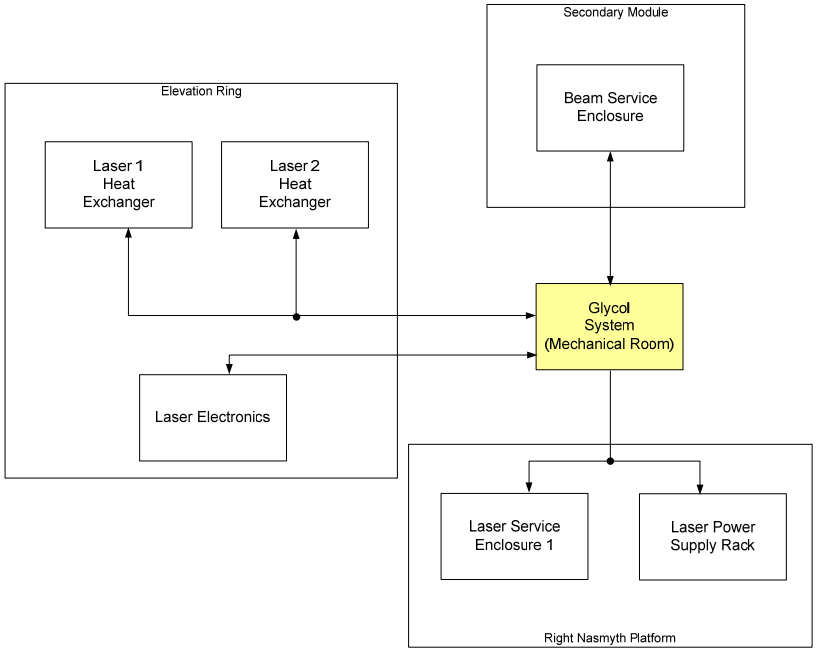

Figure 40. Glycol cooling for the laser system.

3.4.4 Laser Safety System

The safety system will assure the entire laser system and its components will operate to maintain a safe environment for personnel, as well as equipment. The safety system is shown in Figure 42. To make the determination to shutter laser light, the safety system will sense environmental changes or user commands from the Laser System Interface (see section 3.5.2.2.2). Termination of laser radiation will be done at different locales depending on the threat of laser radiation. At the laser, it will close the laser shutters prior to the beam relay system or turn off power to the entire laser system. At the beam steering system, it will close a final shutter prior to launching of the beam into the beam telescope. To make proper determination, the safety system will sense inputs from the laser, beam steering system, glycol system, laser enclosures, aircraft detection and spotter system, and user inputs via the Laser System Interface.

In addition to terminating laser radiation, the safety system will also provide laser status for personnel entering laser zones that may be hazardous. This will ensure laser or summit personnel will not accidentally walk into exposed laser radiation. The safety system controller is expected to be a programmable logic device. It will sense inputs from multiple subsystems on and off the telescope, as well as commands via the network from the Laser System interface.

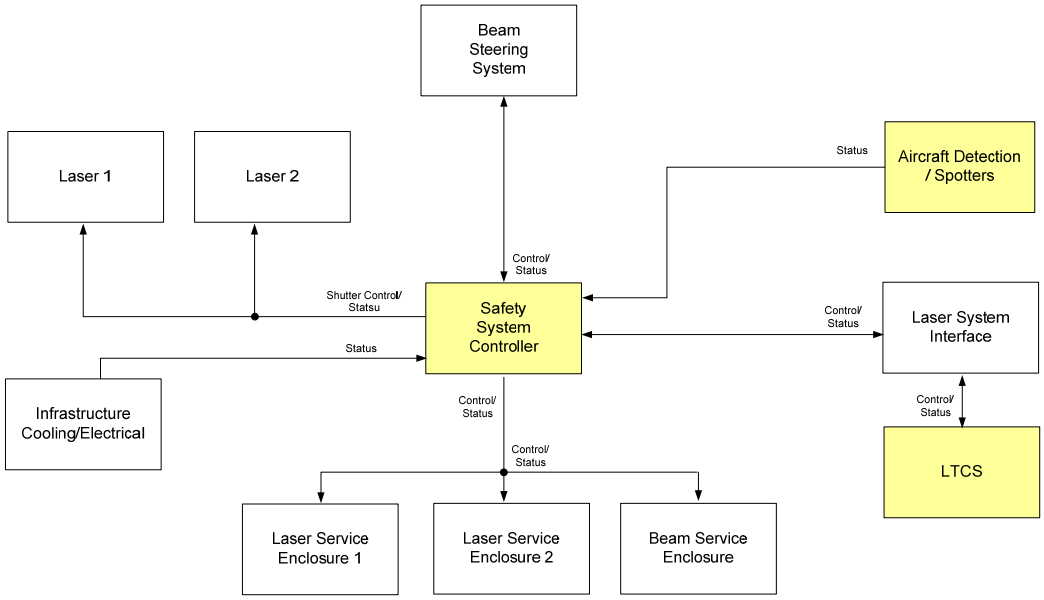

Figure 41: Safety system.

The Keck safety officer, Steve Shimko, has made a preliminary analysis of the increased safety hazards with the NGAO lasers. The increase in power from current systems with 10-20 W to a future system with three 50W lasers means that the potential for property damage and personnel injury is increased proportionally. In addition, the power of IR pump beams will also be increased over corresponding beams in the current lasers. The NGAO lasers will be class 4 lasers, the same as the current Keck lasers. As such, the laboratory engineering controls and procedures are the same as any class 4 laser controlled area. Measures include door interlocks, lighted signs, laser protective eyewear, written procedures, and training. For the large diameter beams leaving the laser launch telescope, the Nominal Hazard Zone (NHZ) for diffuse reflections is essential zero. In contrast, specular reflections would have a very long Nominal Ocular Hazard Distance (NOHD) for the NGAO lasers. As with any sodium Laser Guide Star in navigable airspace, the beam(s) are a threat to aircraft. This will require safety observers and annual request to the FAA for a letter of no-objection. These are currently the standard practices at the observatory for LGS operations. A complete safety analysis would be completed as part of the planning for the laser installation.

Aircraft safety for Keck LGS AO observations is currently provided by aircraft spotters as recommended by the FAA. WMKO recently began working with the G10-T Laser Safety Hazards subcommittee of the Society of Automotive Engineers that sets the relevant aircraft safety standards used by the FAA. This committee has decided, based on a presentation by Paul Stomski (a WMKO staff member), to address the issue of facilitating a consistent approach to approving control

measures. This opens the door to approval of automated aircraft detection systems that do not require spotters or radar. Gemini Observatory is developing an all sky camera for aircraft detection that will be implemented as a shared resource on Mauna Kea.

We will use the same procedures for satellite avoidance and for not interfering with the observations of other Mauna Kea telescopes as are currently used for Keck LGS AO observations. A discussion of the impact on observing efficiency of these items, and potential changes, are discussed in section 3.6.1.2.

3.4.5 Laser Upgrades and Advanced Technology

KAON 570 also briefly discusses the following technologies that could potentially provide large performance gains for NGAO including dual wavelength lasers, fiber lasers and fiber transport, pulsed laser formats and uplink AO. Because of the uncertain or unproven performance of these technologies they have not been selected in our baseline design. We will continue to follow these technologies to determine if they may become appropriate.

3.5 Control Electronics and Software

This part of the design manual, derived from KAON 569, is broken into three sections: the overall controls infrastructure, the non-Real Time Control (RTC) control and the RTC control.

3.5.1 AO Controls Infrastructure

The entire NGAO system can be viewed as a distributed controls system, in which many different components communicate with each other in various client/server or master/slave relationships using possibly several communication networks and protocols. Figure 42 shows a high-level abstraction of the NGAO system control.

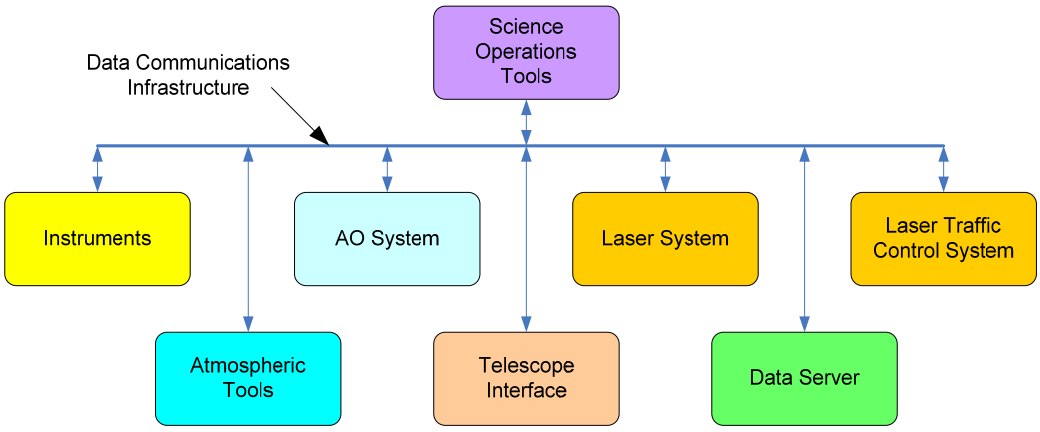

Figure 42. A distributed controls system block diagram of the NGAO system.

Each block in the diagram represents a set of control functions peculiar to a particular system or subsystem that can logically be grouped together. The grouping is an abstraction, as the various functions represented by each block may actually be implemented using multiple software and

hardware components that are also distributed. The primary data communications paradigm used by the NGAO system components has not yet been specified however, it is likely that it will be the keyword system already employed at the observatory.

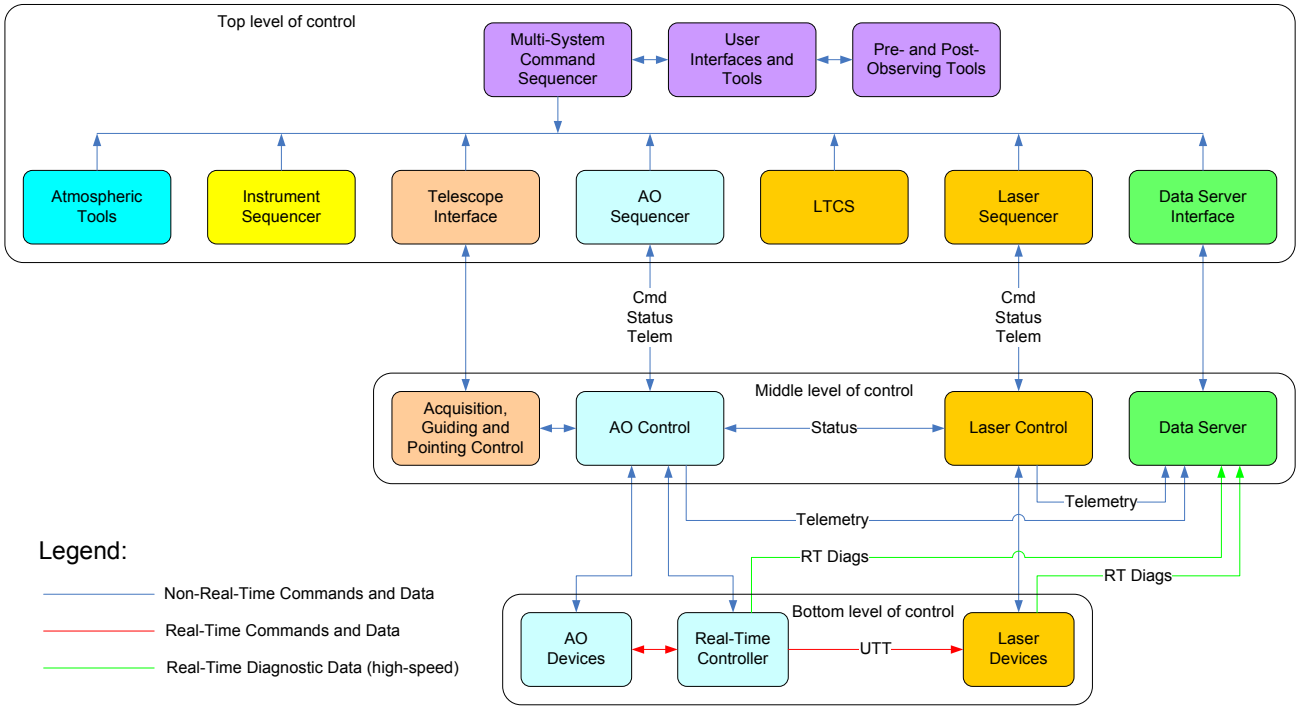

Figure 43. AO controls infrastructure block diagram.

A more detailed block diagram of the AO infrastructure is shown in Figure 43 where the control systems are represented by a hierarchy. At the top level are the main interfaces to the various subsystems (some of these interfaces are referred to as sequences in the diagram). All user commands to the subsystems pass through these top level interfaces. The middle level of the hierarchy represents an abstraction of more complex lower level control tasks, namely the basic control functions for that subsystem. Users do not access the system at this level except for engineering or troubleshooting purposes. Finally, at the bottom level of the hierarchy are the devices controlled by the control system themselves. These three levels of hierarchy will be discussed in more detail.

3.5.2 Non-real-time Control

3.5.2.1 Electronics

Two categories of electronics are discussed: motion control and device control electronics.

3.5.2.1.1 Motion Control Electronics

A preliminary spreadsheet has been developed to document the large number of motion control devices. This will also be used in the preliminary design phase to document their requirements

(range, accuracy/repeatability, run-out, etc.). The laser system architecture is less well determined than the AO architecture at this point, so the laser system motion control requirements can only be estimated. The devices requiring motion control listed in the spreadsheet are organized according to the following breakdown (degrees of freedom required shown in parentheses):

- Vibration sensor (3 DOF)
- Calibration source (4 DOF)
- Rotator (1 DOF)
- LGS WFS assembly (61 DOF)
- Dichroic changer (2 DOF)
- Interferometer pickoff, pointing and centering (5 DOF)
- Acquisition camera pickoff, focus (2 DOF)
- LOWFS assembly (22 DOF)
- NGS WFS and truth sensor (14 DOF)
- Visible imager (5 DOF)
- NIR imager (3 DOF)
- OSIRIS pickoff (1 DOF)
- Laser pointing and centering (36 DOF)
- Laser constellation generator (19 DOF)
- Other laser motion control (11 DOF)

Although still preliminary, the total number of degrees of freedom requiring motion control is approximately 190. The existing Keck AO optics bench has on the order of 40 devices requiring motion control, compared to ~125 for the NGAO optics bench. Moreover, many of the assemblies with multiple devices require complex and coordinated control. A key task during the preliminary design will be to simplify the design to minimize the complexity of the motion control requirements.

Another key preliminary design task will be to develop a comprehensive motion control philosophy and architecture for the system, which will include:

- Selection of a motion control architecture (i.e., distributed vs. centralized servo control)
- Standardization of motors and servo amplifiers
- Specification of the motion control electronics to be used
- Location of the electronics relative to the AO system components and the cold room
- Motion control system reliability

Standardization of the motion control architecture will greatly simplify the design and implementation of such a large number of motion control devices.

3.5.2.1.2 Device Control Electronics

The remaining electronics in the AO system can be characterized as device control electronics. This consists of detector, mirror, real-time controller and environmental control. This basic device control includes power control, initialization, basic parameter control, etc.

The devices to be controlled are as follows:

- Detectors
  - Vibration sensor
  - LGS WFS cameras (9)
  - NGS acquisition camera
  - LOWFS tip-tilt sensors (2)
  - LOWFS TWFS camera
  - LOWFS TTFA camera
  - NGS WFS camera
  - NGS TWFS camera
- Mirrors
  - Woofer DM/TT
  - Tweeter DM/TT
  - LOWFS DM/TT (3)
  - d-IFS DM/TT (6)
  - UTT mirror (1 or 9)
- RTC control
- Environmental control
  - Power
  - Temperature
  - Humidity
  - Particulates
  - Instrument glycol or other cooling
- Laser system control
  - Diagnostics cameras
  - Power and environmental control

These devices have not yet been specified, so it is difficult to define the electronics control required. Based on past experience, we expect that two or three hard-real-time controllers (e.g., VxWorks VME crates) will be required for the AO system, and one or two for the laser system. We also expect that one or two soft-real-time controllers (e.g., Unix workstations) will be required for the AO system and at least one for the laser system. A number of miscellaneous analog and digital IO cards will be required to interface the various electronics devices to the control systems. One or more Unix workstations or VxWorks VME crates may be required for camera control.

3.5.2.2 Software

3.5.2.2.1 AO System Software

Figure 44 shows a block diagram of the AO system control hierarchy. The top level of the hierarchy is the AO sequencer, which is the main interface between the AO controls and the rest of the NGAO system. The intermediate level shows the main control functions grouped by control type and the bottom layer shows the devices that are to be controlled.

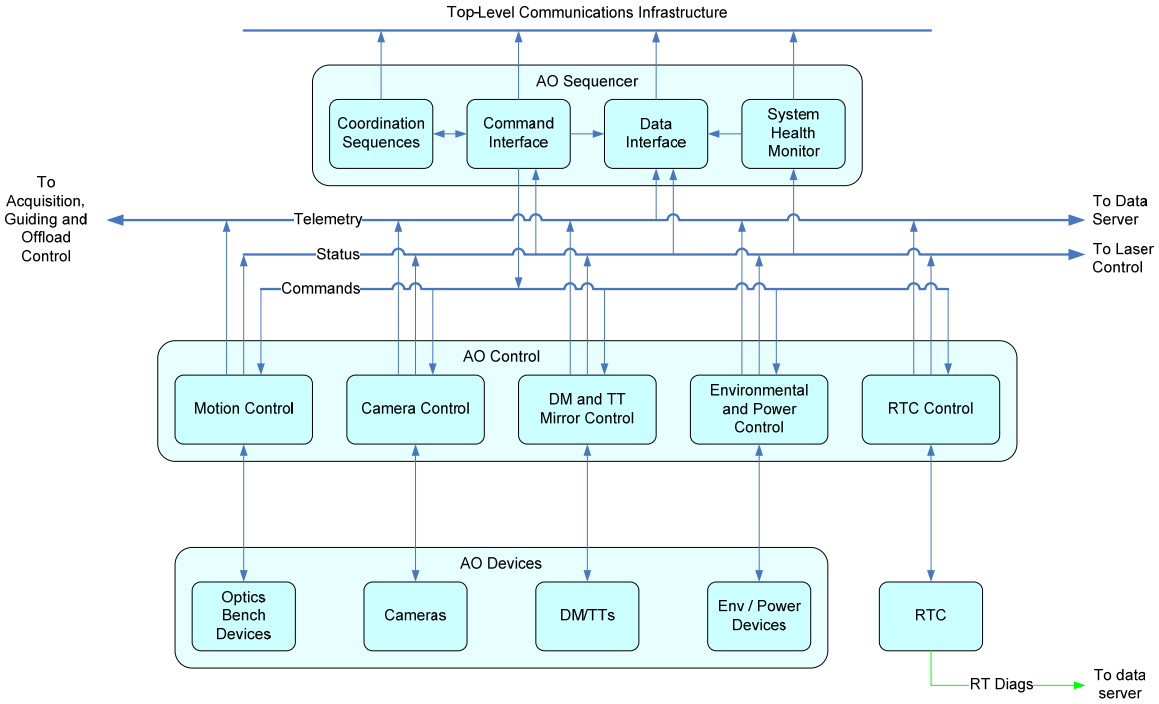

Figure 44. AO systems control hierarchy block diagram.

3.5.2.2.1.1 Sequencer

The AO sequencer is the main interface between the AO controls functions and the rest of the NGAO system. The sequencer has four main components: a command interface, a set of coordination sequences, a data interface and a system health monitor. The grouping of these functions into a "sequencer" is an abstraction, as they may be implemented using multiple software and hardware components that are distributed. Those tasks requiring only soft-real-time control will most likely be implemented on Unix workstations, while those tasks requiring hard-real-time control will likely be implemented using VME crates and CPUs running VxWorks and EPICS (or some similar controls architecture). The use of the term "hard-real-time" refers to the type of control where timing and response times are critical to correct control and operation of a particular device.

The functions of these four main components are as follows:

- Command interface. The command interface represents the main interface for the AO controls. In the current AO system, it consists of the basic interfaces to the devices to be controlled (e.g., keywords, EPICS). This is the most basic command interface for parameter updates and commands not requiring any kind of complex coordination or monitoring.
- Coordination sequences. The coordination sequences are a collection of state machines which implement complex sequences of commands for the underlying control systems. A coordination sequence allows the user to send a simple command to the sequencer, while it performs the many tasks required by this command and returns the status to the user. Examples are: the main AO sequence that is used to startup, initialize, standby, and shutdown the system; and a setup sequence that sets up the AO bench devices, WFS cameras, and the RTC for a particular observing mode (see KAON 550: System Configurations Spreadsheet).
- Data interface. The data interface is the interface between the rest of the NGAO system and data produced by the AO system, primarily in the form of low bandwidth telemetry and system status data (high bandwidth telemetry data and diagnostic data are available through the data server, discussed later in this document).
- System health monitor. The system health monitor is a task that monitors the status of all the important AO system functions and initiates alarms or other fault indications to the rest of the NGAO system if problems are detected.

3.5.2.2.1.2 Motion Control Software

The motion control software functions are organized as shown in Figure 45. They consist of two main components: the low-level and high-level motion control sequences.

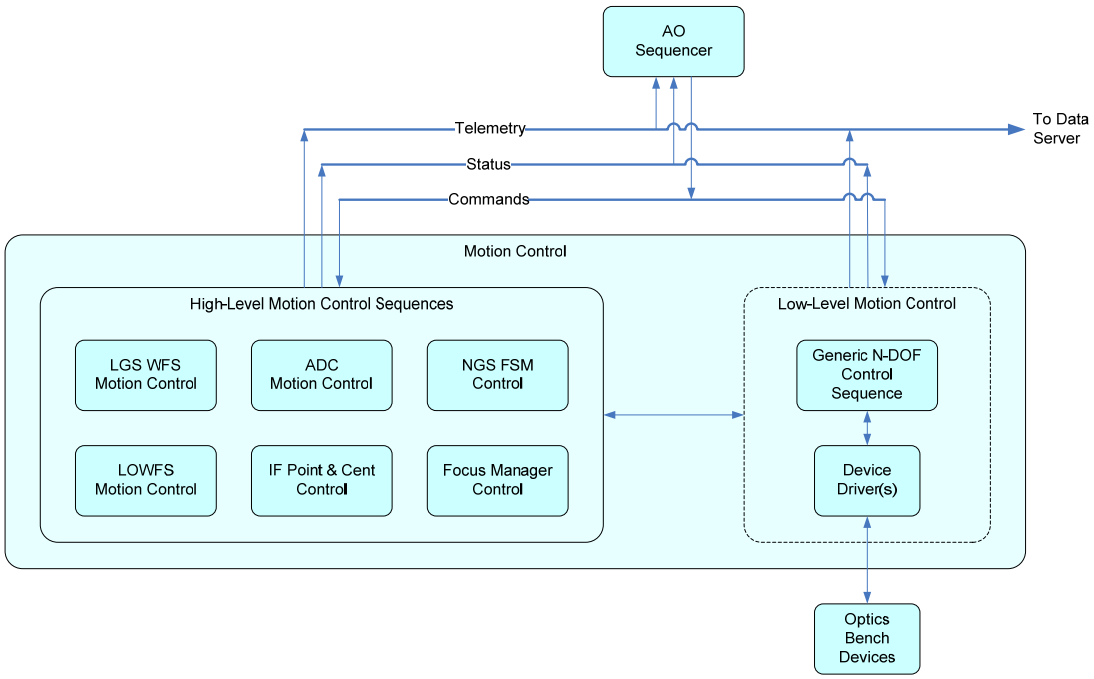

Figure 45. Motion control software architecture block diagram.

The low level motion control functions consist of one or more device drivers that implement an API for interacting with the motion control system to provide the most basic level of motion control. This device driver will most likely be supplied by the manufacturer of the motion control electronics. Layered on top of the manufacturer's device driver will be another driver providing an interface to the AO control system (e.g., EPICS). At the top of this control block is a generic state machine that implements the basic coordinated functions required for controlling a motion control device with an arbitrary number of degrees of freedom. This concept is used in the existing Keck AO system.

The high-level motion control sequences are a set of state machines that implement the complex coordinated control required by many of the assemblies in the AO system. They accept high level commands from the AO sequencer and issue the appropriate commands to the low-level motion control block described above. The sequences will be implemented using a state machine compiler (e.g., EPICS State Notation Language, or the generic state machine compiler developed at Keck). The high level motion control sequences identified thus far are:

- LGS WFS: Coordinated control of the LGS WFS assembly housing 9 wavefront sensors and their associated optics.
- ADC: Generic control for the ADCs used throughout the AO system.
- FSM control: high-level control for the NGS WFS and interferometer field steering mirrors used in coordination for target offsets and dithers.
- LOWFS: Coordinated control of the LOWFS assembly housing the various TT, TTFA, and TWFS sensors and their associated optics.
- Focus Manager: Coordinated control of focus throughout the AO system.

The LGS WFS and interim LOWFS motion control sequences will be the most difficult due to the large amount of motion control and present some level of risk. The arms must be prevented from colliding with one another, which implies that the motors cannot move through their entire range of motion during startup, as is done with devices in the current AO system.

3.5.2.2.1.3 Device Control Software

The device control software functions implement the remaining control blocks in the intermediate control level shown in Figure 44. The main control functions are: camera control, DM/TT control, environmental control, and RTC control. A block diagram illustrating the generic control paradigm for a number of devices is shown in Figure 46. At the bottom level are device drivers that implement a low-level application programmer interface (API) allowing basic control of each device. These device drivers are usually provided by the manufacturer. Layered on top of these device drivers, also at the same low level, are drivers for the AO control system (e.g., EPICS). If control system drivers do not exist for the device drivers or cameras, they will have to be written. The upper level consists of one or more control sequences (state machines) for each device that provide a high-level of control to implement coordination of complex tasks and sequences of commands.

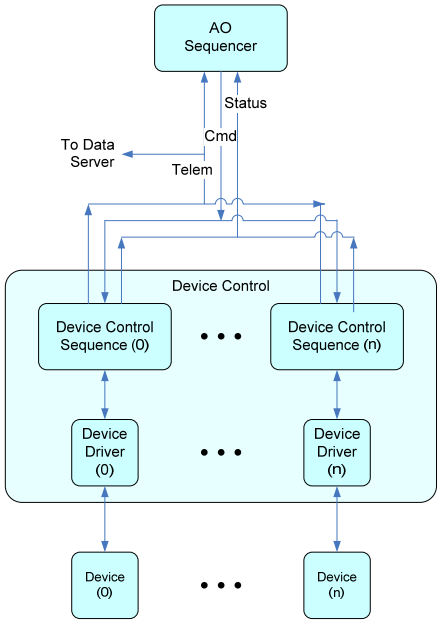

Figure 46. Generic device control paradigm block diagram.

At a minimum, all devices will require some generic functions: start up, initialize, stand by, shut down, etc. The specific devices to be controlled and the control functions we have identified thus far are listed below.

- Camera control
  - Devices: Vibration sensor, wavefront sensors, tip-tilt sensor, acquisition camera
  - Control functions: Frame rate, exposure time, program select, background recording, flat field recording
- Mirror control
  - Devices: Woofer and tweeter DM/TT, LOWFS/d-IFS DM/TT, LGS TT
  - Control functions: voltage control for mirror drive amplifiers (ramp up/down, relay control, etc.)
- Environmental control
  - Devices: controllers for power, temperature, humidity, particulates, instrument cooling, etc.
  - Control functions: Basic parameter control
- RTC control. RTC control RTC device control refers to basic control and parameter passing for the RTC itself. Low level communication will be provided by a device driver which will implement the RTC command set. Any higher level coordination required will be implemented using state machines. Commands similar to the following are expected:
  - Loading DSP & FPGA code
  - Setting scalar parameters (e.g., loop gains)
  - Setting array parameters (reconstruction matrix, centroid origins, servo control laws, etc.)
  - Compute interaction (system) matrix

3.5.2.2.2 Laser System Software

A block diagram of the laser system control hierarchy is shown in Figure 47. The functions of the various levels are similar to those described earlier for the AO system. The laser system controls are responsible for controlling the laser optical devices (beam transport control), the laser device itself, the laser cameras, environmental and power control, and possibly, depending on its architecture, the laser safety system as well.

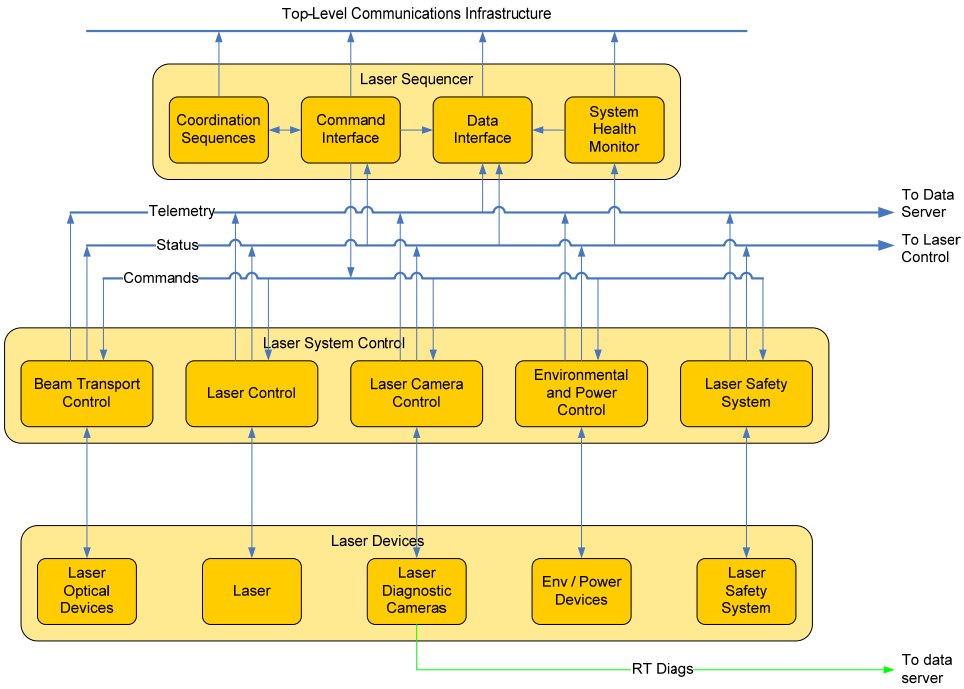

Figure 47. Laser system controls hierarchy block diagram.

3.5.2.2.2.1 Laser Sequencer

The laser sequencer is similar in design to the AO sequencer discussed above and is not discussed in detail here. A key task during the preliminary design will be to identify all of the coordination sequences required for the laser sequencer and their requirements.

3.5.2.2.2.2 Laser Motion Control (Beam Transport Control)

The laser motion control software functions are organized as shown in Figure 48.

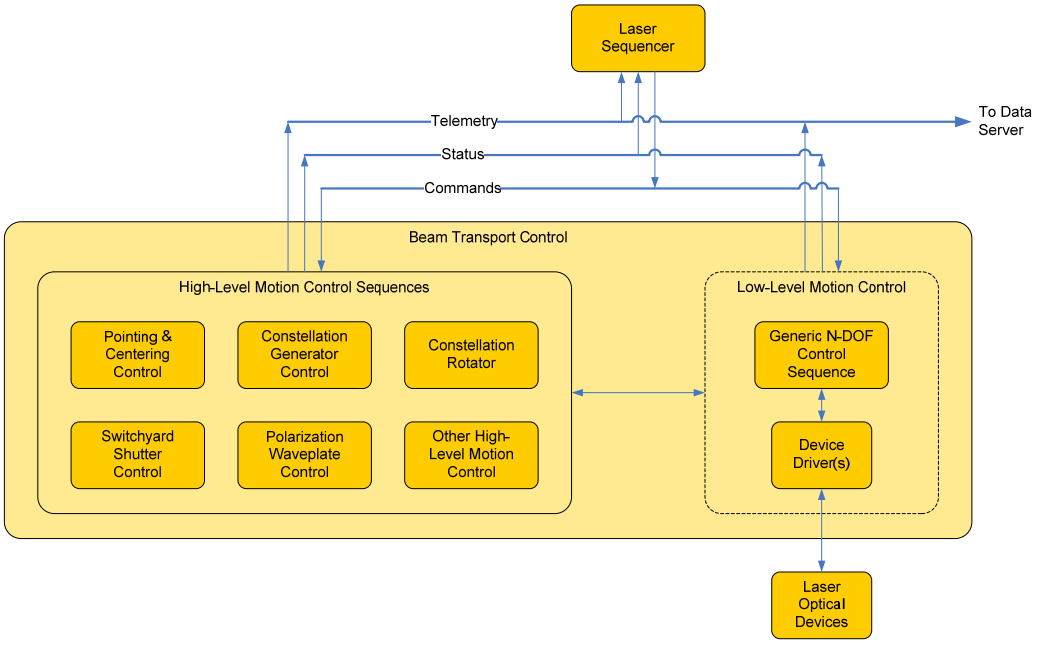

Figure 48. Laser motion control software architecture block diagram.

The low-level motion control functions are similar to the ones discussed earlier for the AO system and are not discussed further here. The same low-level software developed for the AO low-level motion control functions will likely be reused here.

The high-level motion control sequences are a set of state machines that implement the complex coordinated control required by some of the assemblies in the laser system. They accept high level commands from the laser sequencer and issue the appropriate commands to the low-level motion control block. The sequences will be implemented using a state machine compiler (e.g., EPICS State Notation Language, or the generic state machine compiler developed at Keck). The high level motion control sequences identified thus far are:

- Pointing and centering: coordinated control of the 9 laser beams to compensate for flexure due to the changing gravity vector when the telescope moves in elevation.
- Constellation generator: coordinated control of the 9 laser beams to position the lasers as required in the asterism.
- Constellation rotator: coordinated control of the overall rotation of the asterism to keep it fixed on the sky or stationary as required by the particular observing mode.
- Polarization waveplate control: coordinated control of the polarization waveplates to provide polarization control for each of the 9 laser beams.
- Shutter control: coordinated control of the many shutters in the laser switchyard.

3.5.2.2.2.3 Laser Device Control

The laser device control software functions implement the remaining control blocks shown in Figure 47. The main control functions are laser control (control of the laser device), camera control, environmental control, and control of the laser safety system. The device control paradigm and camera and environmental control functions are similar to those described for the AO system. Wherever possible, common camera and environmental control software will be used to support the AO and laser systems. The remaining functions are laser control and laser safety system control:

- Laser control. We assume that the laser will be provided with a software interface that allows for the basic passing of commands and return of status data. We may have to provide a driver to interface the laser to our controls system architecture (e.g., keywords, EPICS). We will also develop coordination sequences (state machines) to coordinate complex sequences of commands to simplify the command and user interface to the laser.
- Laser safety system control. Control of the laser safety system refers to basic control and parameter passing for the laser safety system itself. The control interface consists of a device driver to provide a control interface to the safety system (e.g., EPICS), and possibly some high-level coordination sequences that will be part of the laser sequencer to coordinate sequences of complex safety system commands.

3.5.2.3 Acquisition, Guiding and Pointing Control

A block diagram for the Acquisition, Guiding, and Pointing Control function is shown in Figure 49. The control consists of two main functions: acquisition and guiding, and pointing control. The functions will be implemented in some combination of hard-real-time and soft-real-time control applications.

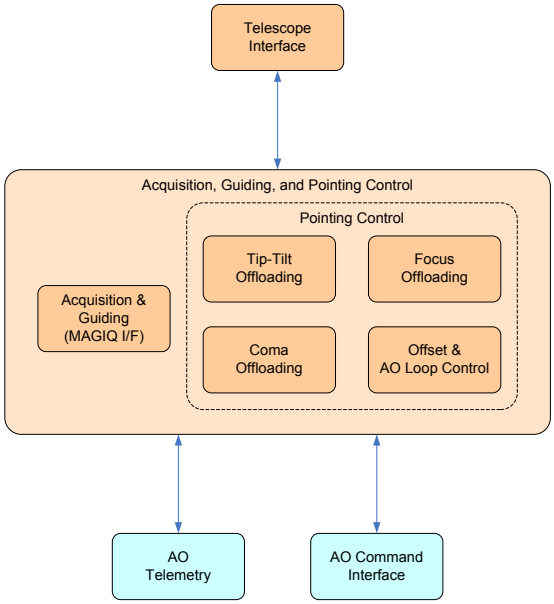

Figure 49. Acquisition, guiding and pointing control software architecture block diagram.

The acquisition and guiding control block is the interface between the AO system and the new Keck standard MAGIQ guider. It represents the hardware and software "glue" required to connect the acquisition camera to the MAGIQ guider system used at the observatory. Some upgrades to the MAGIQ system may be required to support all of the NGAO acquisition requirements. See section 3.6.2.4 for more details on acquisition.

The pointing control function is the interface between the AO system and the pointing functions of the telescope. This includes pointing offsets for tip-tilt and coma offloading, secondary offsets for focus and coma offloading, and an offset control that interfaces to the AO loop commands to control the AO system during telescope offsets and dithers. The offload functions take the appropriate AO telemetry as inputs and compute the required pointing and secondary offsets.

3.5.2.4 Data Server

A block diagram of the data server is shown in Figure 50. The server consists of a dedicated server-class CPU and RAID storage system and data recording and server tasks. The data recording hardware interfaces are expected to be similar to those of the existing AO system telemetry server, which uses a fiber channel interface for high speed data and GBit ethernet for the moderate and slow speed data. The data recording task receives data from the recording interfaces and stores it directly into a database on the RAID storage system. The server task supports remote connections and near-real-time query capability of the database through the data server interface.

The data storage requirements for the system are expected to include the following:

- High speed telemetry and diagnostics data from the real time controller
- WFS, acquisition, and truth sensor camera data
- TT sensor data
- System configuration and parameter data

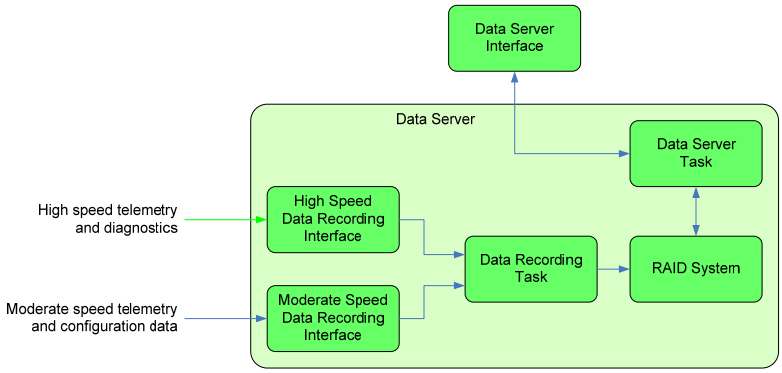

Figure 50. Data server architecture block diagram.

The requirement for the long term data storage is yet to be defined. The tools that will make requests to the data server are the NGAO diagnostic tools, the performance and system monitoring tools, the

PSF reconstruction tools, and the data storage and delivery tool (tool that sorts out and manages the data that will be stored and the data the observer will take home).

3.5.3 Real Time Control

3.5.3.1 Introduction

The Real Time Controller (RTC) is a specialized computer system designed to perform all of the wavefront sensing, tomography calculations, and deformable mirror control processing at rates that keep up with atmospheric turbulence induced optical aberrations. The RTC data flow and computer architectures have been designed to achieve the tomography precision, noise suppression, and bandwidth requirements implied by the science-case driven wavefront error budgets.

An equally important consideration in the RTC design is the need to keep the cost and complexity manageable. Simply scaling earlier implementations of single conjugate AO RTC reconstructors using traditional central processing units (CPUs) is infeasible because of the multiplying effect of multi-guidestars and multiple deformable mirrors on computer speed requirements. To address this issue, we have taken advantage of the parallelizability of wavefront reconstruction and tomography algorithms and mapped them on to a massively-parallel processing (MPP) compute architecture. This architecture scales in size and complexity much more favorably than doing the same calculations on CPUs, and can be readily implemented with commercial off the shelf technology building blocks called field programmable gate arrays (FPGAs). Additional details of this design approach are given in a later section on implementation later in this report, and given in still greater detail in KAON 553.

We first describe the main line real-time tasks that the RTC must perform. Then we describe the essential ancillary support tasks relevant to the RTC such as communicating with the supervisory controller configuration and calibration information, providing offload signals, and providing diagnostic data. In the final section we explain the MPP implementation, describing processor hardware, interface hardware, and software development methodology.

3.5.3.2 RTC Tasks

The RTC, at the core, performs the following tasks in LGS mode:

- Accept digitized pixel data from the LGS WFS and LOWFS, and perform basic image processing (dark and bias subtraction, flat-fielding).
- Calculate wavefront tilts from the LGS WFS and LOWFS using a choice of noise-optimal centroiding algorithms, and compensate for non-linearities in the centroiding methods.
- Reconstruct wavefront phase at each sensor and transmit this information to the tomography processor.
- Use cone-beam projection tomography techniques to reconstruct the three-dimensional volume of atmospheric index-of-refraction variations above the telescope and over the field of view of interest, given the wavefronts from various directions as measured by each wavefront

sensor. This algorithm also takes inputs from the tip/tilt and tip/tilt/focus/astigmatism sensors to break volume solution ambiguities inherent in laser wavefront measurements.

- Integrate through the volume of index estimates along paths to the science instruments – either on-axis for the narrow field science modes, or along up to six different directions for the deployable integral field spectrograph science mode.
- Compensate for deformable mirror influence functions and nonlinearities, deriving voltage commands for the DMs given desired wavefront distortion corrections to be placed on them. Split the control between commands to the tip/tilt mirror, low-order (woofer) DM, and high order (tweeter) DMs.
- Incorporate control compensation dynamics to keep the system stable and achieving a given temporal bandwidth.

In LGS mode the RTC also computes high-order wavefront control commands for DMs in the tip/tilt sensors, sharpening the IR tip/tilt stars.

In natural guidestar (NGS) mode, the RTC acts as a traditional single conjugate AO system. It takes inputs from one natural guidestar wavefront sensor, reconstructs the wavefront, and computes commands to be split up amongst the tip/tilt mirror, woofer DM, and tweeter DM in the narrow field science path.

All these RTC tasks take place at the frame rate of the fastest wavefront sensor camera, up to 2,000 frames per second.

As shown in the Figure 51 schematic, large chunks of compute tasks are associated with either wavefront sensors or DMs and thus can be parallelized across them. Thus some of the dedicated processing units will be assigned specifically to hardware. Furthermore, algorithms within the subunits, as well as within the tomography unit itself (Figure 52), are highly parallelizable when implemented in the Fourier domain, and thus will each map onto an MPP architecture as described earlier.

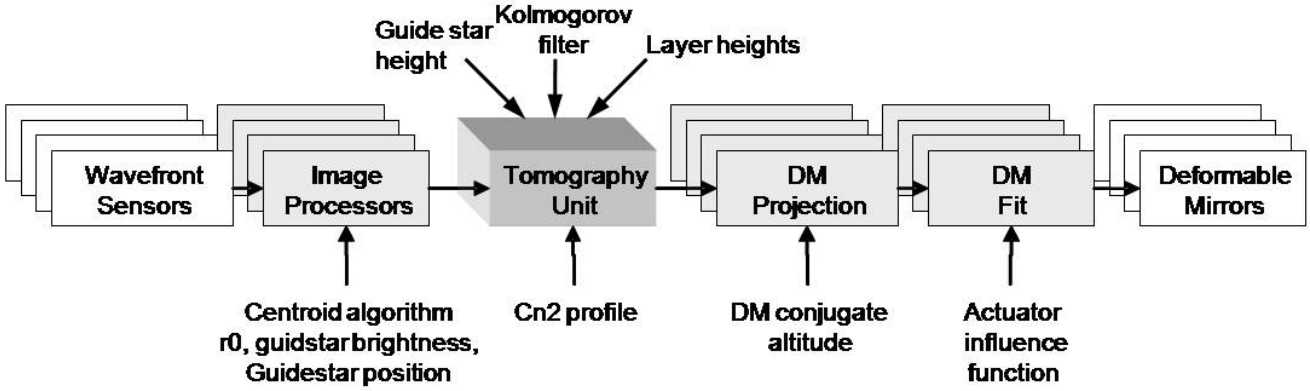

Figure 51. Multi-guide star tomography data flow and parallel processing.

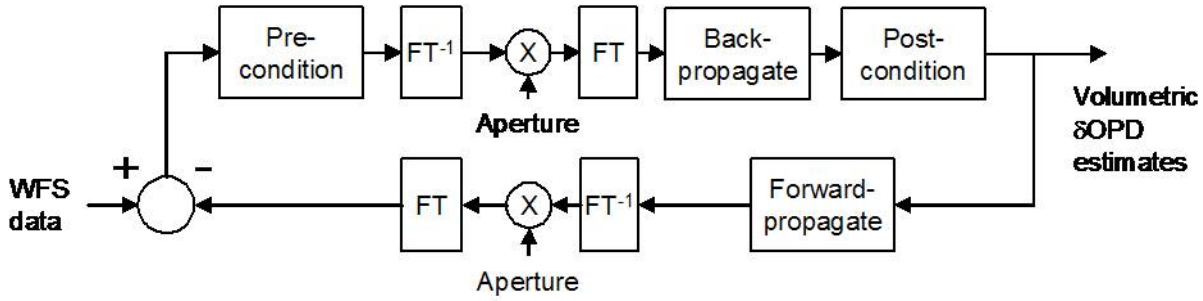

Figure 52. Tomography algorithm.

3.5.3.3 Parametric Input, Optimization, and Reconfigurability

3.5.3.3.1 Minimum Variance Reconstruction Optimization

The RTC algorithm computes the statistical minimum variance solutions for wavefronts at each science instrument, given the measured wavefront data from the guide stars. The minimum variance solution depends on certain a-priori data, which the RTC accepts as parametric input. These include:

- Volumetric turbulence strength (Cn2 profile, discretized at layers)
- Number of layers of turbulence
- Brightness of guide stars
- Wind speeds at layers

Cn2 can be provided either as a-priori input, or as derived from external measurements, for example, from a MASS/DIMM sensor. The preparation and processing of this data is left to the external supervisory control system; the RTC simply takes in a set of normalized Cn2 strength numbers, one per layer, at a rate that is slow (say once/second) with respect to the real-time tasks. As an option, the RTC's tomography engine will provide statistical average rms aberrations resolved by layer, which can be used to adjust Cn2 profile numbers dynamically.

Similarly, wind speeds can be incorporated from external data or deduced internally from past histories of estimates.

3.5.3.3.2 Calibration Parameters

Truth wavefront sensors will provide long-term average wavefront data designed to normalize out systematic biases due to either non-common path optical aberration or Hartmann sensor biases due to variations in the sodium layer thickness and altitude. The RTC will process these wavefront sensor data like any other wavefront sensor and use the results to adjust zero-set points in the overall reconstructor.

In a like manner, prior measurements will have determined calibration set points for each wavefront sensor, giving the definition of a "flat" wavefront for each sensor. The set points for LGS wavefront sensors will depend on field position and zenith angle. Thus the multi-system command sequencer,

with knowledge of the telescope and AO system configuration, will periodically update the RTC wavefront sensor sub-processors as to which parameter set to apply to the wavefront reconstruction.

3.5.3.3.3 Reconfiguration

The processing units and algorithm will be made reconfigurable to allow for each of the observing modes envisioned for NGAO. Configuration parameters include:

- Number and field-positions of laser guide stars.
- Number and field-positions of tip/tilt guide stars.
- Field position of TTFA (tip/tilt/focus/astigmatism) sensor.
- Field positions of deployable integral field science wavefront correctors.

Furthermore, the scalloped pupil of the Keck primary mirror will rotate with respect to the wavefront sensors and DMs in some science observing scenarios. The wavefront and tomography reconstructors utilizes a model pupil as a "valid data" mask, so this model will be set and updated at the appropriate rate within the RTC.

3.5.3.4 Interfaces

3.5.3.4.1 Offloading

The RTC will provide offload signals to the telescope so that the high speed wavefront controllers don't saturate. The offload signals flow to the non-RTC supervisory controller at a relatively low data rate, on the order once per second. Offloading signals include:

- Tip/tilt to the telescope guider.
- Focus to the secondary piston.
- Other low order modes TBD to the telescope primary segment control system.

3.5.3.4.2 Diagnostics and Telemetry

Diagnostic data is defined as data intended for monitoring the health of the RTC and AO system, and for display to the operator. Centroid data from wavefront sensors, signals going to DMs, and other indicators are transmitted at relatively low, human readable, data rates to the external systems.

Telemetry data is defined as up to full-frame rate streaming of portions or all of the intermediate data to high-speed data capture units. This data is useful for a number of post processing tasks such as

- Debugging or tuning of parameters.
- Analysis of seeing conditions and performance of the AO system.
- Point spread function determination.

Data that would be streamed for data capture include:

- All wavefront sensor centroids, intensities, and wavefront sensor reconstructed phases.

- All tip/tilt and TTFA sensor centroids and intensities.
- All commands to the DMs and tip/tilt mirrors.
- All tomography volume estimate data.
- Ancillary information associated with the operations so as to be able to reconstruct the state of the RTC at the time, including internal data tables, Cn2 numbers, wind numbers, calibration sets etc.

Additional data storage capability will be needed to record full frame rate raw pixel data from the wavefront and tip/tilt sensors.

3.5.3.4.3 Command State

The RTC at any time will be operating in one of a number of possible states. Examples of such states include:

- Narrow field science LGS AO control (hybrid closed loop on the woofer and open loop on the narrow field tweeter and tip/tilt and TTFA tweeters).
- Wide field science LGS AO control (hybrid closed loop on the woofer and open loop on the deployable IFS unit tweeters and tip/tilt and TTFA tweeters).
- Narrow field science NGS AO control (closed loop on the woofer and tweeter).
- Control on tip/tilt only.
- Calibration modes (for alignment/registration, push matrix generation, linearity calibrations).
- Uncontrolled or idle, with static values as loaded for the DMs and tip/tilt mirrors.

The supervisory control system will transmit the state transitions to the RTC which will configure accordingly (and also report back its state on demand). The maintenance of state transition rules will be the responsibility of the multi-system command sequencer.

Additional flags will be maintained for turning on and off various diagnostic and telemetry streams.

3.5.3.5 Implementation

3.5.3.5.1 Algorithms

Algorithms for wavefront phase reconstruction from Hartmann slope data have been analyzed since the beginning days of AO. We anticipate using a modern fast-iterative technique such as the ones described in references 1 and 2. Such techniques can take advantage of parallelism if they are implemented in the Fourier domain. Regularizations taking into account the signal-to-noise of the measurement and filters for suppressing the waffle mode can also be implemented in the Fourier domain. The pupil boundary conditions (outside of which the measurements must not be assumed as zero but allowed to be free variables) force the algorithm to be iterative as described in the above references, but 3-5 iterations using a Fourier-domain pre-conditioned conjugate gradient (FD-PCG) method have been shown to be adequate for meeting our error budget.

Inverse tomography algorithms using wavefront measurements from multiple directions have been developed recently (see references 2 and 3). These methods are also made parallel through the use of the Fourier domain but again must be iterated because of the finite spatial extent of the pupil-apertured data. Again, the FD-PCG method has proven adequately stable and rapidly converging in simulation studies (KAON 475).

Finally, fitting the deformable mirror to the desired wavefront correction can be accomplished with parallel processor implementations that carry an inverse model of each DM.

- MEMS open loop control is decoupled into a linear cross-coupling, which is solvable in the Fourier domain, and independent nonlinear functions for each actuator, solvable with nonlinear lookup tables in parallel. The MEMS are repeatable go-to devices and this open-loop model has been proven to be quite accurate (see reference 5).
- The woofer DM, likely a piezo-actuator device with cross-coupling and hysteretic effects, will be controlled via a linear Fourier domain deconvolution only. We will rely on the fact that this mirror is in "closed loop" (upstream of the wavefront sensors) and so any residual mis-fitting will be measured and sent to the more accurately responding tweeters. Bandwidth shouldn't suffer because the woofer is correcting the lower order, and hence slower evolving, atmospheric modes.

More details on algorithm implementation are given in KAON 553.

3.5.3.5.2 Hardware

The multi-processor units are implemented as banks of field-programmable gate arrays (FPGAs) arranged on custom circuit boards. The technology of FPGA programming has advanced to the point that the design and configuration of these boards, intimately coupled to the algorithm distribution on the processor chips themselves and data flow needs, is accomplished entirely using standardized computer aided design and simulation tools. The details of distributing the NGAO RTC architecture onto these processor units are given in KAON 533, sections 4 and 5.

The processor units end up being many repetitions of identical processing elements, making them interchangeable and therefore easy to spare. Except for specialized I/O interfaces, the boards can be configured to process wavefront sensor data, do a piece of the inverse tomography, or process DM commands.

3.5.3.5.3 Hardware Interfaces

High throughput I/O must be used to get data from wavefront sensors to processor units and DM command data to the D/A converter hardware associated with each DM or tip/tilt mirror. Similarly, high throughput I/O must be used to get telemetry data to data storage units. For the most part, industry standard hardware is now commonly available that will handle our anticipated data rates, and an industry standard protocol (LVDS) is called out in the conceptual design. These data interconnects will be implemented on reliable high speed interconnects, such as fiber optic links.

3.5.3.5.4 Programming and Design Process

There are a number of FPGA manufacturers and each has commercial design packages to aid in the design of the programming and interconnections. MPP programming is in common practice today in industry and the required skills are taught in university computer and electrical engineering courses.

3.5.3.5.5 Physical Implementation

Space, power usage, and thermal load considerations are taken into account in the design. We have estimates of these for the conceptual NGAO RTC implementation (KAON 533 Table 5-6) which will be refined as we make trades and design choices in the later system design phases. The physical parameters are expected to be compatible with locating the RTC in a separate electronics enclosure located on the Nasmyth platform.

3.5.3.6 References

1. Vogel, C. R.; Yang, Q., *Multigrid algorithm for least-squares wavefront reconstruction*, **Applied Optics IP**, vol. 45, Issue 4, pp.705-715, (2006).
2. Gilles, Luc; Ellerbroek, Brent L.; Vogel, Curtis R., *Preconditioned conjugate gradient wave-front reconstructors for multiconjugate adaptive optics*, **Applied Optics**, Volume 42, Issue 26, pp. 5233-5250, (2003).
3. Gavel, Donald T, *Tomography for multiconjugate adaptive optics systems using laser guide stars***,** Advancements in Adaptive Optics, **Proceedings of the SPIE**, Volume 5490, pp. 1356-1373 (2004)
4. Gavel, Donald; Reinig, Marc; Cabrera, Carlos***,*** *Fast hardware implementation of tomography for multi-guidestar adaptive optics*, Astronomical Adaptive Optics Systems and Applications II, **Proceedings of the SPIE**, Volume 5903, pp. 138-147 (2005).
5. Morzinski, Katie M.; Gavel, Donald T.; Norton, Andrew P.; Dillon, Daren R.; Reinig, Marco R., *Characterizing MEMS deformable mirrors for open-loop operation: high-resolution measurements of thin-plate behavior***,** MEMS Adaptive Optics I,. **Proceedings of the SPIE**, Volume 6888, pp. 68880S-68880S-12 (2008).

3.6 Science Operations

This section discusses the hardware and software needed to control the overall NGAO facility for science operations at both the operator and astronomer levels and the pre- and post-observing support tools.

3.6.1 Science Operation Model

The overall goal of NGAO science operations is to maximize the science return from the allocated observing time, given i) the science cases, ii) a performance budget for the instrument suite, iii) an operation-cost for the Observatory and iv) a scientific skill set for the astronomers. There exists a

wide range of science operations models to accomplish this overall goal, as a function of the instrument functionalities, the Observatory budget and the *modus operandi* and size of the scientific community.

Two important aspects were studied during the system design: the observing model and the science operation requirements.

3.6.1.1 Observing Model: classical with built-in flexibility tools

A trade study of possible observing models was performed in KAON 476: it recommended that NGAO science operations be following the Keck classical observing model. NGAO nights, particularly LGS nights are scheduled and allocated 6-month in advance. Astronomers, assisted by Keck Observatory support personnel, are performing the observations remotely either from Keck HQ or from a partner institution: the astronomers-observers are therefore fully engaged in their observations and can make on-the-fly decisions for the observing strategy.

The suite of NGAO pre-observing tools including simulation and observations planning tools should allow the astronomer to easily and quickly assess the feasibility of a scientific program during the observing proposal submission phase or any phase prior to the observations, and make the best use of the allocated time. Astronomers will want to adapt the scientific program with the observing conditions for the scheduled observing night(s). Using the planning tools, they can make on-the-fly decision on the observing strategy and take advantage of the various observing configurations with NGAO: NGS/LGS switch, AO science instrument switch, non-AO instrument switch during any night.

One of the risk encountered with the classical observing model is that the data collected be not complete (e.g., due to bad weather or low observing efficiency) preventing the astronomers from fully exploiting the data and publishing, resulting in a lower science return and visibility for the AO instruments. Our model trade study proposes a scenario that can be phased in with NGAO science operations with low impact on the Observatory support: Each TAC may decide to encourage its astronomers' pool to collaborate for a subset of TAC-allocated nights: the scientific programs could be ranked as a function of required observing conditions, and be given observing priorities till the data is complete. This level of schedule flexibility would likely benefit the overall science return while maintaining Observatory operation costs. The flexibility and scheduling burden would be distributed among the astronomers within the partner institutions. The experiment could be stop at any time should it be not satisfying.

3.6.1.2 Science Operation Requirements: Observing Efficiency

The requirements from the NGAO science cases (KAON 455) and the observing scenarios for these science cases (KAON 571) led to a set of requirements for the science operations from the astronomer point-of-view that are detailed in the System Requirement Document - SRD (Sect. 6.1.4 in KAON 456). In addition, we have reported on the lessons learned from the LGS science operations at Keck (KAON 463) including weather impact on LGS and observing efficiency budget. From this

report and other sources, we have developed a second set of Observatory Operational requirements for the science operations in the SRD (Sect. 6.2.5 in KAON 456).

One of the most important requirements is the percent of time collecting science quality data. Our goal is to achieve at least 80% open shutter science time for "faint field" observing program (programs requiring 1 to 4 hours of total integration time with individual integration time of > 20 min) and 70 % for "bright field" observing programs (programs requiring less than an hour of total integration time and including many fields through the observing night).

In accounting for the open shutter science time, we make the following assumptions:

- Weather impact is not included in the calculation of the open shutter science time. Time loss due to weather in LGS mode accounts for ~25% of the total allocated time (KAON 463). We will track the statistics from time losses due to weather in both LGS and NGS mode. Yet given the Observatory option for the classical observing model, this loss cannot be accounted against the NGAO science operation efficiency. The weather statistics will be included in more general discussion on observing model.
- Open shutter time spent on science acquisition, centering the object, checking the SNR, etc is considered overhead.
- Open shutter time spent for on-sky telluric, photometry, astrometry, PSF calibration is considered science time but we will keep track of its contribution to the total time.

While developing the observing scenarios (KAON 571), we have created a simple efficiency budget tool (http://www.oir.caltech.edu/twiki_oir/bin/view/Keck/NGAO/NGAOObservingScenarios) that can be used for each science case and provide a preliminary assessment on the observing efficiency. A snapshot of the tool is presented in Figure 53. The estimates for the overhead during the course of an observing program are detailed in KAON 571 for the general observing sequence and in KAON 567 for the acquisition sequence. We have considered minimum, median and maximum estimate for each of these contributions and calculate a weighted average equivalent to $(min + 4*med + max) / 6$. We estimate for the current study that the maximum values represent instances of technical difficulties. Therefore we have not allocated any additional time for technical problems. These estimates have also been checked against current performance.

We can reach ~83% observing efficiency on the d-IFS, including calibrators. There are still a few contributors to the total overhead whose impact is difficult to mitigate. Any dedicated time for calibration standards has a strong impact on observing efficiency since these objects are "bright field" observed for a few minutes (< 5 to 10 min), with ~100% time overheads (slew, acquisition, SNR check, etc). In the Figure 53 example we have estimated ~27 min for any overhead due to the Laser Traffic Control System (LTCS). LTCS interrupts are due to either 1) a plane flying in the vicinity of the beam, 2) beam collision with other telescopes, 3) planned request for no-propagation (closure event) from the Laser Clearinghouse (LCH), and 4) on-the-fly phone call request for no-propagation at all from the LCH. A recent change in the LCH operations could lead to additional time losses.

The number of interrupts due to planes is estimated to ~2 per year, making it a non-issue. The number of interrupts due to beam collision with other telescopes will be reduced once the new "first

on target" LTCS rule is agreed upon and applied for all Mauna Kea telescopes (currently the new rule is used between the Keck telescopes). Under this rule, the first telescope on target gets priority to keep observing (currently telescopes projecting a laser have lower priority and the laser is shuttered for any collision). One gets the most benefit from this rule if it used in parallel with the collision preview tool that can predict the collisions before the telescope slew to a new target, hence allowing the observer to select a target that is clear of "planned" collisions. The benefit from this new rule has yet to be fully assessed.

	A	B	C	D	E	F	G	H
4			Time (min)					
5			min	med	max	(min+4*med+max)/6	Total	
6								
7	Galaxy Field 1	Telescope slew	1	3	6	3.17		
8		Adjust pointing	0.5	1	2	1.08		
9		NGS acquisition	0.5	1	4	1.42		
10		NGAO acq	2	4	6	4.00		
11		Fine centering	1	2	4	2.17	11.83	
12		Ind. Science integration	15	20	30	20.83		
13		Total Science Integration	90	150	240	155.00	155.00	
14		repeat	6	7.5	8	7.44		
15		Re-Fine centering	1	2	4	2.17		
16		# of re-centering	0	2	4			
17			0	4	16	5.33	5.33	
18		Dither/setup/readout	0.08	0.25	1	0.35		
19		x # of repeats	0.48	1.875	8	2.58	2.58	
20								
21	Telluric calibration 1	Telescope slew	0.25	0.5	1.5	0.63		
22		Adjust pointing	0	0	0	0.00		
23		NGS acquisition	0.5	1	2	1.08		
24		NGAO acq	1	2	3	2.00		
25		Fine centering	0	0	0	0.00	3.71	
26		Ind. Science integration	1	2	3	2.00		
27		Total Science Integration	2	4	8	4.33	4.33	
28		repeat	2	2	2.67	2.17		
29		Dither/setup/readout	0.08	0.25	1.00	0.35		
30			0.16	0.5	2.67	0.75	0.75	
31								
32	**Total field #1**	**Total Observing**					183.54	
33		**Total Open Shutter**					159.33	0.87
34								
35	Flux standard	Open shutter				4.33		
36	(eq. to telluric std)	overhead				0.75	5.08	
37		repeat per night					2	
38	**Total Std Flux**	**Total observing**					10	
39								
40	**LTCS interrupts**	ind integration time	20.83	20.83	20.83			
41		re-fine centering	2.17	2.17	2.17			
42		# of interrupt	0	1	3			
43			0	23	69	26.83	26.83	
44								
45								
46								
47								
48	Available hours/night		9.1	10.25	11.3	10.23		
49			546	615	678	613.50	613.50	
50								
51	Number of field/night					3.14		
52								
53								
54								
55								
56	**Efficiency**	**Total Observing**					613.50	
57		**Total Open Shutter**					509.14	
58		**Total overhead**					104.36	613.50
59		**Observing efficiency**					0.83	
60								

Figure 53. Efficiency estimate for the high-z galaxies science case.

The planned LCH requests for closure on a specific target direction can be included the observing planning tool and can result in minimal impact on the observing time losses *as long as they are less than 10 min and rare*. LCH closure requests were rare and insignificant from 2003 to 2007. LCH has recently released its new "SPIRAL 3" software that uses new rules for possible laser impact (not documented), a half-cone angle of 1.5º for the no-propagation zone and estimates no-propagation time windows for a particular direction. This has resulted in a dramatic increase of up to hundreds of events per night. The preliminary assessment of the new operation mode for the LCH is documented

in KAON 578. Tools have been developed by the WMKO AO operations team to minimize the impact. As it stands, this new LCH closures rate would significantly impact NGAO observing efficiency for extragalactic targets. This issue is being addressed by WMKO in collaboration with other Observatories and will require more attention for NGAO.

Last minute phone call request for no-propagation from LCH have a huge impact on efficiency for the given night since this stops all LGS operations for a certain time period. This happens ~ 5 times per year when using LGS 140 nights/year. Last but not least, the ability to abort a science exposure quickly and either get ready for a new exposure or move to a new target faster should contribute to reduce the impact from LTCS events.

3.6.2 Conceptual Design for System Operations

3.6.2.1 Operation Control Infrastructure

For a given observing model, the observing efficiency is *the* important design requirement for the individual components (e.g., reading out the camera) nut mostly for the integrated system (e.g., offset to sky). The current Keck II LGS system feeding NIRC2 or OSIRIS performs routinely with ~ 30 - 50% overhead depending on the science program (KAON 463). Its limited efficiency as an integrated system is primarily due to the serial architecture for the command interfaces between subsystems (AO/laser/telescope/science instruments) and the lack of multi-system coordination sequences.

To address the efficiency requirement with NGAO as an integrated system, we are proposing a new integrated design. Our conceptual design includes 1) a multi-system sequencer for commanding the sub-systems in parallel (e.g., offset the telescope as the science instrument write the FITS file to disk) and 2) a sequencer for each subsystem (AO, laser, science instrument) to quickly and reliably handle complex command for a given subsystem (e.g., set AO subsystem for NGS field acquisition).

The overall control infrastructure is documented in KAON 569. The three main components of the NGAO science operations are:

1. The Pre- and Post- Observing Tools
2. The Operation Control GUIs
3. The Multi-system Command Sequencer

In Figure 54, we present a block diagram for the science operations architecture using a view that complements the architecture information from KAON 569. The configuration for the NGAO and the science instrument depends on the science program and the observing strategy and is determined during the pre-observing phases. Using a set of planning tools, the astronomer will develop the detailed observing plan and save all relevant parameters in configuration files. These configuration files can be loaded by the Operation Control GUIs. From the Operation Control GUIs, the operator and the observer will command & control the observation sequences: AO & science acquisition, system tune-up, observing sequences (snapi, dither, offset, filter, etc). The observation sequences are managed by the Multi-system Command Sequencer (MCS): complex sequences for one subsystem

are handled by the subsystem sequencer (e.g., "setup AO bench for NGS" is performed by the AO sequencer) or executed directly from the MCS for simple command.

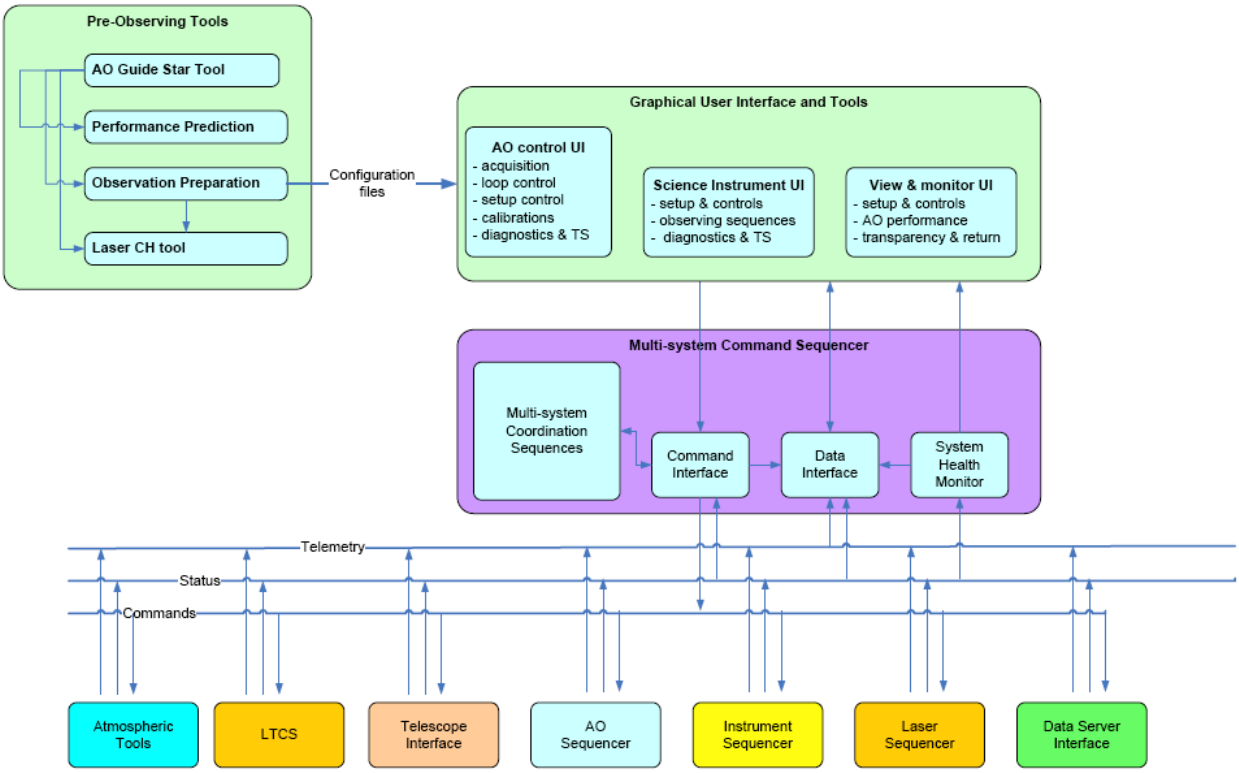

Figure 54. Science operations tools block diagram.

The post-observing tools have been omitted in Figure 54. The pre- and post- observing tools are described in more detail in the next section.

3.6.2.2 System Configurations Matrix

The purpose of the system configuration matrix is to help map requirements to components. The NGAO system configuration is presented in KAON 550 and is partly represented in Figure 55 below. It represents a total of 10 different configurations in NGS mode and 11 in LGS mode for acquisition, calibrations and science observations with one or two of the science instruments (interferometer, visible and NIR camera, OSIRIS, d-IFS). Some of the configurations include more options (e.g., rotator mode in fixed field or fixed pupil, LGS asterisms narrow, medium or wide, etc). This matrix is also key to the design the sequences of commands to the subsystems and individual components during calibrations, setup and observing sequences.

#	Configuration	Science !	Science Field Diameter	Rotator Mode	Projected LGS Asterism	LGS Asterism Rotation	Woofer	LGS dichroic	LGS WFSs	Post Relay 1 Dichroic	Interferometer Fold	NGS Acquis Fold	TWFS Diff Trackin	LOWFS & PSF ADC	LOWFS + Tweeter	1st relay Truth Sensor
NGS Science Modes																
2a	**Interferometry** of			Fixed field						transmit /						
2b	bright on-axis NGS	H - L	! 2"	Fixed pupil			Yes	Out		vis reflect	Mirror	Out				
3	Dual star **Interferometry**	H - L	! 60"	Fixed field			Yes	Out		transmit / vis reflect	Mirror	Out				
4a			! 30"	Fixed field												
4b	**NIR Camera**	z - K	! 2"	Fixed pupil			Yes	Out		Mirror						
5a			! 30"	Fixed field												
5b	**Visible Camera**	I - Y	! 2"	Fixed pupil			Yes	Out		Mirror						
6a			! 30"	Fixed field												
6b	**OSIRIS**	z - K	! 2"	Fixed pupil			Yes	Out		Mirror						
7a			! 30"	Fixed field												
7b	**NIR & Vis Cameras**	I - K	! 2"	Fixed pupil			Yes	Out		Mirror						
8a	NIR Camera &		! 30"	Fixed field												
8b	OSIRIS	z - K	! 2"	Fixed pupil			Yes	Out		Mirror						
9a	**Faint NGS + NIR**		! 30"	Fixed field												
9b	**Cam or OSIRIS**	J-K	! 2"	Fixed pupil			Yes	Out		Mirror						
	TBD															
10	**Field Acquisition**	Current	Full	Current			Flat	Out		Vis transmi	Out	Mirror				
LGS Science Modes																
1	**d-IFS**	z - K	! 120"	Fixed field	Wide	Yes for field	Yes	In	9	Out	Out	Out	No	Tracking	3	Yes
2a	**Interferometry** of			Fixed field		Yes for field					J transmit /	Out				Yes, on-
2b	faint on-axis NGS	H - L	! 2"	Fixed pupil	Narrow	No, fixed	Yes	In	6	Out	HK reflect	Out	No	Tracking	1 on-axis	axis
3	Dual star **Interferometry**	H - L	! 60"	Fixed field	! Medium	Yes for field	Yes	In	9	Out	J transmit / HK reflect	Out	No	Tracking	3	Yes
4a			! 30"	Fixed field	! Medium	Yes for field			9	transmit /			Option		3	Option
4b		K	! 2"	Fixed pupil	Narrow	No. fixed			6	K reflect			No		1 on-axis	Unlikely
4c			! 30"	Fixed field	! Medium	Yes for field			9	J transmit			Option		3	Option
4d		H	! 2"	Fixed pupil	Narrow	No. fixed			6	/ H reflect			No		1 on-axis	Unlikely
4e			! 30"	Fixed field	! Medium	Yes for field			9	H transmit			Option		3	Option
4f	**NIR Camera**	z - J	! 2"	Fixed pupil	Narrow	No. fixed	Yes	In	6	/zJ refl	Out	Out	No	Tracking	1 on-axis	Unlikely
5a			! 30"	Fixed field	! Medium	Yes for field			9	JH			Option		3	Option
5b	**Visible Camera**	0.7-1" m	! 2"	Fixed pupil	Narrow	No, fixed	Yes	In	6	transmit /	Out	Out	No	Tracking	1 on-axis	Unlikely
6a			! 30"	Fixed field	! Medium	Yes for field			9	transmit /			Option		3	Option
6b		K	! 2"	Fixed pupil	Narrow	No. fixed			6	K reflect			No		1 on-axis	Unlikely
6c			! 30"	Fixed field	! Medium	Yes for field			9	J transmit			Option		3	Option
6d		H	! 2"	Fixed pupil	Narrow	No. fixed			6	/ H reflect			No		1 on-axis	Unlikely
6e			! 30"	Fixed field	! Medium	Yes for field			9	H transmit			Option		3	Option
6f	**OSIRIS**	z - J	! 2"	Fixed pupil	Narrow	No, fixed	Yes	In	6	/zJ refl	Out	Out	No	Tracking	1 on-axis	Unlikely
7a			! 30"	Fixed field	! Medium	Yes for field			9	transmit /			Option		3	Option
7b		I,K	! 2"	Fixed pupil	Narrow	No, fixed	Yes	In	6	IK reflect	Out	Out	No	Tracking	1 on-axis	Unlikely
7c			! 30"	Fixed field	! Medium	Yes for field			9	J transmit			Option		3	Option
7d		I,H	! 2"	Fixed pupil	Narrow	No, fixed	Yes	In	6	/ IH reflect	Out	Out	No	Tracking	1 on-axis	Unlikely
7e			! 30"	Fixed field	! Medium	Yes for field			9	H transmit			Option		3	Option
7f	**NIR & Vis Cameras**	I,J	! 2"	Fixed pupil	Narrow	No, fixed	Yes	In	6	/ IJ reflect	Out	Out	No	Tracking	1 on-axis	Unlikely
8a	NIR Camera &		! 30"	Fixed field	! Medium	Yes for field			9	Same as			No		3	Option
8b	OSIRIS	z-K	! 2"	Fixed pupil	Narrow	No, fixed	Yes	In	6	NIR Cam	Out	Out	No	Tracking	1 on-axis	Unlikely
	TBD															
10	**Field Acquisition**	Current	Full	Current			Flat	In		Vis transmi	Current	Mirror	Current	Current	Current	Current
11a								In								
11b	**LGS Acquisition**	Current	Full	Current	Current	Current	Flat	Out	Current	Vis transmi	Current					

Figure 55. Part of the system configuration for NGAO.
The full system configuration matrix is presented in KAON 550.

3.6.2.3 System Calibration: Routine and Maintenance Calibrations

The calibrations for the NGAO will be defined in the PD and DD phase. They include 1) routine calibrations, and 2) maintenance calibrations. The routine calibrations are calibrations that are required on run-to-run or night-to-night basis such as fine laser alignment and power calibrations, DM to lenslet registration, non-common path aberrations, etc. The maintenance calibrations are performed following a schedule and may include detector response, noise and offsets calibrations, TT and DM interaction matrices (poke matrices), motion control tune-ups, throughput, etc.

We anticipate that the daily calibrations will be performed by the observing support team using the high-level science operation tools. The maintenance calibrations may be implemented at the subsequencer level when applicable. The detail requirements and the algorithm for each routine and non-routine calibration will be developed during the PD and DD phases. The corresponding calibration sequences will be coded and implemented at the MCS and/or at the subsystem sequencer level. Note that the use of the keyword architecture as currently implemented at Keck will allow the

scientists to easily prototype and validate the calibration algorithm using their programming language of choice during the I&T phases.

3.6.2.4 System Operations: Acquisition

The NGS and LGS acquisition requirements and conceptual design are discussed in KAON 567. This includes a trade study between near-IR and visible detector technologies that found that a commercial CCD is sufficient for the NGS acquisition task. The NGS acquisition will also rely on data retrieval from multi-color astronomical catalogs (USNO-B, GCS-II and SDSS). KAON 567 lists and studies the possible risks during the acquisition process. The specifications for the acquisition conceptual design are presented in Table 11.

Table 11. Acquisition conceptual design level specifications.

Title	**Specifications**
Field of view	≥ 150"
IR field identification	a) Image sources in the near-IR (1.0-2.0 μm) b) Image sources in the visible (0.5-1.0 μm) In both cases, use supplementary information about target locations from catalogs and surveys
Point source sensitivity	V=22 or J=19, exposure ≤ 10 s, SNR ≥ 10
Position accuracy	≤ 0.050" rms, random errors in determining source positions in an acquisition camera image
Minimal time overheads	Total acquisition process time typically < 50 s, worst case < 120 s. Includes time for telescope moves, camera exposure, and analysis.
Photometric imagery	Photometric error of 0.2 magnitudes, in standard astronomical bands such as Johnson, UKIDDS, or SDSS
Registration accuracy	≤ 0.020" rms, random error in determining positions of acquisition camera with respect to telescope optical axis
Diagnostics and troubleshooting tools	Report metrics for automatic acquisition and to aid observer decision-making, including manual override by astronomer or observing assistant
Data products	Store acquisition images as FITS files, and appropriate diagnostics, in the NGAO data server
Interface to observer planning tools	Acquisition software will receive target information from the NGAO observer planning tools
Guiding mode	Used for testing when wavefront sensors not available

The telescope pointing accuracy is currently the largest risk for the observing efficiency. The observing efficiency budget depends on the brightness of the NGS and acknowledges the difficulty of acquiring fainter stars. A single camera design is feasible for LGS and NGS acquisition using a CCD sensor. The use of the single CCD sensor will cause relatively minor modifications to the overall

NGS optical design. High level requirements and interfaces to other NGAO subsystems are also discussed in KAON 567.

Table 12 presents a generic description for the acquisition sequence for NGAO with an emphasis on the parallel steps. The NGAO planning tools will assist the astronomer to select the next science target. All relevant configuration information will be loaded by the Operation Control (OC) tools.

Table 12. Generic NGAO Acquisition Scenario.

Step	Observing Step	Parallel Steps	Remarks
0	Select next target: - assess science priority - check target elevation range - check observing conditions - check LTCS conditions	Complete integration on current science target or calibrator. When target selected from Planning Tools, then information is loaded in OC tools.	It is not clear yet whether the astronomer will have to run these checks manually or whether it will be automated.
1	Upon completion of readout of science array, LGS is shuttered, AO loops open and key-system feedback parameters are saved then the operation control tools trigger the telescope slew.	OC tools parses information, and get ready for execution: - NGS parameters for acquisition - AO configuration - Instrument configuration	
2	Telescope slews	The OC tools send commands to the multi-system sequencer. Setup sequences are executed as appropriate by the AO, laser & science instrument sequencers.	
3	Telescope Pointing Adjustment on one of the NGS (brightness allowing). This step is automatically performed by the NGS acquisition subsystem with the visual check of the Observing Assistant (OA). Upon success, pointing corrections are applied and next telescope slew is commanded from the OC tools.	There is no need to use the acquisition camera for the LGS acquisition: LGS pointing model is accurate enough to get all laser spots centered within the capture range for the HO WFS.	This step may be required only when the NGS V>18 mag. (TBC) or when the telescope slews by more than x° in elevation/azimuth range.
4	Telescope coarse registration on the science field. NGS acquisition subsystem runs an automated routine to record and process image, ID the NGS in the field with respect to catalog data then compute required offset.	LGS propagation and acquisition steps initiated. Laser pointing correction and uplink TT correction loops closed with very low gain. Pickoff mirror positioning and LOWFS setup complete	Need to implement the acquisition for the vibration/wind shake reference. Need additional study for telescope guiding. Not clear if

	Visual check of process by OA. Upon success, position offsets are applied to telescope.	including background.	the HOWFS will require a background.
5	Telescope fine registration on the science field: If photons not detected at the expected SNR on the LOWFS (or NGS not on Pointing Origin), then NGS acquisition subsystem runs a 2nd iteration. Visual check of process by OA. Iterate if necessary (to be detailed). Upon completion adjust telescope pointing model.	Pick-off mirrors for science and TWFS in position	Need to check the conditions for the dichroic during this step. Need to be able to adjust pointing model for telescope even though PO != REF.
6	AO subsystem control: 1) low gain on woofer & MEMs, 2) increase gain on UT, 3) start telescope guiding, 4) adjust woofer & MEMs gain, 5) initiate TWFS + tomography optimization	Science instrument is setup: optics and read modes are set and confirmed. May record first exposure to check centering with point-source and expected SNR/coadd. Monitor image quality and assess optimization progress.	UTT acquisition requires more design. Assuming redundant information from USNO-B, GSC-II & SDSS uncertainty in field centering should be < 0.2".
7	Science integration starts		

The main contributions to the centering error budget during NGAO acquisition in LGS mode are:

1. The accuracy for the knowledge of the separation distance and position angle between the stars and the galaxies from the literature. This information is provided by the astronomer, and can be < 0.01" if the field has been observed (recently) with HST cameras. The USNO-B on-line catalog provides an astrometric accuracy of 0.2", and the astrometric solution for the USNO-B, GSC-II and SDSS catalogs are improved as the proper motions are being calibrated using GSC-I (KAON 467).
2. The pickoff arm positioning accuracy for each science target with respect to the TT closed-loop reference position for the LOWFS, which is the total of:
    a. The internal positioning accuracy and position stability for each individual pick-off arm (science and LOWFS) – the requirement is ≤ 0.005" (KAON 548)
    b. Registration accuracy and stability between LOWFS and science arms including TT stage positioning accuracy.
3. The differential atmospheric refraction between the LOWFS and the science instrument.
4. The total contribution from the optical distortions due to thermal gradient, alignment error, woofer and MEMs positioning between the science array and the LOWFS.

The LOWFS and LGS object selection mechanism study (KAON 559) shows that the positioning accuracy requirement can be met.

3.6.2.5 System Operations: Dithering and Offsetting

Several approaches to dithering and offsetting were proposed and discussed in KAON 558. The rationale for reviewing the dithering and offsetting scenarios comes from the important overhead (~30 seconds per move) it currently takes to perform these important observing steps.

The selected approach recommends avoiding any telescope move and AO pause/resume sequence, unless necessary. Most field repositioning on the science array is performed to account for pixel/spaxel response, background emission or super-sampling and are of relatively small amplitude (< 2"). They could be performed by moving one of the NGAO internal fast-steering optics: tilt on the individual MEMS for the d-IFS, tilt on the second-relay MEMS for the narrow field science, repositioning of the probe arms for the d-IFS. This implementation would leave the LOWFS, TWFS and HOWFS closed during the entire observing sequence, and would allow for maximum flexibility and efficiency for centering the science target, tracking, correcting for DAR, etc. We believe that these internal optics have the required pointing accuracy and could result in minimal overhead (< 5 second).

An alternate scenario that still does not require the telescope to move would require a global tilt on the woofer, and a counter motion for the LOWFS/TWFS, HOWFS probe arms. This requires pausing and resuming the AO operations and may require ~ 5 to 10 seconds.

Alternatively, offsets of larger amplitude are performed by requesting a telescope offset, repositioning the probe arms at a different field location and re-acquiring the guide stars on the AO sensors. This may take about ~ 15 to 30 seconds depending on the detailed implementation.

We are planning to examine these scenarios during the preliminary and detailed designs and develop the detailed requirements. We are confident that the combination of these three scenarios with the possibility of parallel commands to different subsystems will address the efficiency requirement for dithers and offset for the key science cases.

3.6.3 System Control

The high-level control of the system is performed through the Operation Control GUIs and executed by the Multi-system Command Sequencer (MCS). A schematic view for these controls was presented in Figure 54.

3.6.3.1 Multi-System Command Sequencer

The MCS is the main interface between the Operation Control GUIs (configured and controlled the by AO operator, the expert user and the observer) and the control of each subsystem. The important design concept we have opted for, is to have all complex observing sequences under a central

supervisory control system that will send and coordinate commands with the AO, Laser, science instrument(s) and other subsystems. The architecture for the MCS follows the design for the subsystem sequencer (see KAON 569 and section 3.5.2.2.1.1).

The MCS has four main components: a library of multi-system coordination sequences, a command interface, a data interface and a system health monitor. The functions of these four main components are as follows:

- Multi-system coordination sequences. The multi-system coordination sequences are a collection of functions which implement complex sequences of commands for the underlying control subsystems (AO, Laser, etc). A multi-system coordination sequence allows the user to send a simple command to the MCS, while it commands and coordinates all of the many tasks required by this command and returns the status to the user. The coordination sequence receives a command from the user and then sends multiple commands appropriate for the task to be accomplished to the underlying multi-systems using the main command interface discussed below. Examples are: the LGS setup sequence that is used during slew to startup, initialize and setup AO, Laser and science instrument for the next LGS acquisition sequence. The specific coordination sequences have not yet been determined at this early phase of the design. Hence, a key task during the PD phase will be to identify all of the coordination sequences required for the MCS and to specify their requirements. Note that we will likely require some flexibility in the management of this sequence library as we plan to add sequences to the library, mostly diagnostic and troubleshooting sequences, during the I&T and early operation phases of the system. The reliability and efficiency of the NGAO operations strongly rely on the successful implementation of the multi-system coordination sequences.
- Command interface (see Section 3.5.2.2.1.1).
- Data interface (see Section 3.5.2.2.1.1).
- System health monitor. The system health monitor is a task that monitors the status of the MCS functions and tasks.

3.6.3.2 Operation Control (Graphical) User Interfaces

The operation control GUI is the main interface between the Users (AO operator, expert user and observer) and the control of components and execution of sequences with the NGAO and science instrument.

The detailed design for the operation control GUIs for the science instruments is not a component of the science operation tools. Yet we will work with the science instrument teams and define a common design for the interface between the NGAO science operations GUI and the science instrument GUIs during the PD and DD phase.

During the SD phase, we have opted for the following preliminary set of design choices:

- The GUIs will be modular (as shown in Figure 54) and include three main parent components: 1) NGAO controls, 2) science instrument controls and views, and 3) system-view and performance monitoring displays.

- The implementation of these tools should be fully compatible with the pre- and post-observing tools.
- The standard practice in the observatories (Gemini, ESO, STScI, Keck) for the implementation of these operation tools is to use Java and XML programming languages. We would recommend using these standard practices and other similar ones being developed in the context of Virtual Observatories (VO) and National VO.
- Several GUIs may be required during the operations per parent component. We will attempt to limit the total numbers of GUIs. Due to the limited integrated software development, our current LGSAO control includes as many as 30 displays and leads to some confusion during LGS operations.
- The control GUIs will include two type of command controls: controls for direct commands with no parameters e.g., open AO loops, (re-)close AO loops and controls for more complex commands requiring some parameters e.g., an acquisition sequence using a configuration file.
- The operation control GUIs will be designed to be users-friendly and include/display the minimal complexity. All complex commands will be implemented at the lower levels in the MCS and subsystem sequencers. Additional complex commands could be controlled using from specific call to a different set of GUIs (e.g., a somewhat complex calibration widget could be called from the NGAO GUI).
- The user can select the parameters for complex command either by loading a previously saved configuration file (these configuration files are also the outputs of the planning tools) or by manually entering values in the configuration fields.

3.6.4 Pre and Post-Observing Tools

3.6.4.1 Pre-Observing Tools

The pre-observing tools will allow the observer to simulate, evaluate and plan for an observing program using the NGAO and the science instrument(s) any time prior to the observations, particularly during the observing time proposal submission process. The astronomer will likely go through a second phase of observation planning in the month prior to, and days leading to the observations. During the observing night, the observer may use the same sets of tools to check and refine the observing strategy, if necessary.

The pre-observing tools are:

- The AO Guide Star Tool to search adequate astronomical catalogs for natural guide sources, identify and select them, and save all relevant information on the NGS and the science field required to simulate and acquire the target.
- The NGAO Simulation tool to estimate the NGAO performance in terms of Strehl ratio, encircled energy, full-width at half-maximum, etc as a function of the NGAO mode and setup.
- The Exposure Time Calculator to estimate the SNR / seconds and dominant noise regime for the science instruments.
- The Observation Preparation tool prepare, review and save the observing sequences and estimate the observing efficiency.

- The Laser Clearinghouse Planning tool to automate the coordination tasks with the laser clearinghouse.

The requirements for these tools are a combination of derived-requirements from the science cases (KAON 456) and operational requirements (KAON 456). A block diagram for the pre-observing tools architecture design was shown in Figure 54. KAON 577 presents the System Design Report for the pre-observing tools.

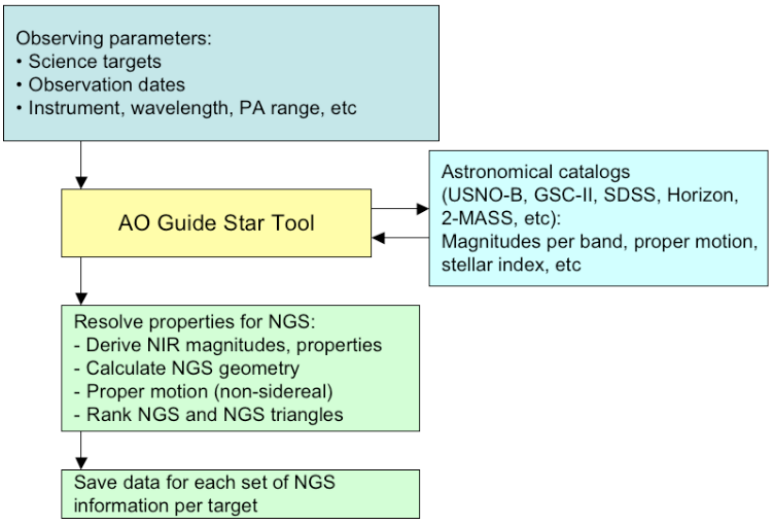

Figure 56. AO guide star tool workflow.

During the proposal phase, the AO Guide Star, the Performance Estimator, the Exposure Time Calculator and the Observation Preparation tools needs to assist the astronomer in identifying suitable Guide Stars and providing a first order estimate for the image quality, the exposure time and expected SNR and the observing strategy, given a basic science instrument setup. The information saved by the user might be inserted in the technical justification of the proposal. The tools needs to be users' friendly and easily portable on most computers' OS.

During the detailed observation planning, the same tools will be used to evaluate, optimize and prepare the observations sequences. The output parameters for the guide stars and instrument configurations will be saved in a format shared by the NGAO observing tools. The information will be loaded by the observing tools during night time operations.

Finally, during the observations, these tools may be used to preview and assist the on-going observations and for any on-the-fly change to the observing strategy.

Figure 56, Figure 57 and Figure 58 succinctly present the workflow for the AO guide star tool, the performance simulation and exposure time calculator, and the observation preparation tools, respectively.

The AO Guide Star Tool is used for both LGS and NGS cases. It is a versatile tool that will make request to astronomical catalogs, resolve target names, find and select AO guide stars for the NGAO science cases based on their derived NIR brightness and save the results. It is required to find a single star for NGS and sets of triplets for LGS. The sets of triplets will be ranked according to the estimated total residual error on the estimation of the TT mode and quadratic null modes. The results will be saved in the valid format for the telescope and the tools.

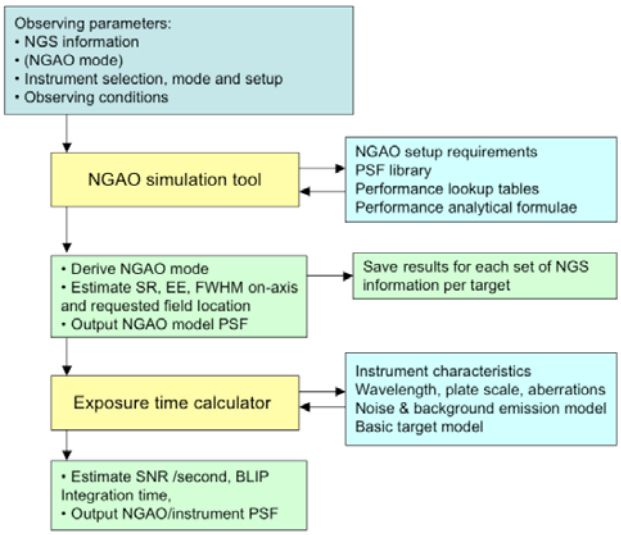

Figure 57. NGAO performance estimation tool and exposure time calculator workflow.

The NGAO performance estimation tool will take as inputs the AO Guide Star(s) information, the AO mode, the selected instrument and the (anticipated) observing conditions. As it will run on the host computer, or through a web-server, it will not be able to (re-)run a full NGAO simulation for each new observing program. Instead, it will make use of a combination of PSF libraries, performance lookup tables and analytical formulae to estimate AO quantities such as SR, EE, FWHM and possibly a 2-D NGAO model PSF for the science field(s). The tool will allow the user to compare performance results from different AO Guide Star(s) and different LGS asterisms configuration. The output results and the parameters used for the simulation will be saved in a file. The parameters and the algorithm for the simulation tools are yet to be defined.

Once the AO performance has been estimated it is then possible to calculate the exposure time to achieve a desired SNR given the instrument selection and setup, the detector read mode, a model for the noise and background emission, as well as a (simple) flux distribution model for the target. The tool will also estimate the background limited performance time and check that the detector is used in its linear range.

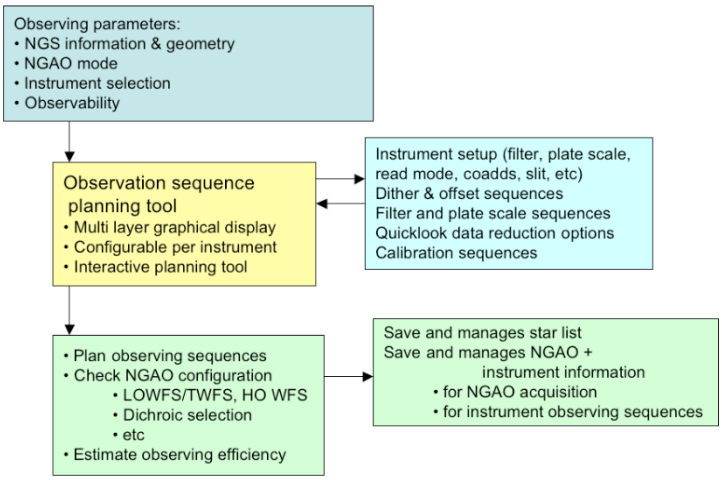

Figure 58. Observation preparation tool workflow.

The observation preparation tool will take as inputs the information from the selected AO guide star(s), the NGAO mode, the instrument selection and when required, the observability of the target. The astronomer will define the parameters for the observing sequences that are possible for this observing mode. The tool will check the NGAO configuration e.g., dichroic configuration and expected NGS flux on the LOWFS compatible with the selected observing wavelength. The parameters to be set for the observing sequences are yet to be defined. The tools are anticipated to allow for flexible and versatile use of the instrument. The configuration for the observing sequences will be saved in files that will be loaded at the time of the observations. We have yet to define how these files will be managed. A manual management for these various configuration files (guide star and science targets information, NGAO configuration, instrument configuration, observing sequence information, etc) could lead to confusion. We will consider implementing an automated file management from the observing proposal phase to the final execution at the telescope.

3.6.4.2 Post-observing Tools

The post-observing tools and interfaces are:

- Data quality metrics: the purpose of this tool is to reduce and analyze data collected during the observations and output quantities such as total residual wavefront error, seeing, photometric stability, Na return, observing efficiency, etc. These quantities have yet to be defined during the PD and DD phases. The results will be saved and stored with the final data product.
- Data product management tool: the observer and the support staff will use this tool to define which data needs to be saved and stored with the science data. This data product management may also help manage the data that does not need to be stored and can be deleted.
- PSF reconstruction tool: based on the WFC data stored on the data server, the Cn2 information, and other system parameters the PSF reconstruction tool will provide an estimate for the PSF in specific locations in the science field. The algorithms for the PSF reconstruction are yet to be defined. We have started the development of a prototype algorithm for the current NGS and LGS system for the on-axis and off-axis cases.

3.7 Science Instruments

3.7.1 Overview

The observing capabilities identified in the NGAO science cases are understood to result in the need for low background moderate resolution (R~ 3000 to 5000) spectroscopy and well sampled diffraction limited imaging over the full NGAO wavelength range.

While some science cases can be satisfied with a slit spectrograph, it appears that IFU spectroscopy with spatial sampling scales down to the diffraction limit can satisfy those science cases as well as meet a common need for spatially resolved spectroscopy to support velocity determinations in various kinds of kinematic studies.

The key impacts of the NGAO system design on instrumentation are the wide wavelength coverage offered by the system, and the availability of two AO corrected science fields. A low order AO relay offers a comparatively wide 120" diameter science FOV (referred to as the "wide field" or "first" relay), with additional FOV (a total of 150" diameter) provided for LGS acquisition and tip-tilt star selection. A high order AO relay offers a 30" FOV (referred to as the "narrow field" or "second" relay) with essentially diffraction-limited performance in the near-IR. The basic optical characteristics of the wide field relay are summarized in Table 13, and for the narrow field relay in Table 14. Additional details on the instrument interface definitions may be found in KAON-555.

Table 13: Wide field relay optical characteristics

Parameter	*Min.*	*Typ.*	*Max.*	*Units*	*Notes*
FOV (diameter)	150	-	-	"	1
Focal ratio	-	*f*/15	-	N/A	
Plate scale	-	1.3751	-	"/mm	
Focal plane radius of curvature	-	-1430	-	mm	2
Wavelength range	0.97	-	2.40	μm	3
Transmission	80	-	-	%	4
Pupil telecentricity	100	-	-	%	5

Notes:
1. Unvignetted field of view. The central 120" is fully accessible to the d-IFS and the tip-tilt sensors; the outer 30" is reserved for the tip-tilt sensors.
2. Positive radius of curvature describes an AO relay output focal plane where a given point in the AO relay output focal plane not located on the optical axis is displaced in the +z direction away from the AO relay focal plane. This value is correct for the NGAO Zemax model "KNGAO_2-tier_folded-2nd-relay_v4_wtelescope.ZMX".
3. This definition is consistent with KAON-530.
4. From the output of the telescope (Nasmyth focus) to the output of the low order AO relay.
5. At all field points over the unvignetted FOV.

NGAO is expected to support science observations over the wavelength range of 0.7 to 2.4 μm. In addition there is a goal of reaching the Hα line at ~656.3 nm with useful Strehl (>10%) and reasonable throughput. In the current design the wide field relay supports a deployable near-IR integral field spectrograph (d-IFS), the near-IR tip-tilt sensors, and the LGS wavefront sensors.

Table 14: Narrow field relay optical characteristics

Parameter	*Min.*	*Typ.*	*Max.*	*Units*	*Notes*
FOV (diameter)	30	-	-	"	1
Focal ratio	-	*f*/46.5	-	N/A	
Plate scale	-	0.4436	-	"/mm	
Focal plane radius of curvature	-	-277.53	-	mm	2
Wavelength range	0.680	-	2.40	μm	3,4
Transmission	75	-	-	%	5
Pupil telecentricity	100	-	-	%	6

Notes:
1. Unvignetted field of view.
2. Positive radius of curvature describes an AO relay output focal plane where a given point in the AO relay output focal plane not located on the optical axis is displaced in the +z direction away from the AO relay focal plane. This value is correct for the NGAO Zemax model "KNGAO_2-tier_folded-2nd-relay_v4_wtelescope.ZMX".
3. Goal range of 0.620 μm to 2.40 μm.
4. This definition is consistent with KAON-530.
5. From the output of the telescope (Nasmyth focus) to the output of the high order AO relay.
6. At all field points over the unvignetted FOV.

As discussed in §3.3 the wide field relay is also used to feed the narrow field relay in a "woofer/tweeter" arrangement. Since the tip-tilt sensors located at the wide field relay are required for all observing modes, selectable dichroic beam splitters are used to share the light between the narrow and wide field. A fold mirror can also be inserted prior to the wide field focal plane to fold the 150" field to a NGS/LGS acquisition camera. In addition, the light at 589 nm is directed to the LGS wavefront sensors through a fixed dichroic beam splitter located within the wide field relay.

The result of this configuration is that the wide field supports science only for the near-IR wavelength range. The narrow field relay on the other hand is intended to support both near-IR and visible wavelength observing. Additional dichroics are provided to share the light as required between the near-IR and visible wavelength ranges to support the instruments as well as a NGS wavefront sensor and a "truth" wavefront sensor.

The proposed instruments for the narrow field relay are a visible imager with an add-on IFU, a near-IR imager with a coronagraph, and a near-IR single object IFU. As a starting point we are planning to use the existing OSIRIS instrument for first light operations, with a future possibility of a new instrument with a somewhat wider FOV.

As discussed in the following sections, performance improvements in both CCDs and IR arrays allows some interesting and potentially useful overlap in wavelength coverage in the vicinity of 1 μm. As a consequence the narrow field relay passbands defined for near-IR and visible wavelength observing are specified with an overlap to allow instruments to take advantage of the opportunities in this wavelength range.

The resulting NGAO system passbands are shown in Figure 59 along with the NGAO nominal observing bands. The cut-on and cut-off (50% points) wavelengths are summarized in Table 15. Additional details on the NGAO passband definitions may be found in KAON-530.

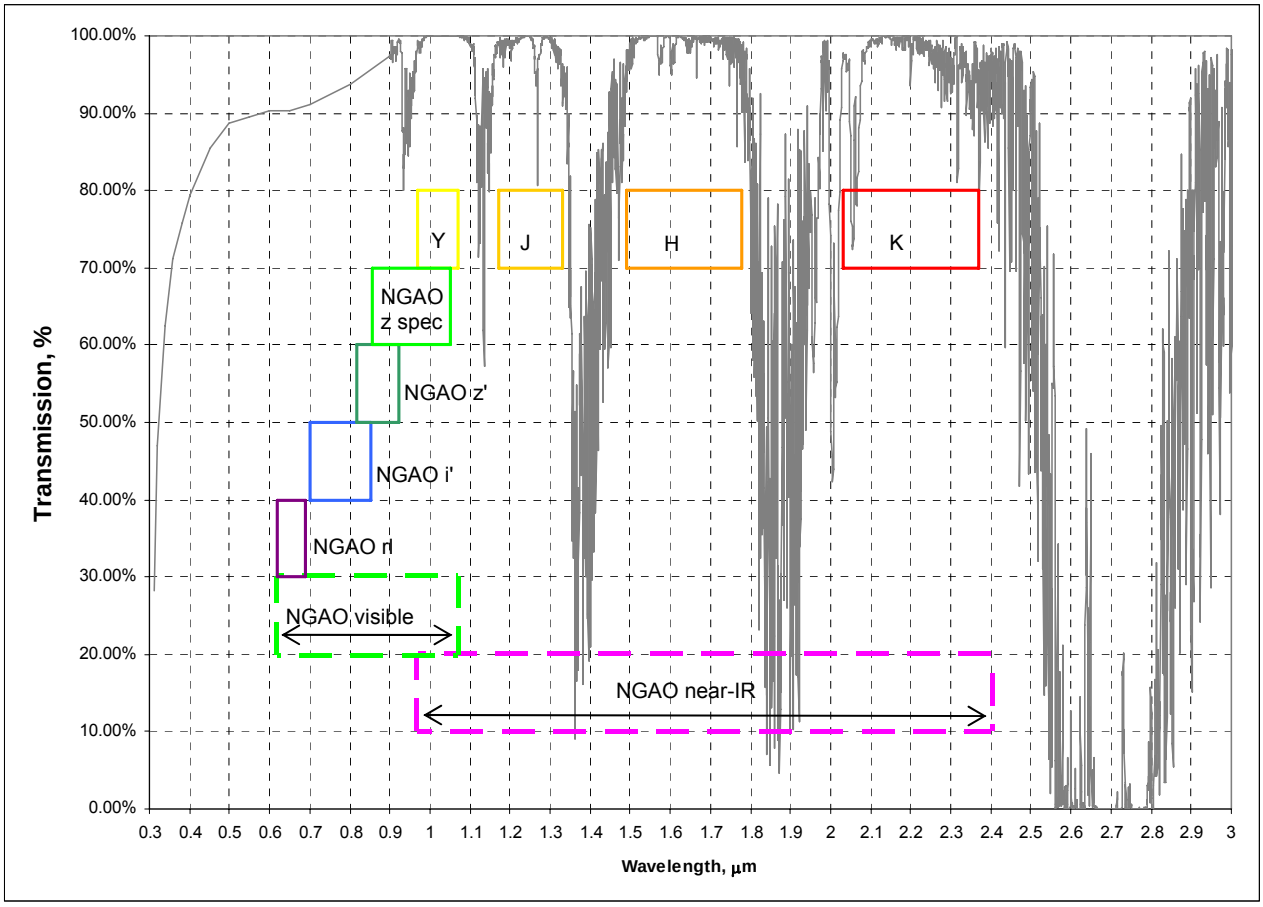

Figure 59: NGAO Passbands

Table 15: NGAO system passband and observing band characteristics

Passband name	**Cut-on λ (μm)**	**Cut-off λ (μm)**	**Notes**
NGAO Visible	**0.68 (0.62 goal)**	**1.07**	Goal is useful Strehl at Hα
NGAO rl	0.620	0.689	rl = "r band long", cut-on may be set higher depending on filter characteristics
NGAO i'	0.702	0.853	SDSS i' band
NGAO z'	0.818	0.922	SDSS z' band
NGAO z spec	0.855	1.050	Custom NGAO z band for spectroscopy
NGAO Near-IR	**0.97**	**2.40**	
NGAO Y	0.970	1.07	UKIDSS photometric
NGAO Y spec	0.970	1.120	
NGAO J	1.170	1.330	UKIDSS/Mauna Kea photometric
NGAO J spec	1.100	1.400	
NGAO H	1.490	1.780	UKIDSS/Mauna Kea photometric
NGAO H spec	1.475	1.825	
NGAO K	2.030	2.370	UKIDSS/Mauna Kea photometric
NGAO K spec	2.000	2.400	

3.7.2 Deployable Integral Field Spectrograph

3.7.2.1 Requirements

All of the d-IFS science cases have common requirements for observations in the three near-IR bands from 1 μm to 2.40 μm. There also may be requirements for observations below 1 μm and coverage in this range will be considered during the system design phase for the d-IFS.

A key element in the extragalactic science cases is the need to obtain large numbers of observations in order to develop the appropriate statistics for object populations and the variability in the characteristics and distributions. Consideration of the available target densities (see Table 16) leads to the conclusion that multi-object observations would be a major gain. Depending on the target selection criteria, areal densities range from 1 to 10 targets per square arc minute on the sky. In order to take best advantage of the high areal densities of targets, it is desirable to be able to deploy of order 6 to 12 AO-corrected IFS over a FOR of 3 to 5 square arc minutes.

The 120" diameter FOR provided to the d-IFS results from a trade study considering the number of LGS beacons required for tomographic wavefront measurements and also a desire to limit the size of the input K-mirror image de-rotator. Consideration of the available target densities indicates that this FOR is large enough to make efficient use of 6 object channels for the majority of the science cases.

For most of the science cases coverage of a full band in a single exposure is desirable, with a spectral resolution of R ~4,000 to allow resolving out the OH sky features and allow distinguishing the key diagnostic emission lines. For higher precision radial velocity measurements at the galactic center a higher resolution mode, of R ~10,000 is desirable, and consideration of a provision for this mode will be made during the system design phase.

The baseline spatial sampling for the IFS is 50 mas. For integral field spectroscopy, we are interested in how well the PSF delivered by the AO system matches this spatial sampling, that is, the encircled energy (EE) in each spatial sample. For the simulations performed to date we have used 50% EE in one spatial sample, a value that is consistent with the predicted performance of the MOAO mode of NGAO with ~30% sky coverage. Under some conditions, the current AO system simulations indicate that a 70 mas spatial sampling is required to achieve the 50% EE fraction in one sample. Optimizing the spatial sampling to balance spectroscopic efficiency and spatial resolution will require further study as the performance estimates for the AO system are refined.

The typical size of target galaxies for extragalactic observations is ~1". In order to permit simultaneous observation of the sky background, the baseline FOV is a 1" x 3" rectangle. This allows on-IFS dithering for sky subtraction, making exposures more efficient and eliminating calibration concerns that arise with separate sky observations.

Table 16: Space densities of various categories of extragalactic targets

Type of Object	~Density per arc minute^2	Reference
SCUBA sub-mm galaxies to 8 mJy	0.1	Scott et al. 2002
Old and red galaxies with 0.85 < z < 2.5 and R < 24.50	2	Yamada et al. 2005; van Dokkum et al. 2006
Mergers with emission lines in JHK windows & R < 24	2-5	Conselice et al. 2003
Field galaxies w/ emission lines in JHK windows 0.8 < z < 2.2 & R < 25	> 10	Steidel et al. 2004; Coil et al. 2004
Center of distant rich cluster of galaxies at z > 0.8	> 20	van Dokkum et al. 2000
All galaxies K < 23	> 40	Minowa et al. 2005

A direct imaging mode is also proposed. At least a basic imaging mode is needed for calibration of the MOAO relay, and since there is no wide field imager for NGAO, this mode can also be useful for direct imaging to compliment IFU spectroscopy in areas such as cluster scale lensing. This mode is also suitable for imaging to detect specific diagnostic lines in conjunction with narrow band filters.

For several science cases, particularly cluster scale lensing, galactic observations, and even IFU observations of Jupiter, a close packed mode is desirable for the IFS fields. The close packed configuration of the six d-IFS fields is shown in Figure 60.

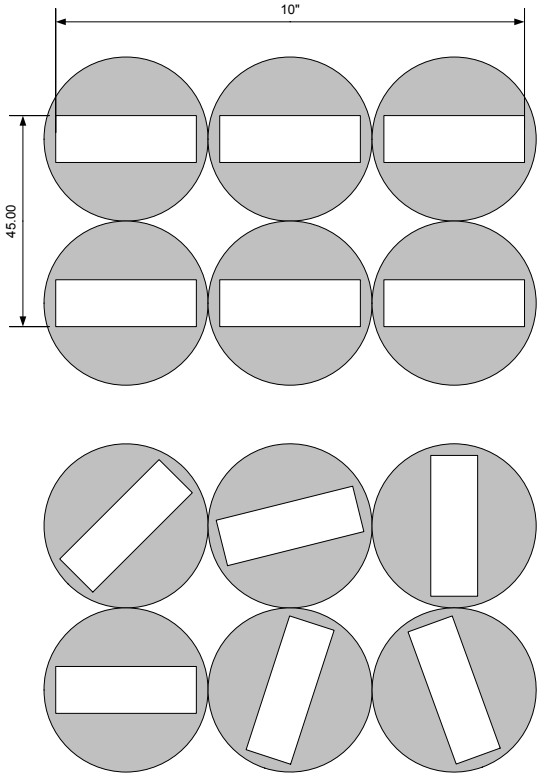

Figure 60: Close packing of d-IFS fields
Top: the d-IFS close packed footprint is 10" x 45", an area of 10" x 25" can be acquired in six overlapping exposures. Bottom: the FOV of each probe can be oriented as required by the observation.

Initial considerations of close packing suggest that a mode with gaps of ~0.5" between IFS fields is possible, and using a suitable dither pattern of six exposures a contiguous area of 10" x 25" can be observed using all 6 object channels of the d-IFS. Various configurations are supported by the provision of individual field rotation for each IFS channel, and by a probe tip design that permits close packing in a 2 x 3 array. An illustration of close packing and field rotation are shown in Figure 61 for a cluster scale lensing observation.

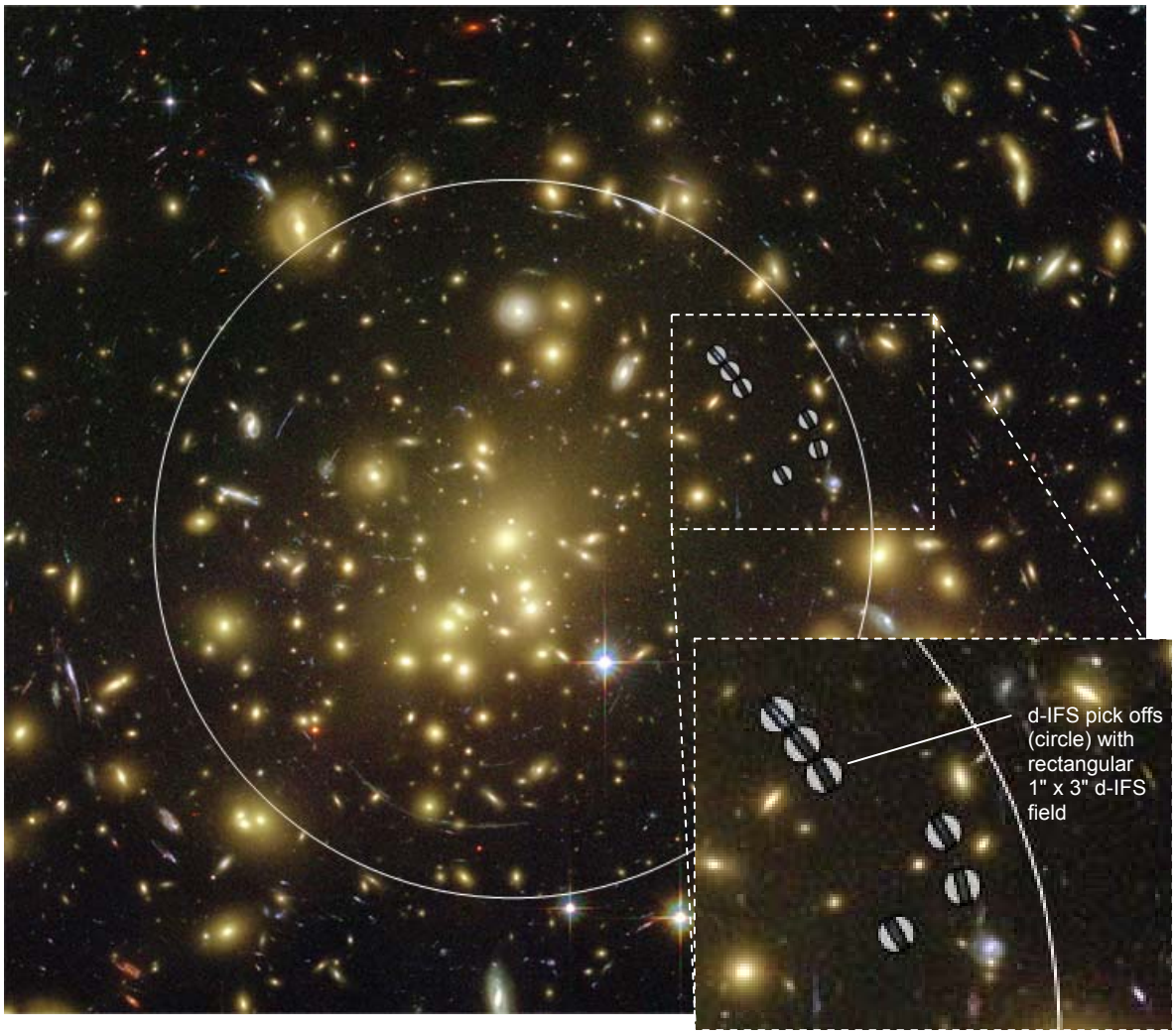

Figure 61: Illustration of a cluster scale lensing observation using the close packed mode of the d-IFS
This example (HST ACS image of Abell 1689) shows the 120" wide field relay science FOR (white circle) and the six IFS fields deployed to observe four different lensed images, one using close packing of three IFS fields. HST image credit: NASA, ESA, L. Bradley (JHU), R. Bouwens (UCSC), H. Ford (JHU), and G. Illingworth (UCSC).

NGAO is expected to provide a significant gain in sensitivity over the current Keck telescope AO systems. This is due to the improved Strehl ratio, and due to improved background and transmission. For some science cases such as high-z galaxies, the desired sensitivity is constrained by the duration of reasonable spectroscopic exposures. Science programs concerned with surveys place a premium on achieving background-limited observations with shorter integration times. We have adopted a standard of 5σ detection with a one-hour integration time as the reference point for point source limiting magnitude, with one hour representing a reasonable time for programs such as extragalactic surveys with relatively large numbers of targets. The current performance estimates for NGAO point source limiting magnitudes range from 26.5 in J band to 25 in K band.

Control of background flux from the telescope and AO system is essential to maximize the SNR of the observations and to reach the required sensitivity in reasonable integration times. At wavelengths shorter than ~2 μm the background in a well designed optical system free from scattered light is due to night sky emission. For wavelengths > 2 μm, background flux due to thermal emission from the telescope and AO system becomes significant. Our studies of the impact of background on sensitivity for near-IR observations have resulted in a requirement that the AO system+instrument should not increase the unattenuated background from the sky+telescope by more than 30%, with a goal of 20%.

Simulations based on the predicted performance of Keck NGAO show a factor of 3 to 6 improvement in signal to noise ratio (SNR) using an IFS with NGAO compared to Keck's OSIRIS and the current LGS AO system. For background-limited measurements, this would yield exposure-time reduction factors of 9 to 36. Multiple IFS will further multiply the efficiency. Thus, our nominal 6 object channel d-IFS with MOAO would yield a dramatic total gain of 50 to 200 in the completion rate for survey-level programs, relative to the current LGS AO OSIRIS system. This is a major advance in the potential of AO systems for deep spectroscopic surveys of the distant universe.

Based on these considerations, the science driven requirements for the d-IFS are summarized in Table 17.

Table 17: Summary of the d-IFS science driven requirements

Performance requirements	**Value(s)**
Wavelength range	1 to 2.40 μm (J, H, K bands), one entire band in a single exposure.
Spatial Sampling	< 70 mas, goal of 50 mas, with the required EE fraction
Encircled Energy	≥ 50% in one spatial sample for 30% sky coverage
Field of view	1" x 3" per object channel
Field of regard	120" diameter
Background	<30% over the unattenuated background from sky+telescope, goal of <20%
Sky coverage	≥ 30%
Observing modes	
Number of object channels	6 to 12
Imaging	Direct imaging through slicer
Close packing	2 x 3 pattern with a goal of ~0.5" gaps between IFS channels
Spectroscopy	
Spectral resolution	R ~ 4,000
Sampling	~2000 pixels per spectra

3.7.2.2 Instrument Concept

The concept for the NGAO d-IFS is based on two major subsystems; the OSM feeding six or more MOAO corrected object channels with image sampling, each followed by a reflection grating spectrograph. A block diagram of the deployable multi-object instrument is shown in Figure 62.

Starting at the left side of the diagram the AO system input consists of a K-mirror image de-rotator followed by the wide field AO relay. The near-IR light from the wide field relay then goes to the near-IR OSM. This OSM provides object selection for the deployable IFU and for the three near-IR tip-tilt sensors. Not shown is a dichroic beam splitter that will be realized as a set of selectable beam splitters for use in the narrow field mode where near-IR light must be shared between the tip-tilt sensors and the narrow field instruments.

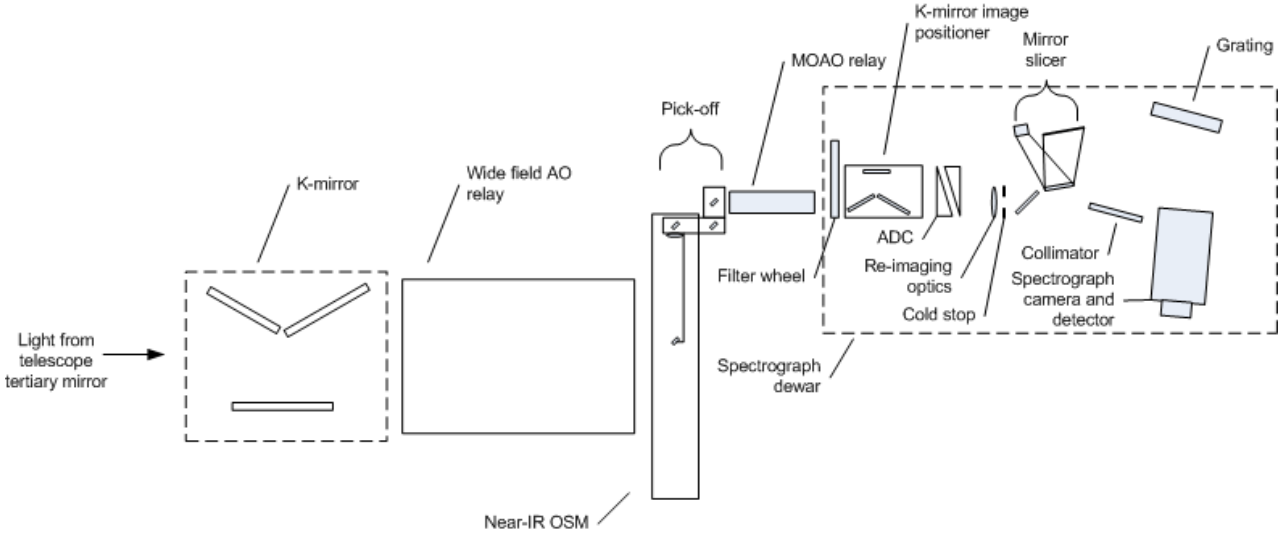

Figure 62: d-IFS block diagram

After the OSM one spectrograph channel is illustrated, starting with the MOAO relay. Each MOAO relay uses a 32 x 32 MEMS deformable mirror. The relays used for the deployable IFU and the tip-tilt sensors will be similar, but the FOV requirements of the tip-tilt sensors are more modest.

All of the AO system optics, including the near-IR OSM and the MOAO relays are enclosed in a cooled enclosure (~260 K) with a window located prior to the K-mirror (not shown in the figure) to isolate the enclosure from the dome environment. A calibration source (PSF, wavelength and flat field) is also provided as part of the AO system for use in all of the AO modes and with all of the instruments.

The output of the MOAO relay is directed to the spectrograph dewar containing the balance of the IFS optical system. After the cryostat entrance window a set of selectable order sorting filters are followed by a small K-mirror rotator to allow setting the on-sky orientation of the IFS FOV. An atmospheric dispersion corrector, re-imaging optics and a cold stop follow the K-mirror. The re-imaging optics form an intermediate image of the telescope focal plane on the slicer mirror. The slicer mirror is followed by formatting mirrors that organize the image slices into a pseudo long slit

image on a series of slit mirrors. After a stop at the entrance to the spectrograph, the light from the pseudo long slit is collimated and then dispersed by a reflection grating. The dispersed light is then imaged onto the detector by a refractive camera. The grating can be replaced by a plane mirror to permit direct imaging through the slicer.

Each spectrograph will use a H2RG detector and sidecar ASIC. The MEMS DM drive and control will be supplied by the AO system. The remaining electronics will be based on heritage designs from other near-IR instruments (OSIRIS, MOSFIRE).

Much of the control software will be based on the MOSFIRE heritage to provide keyword level control of each spectrograph, and existing tools (OSIRIS Quicklook II) are available for image display including data cubes. Data reduction tools may also be based on a pipeline system similar to OSIRIS, but the mirror slicer design and full coverage of each band should reduce the calibration complexity and difficulty.

3.7.2.3 Key Technical Issues

The concept described here is the starting point for the system design phase of d-IFS. In this first design phase we will carry out a process of iteration between the concept and the science requirements. At this point, we can identify a number of technical issues that need to be considered, in effect representing the trade space for this design. Our overall approach to the design will include design to cost considerations as well as strategies to balance risk, particularly by choosing conservative, heritage based designs where they are suitable and do not compromise performance. In the sections that follow we briefly discuss the major design issues and identify the key related activities that will take place during the system design. To structure this discussion we have organized the issues according to the top levels of the product structure associated with the current design concept.

3.7.2.3.1 Overall Parameters and Performance

Key parameters of the instrument depend on the level of performance achieved for the corresponding AO system parameters, illustrating the fact that the AO system and its instruments cannot be specified or designed in an independent fashion. Within this category of systems engineering, we have identified the following activities as part of the system design process:

- End to end throughput and background modeling (AO+instrument)
- Evaluating pupil registration over the FOR
- Impact of low order relay performance on the MOAO relay design and performance
- Near-IR beam splitter requirements drivers from this instrument
- ADC performance requirements
- Integration of the instrument with the AO system: optical, mechanical, electronics and software
- Observation planning, AO and instrument control and configuration during observing
- Calibration facility requirements drivers from this instrument

3.7.2.3.2 Object Selection Mechanism

The OSM is based on the "probe arm" concept. Each probe arm incorporates collimation optics and the necessary fold mirrors to allow radial positioning of the pick-off mirror and sector motion over a portion of the OSM field. The probe arm FOV will be at least 3" in diameter. The currently available heritage design for the basic probe arm concept is the Gemini on instrument wavefront sensor, (Thornton et al. 1998). This design carries the wavefront sensor detector as part of the assembly and does not have the range of motion required from the OSM of the d-IFS. A design closer to our requirements is the probe arm of the KMOS instrument (Sharples et al. 2006, Dowling et al. 2005) under development for the VLT. Review of the evolution of this design (Sharples et al. 2004, Sharples et al. 2006) shows some of the challenges in implementing a probe arm with low flexure and reasonably efficient close packing.

In particular, we note the following design issues for the OSM design:

- Pick-off design with respect to flexure and positioning accuracy
- Focus adjustment due to the curved focal plane
- Pick-off size and capability for close packing and dithering over contiguous fields
- Software control and failsafe procedures for pick-off motion
- Most efficient method to obtain sky background measurements
- Observation planning tool requirements
- AO system requirements drivers on the OSM design for the tip-tilt sensors

3.7.2.3.3 MOAO Relay

From the OSM, each object channel of the d-IFS feeds a high order MOAO relay. This relay uses a 32 x 32 MEMS DM operating in open loop to provide high order AO correction for the object channel FOV using tomographic information about the atmosphere over the telescope acquired by the multiple LGS beacons and wavefront sensors. The MOAO relay will need to be compact in order to fit one per object selection channel around the OSM focal plane. A 1024 actuator (32 x 32) MEMS DM with open loop performance consistent with our requirements has been demonstrated in the lab. The current ViLLaGES experiment at UCO/Lick is performing on-sky tests of the MOAO open loop concept using a 32 x 32 MEMS device.

The key MOAO issues we will consider in the system design phase of this instrument are:

- MOAO performance and sky coverage/encircled energy trade offs
- MOAO relay calibration

3.7.2.3.4 IFS Front End

The front end of the IFS consists of a re-imager that serves to match the sampler's physical size to the desired focal plane sampling. The baseline design is for a single 50 mas spatial sampling scale. The number and format of the samples will be fixed by the image sampler design, but it is possible to change the scale of the samples on the sky by providing more than one set of re-imaging optics. However, this introduces complexity and increases the physical envelope of the front end. A trade

study will be performed to review the chosen spatial sampling scale and consider the benefits of providing more than one scale.

3.7.2.3.5 Image Sampler

The baseline selection of a mirror slicer is based primarily on the anticipated SNR improvement compared to a lenslet-based design. The mirror slicer will provide an anamorphic stretch of the image to ensure Nyquist sampling of the image pixels in the spectral direction. For the 1" x 3" FOV and a 50 mas pixel scale a 20 slice format would produce a pseudo long slit of 1200 spatial pixels. With a 2K x 2K detector in the spectrograph a larger FOV is possible, up to 34 slices for a FOV of 1.7" x 3". It is also possible to share a spectrograph between three object selection channels by using a rectangular mosaic of two 2K x 2K detectors.

The mirror slicer appears to be well suited to a system where the required spatial resolution is not at the diffraction limit. The literature contains several examples of mirror slicer designs including the slicer for the Gemini GNIRS instrument (Content 1998, Allington-Smith 2006) and the slicer for the VLT KMOS instrument (Content 2006). The wavefront quality (~100 nm rms wavefront error) possible with more advanced techniques of slicer fabrication appears to be compatible with the encircled energy requirements of this instrument. The mirror slicer design will fix the sampling format and FOV for the IFS, so a trade study will be required to confirm the suitability of the baseline 1" x 3" format. A consideration in this study is that a rectangular format does not make optimal use of a square detector, so further evaluation of the trade off between FOV, spectrograph design and detector cost will be required.

3.7.2.3.6 Spectrograph

The spectrograph is a relatively simple grating spectrograph. A mirror collimator directs the light from the image slicer's slit mirrors onto a fixed grating, providing spectra for J, H and K bands in orders 5, 4 and 3. A refractive camera then formats the dispersed spectra onto a 2K x 2K Hawaii-2RG detector.

The image sampler and spectrograph optical systems will operate at cryogenic temperatures to control thermal background. The number and size of the required cryostats is an important factor in the complexity and size of the instrument. Complexity could be reduced by sharing a spectrograph with more than one image sampler. A key trade-off in this approach is that sharing will require a larger acceptance angle for the spectrograph collimator resulting in increased aberrations and larger optics. The grating, spectrograph camera and detector will represent significant cost items, making a trade study of spectrograph design concepts and variations in sharing of spectrographs by the object channels an important part of the design to cost effort.

The baseline requirement for spectral resolution is R ~ 4,000 to permit resolving out the OH lines. There may also be a case for higher resolution for more precise spectral diagnostics and for higher radial velocity precision. This would lead to a grating changer, adding cost and complexity. A trade study will be required to consider the scientific benefits of a second higher resolution mode.

3.7.3 Narrow Field Instruments

The narrow field instruments will address a wide range of science cases, including extragalactic science (quasar host galaxies, galaxy scale lensing, nearby AGNs), Galactic science (Galactic center, extrasolar planets,) and planetary science. Accommodating this diverse range of observations necessitates some compromises, but throughout the development of the narrow field instruments the primary goal will be to balance and optimize each of the science driven requirements for these instruments in order to best serve all of the science cases.

As noted earlier, performance improvements in both CCDs and IR arrays have resulted in the possibility of using substrate removed IR arrays into the upper part of the visible wavelength range, and thick substrate CCDs allow exceptional QE in the 800 to 1000 nm range without detectable fringing. As a consequence we have selected as the baseline detectors for instrumentation HgCdTe infrared arrays for the near-IR (1.0 to 2.4 μm) and thick substrate high resistivity CCD detectors for the visible wavelengths to from ~650 to ~1000 nm.

Specifically the current instrument concepts employ the following detectors:

1. Teledyne Scientific & Imaging MBE processed substrate-removed HgCdTe Hawaii-2RG (H2RG) 2k x 2k and Hawaii-4RG (H4RG) 4k x 4k infrared arrays for the near-IR
2. Lawrence Berkeley National Laboratory (LBNL) fully depleted, high resistivity thick substrate 4096 x 4096 pixel CCDs for the visible wavelengths

These detectors offer state of the art QE performance over their design wavelength ranges. For the purposes of this discussion the portion of the QE curve that we are concerned with is the cut-off wavelength of the visible wavelength detector, and the cut-on and cut-off wavelengths of the near-IR detectors. Cut-on wavelength is defined here as the wavelength where the detector's QE rises to 50% of the mean detector QE. Cut-off wavelength is defined here as the wavelength where the detector's QE drops to 50% of the mean detector QE. The relevant portions of the two QE curves are shown in Figure 63. These data are based on Figer et al. 2004, and private communications regarding JWST NIRCAM detectors (McLean 2007) and LBNL detectors (Stover 2007).

The substrate-removed versions of the H2RG have useful QE throughout our wavelength range of interest. However, these devices are considerably more expensive than the LBNL CCDs. They also require colder operating temperatures, and exhibit higher read noise. It is also likely that instrument camera optical design will encounter some significant additional challenges if it is necessary to cover both the visible and near-IR wavelength ranges in one camera. For these reasons the use of CCDs for the visible wavelength range appears to be the best choice at this time.

The potential of the LBNL CCDs is illustrated in Figure 63. This figure shows the standard photometric visible wavelength r and i bands, and a photometric definition of the near-IR Y band (UKIDSS, Hewett et al. 2006). The QE of the LBNL CCD extends well beyond the i band, and has useful response into the middle of the near-IR Y band. This suggests that the long wavelength cut-off for the NGAO visible mode could be usefully extended for photometry by including both a

photometric z' band and Y band, and for spectroscopy a passband that includes the ~920 to 970 nm wavelength range.

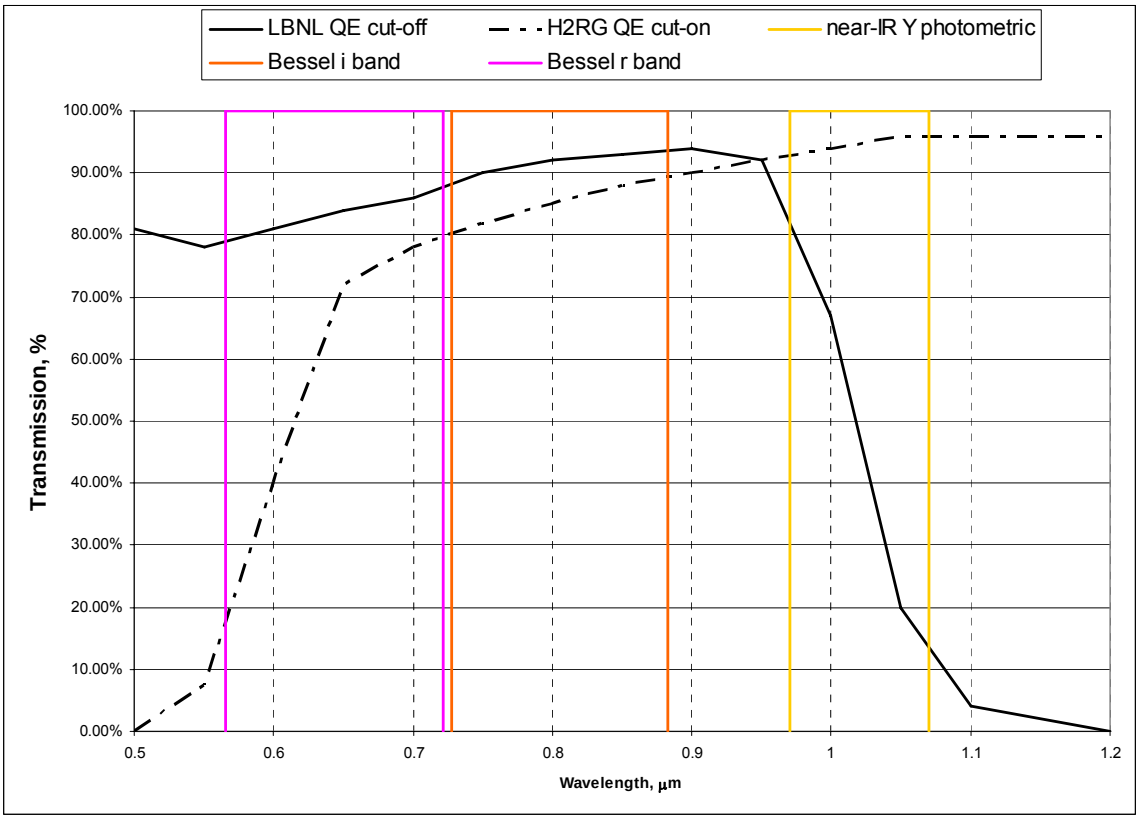

Figure 63: Detector QE cut-on and cut-off characteristics

3.7.4 Near-IR Imager

3.7.4.1 Requirements

The science driven requirements for the near-IR imager are summarized in Table 18.

Table 18: Summary of the near-IR imager science driven requirements

Performance requirements	**Value(s)**
Wavelength range	0.97 to 2.45 μm (Y, J, H, K bands)
FOV	30"
Pixel scales	10 mas (2 pixel sampling in Y band) 6.7 mas (3 pixel sampling in Y band)
Background	<30% over the unattenuated background from sky+telescope, goal of <20%
Observing modes	
Imaging	Adjustable Lyot stop
Coronagraphy	6λ/D apodized pupil Lyot coronagraph
Filters	Photometric Y, J, H, K, also K', Ks, narrow band TBD

The near-IR imager is intended to provide well sampled diffraction limited imaging over the NGAO narrow field FOV of 30" diameter. For simplicity and stability there is a strong goal to have a fixed plate scale. While many science cases are satisfied by 2 pixel sampling, the minor planets science cases have a preference for 3 pixel sampling. Since the available detectors have square areas, and the narrow field FOV is circular, we have the usual choice of an inscribed or exscribed detector area. Two options are illustrated in Figure 64, one using a H2RG, and the other using a H4RG.

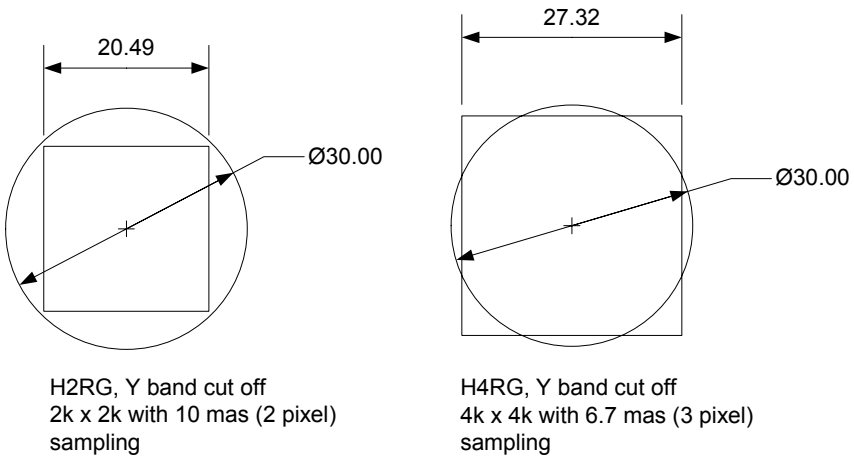

Figure 64: Near-IR imager FOV options
(All dimensions in arc seconds)

As can be appreciated the choice of 3 pixel sampling at the Y band cut off is just one of the possibilities in the trade space of sampling and FOV. For example, selecting the J band cut off results in a 33" x 33" FOV for 3 pixel sampling, and is a little more than 2 pixel sampling at the Y band cut off. This is clearly an area where a trade study involving further simulations to optimize the sampling will be required.

The high contrast science cases, primarily extrasolar planets, require a high performance coronagraph. A study of NGAO high-contrast and companion sensitivity (KAON-497) examined the apodized pupil Lyot coronagraph over a range of occulting spot sizes from 6λ/D to 14 λ/D. The study was not optimistic for some of the more demanding Extrasolar planet cases, but concluded that with excellent control of static non-common path aberrations, as well has highly precise PSF subtraction at least 50% of the science cases were achievable at the 6 to 8 σ confidence level.

3.7.4.2 Instrument Concept

The near-IR imager concept is illustrated in Figure 65. The imager is fully cryogenic instrument with refractive optics.

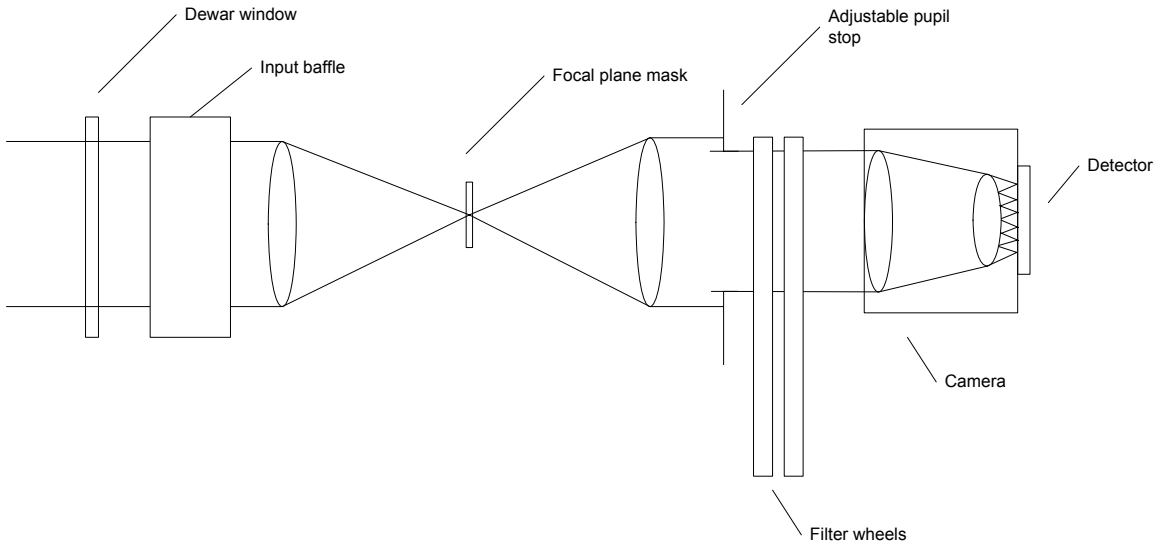

Figure 65: Near-IR imager block diagram

The NGAO focal plane is located inside the dewar where a focal plane baffle is followed by a refractive relay that images the focal plane on a deployable apodized occulting spot. The beam is then collimated and passes through an adjustable Lyot stop located at the pupil plane, followed by the filter wheels. The pupil image is ~68 mm in diameter, with the filters slightly oversize at 70 mm clear aperture. A filter wheel ~260 mm in diameter will accommodate six filters, allowing 2 wheels to support a total of 12 filters. Although the Lyot stop is currently envisioned as circular, it is also possible to provide a hexagonal mask with serrations to match the Keck telescope pupil.

Assuming a H4RG detector with 10 micron pixels, the camera will operate at ~ $f/31$.

Additional features of the design will include a pupil imaging mode to ensure accurate registration to the AO pupil image, and provisions for calibration of instrument wavefront error to aid in optimizing non-common path errors.

Locating the instrument on the NGAO bench optimizes the stability with respect to the AO system, but places additional demands on the performance of vibration isolation for the closed cycle cooling system. This requirement can be met by a pulse tube cooler.

With the exception of the tolerances for the coronagraph, the instrument is relatively straightforward and can make use of heritage designs from earlier WMKO instruments, particularly OSIRIS and MOSFIRE. Both OSIRIS and MOSFIRE use the same basic mechanism design for filter wheels (although MOSFIRE's are much larger), and MOSFIRE also has an adjustable pupil mask. MOSFIRE uses a H-2RG detector with the Teledyne Sidecar ASIC for readout, and the complete mounting and interconnection design should be able to be reused with minor adjustments for the H-4RG in the NGAO near-IR imager.

Similarly, software based on the MOSFIRE heritage can be used for keyword level control of the near-IR imager, and existing tools are available for image display. A number of science cases have specialized data reduction needs, and further consideration of the optimal way to provide data reduction tools will be required.

3.7.5 Visible Imager and IFU

3.7.5.1 Requirements

The science driven requirements for the visible imager and IFU are summarized in Table 19.

Table 19: Summary of the visible imager and IFU science driven requirements

Performance requirements	**Value(s)**
Wavelength range	0.7 to 1.05 μm
FOV Imaging IFU	 30" 2" x 2"
Pixel scales	4.8 mas (3 pixel sampling in i' band) goal of 4 mas (3 pixel sampling in NGAO rl band)
Background	<30% over the unattenuated background from sky+telescope, goal of <20%
Observing modes	
Imaging	Adjustable Lyot stop
Spectroscopy	IFU with 13 mas sampling (diffraction limited in NGAO rl band), R ~100
Coronagraphy	10λ/D apodized pupil Lyot coronagraph
Filters	Photometric NGAO rl, i', z', NGAO z spec, other narrow band filters (Hα, CaII triplet) TBD.

Many of the science cases will expect to use the visible imager to reach shorter wavelengths for the same kinds of observations they will conduct in the visible wavelengths. However, for Galactic center and studies of QSO host galaxies there is significant demand for specialized operation to support narrow band imaging for the Ca II triplet (around 850 nm). Some science cases also will benefit from the availability of a coronagraph, and if NGAO performance reaches the goal of useful Strehl at Hα (656.3 nm) then the visible imager will be expected to support imaging with an Hα filter, moving the short wavelength cut off down to ~620 nm (to allow for reasonable wings on the Hα bandpass).

A more challenging, and perhaps even controversial feature of the visible imager is the requirement, or perhaps goal, to provide an IFU with diffraction limited spatial sampling. This is an extremely demanding requirement, and may not be possible to achieve with useful throughput using a fiber sampling arrangement, while other approaches such as a mirror slicer are not likely to provide the required wavefront quality. This will be an area for significant early study during the instrument's development, and may become a second light addition to the basic NGAO visible imager.

3.7.5.2 Instrument Concept

The concept for the visible imager is shown in Figure 66. The imager uses refractive optics and operates at the AO enclosure temperature with the exception of the detectors, which are in a cooled dewar.

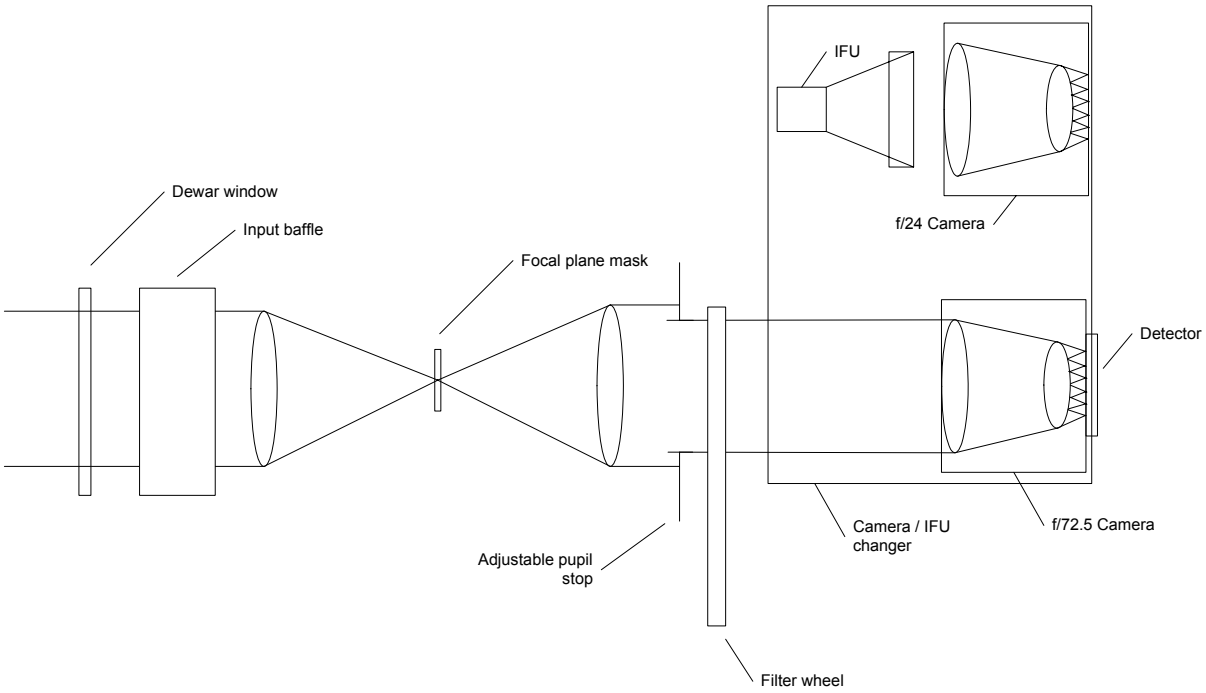

Figure 66: Visible imager block diagram

The APLC is similar in design to the near-IR imager, but with a central occulting spot of 10λ/D. An adjustable Lyot stop is provided to aid in controlling background, particularly at the long wavelength end of the instrument's passband. The same basic filter wheel design developed for the near-IR imager can also be employed, but without the requirement for cryogenically compatible moving parts. Depending on the number of specialized narrow band filters needed, one filter wheel with six filter positions may be sufficient. Assuming a 4k x 4k LBNL detector with 15 micron pixels, the camera will operate at ~ f/72.5 with the 4 mas pixel scale.

In IFU mode the initial concept is a fiber optic image slicer covering a 2" x 2" FOV with 13 mas spatial samples. The image slices are reformatted into 6 virtual slits of ~3950 samples per slit and dispersed using a VPH grism through a second camera (at f/24) onto the detector. This format gives ~680 pixels per spectra, more than enough for the R ~100 spectral resolution. The off center optical path allows a simple rotary mechanism to interchange the IFU/grism and camera with the imaging camera.

Additional features of the design will include a pupil imaging mode to ensure accurate registration to the AO pupil image, and provisions for calibration of instrument wavefront error to aid in optimizing non-common path errors.

Locating the instrument on the NGAO bench optimizes the stability with respect to the AO system, but also raises concerns for vibration if closed cycle refrigeration is used. Detector cooling may be accomplished either with a Cryotiger (vibration concerns) or a small pulse tube cooler (minimal vibration concerns).

With the exception of the IFU, the instrument is relatively straightforward and can make use of heritage designs from earlier WMKO instruments, including similar, but non-cryogenic designs for the filter wheel and adjustable pupil stop as used in MOSFIRE. The detector mounting and dewar can be based on existing designs for instruments such as the UCO/Lick APF spectrograph which uses a Cryotiger cooler. The detector readout can be provided by an Astronomical Research Cameras system, with DSP code and related electronic hardware likely derived from the red detector upgrade currently under development for LRIS.

Similarly, software can be based on existing designs for the keyword level control of the visible imager, and existing tools are available for image display. A number of science cases have specialized data reduction needs, and further consideration of the optimal way to provide data reduction tools will be required.

3.7.6 Single Object Near-IR IFU

Studies of the Galactic center and several of the planetary science cases have a requirement for a single object near-IR IFU operating at the diffraction limit provided by the narrow field relay. The science driven requirements for this instrument are summarized in Table 20.

Table 20: Summary of the single object near-IR IFU science driven requirements

Performance requirements	**Value(s)**
Wavelength range	0.97 to 2.45 μm (Y, J, H, K bands)
Spatial Sampling	20 mas (λ/D in Y band) 35 mas (λ/D at ~mid-H band)
Field of view	1" x 1" up to 4" x 4"
Background	<30% over the unattenuated background from sky+telescope, goal of <20%
Observing modes	
Spectroscopy	
Spectral resolution	R ~ 3,000 to 4,000, goal of R ~ 15,000
Sampling	~2000 pixels per spectra
Filters	Spectrometer Y, J, H, K, narrow band TBD

As noted earlier, the existing OSIRIS instrument used with the Keck II AO system is being considered as the initial single object near-IR IFU for NGAO. OSIRIS is a fine instrument that is producing significant science results. It has a selection of spatial sampling scales, including 20, 35, 50 and 100 mas. The internal wavefront error of the instrument is low enough to support diffraction limited performance down to 20 mas. OSIRIS offers broadband filters, allowing 16 x 64 spatial

samples over the FOV, and a selection of narrow band filters with the corresponding FOVs ranging from 48 x 64 spatial samples down to 16 x 64 for some filters. The resulting FOVs for broadband imaging are 0.32" x 1.28" with the 20 mas spatial sampling, and 0.56" x 2.24" with the 35 mas spatial sampling. In narrow band mode the corresponding FOVs are 0.96" x 1.28" and 1.68" x 2.24" for the filters supporting 48 x 64 spatial samples.

Experience gained with OSIRIS has identified two important issues that make it less than ideal for NGAO. The first is the limited FOV at the 20 and 35 mas scales in broadband mode. Even in narrowband mode the 20 mas FOV barely meets the requirement for Galactic center science, but fails to meet the requirement for the planetary science cases (3" to 4"). The second is that due to some limitations on the sizing of pupil stops for the various plate scales OSIRIS has some performance limitations with respect to sensitivity and background. It is possible that these issues are fundamental enough that the instrument may not be able to satisfy the NGAO background requirement. However, it should be pointed out that a significant part of the apparent limit on OSIRIS sensitivity is due to the high background of the current Keck II AO system, a particular issue that NGAO addresses by cooling the entire AO system.

OSIRIS offers a spectral resolution of R~ 3,800 for the 20 through 50 mas spatial sampling scales, within the range needed for all but the most demanding radial velocity measurements needed for the study of relativistic effects around the central black hole in our galaxy. This science case is thought to require up to R ~15,000 which will be a very difficult requirement to meet with a diffraction limited (lenslet based) IFU and a reasonable FOV.

For reasons of schedule and cost, the current plan is to use OSIRIS as the initial near-IR IFU, and consider the construction of an instrument more closely matched to the requirements of the full compliment of NGAO narrow field science at a future time.

It should also be noted that OSIRIS is designed to operate with a $f/15$ input beam, so operation with the NGAO narrow field relay will require additional optics to reduce the $f/46.5$ beam to $f/15$. A deployable fold mirror is incorporated at the narrow field relay output to permit directing the output beam to a location suitable for OSIRIS within the AO enclosure. OSIRIS is currently a moveable instrument, with electronics mounted directly to the OSIRIS cart. These electronics cannot be located inside the cooled AO enclosure for NGAO, so OSIRIS will require repackaging of its electronics to locate them outside of the AO enclosure.

At least some of these modifications are already planned to allow OSIRIS to move in 2009 to the fixed location with the upgraded Keck I LGS AO system.

3.7.7 Interferometer

It is a requirement for the Interferometer to be supported by AO on both telescopes in the NGAO era. This could be a direct feed from NGAO, most likely after the first relay, or by a separate AO system, which imposes a requirement on being able to exchange AO systems. A trade study was performed on the issue of Keck Interferometer support that is documented in KAON 483. The primary

requirements are to achieve at least the current level of performance while maintaining a common field orientation and polarization from both telescopes.

3.7.8 'OHANA

Both existing Keck AO systems accommodate an 'OHANA fiber injection module at the output of the AO systems. NGAO should provide an output port where this or a similar fiber injection module could be located, and whose output could be successfully interfered with the light from another telescope.

3.7.9 Thermal NIR Imager

A thermal NIR imager has not been given a high priority and therefore no significant evaluation has occurred for this instrument. An evaluation of the reuse of NIRC2, which extends out to L and M-bands, was performed as part of KAON 493.

3.7.10 References

1. Hewett, P. C.; Warren, S. J.; Leggett, S. K.; Hodgkin, S. T., "The UKIRT Infrared Deep Sky Survey ZY JHK photometric system: passbands and synthetic colours," MNRAS, Volume 367, Issue 2, pp. 454-468, 2006 RAS.

2. Tokunaga, A. T.; Simons, D. A.; Vacca, W. D., "The Mauna Kea Observatories Near-Infrared Filter Set II. Specifications for a New JHKL'M' Filter Set for Infrared Astronomy," PASP, Volume 114, Issue 792, pp. 180-186, 2002 The Astronomical Society of the Pacific.

3. Robert J. Thornton, Jr., Jeffrey Douglass, Klaus Hodapp, Tony Young, and Hubert Yamada "Gemini near-infrared imager on-instrument wavefront sensor gimbal tilt stage," Proceedings of the SPIE Volume 3354, Infrared Astronomical Instrumentation, pp. 187-200, SPIE 1998.

4. Sharples, Ray; Bender, Ralf; Bennett, Richard; Burch, Keith; Carter, Paul; Casali, Mark; Clark, Paul; Content, Robert; Davies, Richard; Davies, Roger; Dubbeldam, Marc; Finger, Gert; Genzel, Reinhard; Haefner, Reinhold; Hess, Achim; Kissler-Patig, Markus; Laidlaw, Ken; Lehnert, Matt; Lewis, Ian; Moorwood, Alan; Muschielok, Bernard; Förster Schreiber, Natascha; Pirard, Jeff; Ramsay Howat, Suzanne; Rees, Phil; Richter, Josef; Robertson, David; Robson, Ian; Saglia, Roberto; Tecza, Matthias; Thatte, Naranjan; Todd, Stephen; Wegner, Michael, "Design of the KMOS multi-object integral-field spectrograph," Proceedings of the SPIE Volume 6269, Ground-based Instrumentation for Astronomy, pp. 62691C, SPIE 2006.

5. Dowling, M.; McMahon, P.; Ramsay Howat, S.; Robertson, D. J.; Parr-Burmann, P.; Sharples, R.; Cunnigham, C.; Dickson, C.; Schmoll, J.; Hastings, P.; Lee, D.; Luke, P.; Phillips, N.; Wells, M.; Dipper, N., "A prototype cryogenic pickoff arm for multi-IFU spectrometers," Proceedings of the 11th European Space Mechanisms and Tribology Symposium, ESA SP-591, pp. 289 – 297, 2005.

6. Sharples, Ray M.; Bender, Ralf; Lehnert, Matthew D.; Ramsay Howat, Suzanne K.; Bremer, M. N.; Davies, Roger L.; Genzel, Reinhard; Hofmann, Reiner; Ivison, Rob J.; Saglia, R.; Thatte, Niranjan A., "KMOS: an infrared multiple-object integral field spectrograph for the ESO VLT," Proceedings of the SPIE, Volume 5492, Ground-based Instrumentation for Astronomy, pp. 1179-1186, SPIE 2004.

7. Content, Robert, "New design for integral field spectroscopy with 8-m telescopes," Proceedings of the SPIE Volume 2871, Optical Telescopes of Today and Tomorrow, pp. 1295-1305, SPIE 1997.
8. Allington-Smith, J. R.; Content, R.; Dubbeldam, C. M.; Robertson, D. J.; Preuss, W., "New techniques for integral field spectroscopy - I. Design, construction and testing of the GNIRS IFU," MNRAS, 371, 1, pp. 380-394, 2006.

9. Content, Robert, "Optical design of the KMOS slicer system," Proceedings of the SPIE Volume 6269, Ground-based Instrumentation for Astronomy, pp. 62693S, SPIE 2006.

10. Figer, Donald F.; Rauscher, Bernard J.; Regan, Michael W.; Morse, Ernie; Balleza, Jesus; Bergeron, Louis; Stockman, H. S., "Independent testing of JWST detector prototypes," Proceedings of the SPIE, Volume 5167, pp. 270-301, SPIE 2004.

11. McClean, I.S., private communication, 2007.

12. Stover, R., private communication 2007.

4 PERFORMANCE BUDGETS

In support of the flowdown of requirements from the Science Case and high-level Functional Requirements to component specification, eight system performance metrics were identified in the Science Requirements Document. For three of these metrics, background and transmission, wavefront error and ensquared energy, and high-contrast performance, we have produced associated quantitative performance budgets to identify key performance drivers. For photometric precision, astrometric accuracy, and polarimetry we have identified key drivers and documented these in technical reports that have informed the NGAO design. The final two metrics, observing efficiency and observing uptime, have been given only preliminary consideration and will be further developed in the preliminary design phase.

A concise summary of the various performance budgets developed during the SD phase is presented in KAON 491.

4.1 Background and Transmission

The background and transmission performance budget is developed in KAON 501.

Both AO relays must efficiently transmit the science wavelength light from 0.7 to 2.4 μm (with a goal of 0.656 to 2.4 μm, so as to include Hα). The first relay must also efficiently transmit sodium wavelength light (589 nm) and the additional L-band light (3.4 to 4.2 μm) for the interferometer. This wavelength range must be efficiently divided between the various sensors (LGS and tip-tilt) and the instruments.

Near-IR light will be shared between the tip-tilt sensors and the narrow field instruments. This will require the near-IR beamsplitter for the OSM to be a set of selectable dichroics. This will send some of the near-IR light (for example J and H bands) to the tip-tilt sensors while sending the balance to the narrow field instruments (visible and K band for example).

The transmission budgets developed in KAON 501 take into account all surface counts in the various NGAO system paths. As some resultant NGAO (only) transmissions are:

- K-band Narrow-Field Science Transmission 52.7%
- K-band Wide-Field Science Transmission 56.2%

Where the science path considered is from before the telescope M1 to the interior of an instrument entrance window, including atmospheric dispersion corrector surfaces. For the high-order LGS wavefront sensor path, we have NGAO (only) transmission:

- 589 nm LGS WFS Transmission 38.9%

based on a conservative laser transmission of 0.98 per reflective or refractive surface. In the preliminary design phase, we will work to refine these budgets on a per-coating basis to better optimize system transmission. Excellent coatings and cleanliness will be required for all surfaces.

KAON 501 also contains a detailed analysis of thermal background, particularly for K-band science where the current Keck AO system is known to contribute detrimentally to overall background. The basic result in KAON 501 is that all of the architectures considered for NGAO required approximately the same system cooling, between 259K and 263K to meet science requirements. The design choice we have adopted to achieve the K-band background requirement is to cool the AO optics to 260 K.

The sensitivity delivered by the NGAO system is significantly affected by the total background seen by the instruments. In the present Keck telescope AO systems background is recognized as a significantly limiting sensitivity, particularly for the K band.

Part of the solution to reducing background is the control of scattered light through careful design and implementation, and the use of hexagonal, rotating cold stops matched to the shape of the telescope pupil in the near-IR instruments. However, thermal emission is a significant factor for near-IR observations, particularly longward of 2 μm. Using data from the current Keck II telescope AO system we have developed a model of the background contributed by sky + telescope + AO system that indicates the AO system optics should be cooled to 260 K.

4.2 Wavefront Error and Ensquared Energy

A wavefront error budget for NGAO has been developed using Excel spreadsheet tools developed over several years for the engineering evaluation of AO system performance. The primary purpose of the spreadsheet is to compute AO and instrumental wavefront error budgets for different architectures and science cases, along with Strehl ratios computed using the Marechal approximation. The spreadsheet also computes ensquared energy fractions using a core/halo model for the point spread function, and calculates sky coverage estimates for tip-tilt guide stars employed in LGS architectures from common star density models. The spreadsheet has been validated by comparing the spreadsheet predictions to the current performance of the Keck II LGS AO system with good agreement.

The wavefront error budget is described in KAON 471. The primary tool is an excel spreadsheet (current version Wavefront Error Budget Tool v1.35.xls). This budget is supported and anchored by a number of KAONs. The atmospheric assumptions summarized in KAON 503 are based on previous seeing studies (KAON 303) and new TMT site monitoring data (KAON 415 and 496). The sodium return assumptions are based on sodium density from Keck LGS photometry (KAON 416), long term LIDAR measurements on Haleakala (KAON 417) and comparisons to measured returns from Gemini and Keck (KAON 419). The wavefront error budget tool has been anchored to the performance of the existing Keck AO system in KAON 461. The contribution of Keck telescope segment figure errors is determined in KAONs 468 and 469, and the overall contribution of the telescope to the wavefront errors is determined in KAON 482. Finally, several tomography codes were compared (KAON 475) in order to validate the tomography assumptions used in the wavefront error budget and the null and quadratic mode tomography errors were evaluated (KAON 492).

Related analyses include sky coverage modeling (KAON 470) and performance versus field of view for low order wavefront sensor guide stars (KAON 504).

In order to test and anchor the NGAO error budget tool, a detailed assessment of the Keck II AO performance was performed in KAON 461. Table 21 from this KAON demonstrates the capability of the NGAO tool to model the Keck II AO performance, albeit under somewhat different conditions and with some unknowns (such as d0). More recently we have demonstrated that the NGAO tool can be used to accurately model the demonstrated performance of the Keck II AO system after the Next Generation Wavefront Controller upgrade as shown in Table 22. The NGAO tool has also been used in this Table to support predictions of the performance of the Keck I LGS AO upgrade that is currently underway.

	NGS bright star		**LGS (10th mag)**		**LGS (18th)**	
	Meas-ured	NGAO tool	Meas-ured	NGAO tool	Meas-ured	NGAO tool
Atmospheric fitting	139	110	128	110	128	110
Telescope fitting	60	66	60	66	60	66
Camera	113	110	113	110	113	110
DM bandwidth	103	115	157	146	157	146
DM measurement	17	16	142	150	142	150

TT bandwidth	75	91	109	94	300	243
TT measurement	9	5	23	11	300	349
LGS focus error	0	0	36	36	36	91
Focal anisoplanatism	0	0	175	208	175	208
LGS high-order error	0	0	80	80	80	80
Miscellaneous	120	0	120	0	120	0
Miscellaneous (NGAO)	0	106	0	72	0	72
Calibrations	0	30	0	30	0	30
Total wavefront error	258	250	378	372	557	563
K-band Strehl	0.58	0.57	0.31	0.30	0.08	0.08
Percentile Seeing	75%	65%	75%	65%	75%	65%

Table 21. NGAO error budget tool anchoring to Keck II AO performance.

Error Term	KII NGWFC upgrade	K I (linear pol.)	KI (circular pol.)
Atm. Fitting	118	118	118
Tel. Fitting	66	66	66
Camera	110	110	110
DM Band	125	96	88
DM Measure	152	104	96
TT band	102	102	102
TT measurement	23	23	23
LGS focus error	46	19	19
Focus Aniso.	164	164	164
LGS HO error	80	50	50
Miscellaneous	70	70	70
Calibrations	30	30	30
Total Wavefront Error	348	312	306
K band Strehl	0.37	0.45	0.46

Table 22. The NGAO error budget tools accurately models the upgraded Keck II AO performance.

4.2.1 Key Flowdowns from the Wavefront Error Budget

The AO system architecture is driven by the required wavefront error and related performance budgets to incorporate a number of innovative subsystems that work together to achieve NGAO science goals for optimized cost and technological risk. Key new features of NGAO include multiple LGS beacons and a corresponding number of LGS wavefront sensors, multiple tip-tilt stars, a tomographic wavefront reconstructor and high order correction.

Although a shallow optimization, we find that 64 x 64 actuators is required over the telescope pupil to overcome both atmospheric turbulence and residual figure errors in the Keck telescope primary mirror (KAON's 468 and 469). We believe this is most practically achieved using a small MEMS deformable mirror to correct over a narrow field of view. (A comparison with a large classical DM architecture is presented in KAON 499.) Our requirements for high sky coverage fraction and wide-field d-IFS science leads us to require a large technical field of view. We considered an entirely open-loop control architecture wherein the LGS beams would see no correction, but determined this to be too risky as we would require extremely linear LGS WFS's possessing a very large dynamic

range To address the problem we adopted a two-stage correction architecture, with a first DM with 20 x 20 actuators providing low order correction for the LGS in a closed loop. A second, MEMS, DM is operated in a feed forward or "go to" control mode. We have allocated 40 nm rms to residual go-to control errors (driven primarily by imperfect knowledge of the woofer mirror position), and intend to verify our ability to meet this flowdown specification during the preliminary design phase (using resources at UCSC's LAO). To meet sky coverage goals, we further employ separate, lower order MEMS in each of the tip-tilt sensors, and within each head of the multi-object deployable near-IR IFS instrument (d-IFS).

Our study of the performance of the selected AO system architecture shows that it is quite robust, permitting optimization of the residual wavefront error for a wide range of observing conditions. The spreadsheet tool was configured to optimize the H band Strehl ratio, and certain parameters such as LGS constellation radius, high order update rate, and tip-tilt update rate were allowed to vary within appropriate constraints in order to optimize the Strehl ratio. By allowing for reconfigurable science and LOWFS star laser asterism, we find performance reductions can be mitigated even in poor seeing, low sodium abundance, or in the event of sub-optimal laser power output. An example report from our wavefront error budget tool is shown in Figure 67. Additional examples are provided as an Appendix to this report (section 9).

Keck Wavefront Error Budget Summary

Version 1.35

Mode: **NGAO LGS**
Instrument: **TBD**
Sci. Observation: **KBO**

	Science Band								
	u'	g'	r'	i'	Z	Y	J	H	K
λ (μm)	0.36	0.47	0.62	0.75	0.88	1.03	1.25	1.64	2.20
δλ (μm)	0.06	0.14	0.14	0.15	0.12	0.12	0.16	0.29	0.34
λ/D (mas)	7	10	13	15	18	21	26	34	46

Science High-order Errors (LGS Mode)		Wavefront Error (rms)	Parameter	Strehl Ratio (%)
Atmospheric Fitting Error		48 nm	64 Subaps	
Bandwidth Error		50 nm	**53 Hz (-3db)**	
High-order Measurement Error		60 nm	100 W	
LGS Tomography Error		54 nm	**3 beacon(s)**	
Asterism Deformation Error		22 nm	0.50 m LLT	
Multispectral Error		22 nm	30 zenith angle, H band	
Scintillation Error		13 nm	0.34 Scint index, H-band	
WFS Scintillation Error		10 nm	Alloc	
	112 nm			
Uncorrectable Static Telescope Aberrations		43 nm	64 Acts	
Uncorrectable Dynamic Telescope Aberrations		33 nm	Dekens Ph.D	
Static WFS Zero-point Calibration Error		25 nm	Alloc	
Dynamic WFS Zero-point Calibration Error		40 nm	Alloc	
Leaky Integrator Zero-point Calibration Error		15 nm	Alloc	
Go-to Control Errors		38 nm	Alloc	
Residual Na Layer Focus Change		34 nm	30 m/s Na layer vel	
DM Finite Stroke Errors		0 nm	4.0 um P-P stroke	
DM Hysteresis		13 nm	from TMT	
High-Order Aliasing Error		16 nm	64 Subaps	
DM Drive Digitization		1 nm	16 bits	
Uncorrectable AO System Aberrations		30 nm	Alloc	
Uncorrectable Instrument Aberrations		30 nm	TBD Instrument	
DM-to-lenslet Misregistration		15 nm	Alloc	
DM-to-lenslet Pupil Scale Error		15 nm	Alloc	
	103 nm			
Angular Anisoplanatism Error		23 nm	**1.5 arcsec**	
Total High Order Wavefront Error	152 nm	**154 nm**	**High Order Strehl**	0.00 0.01 0.09 0.19 0.31 0.42 0.56 0.71 0.83

Science Tip/Tilt Errors		Angular Error (rms)	Equivalent WFE (rms)	Parameter	Strehl ratios (%)
	Sci Filter				
Tilt Measurement Error (one-axis)		1.95 mas	33 nm	13.6 mag (mH)	
Tilt Bandwidth Error (one-axis)		1.07 mas	18 nm	25.0 Hz (-3db)	
Tilt Anisoplanatism Error (one-axis)		2.93 mas	50 nm	**33.6 arcsec off-axis**	
Residual Centroid Anisoplanatism		1.10 mas	19 nm	10 x reduction	
Residual Atmospheric Dispersion	*H*	0.26 mas	5 nm	20 x reduction	
Induced Plate Scale Deformations		0.00 mas	0 nm	0 m conj height	
Science Instrument Mechanical Drift		1.25 mas	21 nm	Alloc 15 mas / hr	
Long Exposure Field Rotation Errors		1.25 mas	21 nm	Alloc 15 mas / hr	
Residual Telescope Pointing Jitter (one-axis)		2.12 mas	36 nm	29 Hz input disturbance	
Total Tip/Tilt Error (one-axis)		**4.7 mas**	86 nm	**Tip/Tilt Strehl**	0.29 0.41 0.55 0.64 0.71 0.77 0.83 0.90 0.94
Total Effective Wavefront Error			**175 nm**	**Total Strehl (%)**	0.00 0.01 0.05 0.12 0.22 0.33 0.46 0.64 0.78
				FWHM (mas)	8.7 10.8 13.6 16.2 18.9 21.9 26.3 34.2 45.8

		Spaxel Diameter (mas)	15	34	50	70	80	160	240	480	1000		320
Ensquared Energy	*H*		0.12	0.40	0.60	0.70	0.71	0.74	0.77	0.84	0.88		0.80

Sky Coverage Galactic Lat. 30 deg

Corresponding Sky Coverage	**10.0%**	This fraction of sky can be corrected to the Total Effective WFE shown

Assumptions / Parameters

						LGS power	100 W at laser(s)	Excitation (all LGS 90km)	9913 ph/cm^2/sec
r0	**0.147 m**	**at this zenith**	Wind Speed	11.0 m/s		Zenith Angle	30 deg		
Theta0_eff	**2.14 arcsec**	**at this zenith**	Outer Scale	50 m		HO WFS Rate	1067 Hz	SH using	CCID56
Sodium Abund.	4 x 10^9	atoms/cm^2	LGS Ast. Rad.	0.08 arcmin		HO WFS Noise	1.8 e- rms		
Science AO Mode:	MOAO		HOWFS Trans	0.18		HOWFS anti-aliasing	NO		
LOWFS AO Mode:	MOAO Point and Shoot					LO WFS rate	667 Hz	SH using	H2RG
LOWFS Star Type:	M	Num TT 2	Num 3x3	0		LO WFS Noise	4.5 e- rms		
Max Exposure Time	300 sec	Num TTFA 1	Num HOWFS	0		Max mechanical tip/tilt rejection bandwidth		100 Hz	

Figure 67. Science target wavefront error budget for the Kuiper Belt Object Companion Survey Key Science Case.

In addition the science target WFE budget, we also maintain a separate WFE error budget for the sharpening of the LOWFS NGS stars. An example of this budget, corresponding to the science case in Figure 67 is shown in Figure 68.

Keck Wavefront Error Budget Summary Version 1.35

Mode: **NGAO LGS**
Instrument: **TBD**
Sci. Observation: **KBO**

	Science Band								
	u'	g'	r'	i'	Z	Y	J	H	K
λ (μm)	0.36	0.47	0.62	0.75	0.88	1.03	1.25	1.64	2.20
δλ (μm)	0.06	0.14	0.14	0.15	0.12	0.12	0.16	0.29	0.34
λ/D (mas)	7	10	13	15	18	21	26	34	46

LOWFS High-order Errors (Mode)	35.3 arcsec off-axis	Wavefront Error (rms)	Parameter	Strehl Ratio (%)
Atmospheric Fitting Error		85 nm	32 Acts Across	
Bandwidth Error		50 nm	53 Hz (-3db)	
High-order Measurement Error		64 nm	10% Pupil Shear Criterion	
LGS Tomography Error		125 nm	Point and Shoot	
Asterism Deformation Error		22 nm	0.50 m LLT	
Multispectral Error		22 nm	30 zenith angle, H band	
Scintillation Error		13 nm	0.34 Scint index, H-band	
WFS Scintillation Error		10 nm	Alloc	
	175 nm			
Uncorrectable Static Telescope Aberrations		59 nm	32 Acts Across	
Uncorrectable Dynamic Telescope Aberrations		2 nm	Short exposure	
Static WFS Zero-point Calibration Error		25 nm	Alloc	
Dynamic WFS Zero-point Calibration Error		40 nm	Alloc	
Leaky Integrator Zero-point Calibration Error		15 nm	Alloc	
Go-to Control Errors		38 nm	Alloc	
Residual Na Layer Focus Change		34 nm	30 m/s Na layer vel	
DM Finite Stroke Errors		15 nm	1.5 um P-P MEMS stroke	
DM Hysteresis		2 nm	from LAO	
High-Order Aliasing Error		16 nm	64 Subaps	
DM Drive Digitization		1 nm	16 bits	
Uncorrectable AO System Aberrations		30 nm	Alloc	
Uncorrectable Instrument Aberrations		30 nm	TBD Instrument	
DM-to-lenslet Misregistration		15 nm	Alloc	
DM-to-lenslet Pupil Scale Error		15 nm	Alloc	
	106 nm			
Angular Anisoplanatism Error		0 nm	On LOWFS axis	
Total High Order Wavefront Error	205 nm	**205 nm**	**High Order Strehl**	0.00 0.00 0.01 0.05 0.12 0.22 0.35 0.54 0.71

Assumptions / Parameters

	10%-shear fraction:	0.86	Effective PnS GS radius	0.21 arcmin	LGS power	100 W at laser(s)	LGS return (all beacons)	9913 ph/cm^2/sec	
r0	0.147 m	at this zenith	Wind Speed	11.0 m/s	Zenith Angle	30 deg			
Theta0_eff	2.14 arcsec	at this zenith	Outer Scale	50 m	HO WFS Rate	1059 Hz	SH	using	CCID56
Sodium Abund.	4 x 10^9	atoms/cm^2	LGS Ast. Rad.	0.08 arcmin	HO WFS Noise	1.8 e- rms			
Science AO Mode:	MOAO		HOWFS Trans	0.18	HOWFS anti-aliasing	NO			
LOWFS AO Mode:	MOAO Point and Shoot				LO WFS rate	808 Hz	SH	using	H2RG
LOWFS Star Type:	M	Num TT 2	Num 3x3 0		LO WFS Noise	4.5 e- rms			
Max Exposure Time	300 sec	Num TTFA 1	Num HOWFS 0		Max mechanical tip/tilt rejection bandwidth	50 Hz			

Figure 68. LOWFS NGS wavefront error budget for the KBO Companion Survey Science Case. The NGS is 35" off-axis. We expect such a star to be sharpened to about 35% J-Strehl using MOAO correction based on multi-LGS tomography.

4.2.2 Laser Power considerations

Our error budget analysis indicates to us that for most narrow-field science cases, an equivalent of 100W of sodium laser power (assuming an SOR-type laser return per Watt, providing about 8,500 total photons/cm^2/sec returning to the telescope aperture at zenith) is sufficient to meet nearly all of our narrow-field science performance objectives. This power will be divided to form between 6 and 9 laser beacons (3 to 6 science beacons and 3 point-and-shoot LOWFS beacons). Because of the geometry of projection, we expect the point-and-shoot beacons to substantially sample the atmospheric column in the science direction, allowing us to use all return laser photons to determine the MOAO correction for the narrow-field science instruments.

Prior analyses indicate that performance is a weak function of the detailed distribution of laser power among beacons (CELT Report #9) and we feel the greater uncertainty lies in meeting our tomography performance goals. Flexibility in asterism configuration represents to us a key strategy for risk mitigation in meeting our tomography error specification. The primary cost, therefore of the point-and-shoot sharpening strategy is the need to rebuild the science reconstructor for every observation to account for different LGS asterism geometry, but this is not considered computationally prohibitive (or can be pre-computed based on known LOWFS star geometry).

For the wide-field dIFS instrument science cases, we find that 100W equivalent return is insufficient to robustly meet current science requirements. Fundamentally, this is because wide-field science requires us to measure the atmospheric wavefront error over a larger volume of atmosphere, reducing the signal-to-noise ratio per atmospheric volume element. We find that 150W equivalent return (about 13,000 total photons/cm^2/sec returning to the telescope aperture at zenith) is sufficient to meet the d-IFS science goals. Thus we plan on 100W baseline, with a 50W additional increase to support the d-IFS instrument when commissioned.

In addition, the increase to 150W total equivalent power will make NGAO even more robust to conditions of poor seeing or low sodium abundance. For one key science case, the study of exo-Jupiters with LGS, performance particularly high-contrast performance, will also be improved with the additional laser power, as this case is dominated by high-order wavefront errors (tip/tilt being provided by a relatively bright science target.)

4.2.3 Performance Summary

A summary of wavefront error performance is presented in Table 23.

Observation	Int. time	TT reference	Science LGS aster. diameter	TT error, mas	Sky coverage	High order wavefront error, nm	Effective wavefront error, nm	Strehl (1.65 μm)	Strehl (2.2 μm)
Io	10 s	Science target	NGS	2.7	NGS	104	112	83%	90%
KBO Companior Survey	300 s	Field star	11”	4.7	10%	154	175	64%	78%
Exo-Jupiters with LGS	300 s	Science target	11”	2.4	N/A	152	157	69%	82%
Galaxy / Galaxy Lensing	1200 s	Field star	11”	9.5	30%	159	226	47%	66%
High-Redshift Galaxies	1800 s	Field star	51”	9.3	30%	204	257	55%*	63%*
Galactic Center	30 s	IRS 7	11”	3.0	N/A	177	184	61%	76%

Table 23. Wavefront error budget summary for several NGAO science cases.
The performance metric for the high-redshift Galaxies science cases is ensquared energy in a 70 x 70 mas spaxel. For all other cases, it is Strehl ratio.

The first column of the table indicates the observing scenario. The second column indicates the integration time assumed for the science exposure. The third column indicates the tip-tilt reference used, and the fourth column gives the diameter of the LGS variable radius constellation. The fifth column indicates the tip-tilt error that results from the assumed angular offset of the tip-tilt star. The sixth column gives the sky coverage fraction over which the tip-tilt error will be less than or equal to the error given in column five. This estimate results from the use of common sky coverage models (Spagna and Bachall-Soneira). The last three columns give the high order wavefront error, the total wavefront error with tip-tilt errors, and the H band Strehl. For the extragalactic case, the figure of merit is ensquared energy rather than residual wavefront error, for the 50 mas spatial sampling of each head of the multi-object deployable IFU the ensquared energy is 55% in H-band, assuming full 150W of power and a total of 9 LGS beacons.

These results show that the variable radius LGS constellation and the performance levels assumed for the tomographic wavefront reconstruction, LGS wavefront sensors and near-IR tip-tilt sensors are capable of providing performance that is generally at the level required by the science cases. Initial estimates of NGAO system performance based on laser tomography AO resulted in the adoption of three representative values of residual wavefront error for the science case simulations: 140 nm, 170 nm and 200 nm. This has led to further work to develop additional techniques for performance improvement including the additional three freely positionable LGS and the additional tip-tilt sensors.

The sky coverage fractions required by the extragalactic and Galactic science cases requires optimizing the offset and brightness of the tip-tilt stars. This is accomplished by increasing the faint magnitude limit for tip-tilt stars through the use of tip-tilt sensors operating at near-IR wavelengths combined with MOAO correction using deployable LGS beacons specifically for tip-tilt reference sharpening, and by providing a 150" field of view for tip-tilt star selection.

4.3 Photometric Precision

Requirements for photometric measurements in the NGAO science cases range from 0.05 to 0.1 magnitudes in relative photometry, and ≤ 0.05 magnitudes for absolute photometry. The fundamental condition for high photometric accuracy is stability of the PSF. Because of the high Strehl delivered by the NGAO system, a more stable PSF is expected. Many of the science cases that require the highest photometric accuracy are observing a science target of sufficient brightness (H < 16) to permit use of the science target as an on-axis tip-tilt reference, further improving Strehl performance.

Detailed consideration of the physical effects that can degrade NGAO system photometric precision is documented in KAON 474, including AO system performance, stellar crowding, scintillation, atmospheric attenuation, and detector non-uniformities. The key result of KAON 474 is that in order to meet the scientifically required photometric precision, NGAO will need to provide the astronomical user with detailed and reliable information regarding the NGAO point spread function (PSF) on an exposure-by-exposure basis.

We envision ‘on-axis’ PSF information provide by AO system control and sensing telemetry, in the absence of an appropriate stellar point source reference (which if known will always provide a more

accurate, direct measure of the PSF). NGAO will also provide an estimate of the field-dependent PSF based upon integrated recording of $C_n^2(h,t)$ information from the called-for atmospheric profilometer on the Mauna Kea summit ridge. Recent work at Palomar (Britton 2006) has shown that real time turbulence monitoring giving C_n^2 data during the observation is also useful in improving the results of PSF post processing. This post processing will also be supported by facility PSF deconvolution software.

4.4 Astrometric Precision

Astrometry is important for a number of the Galactic and Solar System science cases. The most demanding requirements are for observations of the Galactic Center where precision of 100 μas is required. The current Keck II LGS AO system with the NIRC2 instrument is able to achieve best-case precision of 250 μas. The high Strehl of the NGAO system (~3 times that of the current LGS AO system under similar conditions) will make a significant contribution to improved accuracy of astrometric measurements by reducing source confusion. In addition, studies of the astrometric precision of the current Keck II LGS AO system indicate that geometric distortion, differential tilt anisoplanatism between the science target and off axis tip-tilt stars (increasing with increasing distance between the two), and differential atmospheric refraction all contribute to the error in astrometric measurements.

Detailed consideration of the physical effects degrading astrometric accuracy for NGAO was documented in KAON 480, including differential atmospheric tilt jitter, geometric distortion, atmospheric refraction, and stellar confusion. Better Strehl ratio and point source contrast from NGAO will help overcome astrometric errors due to stellar confusion in crowded fields, as well as improving point source sensitivity for all observations, thus providing a richer reference field for astrometric calibration.

The same features provided to monitor the PSF and monitor atmospheric turbulence for photometric accuracy would contribute to NGAO astrometric precision. Geometric distortion in the AO system and instruments will be minimized during design and facilities will be incorporated for mapping residual distortion during commissioning. The optical design choice of having mutual optical conjugation of the 1st and 2nd relay DM's is an intention strategy of mitigating NGAO-inducing plate scale distortions into the science focal planes. (Because the systematic error floor will be rapidly reached, we are more concerned about long-term stability and place less emphasis on the potential correction of differential atmospheric tilt jitter afforded by MCAO architectures.) Improved mechanical stability is also a fundamental part of the design of the NGAO system and instruments.

The NGAO system will also incorporate an ADC to reduce the effects of atmospheric refraction, and differential tilt anisoplanatism will be reduced by the use of multiple, optimally located tip-tilt stars. Alignment tools for these multiple tip-tilt stars will minimize plate scale changes due to the AO correction.

4.5 Companion Sensitivity

Another important area for NGAO science is high contrast observations. The Strehl proposed for NGAO is lower than extreme AO systems such as the Gemini Planet Imager, but at the same time, NGAO will provide higher sensitivity and sky coverage that greatly exceeds that of an NGS-only extreme AO system.

Details of the our high-contrast error budget development are presented in detail in KAON 497. One product of this effort is a preliminary numerical budgeting tool (similar in some ways to the wavefront error spreadsheet tool) that allocates contributions to the residual high-contrast 'dark hole' halo to various physical effects, such as atmosphere fitting error, spatial aliasing, control servo lag, measurement noise, and residual tip/tilt errors. In addition, numerical simulations were performed to evaluate the impact of segment gaps (using the grey pixel approximation), segment vibrations, telescope wind-shake, and coronagraph residual diffraction effects. Partial consideration has been made of the residual spatial power spectrum of tomography error, quasi-static LGS calibration errors, telescope static residual errors, and instrument static errors. By taking separate account of the expected residule speckle lifetimes associated with each physical effect, we can predict the achievable contrast for a certain observation in a given integration time.

An example of the high-contrast simulation capability employed in KAON 497 is shown in Figure 69.

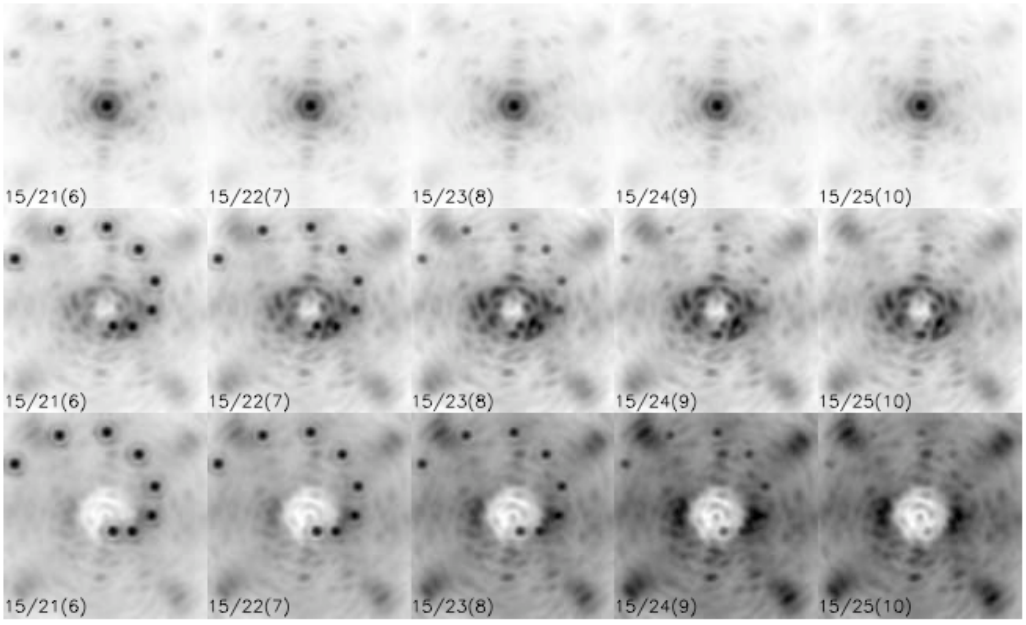

Figure 69. Simulated NGAO J-band science observations with secondary objects inserted.
Top row: AO without coronagraph; middle row: AO + coronagraph with 6 λ/D occulation; bottom row: AO + coronagraph with 10 λ/D occulation. The numbers in the lower left corner of each image indicate the primary /secondary / delta magnitudes, i.e. the format is J_1 / J_2 (ΔJ). The images are stretched (asinh) and individually scaled.

The fundamental conclusion of KAON 497 is that NGAO can indeed serve as a power high-contrast science engine, particularly in the uniqueness space associated with faint science targets (where the NGS-only GPI system will not be usable and where NGAO surpasses in contrast (by an order of magnitude) the LGS-capable PALM-3000 system.)

We found that even with the high-order 64x64 actuator NGAO deformable mirror, residual telescope figure errors lead to speckles with troublesome spatial and temporal scales with the greatest contribution to the high-contrast error budget.

While our analysis of the contrast performance needed indicates that a conventional occulting spot coronagraph with an apodized (hexagonal, rotating) Lyot stop will meet the needs of the majority of the NGAO high contrast science cases, we will also in the preliminary design phase investigate the use of more advanced techniques such as non-redundant aperture masking. To help address specific needs identified in our high-contrast error budget initial analysis, we are expecting further analysis in the preliminary design phase of a variable diameter spatial filter as the field stop for the NGAO NGS HOWFS.

The level of contrast achieved with NGAO will ultimately depend on the control of systematic errors such as non-static, non-common path aberrations, servo lag error and various sources of speckle. Speckle suppression techniques including spatially resolved spectroscopy will be available for NGAO observations and we intend to incorporate to the extent possible the calibration "best practices" discovered by the GPI project.

4.6 Polarimetric Precision

Polarimetric precision was considered only superficially in the system design phase. We identified the K-mirror rotator as a potential detriment to polarimetric precision, but adopted this in our architecture for its other system advantages (simplicity and cost).

We do not yet know how stable or calibratable polarimetry will be with NGAO, but expect to give this further consideration in the preliminary design phase.

One potential strategy for polarimetry for further consideration is the use of the K-mirror rotator in a fixed orientation, allowing the science image to rotate on the sky. For high-contrast polarimetry, this may be an acceptable observing mode, but this will require more careful analysis of all the system implications.

4.7 Observing Efficiency and Uptime

KAON 463 discusses the observing efficiency and uptime of the existing Keck LGS AO system for reference. Observing efficiency has already been discussed in section 3.6.1.2. More detailed efficiency and uptime budgets will be produced in the preliminary design phase.

5 REQUIREMENTS DEVELOPMENT AND COMPLIANCE

The requirements development process is discussed in KAON 573 and is illustrated schematically in Figure 70. The process began by understanding the goals that the Keck community had for a next generation AO capability at WMKO. This was followed by the development of science cases to understand the science drivers and requirements on this NGAO capability. The Science Case Requirements Document (KAON 455) discusses and documents this process and the resultant science requirements. These requirements were developed in parallel with initial performance budgets and analysis to determine feasibility. The science requirements and additional observatory and user requirements were subsequently documented in the System Requirements Document (KAON 456). Both of these documents were intended to be architecture independent. As the team developed an architecture and subsystem designs to satisfy the system requirements the next level of implementation dependent requirements were documented in the Functional Requirements Document (KAON 573). Appendix B of KAON 573 is a printout from the requirements database. The Operations Concept Document and Interface Control Documents will be developed during the Preliminary Design. The document you are currently reading is the System Design Manual shown in the V-diagram as a product of the subsystem architecture definition.

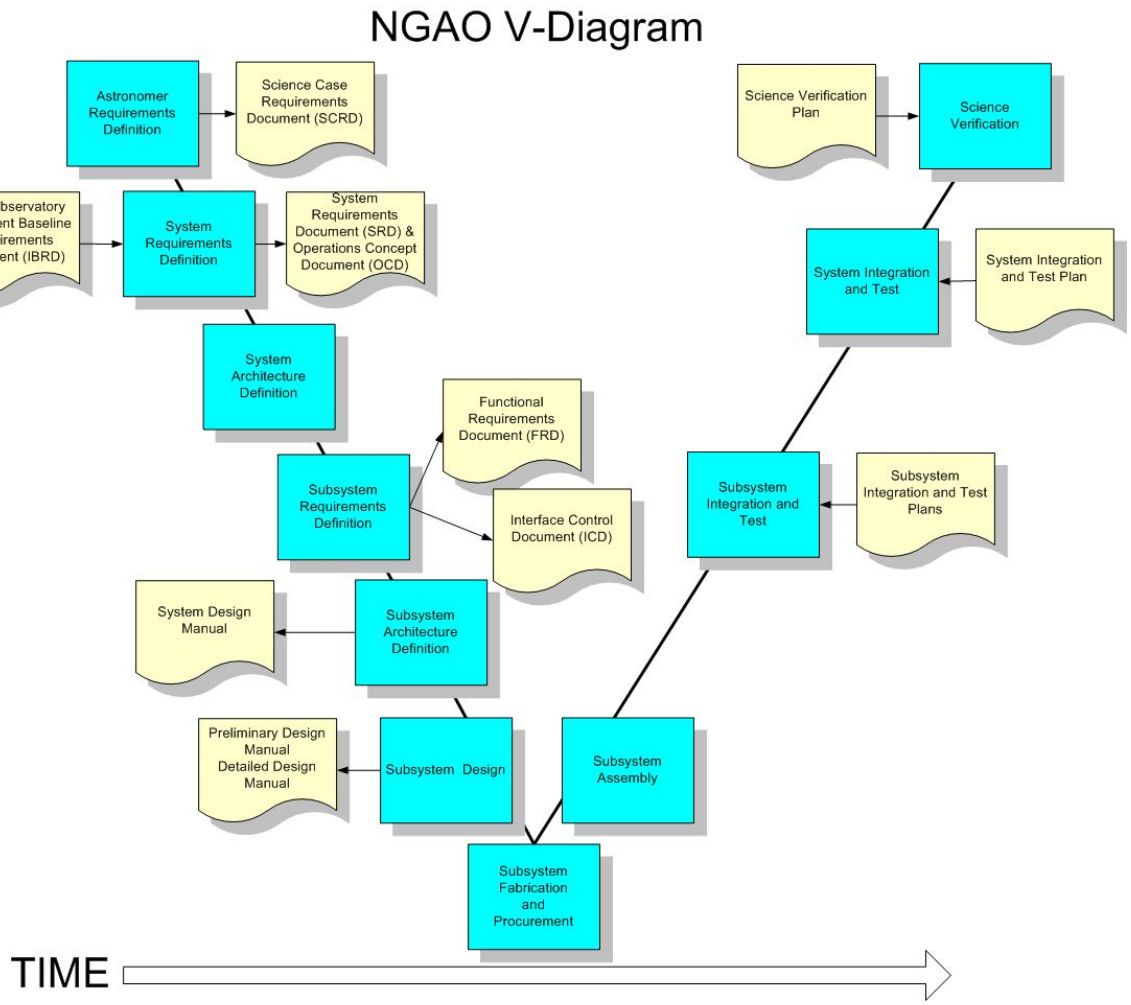

Figure 70. NGAO project V-diagram including the design and development process. *Processes are shown in blue and associated documentation in tan.*

In all levels of the requirements documents, steps were taken to assure that each documented specification is traceable back to its origin or driver. The most relevant sources are the top level NGAO science requirements and essential observatory standards but in many cases requirements are generated based on architectural design decisions, engineering best judgments, or for other reasons. Maintaining requirements traceability enables reasonable change control, so that the systems engineer is able to understand and manage the impact of descopes, engineering "push backs," error budget redistribution, etc.

The science case requirements were summarized in a spreadsheet that was used in the architecture selection process (KAON 499 describes this selection process). The current version of this spreadsheet can be found in KAON 548 or as an Appendix to the System Design Report (KAON 575). The cascaded relay architecture we have selected and developed has been demonstrated in our performance budget analyses (see section 4) to meet the background, wavefront error, encircled energy and sky coverage science case requirements.

Although not yet demonstrated by performance budgets or analysis we are developing the functional requirements and designs to ensure that the astrometric and photometric requirements will be met. A major element of meeting these requirements will be providing a good calibration of the PSF.

The key elements of the selected architecture flowed directly from the science case requirements. At the highest level these can be summarized as follows:

1. Dramatically improved performance at near infrared wavelengths.
   a. Improved IR sensitivity.
      - High Strehls (≥ 80% at K-band) are required over narrow fields. The flowed down requirements are derived from the wavefront error performance budget and assumption about how these error terms can be met. These flowed down requirements include number of actuators in the narrow field, required system bandwidth, number of LGS, number of NGS, required laser power, etc.
      - Lower backgrounds. This is particularly driven by the high redshift galaxy science. This requirement has driven the need for a cooled AO system and the required temperature.
   b. Improved astrometric, photometric and companion sensitivity performance.
      - Improved IR sensitivity is required (see above).
      - It will also be critical to improve the PSF stability and knowledge. The requirements on the PSF stability and knowledge to achieve the astrometric, photometric and companion sensitivity requirements will be developed during the Preliminary Design. The astrometric error budget and PSF reconstruction tools will be developed during the Preliminary Design.

2. Increased sky coverage.
      - Wide field required. This requirement drove us to a wider field than needed for the d-IFS in order to find suitable NGS for tip-tilt sensing. The field requirement was determined via the analysis documented in KAON 504.
      - Ability to use faint NGS. This requirement drove us to the architecture where we provide AO correction of the tip-tilt stars.

3. Efficient extragalactic target surveys.
   a. Science instrument.
      - The need for efficient acquisition of spectral and imaging data drove us to an integral field spectrograph.
      - The availability of multiple targets over a modest (2′ diameter field) and the need to perform surveys efficiently drove us to a multiple head instrument.
      - The need to adapt to the observation field drove us to deployable heads.
   b. Sensitivity.
      - The required image resolution allowed us to work to an encircled energy requirement that required fewer actuators than for the narrow field science.

- This requirement drove us to a choice between multi-conjugate and multi-object AO to achieve good correction over a wide field. Maximizing the performance over narrow non-contiguous fields led to the selection of MOAO.
- The need for low backgrounds drove the need for a cooled AO enclosure.

4. AO correction in the red portion of the visible spectrum.
   - This drove the need to transmit these wavelengths to the visible science instruments and to share visible light with the LGS and NGS wavefront sensors via appropriate dichroics.

5. Science instruments that will facilitate the range of science programs.
   - This drove the selection and conceptual design of the science instruments described in section 3.7.
   - This drove the providing of locations for these science instruments in the design.

We have also mapped each science case to a configuration of the NGAO system as shown in Table 24 to ensure that the NGAO architecture and subsystems can operationally support each science case (the configurations are maintained in KAON 550). The numbers in the NGS and LGS configuration columns refer to NGAO system configurations. A partial view of the configuration spreadsheet is provided in Figure 55.

Table 24. Science case mapping to NGAO configurations.

#	Key Science Drivers	NGS Configuration		LGS Configuration		Notes
		Primary	Secondary	Primary	Secondary	
1	Minor planets as remnants of early Solar System					Differential tracking option needed for LOWFS & truth WFS
	Survey			4e	4a-d,4f	
	Orbit Determination			5a	4ef,5b	
2	Planets around low-mass stars					
	Survey			4c-f,6c-f		
	Spectra			6c-f,4c-f		Narrow band imaging filters may be adequate
3	General Relativity at the Galactic Center					
	Astrometry			4a	4c	
	Radial Velocities with dIFS			1		
	Radial Velocities with OSIRIS			6ac		
4	Black hole masses in nearby AGNs			Vis spectra	6ce	
5	High-redshift galaxies			1		

#	Science Drivers	NGS Configuration		LGS Configuration		Notes
		Primary	Secondary	Primary	Secondary	
1	Asteroid size, shape, composition			5a	4e	Differential tracking option needed for LOWFS & truth WFS
2	Giant Planets and their moons					Differential tracking option needed for LOWFS & truth WFS
	Imaging	4a	5a, 7a	4ace	5a, 7ace	
	Spectroscopy	6a		6ace		
3	Debris disks and Young Stellar Objects					
	Imaging	4ab		4a-f		Need coronagraph. Polarimetry useful.
	Spectroscopy	6ab		6a-f		
4	Astrometry in sparse fields			4ace		
5	Resolved stellar populations in crowded fields			4ace		
6	QSO host galaxies					
	Imaging			4ace		
	Spectroscopy			6ace		
7	Gravitationally lensed galaxies by other galaxies					
	Imaging			4ace	5a	
	Spectroscopy			6ace		
8	Gravitationally lensed galaxies by clusters					
	Imaging			4ace		
	Spectroscopy			1		
9	Backup Science					
	Faint NGS science	9ab				

6 ALTERNATE SYSTEM ARCHITECTURES

During the selection of the system architecture described in this document several alternate architectures were also evaluated and ranked. Each of these architectures, along with our adopted cascaded relay, are described and evaluated in KAON 499.

1. Split relay. The LOWFS, NIR deployable IFU and LGS wavefront sensor are fed directly from the telescope (and therefore must rotate). The narrow field science instruments are fed by a refractive AO relay including a K-mirror and ADC. Some technical evaluation details for this architecture are discussed in KAON 506.
2. Adaptive secondary mirror. All of the science instruments and wavefront sensors are fed directly by the telescope. An adaptive secondary trade study was performed in KAON 485. The existence of an adaptive secondary could potentially improve the performance on seeing

limited instruments, and would offer the optimal approach to a ground layer AO system (see KAON 472).

3. Large relay. A large rotator and AO relay feed all of the science instruments and wavefront sensors. This is the architecture that was described in the NGAO proposal (KAON 400).
4. Keck I upgrade. Quite similar to the selected cascaded relay approach. The NIR deployable IFU and LGS WFS both follow the existing AO relay. A second, higher order relay feeds the narrow field science instruments. The difference is that this is an upgrade to the existing system, rather than a fresh start. KAONs 500 and 502 describe this upgrade in some detail. During preliminary design, we will look more closely at interim benefits to the Keck I LGS system that could be realized as part of our NGAO risk mitigation.

7 TRADE STUDIES

A number of trade studies were performed early in the system design phase to inform the system architecture down select and design choices. A list of these trade studies is provided in Table 25.

Table 25. List of trade studies performed.

Trade Study Title	KAON #
MOAO & MCAO	452
NGAO Versus Keck AO Upgrades	462
Adaptive Secondary Mirror Option	485
Keck Interferometer Support	483 (& 428)
GLAO for non-NGAO Instruments	472
Instrument Reuse	493
Telescope Wavefront Errors	482
Observing Model	476
Rayleigh Rejection	490
LGS Wavefront Sensor Type & number of subapertures	465
Low Order Wavefront Sensor number & type	470
Low Order Wavefront Sensor Architecture	487
LGS Asterism Geometry and Size	429
Variable Versus Fixed LGS Asterism Geometry	427
Uplink Compensation	509

These trade studies were key inputs to the architecture downselection process described in KAON 499.

7.1 MOAO and MCAO Trade Study

This trade study lists the following top-level conclusions.

The science advantages of MCAO are:

1) Contiguous AO-corrected field of view
    a. Choice of PSF stars in the field
    b. Higher packing density of IFU pickoffs

c. Very extended objects: Jupiter, Saturn, Uranus rings
d. Long exposure of hi-Z field galaxies

2) DMs in closed loop, eliminating DM calibration error and drift

The science disadvantages of the MCAO architecture are:

1) Higher field-dependent anisoplanatic error than a MOAO system
2) Extra surfaces in the relay contribute to background emission and reduce throughput.
3) DMs in series could distort the contiguous field randomly resulting in higher astrometric error.
4) Front-end relay adds field and zenith dependent distortion and aberration into the LGS beams, which even if pre-calibrated, will introduce some amount of wavefront error to the science beams via the closed loop.

The science advantages of MOAO are:

1) Lower isoplanatic error at the science field points
2) MOAO units are deployable on a wider field of regard than MCAO, sky coverage is enhanced by correcting tip/tilt stars with their own MOAO units, allowing dimmer tip/tilt stars than with MCAO.
3) Reduced number of optical surfaces for AO correction that minimizes emissivity and optimizes throughput
4) No field distortion introduced by DMs in series.

Science disadvantages of the MOAO architecture are:

1) Discontinuous field of view hampers crowded field studies, e.g. contamination by nearby stars' seeing halos, which are not imaged and so, cannot be PSF subtracted.
2) Cannot image large extended objects
3) DMs are open loop controlled and are thus subject to calibration and drift error.

The MCAO architecture has the following implementation advantage:

1) AO control of DMs is closed-loop, allowing feedback of mirror shape to the control system.

MCAO has the following implementation disadvantages:

1) Powered relay optics and DMs not conjugate to the ground must be larger diameter than a DM at a pupil.
2) The AO relay introduces non-common-path aberration and pupil distortion and may force custom design of the wavefront sensor optics to compensate. The custom optics may need to have moving components in order to track sodium layer distance change with zenith angle.
3) Pupil size has a lower limit set by physical optics. This size is larger than MEMS DMs produced today

The implementation advantages of MOAO are:

1) MEMS are small, enabling the AO systems to be tucked into instruments, making them ideally suited for compact MOAO units.

2) MEMS are low cost. The marginal cost of scaling to high actuator counts is considerably lower than that for large DMs. For the BMC devices, this number today appears to be around $200-300 per actuator as compared to about $1500 per actuator on a piezoelectric deformable mirror. The low cost makes it practical to have a spare on hand.
3) "Go-to" repeatability – A major advantage of an electrostatic actuation over piezoelectric actuation is the absence of hysteretic effects in the displacement to voltage response curves. This implies that the devices could be driven open loop to given surface deflections.
4) The low cost and small size of MEMS DMs opens up the possibility of "ubiquitous MEMS," i.e. devices sprinkled throughout the system to elegantly solve tough optical problems.

a. MEMS DM in each wavefront sensor: This creates a mini closed loop AO system in which the wavefront detector is kept near null, where its linearity properties are best. The predictable voltage response of the MEMS allows it to be used as the probe of the grosser portion of the wavefront shape, which would be added to the wavefront sensor's residuals to complete the wavefront measurement. A variant of this is to use MEMS DMs to correct for the slowly varying but known non-common path aberrations of LGS wavefronts.

b. MEMS in the tip/tilt sensors: If there are enough degrees of freedom to form diffraction limited cores at the sensing wavelength, fainter guide stars can be used to sense tip/tilt to a given accuracy because centroid error is proportional to the spot size and inversely proportional to square root of brightness. The ability to use fainter guide stars would give us higher sky coverage.

Practical disadvantages of MOAO are:

1) MEMS stroke dynamic range may not be adequate to correct the whole atmosphere, leading to a requirement for dual-mirror "woofer-tweeter" MOAO units. The latest generation of MEMS mirrors under development (a 4000 actuator mirror for the Gemini Planet Imager AO system) should have just enough mechanical stroke to cover 5-σ wavefront variation for the Keck 10 meter tip/tilt removed wavefront.
2) MEMS mirrors have not been shown to work yet in astronomical instruments (this is a risk issue)
3) High-order MEMS are presently available from only one manufacturer (another risk issue)

7.2 NGAO versus Keck Upgrade Trade Study

The authors concluded that a Keck AO upgrade was worth further consideration. Implementation options range from an incremental approach, delivering new science capabilities along the way, to a single implementation effort without the interim disruptions to science.

The pros and cons for a Keck AO upgrade include:

1) Pro - Potentially a lower cost. However, as the costs are further evaluated, they would likely increase.

2) Pro - The interferometer's needs are addressed. This will be a difficult problem for NGAO and might require a complete reconfiguration or AO systems.
3) Con - Likely lower performance ultimately than NGAO
4) Con - Only two science instruments (possibly 3) could be available at any one time, unless the other telescope is also upgraded. Unclear yet how many simultaneous instruments could be offered by NGAO.

A Keck AO upgrade would allow for an incremental approach. The pros and cons for an incremental approach include the following.

1) Pro - Some performance improvements could be available sooner.
2) Pro - The system could be improved as funds became available.
3) Pro - It also might allow for and address the need for periodic replacement and maintenance (and the funds to support these) that could be done as the same time as the upgrades.
4) Pro - This approach doesn't require as much of an all or nothing risk. Although this risk could be mitigated for NGAO, there is the risk that we would not have the funds to complete the system.
5) Con - Periodic shutdowns would be required which would make the system unavailable for science, although a one-time shutdown might take a substantial amount of time if NGAO is installed in one step.
6) Con - Increases the risk to operations due to a system always under development.
7) Con - Increases the risk to the development team schedule from potentially needing to support an operational system.
8) Con - Adds a constant stress to the development team.

7.3 Adaptive Secondary Mirror Options Trade Study

The author of this study noted the following points regarding the use of an adaptive secondary mirror.

1) An ASM offers the lowest emissivity and highest throughput option to the science instrument since it is no longer necessary to have a separate tip/tilt mirror or to re-image the telescope pupil onto a deformable mirror (at least 4 reflections are saved).
2) An ASM combines the tip/tilt, DM, and chopping roles all on the same mirror and therefore provides a more stable thermal background that is easier to subtract.
3) An ASM could potentially be used to replace one or more of the tip/tilt mirror, chopping, and DM roles for the existing AO systems (replace the DM with a flat?) if a Keck AO upgrade path were chosen.
4) There will still be the issue of picking off light for wavefront sensing and dealing with field rotation. A new issue is that the DM (ASM) will be rotating with respect to the wavefront sensing.
5) Space for a laser launch telescope behind the secondary mirror could be built into the ASM design, as opposed to design it into the existing secondary mirror module.

6) The use of an ASM could also allow the AO system to be physically smaller which might allow small field AO systems and science instruments to be placed at Cassegrain. This could also allow the existing AO systems to be left at Nasmyth to feed the Interferometer. Cassegrain would also be the best location for the near-IR deployable IFU since low emissivity is a critical requirement for the extragalactic science.

7.4 Keck Interferometer Support Trade Study

The authors of this study state that no ideal solution has been found for supporting the interferometer with NGAO. The following points are noted about each option:

1) Swapping Keck I/II with NGAO
   a. Hardware costs relatively low, compared to building new AO systems
   b. Cost of moving NGAO is higher than fixed NGAO. This assumes the final design is similar to the proposal design.
2) Matching NGAO to Keck
   a. Challenging to match polarization states
   b. Likely requires NGAO relay with K-mirror and in plane optics
   c. No broad wavelength solution found
   d. Lower cost compared to other options, approximately 100K compared to millions
3) Two AO systems
   a. AO secondary on each telescope
      Elegant solution, but costly
      Utility of a shared capability could offset higher costs
   b. MEMs AO for each IF arm
      Relatively inexpensive
      Small footprint allows more mounting/packaging options

The lowest cost option but perhaps the most technically challenging will be matching NGAO to a legacy AO system. A more formal consultation with the Keck Interferometer team was recommended as a next step.

7.5 GLAO for non-NGAO instruments Trade Study

The author of this KAON noted that it is clear that there are potential benefits, ranging from modest to significant, to non-NGAO instruments from a GLAO implementation. If a GLAO system for Keck was pursued (independently of NGAO), such a system would require the existence of an ASM and at least 4 LGS. These might be acquired as part of NGAO or as a separate project. Following the design of these subsystems, the next technical study should investigate the most efficient WFS implementation and look into the technical solutions that have the best cost/capability trade. New WFS modules could be built exclusively for each non-NGAO instrument that wanted to use GLAO. A simpler alternative might be building a single GLAO WFS module that could make GLAO available to all instruments at a given focus, e.g. all Nasmyth instruments or all Cassegrain instruments.

7.6 Telescope Wavefront Errors Trade Study

The main results of this trade study can be summarized as:

1) Full aperture tip tilt errors could dominate the tip/tilt error budget.
    a. Resulting in poor sky coverage
    b. "Encircled Energy Science" might be impacted less
2) Segment motion
    Acceptable error, comparable to NGAO June 2006 proposal and current error budget
3) Segment figures
    Acceptable error, comparable to NGAO June 2006 proposal and current error budget
4) Segment phasing
    Small, needs to be added to NGAO budget, interaction with figure errors not tested
5) Fast guiding on stars outside NGAO corrected field of view appears feasible

The trade study authors' recommendations would be

1) Perform additional analysis of the gains in tracking beyond the simple PI controller considered in this study. Examples would be parametric oscillator and Kalman filters.
2) Understand what might be done to reduce 29 Hz vibrations in telescope segments, secondary, and tertiary.
3) Continue to investigate ways to improve the segment figures. NGAO should leverage information from the TMT study of warping harness at Keck.

Based on this study, it appears that full aperture tilt needs to be given higher priority in the NGAO design and in mitigation efforts with the current Keck AO system. Other telescope wavefront errors appear to be accounted for correctly in the NGAO error budget. It would be advantageous to reduce 29 Hz vibration drivers such as pumps and motors even further, as this is cost effective compared to the cost of an additional "fast guider" for NGAO. The possibility of using seeing limited guide stars outside the corrected field of NGAO appears feasible and should be studied further than the simple scaling law analysis included in this report.

7.7 Observing Model Trade Study

The authors presented a trade study for the NGAO observing models by first defining top-level goals for NGAO science operations. They then reviewed and discussed the existing classical and queue-service models from the published data. They have presented three case-study observing models to further assess a range of possibilities for NGAO. The authors recommend that the NGAO observing model be neither the lean-classical observing model nor the queue-service observing model and they recommend working with the Keck science community to develop a new flexible observing model (possibly phased) for NGAO.

The authors further recommend that the NGAO science operations strongly support the top-level goals that emphasize the need for high quality data products and our given estimate for that effort. They note that this will require designing and building an extensive suite of simulation and observing tools for the AO and the science instruments. It additionally requires the development of reliable and

accurate calibrations methods for photometry and astrometry. This implies knowledge of the PSF across the science field of view. The authors note that a great deal of potential synergy exists between the Observatory and the community to support the science goals and minimize the implementation costs of observational tools.

7.8 Rayleigh Rejection Trade Study

The authors of this study note that fratricide due to Rayleigh scatter is a serious issue for a 5 laser beacon AO system. It is ideal to use a 1-3 micro-sec pulsed laser to mitigate this problem. In the event of this not being available, and mode-locked CW laser being the only option, appropriate background subtraction, projection location, baffles, and stops are to be chosen. The authors note that the effect of fratricide still needs to be quantified more accurately via detailed simulations, though the current study has developed a preliminary model of this effect. The authors advise that NGAO use a center projection method for the LGS. The authors recommend that a safety margin must be included in the error budget to account for the short and long term fluctuations in Rayleigh scatter caused by variations in the atmosphere. Although laser collisions, which is observing through the laser beam projected from another telescope, are to be avoided, it does not actually render the data useless. The effect of a collision is comparable to the sky background at Mauna Kea in the V-band.

7.9 LGS Wavefront Sensor Type and Number of Subapertures Trade Study

The authors of this study recommended that if NGAO chooses to use a CW laser it is best to work with a Shack Hartmann WFS and a radial geometry CCD. Both technologies are mature (as compared to counterparts) and the advantage of pyramid WFS is only a few (less than 5 nm) nm in WFE as presented by current models. In the wide field cases, the majority of the error (288 nm) comes from tomography.

The authors of this study performed a benefit vs. cost (laser power) analysis using Rich Dekany's WFE spreadsheet with the general assumptions described in the report. Additional assumptions and parameters were used to simulate the science observing scenarios: the atmosphere used was based on KAON 303 and pixel charge diffusion was assumed to be 0.3 pixels for the Shack-Hartmann WFS case. With a pyramid WFS, the charge diffusion was assumed to be zero. The Shack Hartmann wavefront sensor charge diffusion and the AO spot size summed in quadrature was used instead of the lenslet diffraction spot size. No MEMS mirror based active correction of the spot size at the WFS was considered.

7.10 Low Order Wavefront Sensor Sky Coverage Trade Study

Based on the results obtained within this study, the authors made the following observations, notes and caveats:

> 1) Near IR sensing is preferable to visible for the NGS WFS. In particular, a combination of J+H bands gives the best performance.

2) Multiple TT stars can significantly improve the tilt estimate. A further improvement can also be achieved if one of the NGS WFS also measures focus, which aids in estimating the combinations of quadratic null modes.
3) A 2 arc min diameter patrol field for finding NGS is sufficient. There is little benefit to making the field larger due to the reduced partial correction and tilt anisoplanatism from being so far off-axis.
4) The radius of the LGS asterism affects the partial correction of the NGS and hence the sky coverage. The LGS asterism radius needs to be optimized as a function of a weighted sum of the tomography error over the science field and the residual TT error from the partially corrected NGS.

7.11 Low Order Wavefront Sensor Architecture Trade Study

The authors made the following recommendation based on this study and the previous one (see section 7.10).

1) 2 near-IR (J+H) tip/tilt sensors with built-in MEMS DM for image sharpening. These sensors may employ a STRAP type optical design adapted to a near-IR detector.
2) 1 near-IR (J+H) pyramid sensor with at least 2x2 sub-apertures and with a built-in MEMS DM for image sharpening.
3) At least 1 LGS dedicated to the LOWFS system for image sharpening.

The STRAP sensor (System for Tip/Tilt Removal with Avalanche Photodiodes) is mentioned here because it is a well documented and routinely used device that has optical properties in common with a pyramid sensor, making it interesting for the current study. It can be regarded as a lenslet-based 1x1 pyramid sensor without modulation. Given the superiority of the PWFS compared to the Shack-Hartmann implementation observed in simulations in the report, even in the 1x1 tip/tilt-only case, the authors recommended a near-IR version of a STRAP type sensor as a preliminary option that could make a good candidate for the tip/tilt LOWFS. With a 2x2 PWFS in slope mode, the configuration listed above gives a total of 12 measurements which is enough to reliably resolve the first nine tomography null-modes (and the authors of this study believed this to be sufficient, compare to KAON 470).

Although it drives up the cost somewhat, in the cost/performance trade-off it seems to make sense to provide for at least one LGS dedicated to the LOWFS system, in order to be always ensured of decent performance of at least one of the sensors. For each observing scenario, based upon the high order WFS asterism and the geometry of candidate low order WFS NGSs, one would direct the low order WFS dedicated LGS to the NGS that would benefit the scenario the most and have the remaining two low-order sensors drive their MEMS DMs from high order WFS telemetry using MOAO reconstruction algorithms. How such a decision matrix might look is beyond the scope of this study, but to a zero-order approximation, although potentially over-simplifying the situation, it might be an acceptable strategy to always use the low order WFS dedicated LGS for the 2x2 PWFS in order to ensure a minimum level of performance by this sensor.

7.12 LGS Asterism Geometry and Size Trade Study

The authors of this study state that based on the science cases it seems clear that the quincunx asterism (5a) will be unable to deliver the required LGS tomography performance in all cases under the given seeing conditions. Barring relaxed requirements from the science cases or a substantial improvement of the average seeing on Mauna Kea, the NGAO system will most likely need to look to alternative asterism that can deliver higher performance levels. Taking into account the points made in sections 2.1, 2.2, and 2.3 of the full report, as well as the realism of having a finite budget for building the instrument, it seems like a reasonable recommendation that future studies and iterations on the NGAO performance budgets should look at asterisms having in the range of 7-9 LGS. The final choice should be deferred until much more comprehensive simulations have been conducted using a tool like e.g. LAOS, but as a starting point, this trade study nominates the three asterisms 7a, 8a, and 9c in the nomenclature of the original report.

7.13 Variable versus Fixed LGS Asterism Trade Study

The authors of this study conclude that for a continuously variable laser guider star asterism:

1) There is little performance benefit in narrow field performance.
2) There is a significant performance benefit for d-IFU science when the mismatch between asterism and target radius exceeds 20 arc sec.
3) Cost overhead in optomechanical hardware is small.
4) Real-time and supervisory control software costs will dominate.
5) In addition, any laser launch costs that may arise due to a continuously variable asterism should be evaluated, as this was not part of the study.

Software and laser launch costs allowing, NGAO should assume a continuously variable asterism in the system design.

7.14 Instrument Reuse Trade Study

The authors made the following conclusions from their study.

NIRC-2 as the NGAO Near-IR imager:

1) This NGAO instrument requires excellent RWFE leading to exquisite imaging quality across the field of view. The NIRC-2 camera optics for all plate scales are not sufficiently high enough quality for this application.
2) Upgrading one or all of the camera channels is not sufficient or cost effective over designing a fixed plate scale imager from scratch.
3) The OSIRIS offset imager is an intriguing alternative and may be suitable for a first light Near-IR imager, especially in J and H, where the oversized pupil stop has less detrimental effect to sensitivity.

NIRC-2 as the L/M band imager:

1) With an approximate 500k optics upgrade to the middle channel of NIRC-2, in addition to upgraded detector electronics, NIRC-2 could satisfy the requirements for the NGAO L and M band imager.
2) The optimum solution for this specific instrument is to incorporate a deformable secondary mirror feeding a Cassegrain mounted imager, designed from scratch.
3) The current M band performance of the Keck telescope combined with the AO system, including K-mirror de-rotator, is poor.

OSIRIS as the Near-IR IFU:

1) As it currently stands OSIRIS does not fulfill the maximum field of view requirements of this instrument, nor the K band background performance requirements at any of the pixel scales, nor the required resolution especially at the largest pixel scale (100mas).
2) If only the fine scales are required for OSIRIS it is possible to consider pupil stop improvements that reduce the amount of contaminating radiation that increases the measured sky background. A replacement of the grating may help increase throughput.
3) Designing an IFU spectrograph offering the large range of plate scales that is found in OSIRIS is technically quite challenging. Considering the incorporation of the coarse scale in the d-IFS instrument, the science team is asked to justify the requirement of both the fine and coarse scales for the Near-IR IFU and therefore clarify the maximum field of view. If the 100mas scale is not required, or does not need to satisfy the requirements of background and resolution stated, then OSIRIS can be considered as a candidate for this NGAO instrument.
4) There may be some issue with implementing OSIRIS without a K-mirror de-rotator in NGAO.

7.15 Up-link AO Trade Study

The purpose of this trade study was to explore the advantages and disadvantages of adaptive optics wavefront control of the outgoing laser in order to correct for atmospheric aberrations on the laser uplink path. The main advantage of uplink correction is the possibility of obtaining a LGS that is smaller in angular extent than one without compensation. Since the wavefront sensor is to first order dependent only on surface brightness of the guide star, the smaller spot needs less total brightness which in turn implies less laser power is required to create it. With each Watt of laser power having a high marginal cost in the overall AO system, improvements that reduce the required power must be taken seriously.

It appears that if one takes pains to use the type of wavefront sensor that can take advantage of it, there is a potential for a very significant reduction of required laser power if the uplink beam is AO corrected. However, the total package, which involves the success of more than one untested technology, is of reasonably high technical risk. Still the benefit potential suggests that even if the more conservative approach is taken during initial design phases, development testing of the new technologies should proceed.

8 GLOSSARY

Table 26. defines the acronyms and specialized terms used in this document.

Table 26. Glossary of Terms

Term	Definition
ACS	Active Control System
ADC	Atmospheric Dispersion Corrector
AO	Adaptive Optics
API	Application Programmer Interface
DCS	Drive and Control System
DM	Deformable Mirror
DOF	Degrees Of Freedom
EPICS	Experimental Physics Industrial Control System
FAA	Federal Aviation Administration
FOV	Field Of View
FPGA	Field Programmable Gate Array
FRD	Functional Requirements Document
FWHM	Full Width at Half Maximum
HOWFS	High Order WaveFront Sensor
IBRD	Instrument Baseline Requirements Document
IFU	Integral Field Unit
KAON	Keck Adaptive Optics Note
KI	Keck Interferometer
KOTN	Keck Observatory Technical Note
LGS	Laser Guide Star
LOWFS	Low Order WaveFront Sensor
mas	milli-arcsecond
MEMS	Micro Electro-Mechanical System
MTBF	Mean Time Between Failures
NGAO	Next Generation Adaptive Optics
NGS	Natural Guide Star
NIR	Near InfraRed
NIRC2	NIR Camera 2
NIRSPEC	NIR SPECtrometer
OA	Observing Assistant
OAP	Off-Axis Parabola
‘OHANA	Optical Hawaiian Array for Nanoradian Astronomy
OMU	Opto-Mechanical Unit
OSIRIS	OH-Suppression InfraRed Integral field Spectrograph
OSM	Object Selection Mechanism
PSF	Point Spread Function
rms	root mean square
SCRD	Science Case Requirements Document
SRD	System Requirements Document
TBC	To Be Completed
TBD	To Be Determined
WFE	WaveFront Error
WFS	WaveFront Sensor
WMKO	W. M. Keck Observatory

9 APPENDIX: NGAO SD PHASE DETAILED WAVEFRONT ERROR BUDGETS

The following are detailed wavefront error / ensquared energy budgets developed using the median turbulence condition Mauna Kea Ridge $C_n^2(h)$ model (KAON 503). This model has:

r_0 (0.5 microns) = 16 cm
θ_0 (0.5 microns) = 2.7 arcseconds
d_0 (0.5 microns) = 4.85 m
L_0 = 50 m

with a $C_n^2(h)$ distribution given by:

Altitude (m)	Mauna Kea Ridge Cn2 Fractional Turbulence
0	0.517
500	0.119
1000	0.063
2000	0.061
4000	0.105
8000	0.081
16000	0.054

KAON 503 also defines a wind velocity model for the Mauna Kea Ridge resulting in:

Greenwood frequency = 27.91 Hz

Keck Wavefront Error Budget Summary

Version 1.35

Mode: **NGAO NGS**
Instrument: **TBD**
Sci. Observation: **Io**

	Science Band								
	u'	g'	r'	i'	Z	Y	J	H	K
λ (μm)	0.36	0.47	0.62	0.75	0.88	1.03	1.25	1.64	2.20
δλ (μm)	0.06	0.14	0.14	0.15	0.12	0.12	0.16	0.29	0.34
λ/D (mas)	7	10	13	15	18	21	26	34	46

Science High-order Errors (NGS Mode)		Wavefront Error (rms)	Parameter	Strehl Ratio (%)
Atmospheric Fitting Error		48 nm	64 Subaps	
Bandwidth Error		30 nm	**100 Hz (-3db)**	
High-order Measurement Error		26 nm	5 mV	
LGS Tomography Error		0 nm	**1 natural guide star**	
Asterism Deformation Error		0 nm	0.50 m LLT	
Multispectral Error		22 nm	30 zenith angle, H band	
Scintillation Error		13 nm	0.34 Scint index, H-band	
WFS Scintillation Error		10 nm	Alloc	
	68 nm			
Uncorrectable Static Telescope Aberrations		43 nm	64 Acts	
Uncorrectable Dynamic Telescope Aberrations		17 nm	Dekens Ph.D	
Static WFS Zero-point Calibration Error		25 nm	Alloc	
Dynamic WFS Zero-point Calibration Error		25 nm	Alloc	
Leaky Integrator Zero-point Calibration Error		15 nm	Alloc	
Go-to Control Errors		0 nm	Alloc	
Residual Na Layer Focus Change		0 nm	30 m/s Na layer vel	
DM Finite Stroke Errors		4 nm	4.0 um P-P stroke	
DM Hysteresis		13 nm	from TMT	
High-Order Aliasing Error		11 nm	64 Subaps	
DM Drive Digitization		1 nm	16 bits	
Uncorrectable AO System Aberrations		30 nm	Alloc	
Uncorrectable Instrument Aberrations		30 nm	TBD Instrument	
DM-to-lenslet Misregistration		15 nm	Alloc	
DM-to-lenslet Pupil Scale Error		15 nm	Alloc	
	79 nm			
Angular Anisoplanatism Error		9 nm	**0.5 arcsec**	
Total High Order Wavefront Error	104 nm	**104 nm**	**High Order Strehl**	0.04 / 0.15 / 0.34 / 0.48 / 0.59 / 0.68 / 0.77 / 0.86 / 0.92

Science Tip/Tilt Errors		Angular Error (rms)	Equivalent WFE (rms)	Parameter	Strehl ratios (%)
	Sci Filter				
Tilt Measurement Error (one-axis)		0.25 mas	4 nm	3.5 mag (mH)	
Tilt Bandwidth Error (one-axis)		0.53 mas	9 nm	50.0 Hz (-3db)	
Tilt Anisoplanatism Error (one-axis)		0.00 mas	0 nm	**0.0 arcsec off-axis**	
Residual Centroid Anisoplanatism		0.00 mas	0 nm	NGS x reduction	
Residual Atmospheric Dispersion	r'	2.39 mas	43 nm	20 x reduction	
Induced Plate Scale Deformations		0.00 mas	0 nm	0 m conj height	
Science Instrument Mechanical Drift		0.04 mas	1 nm	Alloc 15 mas / hr	
Long Exposure Field Rotation Errors		0.04 mas	1 nm	Alloc 15 mas / hr	
Residual Telescope Pointing Jitter (one-axis)		1.06 mas	18 nm	29 Hz input disturbance	
Total Tip/Tilt Error (one-axis)		**2.7 mas**	47 nm	**Tip/Tilt Strehl**	0.56 / 0.69 / 0.79 / 0.85 / 0.89 / 0.91 / 0.94 / 0.96 / 0.98
Total Effective Wavefront Error			**112 nm**	**Total Strehl (%)**	0.02 / 0.11 / 0.27 / 0.41 / 0.52 / 0.62 / 0.72 / 0.83 / 0.90
				FWHM (mas)	7.8 / 10.0 / 13.0 / 15.7 / 18.5 / 21.5 / 26.0 / 34.0 / 45.6

		Spaxel Diameter (mas)	15	34	50	70	80	160	240	480	1000		1080
Ensquared Energy	r'		0.23	0.34	0.35	0.35	0.35	0.38	0.43	0.57	0.78		0.80

Sky Coverage	Galactic Lat.	30 deg		
Corresponding Sky Coverage		**N/A**	This fraction of sky can be corrected to the Total Effective WFE shown	

Assumptions / Parameters

r0	**0.147 m**	**at this zenith**	Wind Speed	11.0 m/s	LGS power	NGS	W at laser(s)	Excitation (all LGS 90km)	NGS ph/cm^2/sec
Theta0_eff	**2.14 arcsec**	**at this zenith**	Outer Scale	50 m	Zenith Angle	30 deg			
Sodium Abund.	4 x 10^9	atoms/cm^2	LGS Ast. Rad.	0.08 arcmin	HO WFS Rate	2000 Hz	SH	using	CCID56
Science AO Mode:	SCAO		HOWFS Trans	0.14	HO WFS Noise	2.4 e- rms			
LOWFS AO Mode:	NGS				HOWFS anti-aliasing	YES			
LOWFS Star Type:	G	Num TT 0	Num 3x3	0	LO WFS rate	2000 Hz	NGS	using	CCID56
Max Exposure Time	10 sec	Num TTFA 0	Num HOWFS	1	LO WFS Noise	2.4 e- rms			
					Max mechanical tip/tilt rejection bandwidth	100 Hz			

Figure 71. Science target wavefront error budget for Io Science Case.

Keck Wavefront Error Budget Summary

Version 1.35

Mode: **NGAO LGS**
Instrument: **TBD**
Sci. Observation: **Gal Cen**

	Science Band								
	u'	g'	r'	i'	Z	Y	J	H	K
λ (μm)	0.36	0.47	0.62	0.75	0.88	1.03	1.25	1.64	2.20
δλ (μm)	0.06	0.14	0.14	0.15	0.12	0.12	0.16	0.29	0.34
λ/D (mas)	7	10	13	15	18	21	26	34	46

Science High-order Errors (LGS Mode)		Wavefront Error (rms)	Parameter
Atmospheric Fitting Error		48 nm	64 Subaps
Bandwidth Error		50 nm	**53 Hz (-3db)**
High-order Measurement Error		60 nm	100 W
LGS Tomography Error		83 nm	**3 beacon(s)**
Asterism Deformation Error		22 nm	0.50 m LLT
Multispectral Error		22 nm	30 zenith angle, H band
Scintillation Error		13 nm	0.34 Scint index, H-band
WFS Scintillation Error		10 nm	Alloc
	128 nm		
Uncorrectable Static Telescope Aberrations		43 nm	64 Acts
Uncorrectable Dynamic Telescope Aberrations		33 nm	Dekens Ph.D
Static WFS Zero-point Calibration Error		25 nm	Alloc
Dynamic WFS Zero-point Calibration Error		40 nm	Alloc
Leaky Integrator Zero-point Calibration Error		15 nm	Alloc
Go-to Control Errors		38 nm	Alloc
Residual Na Layer Focus Change		34 nm	30 m/s Na layer vel
DM Finite Stroke Errors		0 nm	4.0 um P-P stroke
DM Hysteresis		13 nm	from TMT
High-Order Aliasing Error		16 nm	64 Subaps
DM Drive Digitization		1 nm	16 bits
Uncorrectable AO System Aberrations		30 nm	Alloc
Uncorrectable Instrument Aberrations		32 nm	TBD Instrument
DM-to-lenslet Misregistration		15 nm	Alloc
DM-to-lenslet Pupil Scale Error		15 nm	Alloc
	104 nm		
Angular Anisoplanatism Error		63 nm	**5.0 arcsec**
Total High Order Wavefront Error	165 nm	**176 nm**	**High Order Strehl**

Strehl Ratio (%)								
0.00	0.00	0.04	0.11	0.21	0.32	0.46	0.64	0.78

Science Tip/Tilt Errors		Angular Error (rms)	Equivalent WFE (rms)	Parameter
	Sci Filter			
Tilt Measurement Error (one-axis)		0.05 mas	1 nm	7.0 mag (mH)
Tilt Bandwidth Error (one-axis)		1.07 mas	18 nm	25.0 Hz (-3db)
Tilt Anisoplanatism Error (one-axis)		0.48 mas	8 nm	**5.5 arcsec off-axis**
Residual Centroid Anisoplanatism		1.10 mas	19 nm	10 x reduction
Residual Atmospheric Dispersion	*K*	0.12 mas	2 nm	20 x reduction
Induced Plate Scale Deformations		0.00 mas	0 nm	0 m conj height
Science Instrument Mechanical Drift		0.13 mas	2 nm	Alloc 15 mas / hr
Long Exposure Field Rotation Errors		0.13 mas	2 nm	Alloc 15 mas / hr
Residual Telescope Pointing Jitter (one-axis)		2.12 mas	36 nm	29 Hz input disturbance
Total Tip/Tilt Error (one-axis)		**2.7 mas**	50 nm	**Tip/Tilt Strehl**

Strehl ratios (%)								
0.56	0.69	0.79	0.85	0.89	0.91	0.94	0.96	0.98

Total Effective Wavefront Error	**182 nm**	**Total Strehl (%)**	0.00 0.00 0.03 0.10 0.19 0.29 0.43 0.61 0.76
		FWHM (mas)	7.8 10.0 13.0 15.7 18.5 21.5 26.0 34.0 45.6

		Spaxel Diameter (mas)	15	34	50	70	80	160	240	480	1000		120
Ensquared Energy	*K*		0.08	0.31	0.53	0.71	0.75	0.81	0.84	0.90	0.93		0.80

Sky Coverage	Galactic Lat.	30 deg		
Corresponding Sky Coverage		**N/A**	This fraction of sky can be corrected to the Total Effective WFE shown	

Assumptions / Parameters

						LGS power	100	W at laser(s)	Excitation (all LGS 90km)	9913	ph/cm^2/sec
r0	**0.147 m**	**at this zenith**	Wind Speed	11.0	m/s	Zenith Angle	30	deg			
Theta0_eff	**2.14 arcsec**	**at this zenith**	Outer Scale	50	m	HO WFS Rate	1065	Hz	SH	using	CCID56
Sodium Abund.	4 x 10^9	atoms/cm^2	LGS Ast. Rad.	0.08	arcmin	HO WFS Noise	1.8	e- rms			
Science AO Mode:	MOAO		HOWFS Trans	0.18		HOWFS anti-aliasing	NO				
LOWFS AO Mode:	MOAO Point and Shoot					LO WFS rate	667	Hz	SH	using	H2RG
LOWFS Star Type:	IRS7	Num TT 2	Num 3x3	0		LO WFS Noise	4.5	e- rms			
Max Exposure Time	30 sec	Num TTFA 1	Num HOWFS	0		Max mechanical tip/tilt rejection bandwidth		100 Hz			

Figure 72. Science target wavefront error budget for Galactic Center Science Case.

Keck Wavefront Error Budget Summary

Version 1.35

Mode: **NGAO LGS**
Instrument: **TBD**
Sci. Observation: **Exo Jup LGS**

	Science Band								
	u'	g'	r'	i'	Z	Y	J	H	K
λ (μm)	0.36	0.47	0.62	0.75	0.88	1.03	1.25	1.64	2.20
δλ (μm)	0.06	0.14	0.14	0.15	0.12	0.12	0.16	0.29	0.34
λ/D (mas)	7	10	13	15	18	21	26	34	46

Science High-order Errors (LGS Mode)		Wavefront Error (rms)	Parameter	Strehl Ratio (%)
Atmospheric Fitting Error		48 nm	64 Subaps	
Bandwidth Error		50 nm	**53 Hz (-3db)**	
High-order Measurement Error		60 nm	100 W	
LGS Tomography Error		52 nm	**3 beacon(s)**	
Asterism Deformation Error		22 nm	0.50 m LLT	
Multispectral Error		22 nm	30 zenith angle, H band	
Scintillation Error		13 nm	0.34 Scint index, H-band	
WFS Scintillation Error		10 nm	Alloc	
	111 nm			
Uncorrectable Static Telescope Aberrations		43 nm	64 Acts	
Uncorrectable Dynamic Telescope Aberrations		33 nm	Dekens Ph.D	
Static WFS Zero-point Calibration Error		25 nm	Alloc	
Dynamic WFS Zero-point Calibration Error		40 nm	Alloc	
Leaky Integrator Zero-point Calibration Error		15 nm	Alloc	
Go-to Control Errors		38 nm	Alloc	
Residual Na Layer Focus Change		34 nm	30 m/s Na layer vel	
DM Finite Stroke Errors		0 nm	4.0 um P-P stroke	
DM Hysteresis		13 nm	from TMT	
High-Order Aliasing Error		16 nm	64 Subaps	
DM Drive Digitization		1 nm	16 bits	
Uncorrectable AO System Aberrations		30 nm	Alloc	
Uncorrectable Instrument Aberrations		30 nm	TBD Instrument	
DM-to-lenslet Misregistration		15 nm	Alloc	
DM-to-lenslet Pupil Scale Error		15 nm	Alloc	
	103 nm			
Angular Anisoplanatism Error		16 nm	**1.0 arcsec**	
Total High Order Wavefront Error	151 nm	**152 nm**	**High Order Strehl**	0.00 0.02 0.09 0.20 0.32 0.43 0.56 0.72 0.83

Science Tip/Tilt Errors		Angular Error (rms)	Equivalent WFE (rms)	Parameter	Strehl ratios (%)
	Sci Filter				
Tilt Measurement Error (one-axis)		0.11 mas	2 nm	9.2 mag (mH)	
Tilt Bandwidth Error (one-axis)		1.07 mas	18 nm	25.0 Hz (-3db)	
Tilt Anisoplanatism Error (one-axis)		0.00 mas	0 nm	**0.0 arcsec off-axis**	
Residual Centroid Anisoplanatism		1.10 mas	19 nm	10 x reduction	
Residual Atmospheric Dispersion	*H*	0.26 mas	5 nm	20 x reduction	
Induced Plate Scale Deformations		0.00 mas	0 nm	0 m conj height	
Science Instrument Mechanical Drift		1.25 mas	21 nm	Alloc 15 mas / hr	
Long Exposure Field Rotation Errors		1.25 mas	21 nm	Alloc 15 mas / hr	
Residual Telescope Pointing Jitter (one-axis)		2.12 mas	36 nm	29 Hz input disturbance	
Total Tip/Tilt Error (one-axis)		**3.2 mas**	59 nm	**Tip/Tilt Strehl**	0.47 0.61 0.73 0.80 0.85 0.88 0.92 0.95 0.97
Total Effective Wavefront Error			**162 nm**	**Total Strehl (%)**	0.00 0.01 0.07 0.16 0.27 0.38 0.52 0.68 0.81
				FWHM (mas)	8.0 10.2 13.1 15.8 18.5 21.6 26.1 34.0 45.7

		Spaxel Diameter (mas)	15	34	50	70	80	160	240	480	1000		310
Ensquared Energy	*H*		0.13	0.42	0.61	0.71	0.72	0.75	0.77	0.84	0.88		0.80

Sky Coverage	Galactic Lat.	30 deg		
Corresponding Sky Coverage		**N/A**	This fraction of sky can be corrected to the Total Effective WFE shown	

Assumptions / Parameters

r0	**0.147 m**	**at this zenith**	Wind Speed	11.0 m/s	LGS power	100 W at laser(s)		Excitation (all LGS 90km)		9913 ph/cm^2/sec	
Theta0_eff	**2.14 arcsec**	**at this zenith**	Outer Scale	50 m	Zenith Angle	30 deg					
Sodium Abund.	4 x 10^9	atoms/cm^2	LGS Ast. Rad.	0.08 arcmin	HO WFS Rate	1065 Hz	SH	using	CCID56		
Science AO Mode:	MOAO		HOWFS Trans	0.18	HO WFS Noise	1.8 e- rms					
LOWFS AO Mode:	MOAO Point and Shoot				HOWFS anti-aliasing	NO					
LOWFS Star Type:	M	Num TT 2	Num 3x3	0	LO WFS rate	667 Hz	SH	using	H2RG		
Max Exposure Time	300 sec	Num TTFA 1	Num HOWFS	0	LO WFS Noise	4.5 e- rms					
					Max mechanical tip/tilt rejection bandwidth		100 Hz				

Figure 73. Science target wavefront error budget for ExoJupiter LGS Case.

Keck Wavefront Error Budget Summary

Version 1.35

Mode: **NGAO LGS**
Instrument: **TBD**
Sci. Observation: **Galaxy / Galaxy Lensing**

	Science Band								
	u'	g'	r'	i'	Z	Y	J	H	K
λ (μm)	0.36	0.47	0.62	0.75	0.88	1.03	1.25	1.64	2.20
δλ (μm)	0.06	0.14	0.14	0.15	0.12	0.12	0.16	0.29	0.34
λ/D (mas)	7	10	13	15	18	21	26	34	46

Science High-order Errors (LGS Mode)		Wavefront Error (rms)	Parameter	Strehl Ratio (%)
Atmospheric Fitting Error		48 nm	64 Subaps	
Bandwidth Error		49 nm	**54 Hz (-3db)**	
High-order Measurement Error		61 nm	100 W	
LGS Tomography Error		62 nm	**3 beacon(s)**	
Asterism Deformation Error		22 nm	0.50 m LLT	
Multispectral Error		22 nm	30 zenith angle, H band	
Scintillation Error		13 nm	0.34 Scint index, H-band	
WFS Scintillation Error		10 nm	Alloc	
	116 nm			
Uncorrectable Static Telescope Aberrations		43 nm	64 Acts	
Uncorrectable Dynamic Telescope Aberrations		32 nm	Dekens Ph.D	
Static WFS Zero-point Calibration Error		25 nm	Alloc	
Dynamic WFS Zero-point Calibration Error		40 nm	Alloc	
Leaky Integrator Zero-point Calibration Error		15 nm	Alloc	
Go-to Control Errors		38 nm	Alloc	
Residual Na Layer Focus Change		34 nm	30 m/s Na layer vel	
DM Finite Stroke Errors		0 nm	4.0 um P-P stroke	
DM Hysteresis		13 nm	from TMT	
High-Order Aliasing Error		16 nm	64 Subaps	
DM Drive Digitization		1 nm	16 bits	
Uncorrectable AO System Aberrations		30 nm	Alloc	
Uncorrectable Instrument Aberrations		30 nm	TBD Instrument	
DM-to-lenslet Misregistration		15 nm	Alloc	
DM-to-lenslet Pupil Scale Error		15 nm	Alloc	
	103 nm			
Angular Anisoplanatism Error		35 nm	**2.5 arcsec**	
Total High Order Wavefront Error	155 nm	**159 nm**	**High Order Strehl**	0.00 0.01 0.08 0.17 0.28 0.40 0.53 0.69 0.82

Science Tip/Tilt Errors		Angular Error (rms)	Equivalent WFE (rms)	Parameter	Strehl ratios (%)
	Sci Filter				
Tilt Measurement Error (one-axis)		2.76 mas	47 nm	14.0 mag (mH)	
Tilt Bandwidth Error (one-axis)		1.11 mas	19 nm	24.0 Hz (-3db)	
Tilt Anisoplanatism Error (one-axis)		4.72 mas	79 nm	**54.1 arcsec off-axis**	
Residual Centroid Anisoplanatism		1.10 mas	19 nm	10 x reduction	
Residual Atmospheric Dispersion	*H*	0.26 mas	5 nm	20 x reduction	
Induced Plate Scale Deformations		0.00 mas	0 nm	0 m conj height	
Science Instrument Mechanical Drift		5.00 mas	83 nm	Alloc 15 mas / hr	
Long Exposure Field Rotation Errors		5.00 mas	83 nm	Alloc 15 mas / hr	
Residual Telescope Pointing Jitter (one-axis)		2.21 mas	37 nm	29 Hz input disturbance	
Total Tip/Tilt Error (one-axis)		**9.3 mas**	159 nm	**Tip/Tilt Strehl**	0.09 0.15 0.24 0.31 0.39 0.47 0.56 0.69 0.80
Total Effective Wavefront Error			**224 nm**	**Total Strehl (%)**	0.00 0.00 0.02 0.05 0.11 0.19 0.30 0.48 0.65
				FWHM (mas)	11.9 13.4 15.8 18.1 20.5 23.3 27.5 35.1 46.5

		Spaxel Diameter (mas)	15	34	50	70	80	160	240	480	1000		340
Ensquared Energy	*H*		0.09	0.32	0.52	0.66	0.69	0.73	0.76	0.83	0.88		0.80

Sky Coverage	Galactic Lat.	30 deg	
Corresponding Sky Coverage		**30.0%**	This fraction of sky can be corrected to the Total Effective WFE shown

Assumptions / Parameters

r0	**0.147 m**	**at this zenith**	Wind Speed	11.0 m/s	LGS power	100 W at laser(s)		Excitation (all LGS 90km)		9913 ph/cm^2/sec	
Theta0_eff	**2.14 arcsec**	**at this zenith**	Outer Scale	50 m	Zenith Angle	30 deg					
Sodium Abund.	4 x 10^9	atoms/cm^2	LGS Ast. Rad.	0.08 arcmin	HO WFS Rate	1082 Hz	SH	using	CCID56		
Science AO Mode:	MOAO		HOWFS Trans	0.18	HO WFS Noise	1.8 e- rms					
LOWFS AO Mode:	MOAO Point and Shoot				HOWFS anti-aliasing	NO					
LOWFS Star Type:	M	Num TT 2	Num 3x3	0	LO WFS rate	632 Hz	SH	using	H2RG		
Max Exposure Time	1200 sec	Num TTFA 1	Num HOWFS	0	LO WFS Noise	4.5 e- rms					
					Max mechanical tip/tilt rejection bandwidth			100 Hz			

Figure 74. Science target wavefront error budget for Galaxy/Galaxy Lensing Science Case.

Keck Wavefront Error Budget Summary Version 1.35

Mode: **NGAO LGS**
Instrument: **TBD**
Sci. Observation: **Galaxy / Galaxy Lensing**

	Science Band								
	u'	g'	r'	i'	Z	Y	J	H	K
λ (μm)	0.36	0.47	0.62	0.75	0.88	1.03	1.25	1.64	2.20
δλ (μm)	0.06	0.14	0.14	0.15	0.12	0.12	0.16	0.29	0.34
λ/D (mas)	7	10	13	15	18	21	26	34	46

LOWFS High-order Errors (Mode)	54.1 arcsec off-axis	Wavefront Error (rms)	Parameter	Strehl Ratio (%)
Atmospheric Fitting Error		85 nm	32 Acts Across	
Bandwidth Error		49 nm	54 Hz (-3db)	
High-order Measurement Error		65 nm	10% Pupil Shear Criterion	
LGS Tomography Error		139 nm	PnS MOAO	
Asterism Deformation Error		22 nm	0.50 m LLT	
Multispectral Error		22 nm	30 zenith angle, H band	
Scintillation Error		13 nm	0.34 Scint index, H-band	
WFS Scintillation Error		10 nm	Alloc	
	185 nm			
Uncorrectable Static Telescope Aberrations		59 nm	32 Acts Across	
Uncorrectable Dynamic Telescope Aberrations		3 nm	Short exposure	
Static WFS Zero-point Calibration Error		25 nm	Alloc	
Dynamic WFS Zero-point Calibration Error		40 nm	Alloc	
Leaky Integrator Zero-point Calibration Error		15 nm	Alloc	
Go-to Control Errors		38 nm	Alloc	
Residual Na Layer Focus Change		34 nm	30 m/s Na layer vel	
DM Finite Stroke Errors		15 nm	1.5 um P-P MEMS stroke	
DM Hysteresis		2 nm	from LAO	
High-Order Aliasing Error		16 nm	64 Subaps	
DM Drive Digitization		1 nm	16 bits	
Uncorrectable AO System Aberrations		30 nm	Alloc	
Uncorrectable Instrument Aberrations		30 nm	TBD Instrument	
DM-to-lenslet Misregistration		15 nm	Alloc	
DM-to-lenslet Pupil Scale Error		15 nm	Alloc	
	106 nm			
Angular Anisoplanatism Error		0 nm	PnS MOAO	
Total High Order Wavefront Error	214 nm	**214 nm**	**High Order Strehl**	0.00 0.00 0.01 0.04 0.10 0.19 0.32 0.51 0.69

Assumptions / Parameters

	10%-shear fraction:	0.86	Effective PnS GS radius	0.26 arcmin	LGS power	100 W at laser(s)		LGS return (all beacons)	9913 ph/cm^2/sec
r0	0.147 m	at this zenith	Wind Speed	11.0 m/s	Zenith Angle	30 deg			
Theta0_eff	2.14 arcsec	at this zenith	Outer Scale	50 m	HO WFS Rate	1082 Hz	SH	using CCID56	
Sodium Abund.	4 x 10^9	atoms/cm^2	LGS Ast. Rad.	0.08 arcmin	HO WFS Noise	1.8 e- rms			
Science AO Mode:	MOAO		HOWFS Trans	0.18	HOWFS anti-aliasing	NO			
LOWFS AO Mode:	MOAO Point and Shoot				LO WFS rate	632 Hz	SH	using H2RG	
LOWFS Star Type:	M	Num TT 2	Num 3x3	0	LO WFS Noise	4.5 e- rms			
Max Exposure Time	1200 sec	Num TTFA 1	Num HOWFS	0	Max mechanical tip/tilt rejection bandwidth	100 Hz			

Figure 75. LOWFS NGS wavefront error budget for the Galaxy / Galaxy Lensing Survey Science Case. NGS 54" off-axis. We expect such a star to be sharpened to about 32% J-Strehl using MOAO correction based on multi-LGS tomography.

Keck Wavefront Error Budget Summary

Version 1.35

Mode: **NGAO LGS**
Instrument: **TBD**
Sci. Observation: **Extended Groth Strip**

	Science Band								
	u'	g'	r'	i'	Z	Y	J	H	K
λ (μm)	0.36	0.47	0.62	0.75	0.88	1.03	1.25	1.64	2.20
δλ (μm)	0.06	0.14	0.14	0.15	0.12	0.12	0.16	0.29	0.34
λ/D (mas)	7	10	13	15	18	21	26	34	46

Science High-order Errors (LGS Mode)		Wavefront Error (rms)	Parameter
Atmospheric Fitting Error		48 nm	64 Subaps
Bandwidth Error		50 nm	**53 Hz (-3db)**
High-order Measurement Error		49 nm	150 W
LGS Tomography Error		141 nm	**6 beacon(s)**
Asterism Deformation Error		22 nm	0.50 m LLT
Multispectral Error		22 nm	30 zenith angle, H band
Scintillation Error		13 nm	0.34 Scint index, H-band
WFS Scintillation Error		10 nm	Alloc
	168 nm		
Uncorrectable Static Telescope Aberrations		43 nm	64 Acts
Uncorrectable Dynamic Telescope Aberrations		33 nm	Dekens Ph.D
Static WFS Zero-point Calibration Error		25 nm	Alloc
Dynamic WFS Zero-point Calibration Error		40 nm	Alloc
Leaky Integrator Zero-point Calibration Error		15 nm	Alloc
Go-to Control Errors		38 nm	Alloc
Residual Na Layer Focus Change		34 nm	30 m/s Na layer vel
DM Finite Stroke Errors		0 nm	4.0 um P-P stroke
DM Hysteresis		13 nm	from TMT
High-Order Aliasing Error		16 nm	64 Subaps
DM Drive Digitization		1 nm	16 bits
Uncorrectable AO System Aberrations		30 nm	Alloc
Uncorrectable Instrument Aberrations		30 nm	TBD Instrument
DM-to-lenslet Misregistration		15 nm	Alloc
DM-to-lenslet Pupil Scale Error		15 nm	Alloc
	103 nm		
Angular Anisoplanatism Error		23 nm	**1.5 arcsec**
Total High Order Wavefront Error	198 nm	**199 nm**	**High Order Strehl**

Strehl Ratio (%)								
0.00	0.00	0.02	0.06	0.14	0.23	0.37	0.56	0.73

Science Tip/Tilt Errors	Sci Filter	Angular Error (rms)	Equivalent WFE (rms)	Parameter
Tilt Measurement Error (one-axis)		2.20 mas	37 nm	13.9 mag (mH)
Tilt Bandwidth Error (one-axis)		1.28 mas	22 nm	20.8 Hz (-3db)
Tilt Anisoplanatism Error (one-axis)		4.80 mas	80 nm	**55.0 arcsec off-axis**
Residual Centroid Anisoplanatism		1.10 mas	19 nm	10 x reduction
Residual Atmospheric Dispersion	*H*	0.26 mas	5 nm	20 x reduction
Induced Plate Scale Deformations		0.00 mas	0 nm	0 m conj height
Science Instrument Mechanical Drift		5.00 mas	83 nm	Alloc 15 mas / hr
Long Exposure Field Rotation Errors		5.00 mas	83 nm	Alloc 15 mas / hr
Residual Telescope Pointing Jitter (one-axis)		2.54 mas	43 nm	29 Hz input disturbance
Total Tip/Tilt Error (one-axis)		**9.3 mas**	159 nm	**Tip/Tilt Strehl**

Strehl ratios (%)								
0.09	0.15	0.24	0.31	0.39	0.47	0.56	0.69	0.80

Total Effective Wavefront Error	**254 nm**	**Total Strehl (%)**

Strehl (%)								
0.00	0.00	0.00	0.02	0.05	0.11	0.21	0.39	0.58

FWHM (mas)	11.9 13.4 15.8 18.1 20.5 23.3 27.5 35.1 46.5

		Spaxel Diameter (mas)	15	34	50	70	80	160	240	480	1000		340
Ensquared Energy	*H*		0.07	0.26	0.43	0.55	0.57	0.65	0.72	0.86	0.91		0.80

Sky Coverage Galactic Lat. 30 deg

Corresponding Sky Coverage	**30.0%**	This fraction of sky can be corrected to the Total Effective WFE shown

Assumptions / Parameters

						LGS power	150	W at laser(s)	Excitation (all LGS 90km)	14869	ph/cm^2/sec
r0	**0.147 m**	**at this zenith**	Wind Speed	11.0 m/s		Zenith Angle	30	deg			
Theta0_eff	**2.14 arcsec**	**at this zenith**	Outer Scale	50 m		HO WFS Rate	1059	Hz	SH	using	CCID56
Sodium Abund.	4 x 10^9	atoms/cm^2	LGS Ast. Rad.	1.00 arcmin		HO WFS Noise	1.8	e- rms			
Science AO Mode:	MOAO		HOWFS Trans	0.18		HOWFS anti-aliasing	NO				
LOWFS AO Mode:	MOAO Point and Shoot					LO WFS rate	526	Hz	SH	using	H2RG
LOWFS Star Type:	M	Num TT 2	Num 3x3	0		LO WFS Noise	4.5	e- rms			
Max Exposure Time	1200 sec	Num TTFA 1	Num HOWFS	0		Max mechanical tip/tilt rejection bandwidth		100 Hz			

Figure 76. Science target Ensquared Energy error budget for High-Redshift Galaxies. Extended Groth Strip Science Case (for full 150W and 9 beacons)